



**University of
Nottingham**
UK | CHINA | MALAYSIA

Investigating The Role of ZEB1 in Lymphangiogenesis

Zarah Beth Tabrizi BSc

A thesis submitted to the University of Nottingham for the degree of
Doctor of Philosophy (PhD)

Under the supervision of Dr Andrew Benest and Dr Sarah Storr

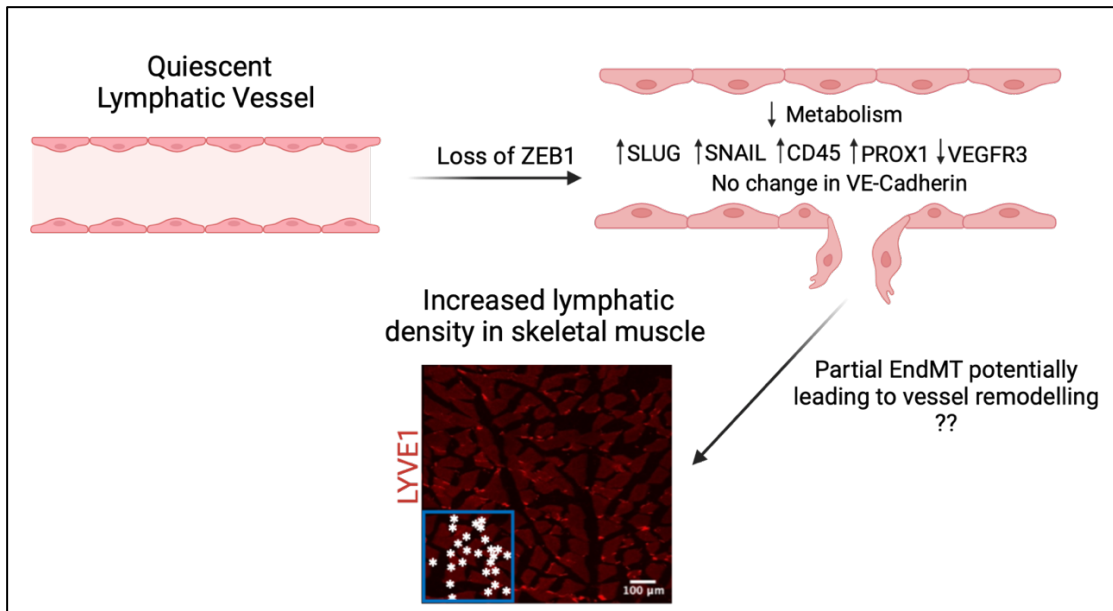
30th September 2023

Abstract

Lymphangiogenesis is the growth of new lymphatic vessels from the existing lymphatic vasculature. Lymphatic endothelial cells (LECs) line all lymphatic vessels and are essential regulators of vessel homeostasis. The switch between LEC quiescence and activation is highly regulated, controlled by multiple signalling pathways and transcription factors. The blood and lymphatic vasculature have shared origins, therefore often governed by similar mechanisms of growth and maintenance. Blood vessel remodelling has been shown to occur via a partial endothelial to mesenchymal transition (EndMT), allowing these cells to migrate from an existing vessel to form a new sprout. Lymphatic vessel remodelling has been relatively understudied, but this same remodelling mechanism is thought to occur. Governing this transition are SLUG and SNAIL, which also regulate epithelial to mesenchymal transition (EMT). Another driver of EMT is the transcription factor ZEB1, which has not been studied at present in EndMT or in the lymphatic system. In the blood vasculature, preliminary work has shown that loss of ZEB1 induces an angiogenic phenotype, therefore we hypothesise that, unlike SLUG and SNAIL, it is loss of ZEB1 which induces a partial EndMT mechanism involved in lymphatic vessel remodelling.

In this thesis, we used a mouse model of inducible endothelial cell knockout (iECKO), and primary human dermal LECs to investigate the role of ZEB1 in the lymphatic vasculature. *In vitro*, following siRNA knockdown of ZEB1, the transcriptome was pro-lymphangiogenic, with a migratory and proliferative phenotype suggested. At a protein level, SLUG and SNAIL were significantly upregulated, and the cell junctional marker VE-Cadherin was unaffected, suggesting a role of ZEB1 in partial EndMT. Mediators of lymphatic growth and identity, VEGFR3 and PROX1, were also dysregulated. In the ZEB1^{iECKO} mice, no change was detected in lymphatic morphology in the dermis of P5 and adult mice. However, in the skeletal muscle, an increase in density of lymphatic vessels following loss of ZEB1 was discovered. Additionally, these lymphatic vessels in the skeletal muscle of both Control and ZEB1^{iECKO} mice were positive for the immune infiltration marker CD45, which has

been suggested as a novel marker of EndMT. This is a significant finding and should be researched further, as this has implications of the fundamental endothelial biology underlying many cell isolation techniques.



A proposed mechanism by which loss of ZEB1 leads to increased lymphatic density.

Quiescent lymphatic vessels express ZEB1, following loss of ZEB1, markers of EndMT are upregulated, leading to a partial EndMT mechanism of vessel remodelling. In the skeletal muscle, this remodelling manifested as an increased lymphatic density, as observed by LYVE1 staining on 20 μm muscle sections. Made with Biorender.com

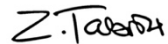
Acknowledgements

I would like to first and foremost my family for their unwavering support throughout these four years. I have appreciated every phone call and facetime, especially when they feature Phoebe. I would also like to thank my friends, the BDI babes, for every cheese and wine evening, every paint and sip, and every Portland trip. I would not have made it through without you all. I am wholeheartedly grateful to my lab group, to Jade, Joe, Nada, and Kathryn, I am so proud of us, I have no doubt we will achieve great things. Thank you to my supervisor Andy, for enabling me to become an independent scientist, and allowing me the opportunities to present my work internationally. I am also grateful to Sarah for teaching me the ins and out of IPA, my RNA chapter would be nothing without it! Finally, thank you to my long-suffering friends, to Kez, El, El and Em, thanks for memorising my thesis title and telling it to everyone, for keeping me sane and always being there to welcome me home.

Author's Declaration

I, Zarah Tabrizi, confirm that the work presented in this thesis was carried out in accordance with the requirements of the University's Regulations and Code of Practice for Research Degree Programs and that it has not been submitted for any other academic award. I confirm that the work and views demonstrated in this thesis are my own. Where information has been derived from other sources, I confirm this has been indicated in the thesis.

SIGNED:



DATE: 25th September 2023

Conferences

Tabrizi Z.B., Mok H., Horder J., Green K.R., Bhalla S.R., Beazley-Long N., Bates, D.O., Benest A.V. Joint Conference of German and British Microcirculation and Vascular Biology; Berlin, Germany. June 2022. Poster Presentation - A potential role of ZEB1 in ischaemic lymphangiogenesis.

Tabrizi Z.B., Mok H., Horder J., Green K.R., Bhalla S.R., Beazley-Long N., Bates, D.O., Benest A.V. Joint International Vascular Biology Meeting, Oakland, San Francisco. October 2022. Poster Presentation - A potential role of ZEB1 in ischaemic lymphangiogenesis.

Tabrizi Z.B., Manning J, Horder J., Green K.R., Bhalla S.R., Beazley-Long N., Bates, D.O., Benest A.V. Lymphatic Forum, Banff, Alberta. June 2023. Poster Presentation - Potential regulation of CD45 by ZEB1 during lymphangiogenesis.

Tabrizi Z.B., Manning J, Horder J., Green K.R., Bhalla S.R., Beazley-Long N., Bates, D.O., Benest A.V. British Microcirculation and Vascular Biology Society Meeting, Edinburgh. June 2023. Poster Presentation - Potential regulation of CD45 by ZEB1 during lymphangiogenesis. **Best Poster Prize.**

Table of Contents

Abstract	2
Acknowledgements	4
Author's Declaration	5
Conferences	6
List of Acronyms and Abbreviations	11
List of Tables	15
List of Figures	15
Chapter 1. Introduction	19
1.1 The Lymphatic System	19
1.1.1 Dysfunctional lymphatics	20
1.2 Transcription factor control of lymphatic quiescence and maturation of lymphatic neovessels in development and physiology	22
1.2.1 Lymphatic development	22
1.2.2 Lymphangiogenic mechanisms	23
1.2.3 Endothelial quiescence as a physiologically active, but not activated state.....	25
1.2.4 Transcription factor regulation of gene expression.....	26
1.2.5 Lymphatic vessels lose quiescence as they grow.....	27
1.2.6 Heterogeneity: How different are each of the endothelial cells within a lymphatic vessel?28	
1.2.7. Prospero homeobox 1 (PROX1) interacts with SOX18 and is key for lymphatic specification	29
1.2.8 Chicken ovalbumin promoter transcription factor II (CouP-TFII) interacts with PROX1 during lymphatic proliferation	33
1.2.9 GATA2 regulates VEGFR3 expression and contributes to lymphatic remodelling	34
1.2.10 FOXC2 plays a key role in lymphatic maturation	35
1.2.11 Control of PROX1 chromatin accessibility regulates downstream gene expression.....	37
1.2.12 Shear stress as a primary determinant of quiescence?	38
1.2.13 MAFB contributes to branching lymphatic morphogenesis	41
1.2.14 ETS-domain transcription factors	42
1.2.15 Lessons from single cell sequencing	43
1.3 Partial EndMT	44
1.4 ZEB1	46
1.5 Preliminary data	50
1.5.1 ZEB1 is present in the quiescent blood endothelium.	50
1.5.2 ZEB1 is present in the quiescent lymphatic endothelium.....	52
1.6 Aims and Hypothesis	53
Chapter 2. Methodology	54
2.1 Cell Culture	54
2.1.1 Model of lymphangiogenic growth	54
2.1.2 siRNA Knockdown	55
2.2 RNA Extraction	56

2.2.1 RNA Sequencing.....	57
2.3 ChIP Sequencing.....	58
2.4 Measuring Oxygen Consumption Rate with Agilent Seahorse.....	64
2.5 Protein Extraction.....	65
2.6 Western Blotting.....	66
2.7 Animal iECKO model.....	67
2.7.1 P5 model.....	68
2.7.2 Adult model.....	68
2.8 Immunofluorescence staining of ear dermis.....	68
2.8.1 Analysis of lymphatic morphology.....	69
2.9 Model of Hindlimb Ischaemia.....	71
2.9.1 Immunofluorescence staining of muscle sections.....	72
2.9.2 Analysis of HLI muscle sections.....	73
2.10 Statistical Analysis.....	75
<i>Chapter 3. The Effect of ZEB1 Knockdown on the Transcriptional Landscape of HDLECs.....</i>	76
3.1 Introduction.....	76
3.1.1. Gene silencing using siRNAs.....	77
3.1.2 RNA Sequencing.....	78
3.1.3 Chromatin Immunoprecipitation.....	79
3.2 Hypothesis and Aims.....	80
3.3 ZEB1 Knockdown RNA Sequencing.....	81
3.3.1 The Top 10 differentially expressed genes are representative of a lymphangiogenic phenotype.....	83
3.3.2 ZEB1 knockdown in LECs affects the RNA expression of known upstream and downstream interactors.....	85
3.3.3 Top canonical pathways.....	88
3.3.4 Loss of ZEB1 has an overall inhibitory effect on the EMT pathway.....	93
3.3.5 Impact on Biological Functions and Disease.....	96
3.3.6 The effect of ZEB1 on transcriptional regulation.....	97
3.4 ZEB1 Chromatin Immunoprecipitation.....	99
3.4.1 Identification of enhancer regions.....	106
3.5 Summary.....	108
<i>Chapter 4. ZEB1 Expression Influences the Protein Expression of EndMT Markers and Adjusts the Metabolic Profile of HDLECs.....</i>	112
4.1 Introduction.....	112
4.1.1 EndMT.....	112
4.1.2 Metabolic changes in EndMT.....	113
4.1.3 Measuring Metabolism using Agilent Seahorse assay.....	115
4.2 Hypothesis and Aims.....	118
4.3 Results.....	119
4.3.1 ZEB1 is differentially expressed in a model of lymphatic endothelial cell growth.....	119

4.3.2 Optimisation of ZEB1 siRNA protocol	120
4.3.3 ZEB1 siRNA knockdown influences expression of SLUG and SNAIL but no other markers of EMT/EndMT	121
4.3.4 ZEB1 knockdown alters the expression of key mediators of lymphatic identity	125
4.3.5 SLUG siRNA knockdown does not induce a change in ZEB1 protein expression	129
4.3.6 ZEB1 knockdown alters the metabolic profile of HDLECs	129
4.4 Discussion	134
Chapter 5. ZEB1 Plays No Major Role in the Early, Post-Natal Extension of the Lymphatic Vasculature of the Ear Dermis, or Adult Maintenance.	141
5.1 Introduction	141
5.1.1 Models of developmental lymphangiogenesis	141
5.1.2 Visualisation and quantification of lymphangiogenesis <i>in vivo</i>	143
5.1.3 Regulation of the lymphatic network in the dermis	144
5.2 Hypothesis and Aims	145
5.3 Results	146
5.3.1 Characterisation of ZEB1 ^{IECKO} transgenic mice	146
5.3.2 Ear dermis as a model of lymphangiogenesis	150
5.3.3 ZEB1 is dispensable in postnatal extension of dermal lymphatic vessels	152
5.3.4 ZEB1 may have a subtle effect on adult dermal lymphatic morphology	155
5.4 Discussion	157
Chapter 6. Loss of ZEB1 Induces Remodelling in Mouse Hindlimb Lymphatic Vessels	163
6.1 Introduction	163
6.1.1 Lymphatic response to inflammation	163
6.1.2 Lymphatic response to ischaemia	164
6.1.3 Quantification of lymphatic remodelling	166
6.2 Hypothesis and Aims	167
6.3 Results	167
6.3.1 Lymphatic vessels in the skeletal muscle ZEB1 ^{IECKO} mice were remodelled in the unoperated limb	169
6.3.2 ZEB1 ^{IECKO} mice have altered lymphatic morphology in the hindlimb regardless of surgery	170
6.3.3 Lymphatic vessels of the mouse hindlimb are CD45 positive	171
6.3.4 Human <i>in vitro</i> data suggests a relationship between ZEB1 and CD45	174
6.4 Discussion	178
Chapter 7. Discussion	188
7.1 The role of ZEB1 in lymphatic endothelial cells	188
7.1.1 Does loss of ZEB1 initiate partial EndMT in LECs?	189
7.1.2 A relationship between ZEB1 and CD45 expression	190
7.2 Limitations	191
7.3 Implications	194
7.4 Conclusion	196
Chapter 8. Appendix	197

8.1 COVID Statement	197
8.2 Professional Industry Placement	197
<i>Chapter 9. References</i>	200

List of Acronyms and Abbreviations

ADP Adenosine Diphosphate
AKT Protein Kinase B
AP1M2 Adhesive Protein Associated Adapter Protein Complex 1
ASPA Animal Scientific Procedures Act of 1986
ATAC-Seq Assay for Transposase-Accessible Chromatin with high-throughput sequencing
ATP Adenosine Triphosphate
BCA Bicinchoninic Acid
BEC Blood Endothelial Cell
BMP Bone Morphogenetic Protein
BSA Bovine Serum Albumin
CD31 Platelet Endothelial Cell Adhesion Molecule 1
CD45 Lymphocyte Common Antigen
CDH2 Cadherin 2
CDH5 VE-Cadherin
cDNA Complementary DNA
ChIP Chromatin Immunoprecipitation
CK-1 α Casein Kinase 1 α
CL-ELISA Chemiluminescence Enzyme-Linked Immunosorbent Assay
CoA Coenzyme A
CouP-TFII Chicken Ovalbumin Promoter Transcription Factor II
CPT1a Carnitine Palmitoyl Transferase 1a
CV Cardinal Vein
CXCL12 C-X-C Motif Chemokine Ligand
CZF Zinc Finger Carboxy-Terminal Cluster
ddPCR digital droplet Polymerase Chain Reaction
DEGs Differentially Expressed Genes
DLL4 Delta-like Ligand 4
DNA Deoxyribonucleic Acid
dsRNA Double Stranded RNA
ECs Endothelial Cells
ECAR Extracellular Acidification Rate
ECM Extracellular Matrix
EDN1 Endothelin 1
EDTA Ethylenediaminetetraacetic Acid
EMT Epithelial to Mesenchymal Transition
EndMT Endothelial to Mesenchymal Transition

EPCAM Epithelial Cell Adhesion Molecule
EGR1 Early Growth Response Protein 1
ERK Extracellular Signal-regulated kinase
ERT2 Estrogen Receptor ligand binding domain
ETS2 ETS Proto-Oncogene 2
ETV2 ETS Variant Transcription Factor 2
ETV3 ETS Variant Transcription Factor 3
ETV6 ETS Variant Transcription Factor 6
FADH2 Flavin Adenine Dinucleotide
FAM83H Family With Sequence Similarity 83 Member H
FAT1 FAT Atypical Cadherin 1
FBS Fetal Bovine Serum
FCCP Carbonyl cyanide-p-trifluoromethoxyphenylhydrazone
FGFR Fibroblast Growth Factor Receptor
FOXC2 Forkhead Box C2
FOXO1 Forkhead Box O1
FOXP2 Forkhead box protein P2
GAPDH Glyceraldehyde-3-Phosphate Dehydrogenase
GATA2 GATA Binding Protein 2
HDLECs Human Dermal Lymphatic Endothelial Cells
HHEX Haematopoietically Expressed Homeobox
HIF-1 α Hypoxia Inducing Factor-1 α
HK2 Hexokinase 2
HUVEC Human Umbilical Vein Endothelial Cell
IB₄ Isolectin B4
iECKO Inducible Endothelial Cell Knockout
IFN γ Interferon Gamma
IgG Immunoglobulin G
IPA Ingenuity Pathway Analysis
IRF Interferon Regulatory Factor
IRF6 Interferon Regulatory Factor 6
JAK Janus Kinase
JNK C-Jun N-Terminal Kinase 1
KEGG Kyoto Encyclopedia of Genes and Genomes
KLF2/4 Kruppel-Like Factor 2/4
LATS Large Tumour Suppressor Kinase
LECs Lymphatic Endothelial Cells
LMs Lymphatic malformations

LYVE1 Lymphatic Vessel Endothelial Hyaluronan Receptor 1
MAF Musculoaponeurotic Fibrosarcoma
MARE MAF Recognition Elements
MEK Mitogen-Activated Protein Kinase Kinase 1
MIB2 Mindbomb E3 Ubiquitin Ligase
mRNA messenger RNA
MT1-MMP Membrane Type 1 Matrix Metalloproteinase
MX2 MX Dynamin Like GTPase 2
MYC MYC Proto-Oncogene, BHLH Transcription Factor
NADH Nicotinamide Adenine Dinucleotide + Hydrogen
NFATc1 Nuclear Factor of Activated T Cells c1
NF- κ B Nuclear Factor- κ B
NO Nitric Oxide
NOTCH1 Neurogenic Locus Notch homologue protein 1
NRP2 Neuropillin 2
NSC Non-Silencing Control
NZF Zinc Finger Amino-Terminal Cluster
OCR Oxygen Consumption Rate
OCT Optimal Cutting Temperature Compound
PAD Peripheral Arterial Disease
PBS Phosphate Buffered Saline
PBS-X Phosphobuffered Saline with Triton X
PCR Polymerase Chain Reaction
PFA Paraformaldehyde
PMSF phenylmethylsulfonyl fluoride
PPAR γ Peroxisome Proliferator-activated Receptor gamma
PROX1 Prospero homeobox 1
PTPase Protein Tyrosine Phosphatase
RAF1 Mitogen Activated 3 Kinase
RIME Rapid Mass Spectrometry of Endogenous Proteins
RIPA Radioimmunoprecipitation Assay Buffer
RIPK1 Receptor Interacting Serine/Threonine Kinase 1
RISC RNA-Inducing Silencing Complex
RNA Ribonucleic Acid
RNASeq RNA Sequencing
RNF213 Ring Finger Protein 213
ROS Reactive Oxidation Species
S1PR1 sphingosine 1-phosphate receptor 1

scRNA-seq Single Cell RNA Sequencing
SDS-PAGE Sodium Dodecyl-Sulfate Polyacrylamide Gel Electrophoresis
siRNA Short Interrupting RNA
SLUG Snail Family Transcriptional Repressor 2
SNAIL Snail Family Transcriptional Repressor 1
SOLiD Sequencing by Oligonucleotide Ligation and Detection
SOX7 SRY-Box Transcription Factor 7
SOX18 SRY-Box Transcription Factor 18
STAT Signal Transducer And Activator Of Transcription
STAT6 Signal Transducer And Activator Of Transcription 6
TAZ TFAZZIN
TBS Tris Buffered Saline
TBS-t Tris Buffered Saline Tween-20
TGF β Transforming Growth Factor Beta
TSS Transcriptional Start Site
TWIST1 Twist Family bHLH Transcription Factor 1
UMAP Uniform Manifold Approximation and Projection
VCAM1 Vascular Cell Adhesion Molecule 1
VEGF Vascular Endothelial Growth Factor
VEGFR Vascular Endothelial Growth Factor Receptor
WNT5B Wnt Family Member 5B
XAF1 XIAP Associated Factor 1
YAP Yes-Associated Protein 1
ZEB1 Zinc Finger E-Box Binding Homeobox 1
ZEB2 Zinc Finger E-Box Binding Homeobox 2
ZMIZ1 Zinc finger MIZ-type containing 1
ZO1 Zona Occludens 1
 α SMA Alpha Smooth Muscle Actin

List of Tables

Table 2.1.2.1 siRNA target sequences of the individual siRNAs which are pooled to reduce target gene expression

Table 2.1.2.2 Constituents of Solutions used in the siRNA knockdown of ZEB1

Table 2.2.1 Quality control for LEC samples sent to Novogene for RNA Sequencing

Table 2.3.1 Reagents required for the precipitation of ZEB1 for Chromatin Immunoprecipitation Sequencing

Table 2.6.1 List of antibodies used for protein expression analysis using Western Blotting

Table 3.3.1.1 Top 10 upregulated and downregulated genes in the Control versus ZEB1 knockdown treated HDLECs

Table 3.3.6.1 Top 10 Transcriptional Regulators predicted inhibited and activated as a result of ZEB1 knockdown

Table 3.4.1 Genes which expression is differentially expressed through the direct binding of ZEB1

Table 4.3.3.1 ZEB1 siRNA knockdown affects ZO-1 and VEGFR2, but no other EMT/EndMT gene expression at an RNA level

Table 4.3.4.1 ZEB1 knockdown downregulates PROX1 at RNA level

Table 4.3.6.1 ZEB1 siRNA knockdown downregulates FOXO1 expression at RNA level

Table 5.3.1.1. Example of a Transnetyx raw data report

List of Figures

Figure 1.2.1.1 Comparison of a lymphatic collecting vessel and a lymphatic capillary

Figure 1.2.2.1 Development, differentiation and separation of the blood and lymphatic networks

Figure 1.2.14.1 Transcriptional insight into establishment and regulation of the quiescent lymphatic endothelial phenotype

Figure 1.5.1.1 Preliminary data demonstrates that ZEB1 is expressed in quiescent HUVECs

Figure 1.5.2.1 Preliminary data shows ZEB1 is expressed in LECs

Figure 2.3.1 Optimisation of sonication of chromatin shearing of HDLECs

Figure 2.8.1 Analysis of lymphatic morphology in the mouse ear dermis using FIJI

Figure 2.9.2.1 Analysis of lymphatic vessels in the hindlimb muscle using FIJI image analysis software

Figure 3.3.1 Consistent knockdown of ZEB1 protein in HDLECs was achieved via siRNA knockdown protocol

Figure 3.3.2 ZEB1 knockdown samples have a distinct transcriptional pattern in comparison to the control

Figure 3.3.3 ZEB1 knockdown results in the differential expression of genes following RNA Sequencing

Figure 3.3.2.1 ZEB1 knockdown results in changes in expression of published interacting molecules

Figure 3.3.3.1 The top five canonical pathways with genes affected by ZEB1 knockdown

Figure 3.3.3.2 ZEB1 knockdown significantly impacts genes associated with the pathway Molecular Mechanisms of Cancer

Figure 3.3.3.3 ZEB1 knockdown significantly impacts genes associated with Interferon Signalling

Figure 3.3.4.1 ZEB1 knockdown significantly impacts genes associated with Epithelial to Mesenchymal Transition by Growth Factors

Figure 3.3.5.1 Summary of Biological Functions and Diseases which are enriched in a dataset of ZEB1 knockdown of HDLECs

Figure 3.4.1 ZEB1 directly interacts with 367 target genes and alters the gene expression of 59 genes in HDLECs

Figure 3.4.2 ZEB1 directly binds to the promoter region of genes identified via ChIPSeq resulting in a significant change in gene expression

Figure 3.4.1.1 Histone modification binding tracks alongside ZEB1 ChIPSeq data allows for identification and visualisation of the TSS, promoter and enhancer regions

Figure 4.1.1 The principles of the Seahorse Mitochondrial Stress Assay

Figure 4.3.1.1 HDLECs exhibit a different protein expression profile when grown in sub-confluent versus confluent conditions as measured by western blot analysis

Figure 4.3.2.1 HDLECs grown to 80% confluency on 60 mm dishes were preferable for consistent protein visualisation on western blot during ZEB1 knockdown

Figure 4.3.3.1 HDLECs treated with ZEB1 siRNA knockdown reduces ZEB1 protein expression

Figure 4.3.3.2 ChIPSeq binding tracks for SNAIL, SLUG and VEGFR2 found no significant peaks between ZEB1 and the IgG

Figure 4.3.4.1 ZEB1 siRNA knockdown induces differential PROX1 and VEGFR3 protein expression as measured by western blot analysis

Figure 4.3.4.2 ChIPSeq binding tracks for PROX1 found no significant peaks between ZEB1 and the IgG.

Figure 4.3.5.1 SLUG siRNA knockdown in HDLECs decreases SLUG protein expression

Figure 4.3.6.1 ZEB1 siRNA knockdown does not affect protein expression of metabolic markers as measured by western blot analysis

Figure 4.3.6.2 Metabolic analysis of HDLECs subjected to ZEB1 siRNA knockdown

Figure 5.3.1.1 Schematic illustration of the loxP sites which flank exon 6 of ZEB1

Figure 5.3.1.2 Mouse trachea was unable to be optimised for quantification of ZEB1 knockdown

Figure 5.3.1.3 No change in the ZEB1 expression between the CD31+ fractions of Mouse A and B

Figure 5.3.1.4 ZEB1 mRNA expression in adult mouse lung tissue in the CD31⁺ fraction of Control and ZEB1^{iECKO} mice

Figure 5.3.2.1 Different lymphatic-rich tissues could be utilised for the investigation of a lymphatic vessel phenotype

Figure 5.3.3.1 No significant morphological changes in the lymphatic vessels of P5 ear dermis of ZEB1^{iECKO} mice were found when knockdown was induced in comparison to the Control

Figure 5.3.3.2 The number of filopodia on sprouting versus non-sprouting lymphatic vessels did not differ between Control and ZEB1^{iECKO} mice

Figure 5.3.4.1 No change in the lymphatic morphology of the dermal ear lymphatics of male and female Control and ZEB1^{iECKO} adult mice

Figure 5.3.4.2 ZEB1^{iECKO} display altered lymphatic networking in comparison to the Control

Figure 6.3.1 Loss of endothelial ZEB1 had no effect on blood flow recovery after successful induction of ischaemia in the hindlimb

Figure 6.3.1.1 ZEB1^{IECKO} mice display increased lymphatic remodeling in contralateral and ipsilateral leg muscles following hindlimb ischaemia surgery

Figure 6.3.2.1 ZEB1^{IECKO} mice have altered lymphatic morphology in skeletal muscle of the gastrocnemius

Figure 6.3.3.1 Lymphatic vessels of the gastrocnemius are LYVE1 and CD45 positive

Figure 6.3.4.1 A potential relationship between ZEB1 and CD45 in HDLECs

Figure 6.3.4.2 Interaction plot predicting effect of ZEB1 knockdown on PTPRC (CD45) protein expression in LECs

Figure 6.3.4.3 Feature plots representing expression profiles of lymphatic endothelial cells in lung fibrotic tissue

Figure 7.4 A proposed mechanism by which loss of ZEB1 leads to increased lymphatic density

Chapter 1. Introduction

1.1 The Lymphatic System

The lymphatic system comprises a network of vessels, organs and tissues which work in tandem to move a transparent liquid called lymph back into the bloodstream. As blood flows around the body, around 20 litres of plasma leak out of pores in the capillaries into the extracellular space, delivering nutrients and oxygen to the surrounding tissues. As these cells respire, they produce waste products which can for the most part (90%) return to the bloodstream. The remaining fluid (10%) must also be returned to circulation, open ended lymphatic capillaries allow this fluid (now termed lymph) to move through the lymphatic network (Tammela and Alitalo, 2010). Lymph moves through the lymphatic circulation through large vessels called collecting vessels and lymph nodes until it reaches one of two major ducts depending on where the fluid originates. Lymph from the left side of the body, abdomen and lower limb goes through the thoracic duct, this runs alongside the aorta and connects with left subclavian vein. Lymph from the upper right arm, thorax and head is returned to the right subclavian vein via right lymphatic duct. The lymph nodes located along the collecting vessels act as a sieve, to cleanse the lymph before it re-enters the blood circulation (Tammela and Alitalo, 2010). Lymph nodes are also a store of lymphocytes and immune cells, playing a role in adaptive and innate immunity (Bujoreanu and Gupta, 2023). Tissues which are exposed to foreign antigens frequently are rich in lymphatic vessels, as immune cells use the vessels as a conduit to execute the immune response (Tammela and Alitalo, 2010). The lymphatic vessels in the small intestine are called lacteals, located in intestinal villi, with collecting vessels located in the mesentery. These lacteals play a role in the absorption of dietary lipids in the form of chylomicrons (Cifarelli and Eichmann, 2019). Lymphatic vessels also have a role in wound healing. Upon injury to tissue, the blood and lymphatic vessels are also damaged, leaving lymph fluid in the tissue, creating oedema. This oedema triggers an inflammatory response. In normal wound healing lymphatic vessels grow (lymphangiogenesis) along with new blood vessels (angiogenesis), this is important, as new blood vessels are leaky, preventing

excessive swelling and clearing the inflammatory response (Renò and Sabbatini, 2023).

1.1.1 Dysfunctional lymphatics

Impaired wound healing can be a result of lymphatic insufficiency. For example, in diabetes, the inflammatory phase is impaired and there is a decreased infiltration of immune cells, this means that the lymphatic vessels are not stimulated to grow, resulting in prolonged oedema (Renò and Sabbatini, 2023). Another example of dysfunctional lymphatics is in Crohn's disease, this condition is a type of inflammatory bowel disease, pathologically linked to a dysfunctional lymphatic system. The recurrent inflammation present results in the development of inflammatory granulomas (a group of macrophages) which eventually block the open-ended lymphatics in the villi (McNamee and Rivera-Nieves, 2017). Induction of lymphangiogenesis has been shown to therapeutically improve gut inflammation in mouse models of inflammatory bowel disease (D'Alessio et al., 2014). In Alzheimer's disease, damage to the meningeal lymphatics promotes amyloid β deposition, increasing accumulation of the amyloid plaques common to the pathology of the disease. This presents a therapeutic avenue of interest whereby recovery or protection of function of the meningeal lymphatics could slow or clear the amyloid β plaque formation, therefore slowing cognitive decline in these patients (Da Mesquita et al., 2018). Lymphoedema is an incurable disease caused by malfunction or damage to the lymphatic vessels. This can be a result of a genetic defect, but more often a consequence of cancer surgery - including one in five people with breast cancer (Ren et al., 2022). This is due to the surgery involved in removing the tumour or biopsied lymph node, which can affect the lymphatic drainage in the affected area. This results in a build-up of lymph, leaving the patient with permanent swelling. This is often in the upper limbs, causing pain and has severe psychological impact on many patients (Al-Niaimi and Cox, 2009). Patients with lymphoedema are also increasingly vulnerable to cellulitis, a skin infection resulting in inflammation. This is due to the accumulation of protein-rich lymph at the lymphoedema site providing a viable growth site for bacteria, which can then not be cleared due to

impaired lymphatic function (Al-Niaimi and Cox, 2009). This results in an impaired immune response and can worsen the swelling at the site of lymphoedema. Currently, treatment focusses on management, such as the use of compression bandages and massages which encourage manual lymphatic drainage (Al-Niaimi and Cox, 2009). Liposuction, not available on the NHS, is currently the only long-term solution, although bioengineered lymphatic grafts are emerging as a potential tool to revascularise the affected area (Kanapathy et al., 2014). Lymphatics have also been implicated in cancer progression. Like blood vessels which undergo tumour angiogenesis, lymphatic vessels are stimulated to remodel in the tumour microenvironment, this remodelling can be in the form of enlargement of existing vessels, as well as the formation of new vessels (Stacker et al., 2014). Lymphangiogenic stimuli is released from the tumour cells and immune cells surrounding the primary tumour, this results in growth of vessels towards the tumour, which facilitates the metastasis of tumour cells to distant organs (Stacker et al., 2014). Restricting and controlling the remodelling of lymphatic vessels in this disease would be beneficial in this case, to restrict the spread of tumour cells to secondary locations.

The lymphatic vasculature has received substantially less attention due to limits in knowledge, elusive morphology, and lack of visibility. However new research suggests that dysfunctional lymphatics are seen in the aetiology of a variety disease pathologies. Therefore, amelioration and replacement of defective or damaged lymphatics should be a bigger focus of upcoming research efforts. This could be by preserving the lymphatic function or by the therapeutic targeting of lymphangiogenic mechanisms.

1.2 Transcription factor control of lymphatic quiescence and maturation of lymphatic neovessels in development and physiology

1.2.1 Lymphatic development

The lymphatic vascular system comprises a hierarchical system of lymphatic capillaries, that drain into higher calibre collecting vessels that return protein rich lymph (generated from interstitial fluid) and trafficking cells (e.g., lymphocytes and myeloid) back into the venous circulation. As the lymphatic system evolved it allowed higher eukaryotes to have a regulated fluid balance system. Lymphatic systems can be found in reptiles, amphibians, birds, and mammals (Adams and Alitalo, 2007). Extravasated water, solutes and cells are forced out the vascular system at higher pressure sites, resulting in fluid leakage from the permeable capillaries into the interstitium. The lymphatic system resorbs this fluid. Insufficient fluid resorption, resulting in fluid accumulation in tissue results in pathological swelling (oedema) (Dagenais et al., 2004). The interstitial fluid enters the lymphatic vessel through modified intracellular junctions (Yao et al., 2012) and is pumped through capillaries to valve containing collecting vessels (Figure 1.2.2.1 (Escobedo and Oliver, 2017)). This occurs via smooth muscle cell mediated coordinated contractions with lymph returned to the vascular network through lymphovenous valves. Lymphatic valves, (and lymphovenous valves) have been identified as containing their own subtype of LECs, a transcriptionally unique signature identified by Takeda et al., (2019) by single-cell RNA sequencing (Takeda et al., 2019).

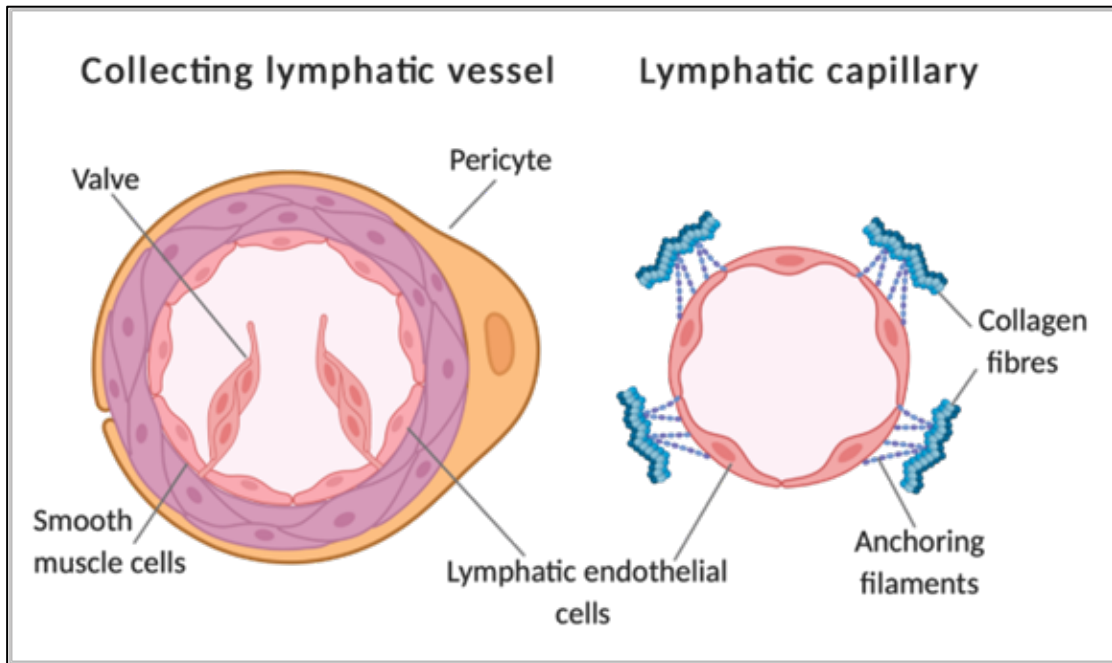


Figure 1.2.1.1. Comparison of a lymphatic collecting vessel and a lymphatic capillary.

Further to lumen calibre differences, additional features of collecting vessels include pericyte coverage, a layer of smooth muscle cells and the presence of valves (made up of LECs) to prevent backflow. Capillaries have discontinuous junctions between endothelial cells, these act as sites of leukocyte entry and increase the permeability of the vessel. Additionally, capillaries are connected to the extracellular matrix by anchoring filaments, these become taut in places of swelling, opening the lumen to allow drainage of tissue fluid. Adapted from Tammela & Alitalo, 2010. Made with Biorender.com.

1.2.2 Lymphangiogenic mechanisms

Lymphangiogenesis is the growth of lymphatic vessels, which occurs primarily from sprouting lymphatic vessels that arise from embryonic vessels during development, but also occurs in adults during wound healing, inflammation, primary and metastatic tumour growth (Ducoli and Detmar, 2021). Each of these conditions results in a significantly altered microenvironment which results in increased inflammation and fluid accumulation which stimulate lymphatic remodelling (Mazzone and Bergers, 2019; Oliver et al., 2020). Blood vessel growth (angiogenesis), largely grow by the formation and extension of filipodia-rich tip cells and the lateral inhibition of neighbouring endothelial cells (ECs) that generate heterogeneity amongst the endothelium and results in differing phenotypes such a stalk, phalanx, and transition ECs (Goveia et al., 2020). Together these form a growing endothelial sprout that will anastomose with nearby sprouts to form a new vessel (Cruys et al.,

2016). Although not currently characterised to the same level of resolution, lymphangiogenic vessels also display some degree of tip/stalk selection (Benest et al., 2008; Xu et al., 2010; Yuan et al., 2002) but it should be noted that lymphangiogenic features (including filopodia extension and proliferation) do appear in canonically non-tip cell or sprout like locations (Baluk et al., 2009; Benest et al., 2008). The lumenised neovessel will undergo further phenotypic switches; remodelling of the basement membrane, formation of endothelial cell junctions and a metabolic shift away from glycolysis and initiate a state of quiescence (De Bock, Georgiadou, and Carmeliet, 2013; Wilhelm et al., 2016). During endothelial cell quiescence, the balance of activating to destabilising factors is in balance resulting in a stable and functional vasculature (Li et al., 2019).

Endothelial phenotypic switching (from quiescence to alternative states) underpins both lymphangiogenesis and angiogenesis; both processes require migration, proliferation, and the metabolic remodelling of a quiescent endothelium (Kalucka et al., 2018). The process of angiogenesis, which has drawn more research interest thus far compared to lymphangiogenesis, can be used as a conceptual model, allowing parallels to be drawn between the processes. From the initial blood islands formed of progenitor cells, a plexus of vascular vessels is formed (Figure 1.2.2.1), these progenitors receive frequent remodelling until the primitive embryonic vasculature is recognisable (De Val and Black, 2009). This is not directly analogous to the entire lymphatic system, but local expansion of local lymphatics in mesentery (Benest et al., 2008), dermal tissue (Braverman and Yen, 1974) and cardiac tissue heart might suggest some analogy (Stone and Stainier, 2019). The specific differentiation mechanisms are excellently described here (Stone et al., 2021).

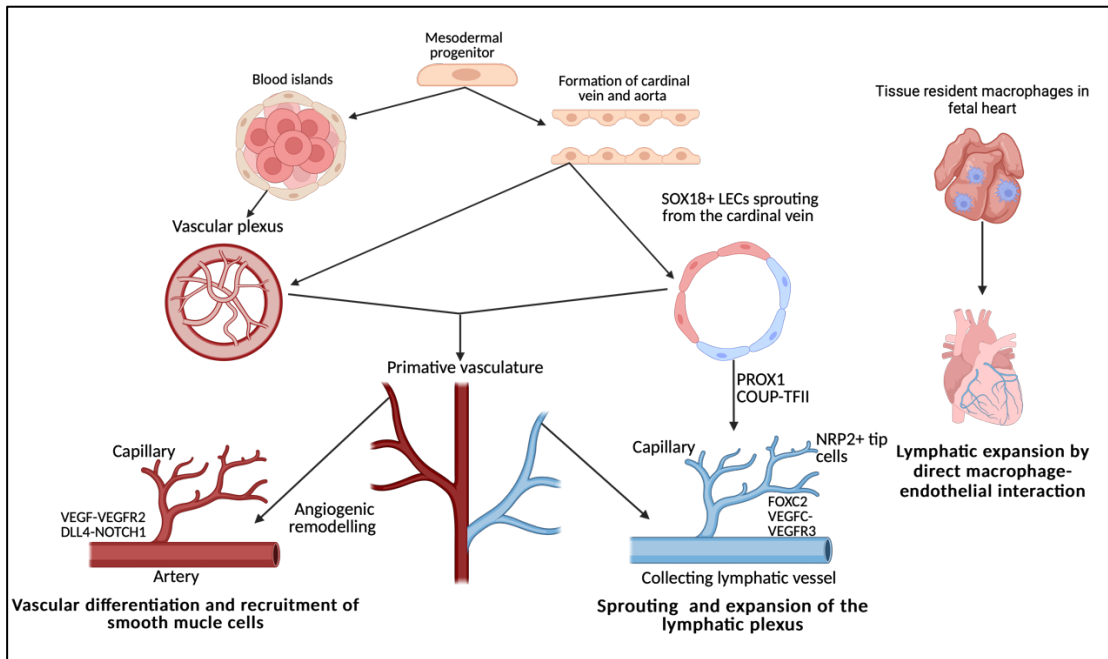


Figure 1.2.2.1. Development, differentiation and separation of the blood and lymphatic networks. Both networks originate from progenitors in the mesodermal layer of the embryo. From the primitive vascular plexus, transcription factors activate the innate genetic program, resulting in extensive remodelling cascades throughout embryogenesis, forming two distinct networks of vessels. In the heart, the lymphatic plexus is remodelled and guided by tissue-resident macrophages through direct interaction between the LECs and the macrophages. Adapted from De Val & Black, 2009 and Adams & Alitalo, 2007. Created using BioRender.com.

1.2.3 Endothelial quiescence as a physiologically active, but not activated state

Endothelial cells which line blood vessels (blood ECs) and lymphatic vessels (lymphatic ECs) metabolise more glycolytically than most cells, therefore consuming very little oxygen in a quiescent, stationary state (Wilhelm et al., 2016). Quiescent ECs still require energy to generate new biomass, protect against oxidative stress and are still involved in homeostatic processes (De Bock, Georgiadou, and Carmeliet, 2013). Oxidative phosphorylation in comparison requires more oxygen, generates reactive oxidative species, and cannot take place in hypoxic regions. Furthermore, as ECs grow they increase their glycolysis which contributes to their proliferation and survival in hypoxic tissue (De Bock, Georgiadou, and Carmeliet, 2013). In order for migration to take place, the cytoskeleton must be remodelled, an energy-demanding process forcing the switch from a low energy state of quiescence to a more active metabolising, migrating state (De Smet et al., 2009). Transcriptionally, these high-energy demanding cells, display a different transcriptional profile than quiescent ECs

(Kalucka et al., 2018). This is also true of the lymphatic endothelium (Wong et al., 2017; Yu et al., 2018).

1.2.4 Transcription factor regulation of gene expression

Transcription factors (TFs) are small proteins which act to increase or decrease the expression of genes by binding to 6-8 base pair target sequences of DNA. TFs contain a DNA binding domain, from which they are classified into families according to its structure, such as SOX proteins. TFs can also be grouped by their three-dimensional structures such as zinc finger proteins. Target segments can be located in the promoter or enhancer region of the DNA. Transcription begins when a TF binds to its sequence in the promoter, beginning a cascade of interactions between multiple proteins and other promoter and enhancer sequences. The result is a transcriptional complex at the promoter, which facilitates initiation of transcription by binding RNA polymerase.

The presence of TFs does not always ensure initiation of transcription. TFs are restricted by their ability to reach their DNA sequences by the conformation of the chromatin. Chromatin is made up of DNA and associated histone proteins, the state of which can restrict gene expression by limiting access of TFs and RNA polymerase to the DNA. The chromatin structure is dynamic, post-transcriptional modification of histones regulate chromatin packaging, making it more or less available to transcriptional activators and repressors. Histone modifications can also recruit enzymes which require ATP to reposition nucleosomes. Histone acetylation requires acetyl coA as a co-factor and involves the transfer of an acetyl group to a lysine side chain. This modification neutralises the positive charge of lysine and weakens the interactions between histones and the DNA. Acetylation sites are enriched in the enhancer and promoter elements, this is thought to facilitate transcription factor access (Bannister and Kouzarides, 2011). Histone phosphorylation involves the transfer of a phosphate from ATP to a hydroxyl group on serines, threonines and tyrosines, this adds a negative charge to the histone, influencing the chromatin structure (Bannister and Kouzarides, 2011; Wang et al., 2008). Methylation does not

change the charge of the histone protein but has been used as a marker of the transcriptional start site (H3K4me3) and of active transcriptional enhancers (H3K4me1). As well as modifying chromatin structure, histone modifications can regulate the binding of effector molecules, for example NuRD is a transcriptional repressor, the H3K4me3 modification prevents the NuRD complex binding to the histone N-terminal tail (Zegerman et al., 2002).

1.2.5 Lymphatic vessels lose quiescence as they grow

To establish the lymphatic network, an innate genetic program is activated by transcription factors in early progenitor cells. In establishing the network, LECs must be able to grow and sprout from existing vessels, this requires the cell to be able to respond to growth signals from the environment, such as vascular endothelial growth factor (VEGF)-C which is recognised by vascular endothelial growth factor receptor-2 (VEGFR2) and 3 (VEGFR3) which are both expressed by differentiated LECs (Deng et al., 2015; Tammela and Alitalo, 2010). VEGF-C can induce translocation of VEGFR2 which results in heterodimers of VEGFR2 and R3 on the cell membrane (Xu et al., 2010; Kaipainen et al., 1995), VEGFR3 can also homodimerize to recognise VEGF-C stimuli (Joukov et al., 1997; Kukk et al., 1996). This activation results in the extracellular signal-regulated kinases (ERK) and protein kinase B (AKT) signalling cascades, which are essential for migration of the LECs (Deng et al., 2015, 2013). In adults, lymphatic growth is often pathological lymphangiogenesis, and normally activated in response to injury or disease (Adams and Alitalo, 2007). For example, during inflammation, VEGF-C is produced by macrophages, encouraging the growth of LECs nearby to sprout toward the injury as well as inducing hypertrophy of the collecting lymphatic vessels (Cursiefen et al., 2004; Maruyama et al., 2005). This facilitates the immune response by mobilising dendritic cells and increasing capacity of vessel to carry lymphatic fluid (Mazzone and Bergers, 2019), and therefore contributes to restoration of tissue homeostasis and resolution of inflammation. When the lymphatic network is established, LECs are quiescent (Sabine et al., 2015); however, upon receiving further cytokine signalling, are stimulated to re-enter the cell cycle (Geng et al., 2020). During a shift back to the quiescent phenotype, the

non-draining lymphatic sprouts will have generated a lumenised vessel resulting in lymph fluid imparting shear stresses upon the lymphatic endothelium (Geng et al., 2020). Integration of mechanotransductive signals with transcriptional regulation is a fundamental mechanism for restoring the lymphatic endothelium to a non-activated, and quiescent phenotype.

1.2.6 Heterogeneity: How different are each of the endothelial cells within a lymphatic vessel?

As we begin to explore underlying mechanisms responsible for heterogeneity within the cells in the lymphatics, it is critical to note there is heterogeneity between different classifications of lymphatic vessel, and terms such as capillaries, collecting, conduit etc., are used to classify the vessels into the 'lymphatic tree hierarchy'. Capillaries and collecting vessels significantly differ in morphology and function (Figure 1.2.2.1). The transcriptional expression profile of these different types of vessels could offer early glimpses into understanding quiescent versus activated phenotypes, as capillaries are the likely site of early phenotyping switching in response to growth stimuli. Any heterogeneity could unveil mechanisms enabling dynamic movement along a spectrum of activated and quiescent phenotypes. Whereas, collecting vessels are mature, established vessels and are likely to be at the quiescent side of the phenotype spectrum. This is a developing area of interest to many, results from a recent publication by Hernández Vásquez et al., (2021) compared the expression profiles of dermal capillary LECs to collecting vessel LECs in adult mice. This work identified several noteworthy genes of interest, including FOXP2 (discussed later) as a major regulator of collecting vessels morphology, whereas LYVE1, MAF and CXCL12 were all significantly enriched in lymphatic capillaries, consistent with a more activated/sprouting phenotype (Hernández Vásquez et al., 2021; Rondon-Galeano et al., 2020). Furthermore, heterogeneity is apparent between lymphatic vessels from different tissue bed, but less is known about the heterogeneity within each specific vessel bed. Most capillary LECs used in experiments are dermal (commonly isolated from foreskin or breast reduction tissue), however delving deeper into different organs we see a difference in

expression of certain transcription factors (Wong et al., 2018). Interestingly, intestinal lymphatics known as lacteals, are continuously regenerated throughout adulthood, which aid the lipid absorption in the intestinal villi (Nurmi et al., 2015; Wong et al., 2018). Facilitating this regeneration was high delta-like ligand 4 (DLL4) expression in these tip cells (Bernier-Latmani et al., 2015). DLL4 is a major driver of blood EC heterogeneity during angiogenesis (Hellström et al., 2007; Suchting et al., 2007) and therefore it is probable that similar mechanisms could underpin lymphatic EC heterogeneity too. The presence of valves, made up of specialised LECs, within collecting vessels (Figure 1.2.2.1) are also a source of heterogeneity amongst the LECs within the vessel. Single-cell RNA sequencing (scRNA-Seq) has enabled researchers to explore cellular heterogeneity at the transcriptomic levels which allows different cellular phenotypes to be identified. Human lymph nodes were disaggregated and scRNA-Seq performed (Takeda et al., 2019) on the LEC populations. A similar approach to explore how quiescence versus activation is manifested in the LEC populations will be an exciting avenue to explore in future work. This is only recently becoming clear from blood endothelial work, but excellent progress has started to explore how collecting lymphatics differ from lymphatic capillaries (Hernández Vásquez et al., 2021) and valve LECs versus non valve LECs (Takeda et al., 2019); offering an insight into intralymphatic endothelium heterogeneity. Thus, heterogeneity between inter-vessel LECs and inter-organ must be considered before truly understanding intra-vessel LEC heterogeneity.

1.2.7. Prospero homeobox 1 (PROX1) interacts with SOX18 and is key for lymphatic specification

The process of LEC differentiation, vessel formation and overall maintenance, requires energy. Therefore, the metabolism of the LECs which form the lymphatic endothelium is a key interest in delineating the mechanisms of developmental and pathological lymphangiogenesis. Metabolic activity in the cell is adapted to its phenotype. ECs can switch between quiescent and proliferating states, and sufficient, differing energy requirements must be met to maintain this state. As the lymph is enriched with nutrients, the LECs must be able to tolerate a high glucose

concentration (which is common to all ECs, whether blood or lymphatic), and a relatively low oxygen concentration (unlike BECs which are oxygen rich)(Moyon et al., 2001; Schoors et al., 2015; Wong et al., 2017). This results in anaerobic glycolysis as a primary source of ATP (Yu et al., 2018; Jiang et al., 2021), allowing for the generation of energy at sites of filopodia formation. Thus, avoiding the need for transportation of ATP from the mitochondria, which are excluded from the thin protrusions (Lee et al., 2018; X. Li et al., 2019). PROX1 regulated gene expression enhances energy production further by binding the carnitine palmitoyl transferase 1a (CPT1a) promoter, an enzyme which shuttles fatty acids in the mitochondria for oxidation, to increase fatty acid oxidation and acetyl CoA production. Consequently, along with acetylase p300, histones associated with lymphangiogenic genes are acetylated (Figure 1.2.14.1) this makes the promoters more accessible to PROX1 for transcription (Li et al., 2019).

Through cloning of the PROX1 promoter and confirmation by chromatin immunoprecipitation (ChIP), it was shown that PROX1 is directly activated by SOX18 which binds to a 4 kB fragment of DNA in the PROX1 promoter, through cooperation of SoxA and B sites (François et al., 2008). PROX1 expression is maintained throughout the vasculature, there are elements within this fragment that regulate the expression of PROX1 in the LECs after SOX18 expression has diminished (François et al., 2008). Examining the differentially expressed genes between BECs and LECs, PROX1 emerged as the major regulator of LEC identity. Out of the 300 differentially expressed genes, PROX1 directly regulated 15 (Petrova, 2002). In addition, when overexpressed in BECs, PROX1 can suppress expression of BEC specific genes such as STAT6 and integrin $\alpha 5$ (Petrova, 2002). The exact signal cascades involved in PROX1 induced LEC differentiation are yet to be fully characterised, but by using PROX1 overexpression and knockdown allowed identification of PROX1 effector proteins to be identified. Mishima et al., (2007) found forced PROX1 overexpression in human umbilical vein endothelial cells (HUVECs) and LECs induced a morphological change, in which a sheet formation was inhibited and altered cell morphology was reported (Mishima et al., 2007). A crucial component of this cascade is integrin $\alpha 9$, which is

transcriptionally regulated by PROX1, and can reverse the morphological changes induced by PROX1 by blocking its activity. LEC motility was increased with PROX1 overexpression, specifically chemotaxis toward VEGF-C, demonstrating LEC identity, migration and shift towards a more plastic and activated phenotype is masterminded by PROX1 (Mishima et al., 2007). This is further reinforced with the finding that PROX1 contributes to transcriptional control of CPT1A expression, which in turns shifts lymphangiogenic metabolism away from oxidative phosphorylation (Yoshimatsu et al., 2011) and towards glycolysis and fatty acid metabolism (Wong et al., 2017).

PROX1 is essential for establishing and maintain lymphatic identity, however over time, its expression is decreased (Ma and Oliver, 2017). Cho et al., (2019) demonstrated YAP and TAZ appear to inhibit PROX1 activity, with YAP/TAZ activity decreased by Hippo pathway signalling. In order for initial LEC budding from the cardinal vein (CV) in mouse embryos, this Hippo signalling is increased, lowering YAP/TAZ and allowing establishment of the early lymphatic vasculature (Cho et al., 2019). VEGF-C stimulation of human dermal LECs induced localisation of YAP in the cytoplasmic compartment along with an observed increase of VEGFR3 phosphorylation. Consistently, there was increased phosphorylation of LATS1/2 and YAP phosphorylation (key mediators of the Hippo pathway), eventually leading to decreased expression of YAP target genes and PROX1 expression. Pinpointing the role of VEGF-C signalling on influencing the expression of lymphangiogenesis dependent transcription factors (Cha et al., 2020).

SOX18 (SRY (Sex Determining Region Y) box 18) is a member of the SRY-related high mobility group (domain family of developmental transcription factors). SOX18 is the first lymphatic marker to be expressed during mouse embryogenesis, prior to PROX1 (François et al., 2008). Detected as early as 9 days post conception, SOX18 positive cells were reported in the CV, and when at later stages the same population of cells expressed PROX1 and CD31, François et al., suggested these cells were precursors to the lymphatic vasculature (François et al., 2008). SOX18 expression is not maintained

through development, as by 14 days post conception, expression had subsided, suggesting that SOX18 acts as a molecular switch to activate differentiation of the ECs to a lymphatic phenotype (François et al., 2008). This switch is induced by ERK signalling, which in turn is regulated by RAF1, a mitogen activated 3 kinase (Deng et al., 2013). Interestingly a study by Deng et al., (2013) which showed excessive RAF1 activation induced uncontrolled blood to lymphatic vessel phenotype (lymphangiectasia), revealing a crucial role of ERK signalling in this early developmental stage (Deng et al., 2013). Vascular cell adhesion molecule 1 (VCAM1) shares a spatiotemporal pattern of expression as SOX18, sparking a suggestion of crosstalk within the pathways controlling the LEC phenotype. VCAM1 is expressed on the surface of activated endothelia, Hosking et al., (2004) discovered three SOX18 binding sites in the VCAM1 gene, and specifically the SoxB site that is essential for transactivation of VCAM1 expression (Hosking et al., 2004) suggesting that careful control of SOX18 expression determines aspects of lymphatic quiescence as VCAM1 is a key mediator of an activated phenotype.

Another SOX factor, SOX7, has also been implicated in controlling the number of lymphatic progenitors from the CV. However, it is loss of SOX7, which was found to induce a lymphatic phenotype (Chiang et al., 2023). In the blood endothelium, expression of SOX7 represses VEGF-C transcription, therefore repressing lymphatic morphogenesis (Chiang et al., 2023). This enables fine tuning of lymphatic growth and patterning, as loss of function of SOX7 at this crucial early stage of specification, resulted in excess LEC progenitors in the dermis, similar to the phenotype seen with a loss of VEGF-C (Chiang et al., 2023). Genome-wide analysis of SOX7 revealed binding to the putative repressive regulatory regions upstream of the VEGF-C transcription start sites (Chiang et al., 2023). This presents SOX7 as a key transcription factor in fine-tuning of the number and spatial distribution of LEC progenitors, essential for the correct migration and assembly of the lymphatic network.

1.2.8 Chicken ovalbumin promoter transcription factor II (CouP-TFII) interacts with PROX1 during lymphatic proliferation

CouP-TFII is an orphan member of the steroid/thyroid hormone superfamily. Expression of CouP-TFII has been reported by Yamazaki et al., to be essential in segregating lymphatic vasculature from the primitive veins. A physical interaction between PROX1 and CouP-TFII was discovered by ChIP, this was found to centre around the cyclin E1 promoter, an important molecule involved in S phase of the cell cycle (Yamazaki et al., 2009; Petrova, 2002). Excess CouP-TFII was found to inhibit the proliferation inducing ability of PROX1. CouP-TFII also acts independently of PROX1, required after the initial sac formation to maintain the lymphatic identity (Frye et al., 2018). As LECs are identified by expression of common markers, loss of this expression can be used as evidence for a change in behaviour of the cell. For example, Lin et al., showed that a CouP-TFII endothelial specific deletion caused a decrease in the expression of classic lymphatic markers such as LYVE1, PROX1, NRP2 and VEGFR3 (Lin et al., 2010). VEGFR3 and NRP2 are both key regulators of lymphatic quiescence and modify VEGF-C signalling in LECs (Bouvrée et al., 2012; Xu et al., 2010; Yuan et al., 2002) which is the major lymphangiogenic signalling pathway, therefore initial lymphangiogenic remodelling requires a shift from quiescence. Interestingly, these ECs ectopically expressed more commonly known BEC markers instead, suggesting CouP-TFII is involved in maintaining the identity of LECs in early vessel formation, prior to full maturation. Specifically, CouP-TFII is a positive regulator of Neuropilin-2 (NRP2) expression, acting through the SP-1 binding site located in the promotor (NGFIA) of NRP2 (Lin et al., 2010). NRP2 has previously been identified as a co-receptor for VEGFR3 (Yuan et al., 2002). Disruption of NRP2 selectively disturbs sprouting of LECs in response to VEGF-C, suggesting NRP2 drives the tip cell phenotype, as stalk cell morphology was unchanged. Tip cells lead new sprouting vessels; thus, a deficiency of tip cells results in less growth of the lymphatic network (Xu et al., 2010).

1.2.9 GATA2 regulates VEGFR3 expression and contributes to lymphatic remodelling

GATA2 is a member of the zinc finger transcription factor family. Work by Frye et al., demonstrated that GATA2 was upregulated in migrating LECs from the CV, analysis revealed that there is a change in matrix stiffness as the ECs migrate into the surrounding parenchyma activating GATA2 expression (Frye et al., 2018). From the CV, LECs begin to form primitive vessels which make up vessel beds (10.5 days post conception), beyond this, the increase in interstitial fluid pressure results in a stretch response, resulting in enrichment of genes involved in cell matrix adhesion, junctional organisation, migration, and vascular development. A specific gene of interest is VEGFR3, which acts as a receptor for VEGF-C, GATA2 binds directly to intron 1 of VEGFR3 to regulate its expression, Coup-TFII also acts independently of PROX1 (Frye et al., 2018). This is important as VEGF-C is crucial for sprouting and migration of LECs. Loss of GATA2 substantially downregulated VEGFR3, and LECs failed to respond to VEGF-C. In normal development, the stretch-activated phosphorylation of VEGFR3 initiates a signalling cascade which activates proliferation and vessel growth. The interstitial flow within the premature vessels is crucial in inducing mechanical forces which further shape the vasculature, for example, through inhibition of Neurogenic Locus Notch homologue protein 1 (NOTCH1) sprouting is promoted and Krüppel-Like Factor 2/4 (KLF2/4) induces proliferation (Frye et al., 2018). By day 15 post conception, the flow at branch points induces a GATA2 and FOXC2-dependent quiescence, as LECs are correctly targeted to important points where the lymphatic vessels and blood vessels connect (Frye et al., 2018). Matrix metalloproteinase signalling was also increased by the change in matrix stiffness as a result of migration, this is crucial for lymphangiogenesis as the surrounding extracellular matrix must be remodelled to facilitate sprouting of the vessels (Detry et al., 2012; Frye et al., 2018).

Collecting lymphatics are distinguishable from capillaries by size, coverage by smooth muscle cells and pericytes, and the presence of valves (Figure 1.2.2.1). These valves are not only present inside the lymphatic vessels but also crucially at the junctions between the lymphatic vessel and the blood vessel. These valves are

formed by intercalations of LECs with a type of vascular endothelial cell which is PROX1 and CD31 positive (Srinivasan & Oliver, 2011). Lympho-venous valves require PROX1 and Coup TF-II complex formation to regulate the dosage of PROX1, deletion of even one copy of PROX1 is enough to induce abnormal connections between the two systems, as differentiation into valve cells is compromised (Srinivasan & Oliver, 2011). GATA2 has also been implicated in valve morphogenesis, as a mechanosensory transcription factor, it recognises the oscillatory shear stress at vessel branch points. By using GATA2 deletions, we can infer importance as the resulting embryos lacked these valves and presented with blood inside the lymphatic vessels, which is a characteristic of improper formation of valves at the lymphovascular junctions (Frye et al., 2018). GATA2 mutations are responsible for Emberger syndrome, carriers of this mutation are predisposed to leukaemia and lymphoedema, this is due to the crucial role of GATA2 in the differentiation of LECs specifically in the lymphovenous valves (Geng et al., 2016).

1.2.10 FOXC2 plays a key role in lymphatic maturation

PROX1 associates with regulatory elements of Forkhead box C2 (FOXC2) (Cha et al., 2016) FOXC2 has roles in angiogenesis, is essential in lymphatic vasculature and is a known marker of the lymphatic valve (Kume, 2008; Norrmén et al., 2009; Takeda et al., 2019; Xiang et al., 2020). In mice, FOXC2 is expressed at 8.5 days post conception in the normal developing heart, blood vessels and limbs, expression in the ECs is recorded between 9.5-10.5 days post conception, along with PROX1 and LYVE1 (Dagenais et al., 2004). This subset of ECs are involved in migration and sprouting to form immature mesh-like networks of vessels, which are organised in a cranial to caudal manner, these separate networks fuse creating major lymphatic pathways (Dagenais et al., 2004; Norrmén et al., 2009). Part of this process includes a dramatic remodelling of the mesenteric plexus; this is where the differentiation of collecting vessels and capillaries becomes apparent. FOXC2 expression is thought to be induced by oscillatory shear stress (Figure 1.2.3.1), as the highest FOXC2 levels were found in ECs which form part of the valves, which are exposed to the most disturbed flow (Sabine et al., 2015). Oscillatory shear stress has significant influence of the gene

expression patterns of LECs, controlling over 800 genes, however when receiving a FOXC2 inducible knockout, these cells responded abnormally to shear stress. Oscillatory shear stress normally induces growth arrest to protect the vessel structure by decreasing cell proliferation. However knockdown FOXC2 *in vitro* generated a TAZ dependent proliferation and increased cell death, suggesting FOXC2 has an important role in maintain quiescence in areas of high shear stress (Sabine et al., 2015). As maturation progresses, FOXC2 expression decreases in the areas not under construction, such as the intraluminal segments between valves (17.5 days post conception) (Norrmen et al., 2009). Even at maturity, high FOXC2 expression is maintained in the valves, suggesting valve LECs are molecularly distinct from neighbouring cells in the trunk of the collecting vessel (Norrmen et al., 2009). It would be interesting to compare the LECs in the collecting lymphatic vessels which are quiescent, to those in the capillaries which are likely heterogenous as they are reactive to lymphangiogenic stimuli. There is also growing evidence that modulating this heterogeneity is the level of VEGFR3 expression (Zhang et al., 2018).

It is suggested that FOXC2 could cooperate with VEGFR3 to specify the phenotype of the lymphatic vessel, as FOXC2 is expressed in valves, required in the larger collecting vessels, compared to smaller capillaries which lack valves, smooth muscle coverage and full coverage by a basal lamina (Alitalo et al., 2005; Oliver and Srinivasan, 2008). VEGFR3 is not downregulated in FOXC2^{-/-} mice, but in VEGFR3^{-/-} embryos, mRNA for FOXC2 is decreased, confirming that VEGFR3 is upstream of FOXC2 and may have a role in its expression (Petrova et al., 2004). FOXC2 regulates the expression of VEGF-C which has been established as an essential chemotrophic factor and an activating ligand for VEGFR3 (Oliver and Srinivasan, 2008), which will permit an autocrine loop regulating the LECs own quiescence.

The nuclear factor of activated T cells (NFATc1 specifically) is a calcium-sensitive transcription factor sharing expression patterns with FOXC2 and regulation by PROX1 (Norrmen et al., 2009). NFATc1 needs to localise into the nucleus where it interacts with other nuclear and transcription factors (such as AP1, nuclear factor κB, Foxp3,

GATA) to form complexes on DNA. VEGF-C acting on VEGFR2 induces translocation of NFATc1 to the nucleus, this receptor is expressed collecting lymphatics and valves, and is thought to promote an increase in vessel size. The importance of this transcription factor is elucidated with experimental deletion of NFAT signalling, whereby lymphatic remodelling and maturation is defective, sharing a similar phenotype to FOXC2^{-/-} mice. The expression of lymphatic capillary markers, lack of valves and impaired sprouting seen in these NFAT^{-/-} mice summarises to a hyperplastic phenotype, which is further exacerbated by loss of a FOXC2 allele. Investigating the link between FOXC2 and NFATc1 further, Norrmén et al., (2009) established that the genes are expressed independently but are found to co-regulate transcription of downstream genes, as ChIP analysis of primary LECs revealed NFAT-binding sites in close proximity of FOXC2 sites (Norrmén et al., 2009). Thus, both NFATc1 and FOXC2 share a role in establishing the collecting lymphatic phenotype.

1.2.11 Control of PROX1 chromatin accessibility regulates downstream gene expression

A novel evolutionary conserved regulatory element was recently discovered, important for the regulation of PROX1, and bound by GATA2, FOXC2, NFATc1 and PROX1 itself (Kazenwadel et al., 2023). This element is an 11 kb transcriptional enhancer, crucial for the temporal and spatial control of PROX1 expression, particularly in the endothelial cells comprising the lymphatic and lymphovenous valves (Kazenwadel et al., 2023). The activity of this enhancer is abolished by the gene edited removal of just five nucleotides within the GATA2 binding site, suggesting GATA2 is essential in this enhancer element's activation (Kazenwadel et al., 2023). GATA2 recruitment to the promoter could act to facilitate a conformational change in chromatin structure, facilitating the binding of FOXC2 and NFATc1 (Norrmén et al., 2009; Kazenwadel et al., 2023). Thus, this PROX1 enhancer element is crucial in the control of lymphatic cell identity through its control of key transcriptional regulators.

Transcriptional co-factors are essential in the activation or repression of transcription, orchestrating gene expression in a cell-specific manner. Zinc Finger MIZ-Type Containing 1 (ZMIZ1) is a known transcriptional co-activator of Notch, p53, Smad3/4 (Li et al., 2006; Lee et al., 2007; Pinnell et al., 2015). A global loss of ZMIZ1 caused embryonic lethality due to vascular defects (Lomelí, 2022). ZMIZ1 is expressed in LECs and has recently been detected as a regulator of PROX1 expression through modifications of chromatin accessibility (Rajan et al., 2023). By using cultured HDLECs, Rajan et al., found that loss of ZMIZ1 altered the gene expression profiles including key developmental genes such as FLT4 (VEGFR3), FOXC2 and PROX1. Using an Assay for Transposase-Accessible Chromatin with high-throughput sequencing (ATAC-Seq), analysis revealed the amount of open chromatin at the promoter regions of PROX1 were significantly less accessible following loss of ZMIZ1 (Rajan et al., 2023). This suggests ZMIZ1 facilitates the chromatin accessibility and therefore gene expression of PROX1. In combination with recent work by Kazenwadel et al., it could be concluded that ZMIZ1 also controls the key lymphatic regulatory genes which bind to the PROX1 enhancer, such as GATA2, FOXC2 and PROX1 itself (Rajan et al., 2023; Kazenwadel et al., 2023).

1.2.12 Shear stress as a primary determinant of quiescence?

Elucidating the FOXC2/NFATc1 pathway further, a newly discovered downstream target, FOXP2, previously implicated in speech development in humans (Co et al., 2020), has been identified as another marker of collecting lymphatics in both mouse and human models (Hernández Vásquez et al., 2021). CHIP sequencing had previously linked FOXC2 and FOXP2 to roles in the lymphatic system (Norrmen et al., 2009), but it only recently this role has been investigated further. The expression of the transcription factor FOXP2 was induced by oscillatory shear stress, acting downstream of FOXC2 to help regulate the collecting lymphatic phenotype and valve development (Hernández Vásquez et al., 2021). The role of oscillatory shear stress is appearing to be a key determinant in examining transcriptional regulation in establishing a functional lymphatic network. But it is not just disturbed, oscillatory shear stress that influences the vessel transcriptional profile, regular laminar stress

present in non-sprouting, mature vessels, acts to maintain quiescence in these cells. LECs at the growing front of sprouting vessels grow via projecting extensions of the cell membrane, these projections are not lumenised, so are not exposed to the circulating lymph, or the fluid dynamics that go with it (Geng et al., 2020). This allows tip cells expressing markers such as DLL4 to enhance VEGF-C signalling and enables lymphatic growth. Meanwhile, stalk cells in these vessels do not express DLL4, Geng et al., (2020) found sphingosine 1-phosphate receptor 1 (S1PR1), a G-protein coupled receptor, antagonises the VEGF-C signalling, enhanced by laminar shear stress independent of S1PR1, allowing the stalk cells to maintain their quiescence. S1PR1 is thought to act by activating Claudin 5, a tight junctional protein, contributing to proper cell-junction formation in mature lymphatic vessels (Geng et al., 2020). Therefore, consolidating the interplay between how shear stress regulates differential transcription factor activity and therefore how this contributes LEC phenotype is one of great promise. Of note, it is well recognised that LECs *in vivo* can grow along 'fluid' channels during tissue regeneration (Boardman and Swartz, 2003). The transcription factor cascades underpinning such events are unknown but would likely reveal novel aspects consolidating the activated migratory and quiescence switching in response to altered fluid dynamics.

LECs are very sensitive to changes in lymphatic flow, functioning in a narrow window of exposure to shear stress (Baeyens et al., 2015). Many pathological conditions such as chronic heart disease (Boehme et al., 2021) and lymphoedema (Scallan et al., 2016) result in chronically elevated lymphatic flow, which can overstimulate the signalling pathways in place to protect the lymphatic endothelium. As described above, through FOXC2, a growth arrest is induced allowing maturation of vessels by repressing the expression of cell-cycle progression genes (Sabine et al., 2015). This allows the cell to adapt to the high stress conditions, limiting damage as cell-cell contacts are reinforced and motility is limited (Sabine et al., 2015). Over time, if this high flow is maintained, the cells face constant interstitial pressure induced-stretch, β 1 integrins on the surface of LECs translate this stretch to VEGFR3 tyrosine

phosphorylation which results in signalling for LEC proliferation (Planas-Paz and Lammert, 2013).

KLF-2 is another mechanosensitive transcription factor, the expression of which is upregulated in both oscillatory and laminar flow (Choi et al., 2017). KLF2 is responsible for the flow-induced expression of VEGF-C (Choi et al., 2017) and disruption of PPAR- γ signalling (Morris et al., 2018). PPAR γ is a part of the nuclear hormone receptor superfamily. In LECs, expression PPAR- γ is decreased in shear stress conditions. In low stress conditions, PPAR γ signalling inhibits expression of NADPH oxidase, increasing bioavailable nitric oxide (NO), an important regulator of vascular tone. LECs exposed to chronic shear stress have increased NADPH expression, increased reactive oxidative species (ROS) - which further scavenge bioavailable NO - disrupting NO homeostasis, this dysfunction is restored with KLF2 knockdown (Morris et al., 2018), isolating responsibility of this transcription factor in this signalling in shear stress conditions.

Hypoxia inducing factor-1 α (HIF-1 α) is a transcription factor commonly associated with inflammatory states and the hypoxic response regulates over 1000 target genes (Semenza, 2013). HIF-1 α has been associated with lymphangiogenesis in malignancy (Schoppmann et al., 2006a, 2006b) but was discovered by Boehme et al., (2021) to have a critical role in turnover of LECs which are chronically exposed to high stress conditions (Boehme et al., 2021). In relation to a pathological model of coronary heart disease, in which there is a chronic increase in pulmonary lymphatic flow, the LECs in the high stress conditions increased HIF-1 α expression despite not experiencing hypoxic conditions (Boehme et al., 2021). This suggests HIF-1 α may be regulated by mechanotransductive forces on the lymphatic endothelium, specifically the ROS from mitochondria experiencing stress, which are central upstream mediators of HIF-1 α . This suggests an interface mechanotransductive signals and quiescence through HIF-1 α involvement (Boehme et al., 2021).

1.2.13 MAFB contributes to branching lymphatic morphogenesis

Recent work by Dieterich et al., (2020) revealed a role of lymphatic V maf musculoaponeurotic fibrosarcoma oncogene homolog (MAFB) in transcriptional regulation of vascular patterning. In LECs, this expression upregulated VEGF-C/R3 signalling via direct binding to MAF recognition elements (MARE) in the promoter and enhancer in the DNA sequence (Dieterich et al., 2020). Transcriptomic analysis indicated MAFB is involved in the early induction of SOX18 expression, thus impacting PROX1 production through this signalling pathway (Dieterich et al., 2015). This work was followed up by Rondon-Galaeno et al., (2020), using a CRISPR/Cas9 mouse model, these mice had a perinatal death associated with cyanosis. Upon investigation, dermal lymphatics in these mice had mild and transient delay in development. However, in the diaphragm, MAFB was necessary for patterning the lymphatics that developed in the mutant mice were broader and covered a larger area of the diaphragm (Rondon-Galeano et al., 2020). Other elements of the signalling cascade linked to MAFB include PROX1, LYVE1 and podoplanin. Global knockout of MAFB induces an hyperbranched phenotype in the developing lymphatic vessels, with decreased overall growth, suggesting MAFB is involved in refining the branching of the lymphatic vessel capillaries, as depletion increased the number of junctions and cord segments (Dieterich et al., 2020). Podoplanin activates platelet aggregation, this separates the primary lymph sac from the CV. Specifically, podoplanin activates c-type lectin receptor 2, which acts on SLP76 to activate syk (a tyrosine kinase) in platelets (Tammela and Alitalo, 2010). Podoplanin is expressed on the membrane of LECs as a glomerular podocyte, promoting adhesion, migration, and tube formation. Pups with podoplanin knockout die at birth from respiratory failure, and displayed defects in lymph patterning and function (Oliver & Srinivasan, 2008). There was an absence in formation of a fluid functional network of lymphatics in these mice, as deeper lymphatics fail to form connections with capillaries at the surface, thus showing defects in migration of LECs and of lumen formation (Oliver & Srinivasan, 2008).

1.2.14 ETS-domain transcription factors

ETS-domain transcription factors are a family of 19 endothelially expressed transcription factors characterized by a highly conserved DNA binding domain and the DNA-binding consensus sequence GGA(A/T) (Hollenhorst et al., 2007). Interestingly, ETS2 and Etv2 were found to be expressed in BECs as well as LECs (Davis et al., 2018; DEJANA et al., 2007; Yoshimatsu et al., 2011). Yoshimatsu et al., (2011) identified the expression of ETS2 and colocalization with PROX1 in nuclei of LECs. Further analysis revealed that ETS2 physically and functionally interact with PROX1. In addition, their work highlights the synergistic enhancement of ETS2 and PROX1 in expression of VEGFR3. Consistent with the effects on expression profile of VEGFR3, ETS2 induces LEC migration towards VEGF-C (Yoshimatsu et al., 2011). In the light of the previous data ETS2 is reported as a pivotal pro-lymphangiogenic factor in collaboration with PROX1 during lymphangiogenesis (Yoshimatsu et al., 2011). Furthermore, another transcription factor of interest, Etv2, has been investigated as a lymphangiogenic initiator directly promoting the expression of VEGFR3 within the posterior CV (Davis et al., 2018). Using *in vitro* differentiated mouse embryonic stem cells, Etv2 ChIPSeq analysis revealed specific Etv2 binding peaks present within VEGFR3 and LYVE1 promoter/enhancer regions (Liu et al., 2015). The VEGFR3 promoter is a likely direct target of Etv2, containing an evolutionarily conserved FOX: ETS domain that is bound by Etv2 and FOXC2 transcription factors (De Val et al., 2008). Further analysis using luciferase reporter studies in zebrafish embryos and ECs suggested Etv2 activates both VEGFR3 and LYVE1 through direct binding to their promoter/enhancer regions, and that the function of these enhancers is conserved among different vertebrates (Davis et al., 2018).

Of the transcription factors regulating endothelial cell physiology, haematopoietically expressed homeobox (HHEX) is composed of a proline-rich domain and a highly conserved homeodomain (Ho et al., 1999). Intriguingly, HHEX was found to be expressed by ECs in both blood and lymphatic vessels from the earliest step of sprouting angiogenesis and lymphangiogenesis from the CV until

adulthood. Further CHIP analysis in blood ECs have revealed putative HHEX binding sites upstream of the PROX1 transcriptional start site. On contrary, HHEX lacks direct binding to enhancer regions of VEGF-C/VEGFR3. Collectively these data support a model where HHEX is an upstream transcriptional regulator of VEGFR3/VEGF-C/PROX1, acting directly to PROX1 transcriptional site (Gauvrit et al., 2018) (Figure 1.2.14.1).

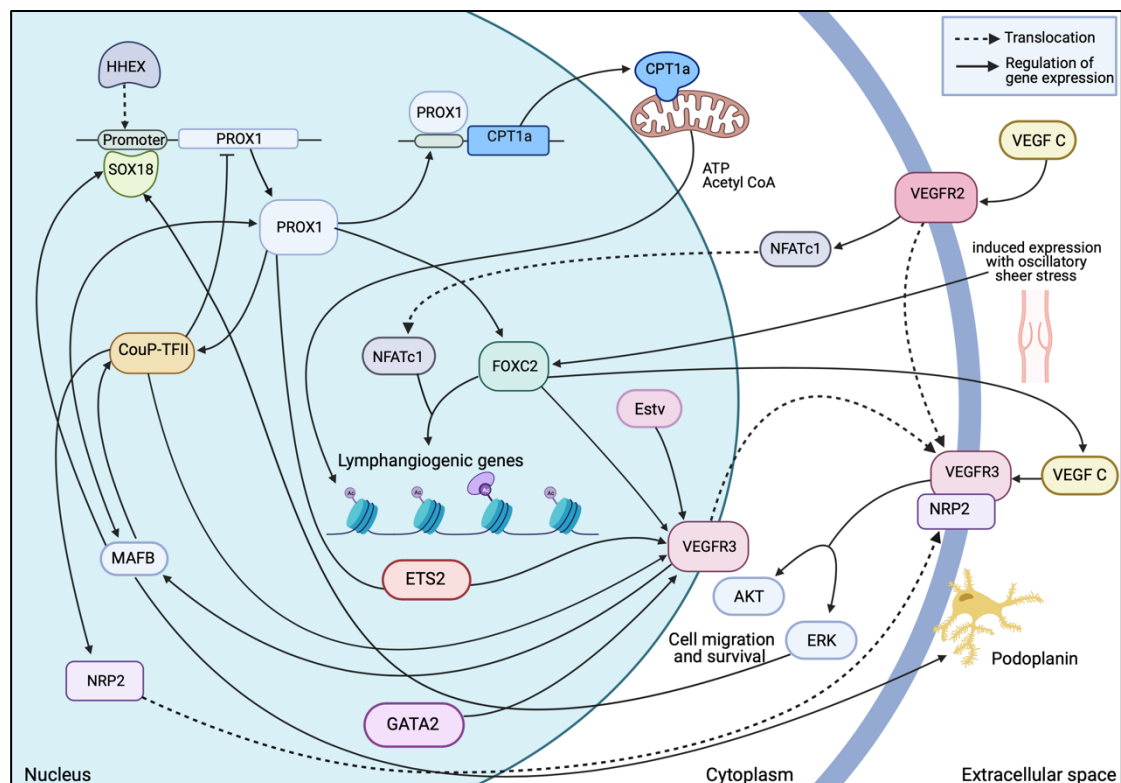


Figure 1.2.14.1. Transcriptional insight into establishment and regulation of the quiescent lymphatic endothelial phenotype. A dynamic and interchangeable network of transcription factors are involved in the complex signalling which differentiates and maintains expression of essential proteins within the cell. This allows the cell to respond accordingly to external stimuli and retain structural stability in areas of high stress. Made with Biorender.com.

1.2.15 Lessons from single cell sequencing

The transcriptomic exploration of lymphatic vasculature has been greatly expanded through the use of scRNA-seq, probing gene-expression data at the resolution of single-cells (Chen et al., 2019; Xiang et al., 2020). Whilst studies had previously suggested heterogeneity among LECs (Iftakhar-E-Khuda et al., 2016; Park et al., 2014; Ulvmar et al., 2014), single-cell techniques have allowed further characterisation of LEC heterogeneity with six transcriptionally distinct PROX1⁺ LEC clusters (clusters I-

VI) being identified in human lymph nodes. Although a highly specialised lymphatic vasculature, such high-resolution analysis has allowed the difference quiescence states to be identified. For example, expression of cell-cell junction, extracellular matrix (ECM)-interacting proteins and inflammatory marker expression demonstrate heterogeneity. Following on from the single cell RNASeq analysis of human lymph node LECs, the group investigated murine lymph node LEC heterogeneity (up to 7 specific identities) and compared the findings with the human results (Xiang et al., 2020). Five mouse LEC clusters were identified as shared between mouse and human. The transcription factor FOXC2, showed high expression levels in cells identified as valve cells and is a shared marker gene between mice and humans (Xiang et al., 2020). Another shared marker gene of lymphatic valve cell was the transcription factor GATA2 (Xiang et al., 2020) which has been previously shown to be critical for the development and maintenance of lymphatic valves (Kazenwadel et al., 2015; Mahamud et al., 2019). Interestingly, the corresponding human LEC cluster to murine valve subset (LEC V) also shows a high expression level of FOXC2 and GATA2 but were detected in a small percentage of cells in the subset. Other transcription factors identified as shared between mouse and human LECs with heterogenous expression across the lymph node include KLF4 (Takeda et al., 2019; Xiang et al., 2020), which has been demonstrated to be a key regulator of the components of flow-induced LEC proliferation (Choi et al., 2017) and RELB (Takeda et al., 2019; Xiang et al., 2020), a member of the nuclear factor- κ B (NF- κ B) family (Yang et al., 2019) known to play a key role in the development and function of lymphatic vessels mediated by LECs (Liang et al., 2019).

1.3 Partial EndMT

Endothelial cells share many characteristics with epithelial cells. They have strong apical-basal polarity, and the ability to undergo a transition to a mesenchymal-like cell. In endothelial to mesenchymal transition (EndMT), ECs lose their endothelial characteristics and gain a mesenchymal phenotype. The hallmarks of this transition include loss of polarity, extension of filopodia and migration into the extravascular space (Bischoff, 2019). This process is seen physiologically in the formation of heart

valve in the embryo (von Gise and Pu, 2012), as well as pathologically in fibrosis (Yoshimatsu and Watabe, 2011). Both epithelial to mesenchymal transition (EMT) and EndMT share the same pathways and effectors, such as SNAIL, SLUG, TWIST1, ZEB1 and ZEB2 (Welch-Reardon et al., 2015). Partial transition of both epithelial and ECs to a mesenchymal phenotype is possible, this is where one or more of the key characteristics of the mesenchymal phenotype is not exhibited. A crucial example of this is in angiogenesis, where it is believed that partial EndMT is involved in the remodelling of blood vessels. The growing sprout is led by a tip cell, which lacks apical basal polarity, has the ability to degrade both the basement membrane and extracellular matrix and encompasses an overall migratory phenotype (Welch-Reardon et al., 2015). This process is termed partial EndMT as the cell-cell junctions remain intact, allowing migration as a train of cells rather than as individual cells (Welch-Reardon et al., 2015). The transcriptional regulation of whether cells undergo full or partial EndMT is unknown, however SNAIL, SLUG, TWIST and ZEB1/2 have been implicated in initiation of the transition in EMT and to a research-limited extent, in EndMT. These transcription factors share the ability to repress E-Cadherin expression (Welch-Reardon et al., 2015), this is a junctional protein which regulates cell adhesion (Loh et al., 2019). In EndMT, E-cadherin is not present in ECs, they instead express VE-Cadherin. Similar patterns of inhibition have not been seen in ECs with SLUG knockdown (Welch-Reardon et al., 2014). SLUG has been implicated as an important regulator of sprouting angiogenesis, regulating membrane type 1 matrix metalloproteinase (MT1-MMP), the lack of effect on cell-cell junctions suggested SLUG has an effect specifically as a driver of partial EndMT (Welch-Reardon et al., 2014). SNAIL was also investigated by Welch-Reardon et al., in the context of *in vitro* sprouting angiogenesis, SNAIL expression was induced during sprouting, but at a later timepoint in comparison to SLUG (Welch-Reardon et al., 2014). Interestingly, loss of both SNAIL and SLUG inhibited endothelial cell sprouting, invasion and lumen formation, suggesting a dual role of these transcription factors in partial EndMT (Welch-Reardon et al., 2014).

The majority of research conducted regarding partial EndMT thus far has been conducted in blood ECs. Due to shared origins, and multiple shared mechanisms of growth, we can consider a similar mechanism may be involved in the remodelling of the lymphatic vasculature. A paper by Wang et al., has investigated EndMT in LECs in relation to contribution to tumour metastasis (Wang et al., 2017). This paper suggested with addition of tumour cell derived WNT5B, induction of partial EndMT was seen, this was established due to increased α smooth muscle actin (α SMA) and vimentin, but maintenance of CD31 expression (an endothelial adhesion molecule). In addition, EMT transcription factors SLUG and SNAIL were increased in these cells, as was lymphatic identity marker PROX1. Using tube formation assays as an *in vitro* model of lymphangiogenesis, Wang and colleagues found that both knockout of either SLUG or SNAIL is necessary for lymphangiogenic remodelling in response to WNT5B (Wang et al., 2017). This is similar to the mechanisms seen in blood vessels whereby angiogenic sprouting is inhibited by loss of SLUG or SNAIL (Welch-Reardon et al., 2014). The involvement of other EMT markers, such as ZEB1, ZEB2 or TWIST have not yet been reported.

1.4 ZEB1

Zinc finger E-box binding homeobox 1 (ZEB1) is a zinc finger transcription factor located on chromosome 10p11.2 (Williams et al., 1992). The ZEB1 protein is comprised of 1117 amino acids, beginning, and ending with a C2H2-type flanking zinc finger amino-terminal cluster (NZF) and carboxy-terminal cluster (CZF) a homologous structural homeodomain is located in the middle (Perez-Oquendo and Gibbons, 2022). The function of the two C2H2-type zinc fingers is to recognise and bind a specific 5'-CANNTG-3' sequence (Comijn et al., 2001). These clusters are thought to regulate cell differentiation and have tissue specific functions (Fan and Maniatis, 1990). The homeodomain region is flanked by the Smad interaction domain, and C-terminal binding interacting domain (CtBP), these regions are essential for the regulation of ZEB1's transcriptional activity (Shi et al., 2003; Postigo, 2003).

ZEB1 can both activate and repress gene expression of target genes by epigenetic mechanisms and recruitment of different co-suppressors or activators (Postigo, 2003; Sánchez-Tilló et al., 2012). ZEB1 can recruit CtBP co-repressors such as histone deacetylases and methyltransferases leading to transcriptional repression (Drápela et al., 2020). ZEB1 repressor activity can be controlled by post translational modification, such as SUMOylation or acetylation, which disrupts ZEB1 binding to CtBF (Long et al., 2005; Sánchez-Tilló et al., 2012). ZEB1 activates transcription of TGF- β responsive genes through recruitment of co-activators such as Smad, histone acetyltransferase p300 and P/CAF (Postigo, 2003; Drápela et al., 2020). This dual role of ZEB1 as transcriptional regulator, enables the control of the expression of over 2000 genes, with roles in cell-cell adhesion, anchorage-independent growth and cell polarity (Maturi et al., 2018; Caramel et al., 2018). The phenotypes under ZEB1 control makes this transcription factor crucial for the EMT program (Caramel et al., 2018).

ZEB1 is under the regulation of several transcriptional and post-translational mechanisms. A widely described mechanism is the feedback loop of ZEB1 and the miR-200 family, this loop regulates cellular plasticity, differentiation and ZEB1 activity in tumour cells (Zhang et al., 2019). Within this loop, ZEB1 inhibits the transcription of miR-200 family members, promoting EMT and drug resistance, while miR-200 members promote mesenchymal to epithelial transition (MET) and drug sensitivity (Brabletz, 2012). Specific disruption of this feedback loop is a target for treatment of therapy resistance and has been shown to alter cell plasticity and slow metastasis *in vivo* (Celià-Terrassa et al., 2018). As an activator of EMT, TGF- β induces ZEB1-dependent mesenchymal transdifferentiation in glioblastoma (Joseph et al., 2014). and colorectal cancer (Flum et al., 2022). This mechanism of ZEB1 induction is through the upregulation of pSMAD2/3 which forms a complex with SMAD2, translocating it to the nucleus, allowing it to bind to the ZEB1 promoter and activate transcription (Joseph et al., 2014). Control of ZEB1 expression through upregulation of TGF- β is therefore conducive to an invasive, metastatic phenotype.

ZEB1 has primarily been implicated in tumour cells and the overall tumour progression, by targeting epithelial gene promoters. High ZEB1 in cancer types such as brain, breast, cervical, colon, endometrial, gastric, liver, and pancreatic to name a few, has been associated with poor prognosis. ZEB1 promotes tumour progression and metastasis by reprogramming the tumour microenvironment and increasing cell motility creating a favourable tumour niche (Perez-Oquendo and Gibbons, 2022). ZEB1 expression in epithelial cells promotes a change in the transcriptional landscape of the cell by suppressing epithelial genes such as E-cadherin and activation of mesenchymal gene such as matrix metalloproteases and epidermal growth factor receptor (Peng et al., 2017; Aigner et al., 2007). This results in the detachment of the cells from the primary tumour, with loss of apical basal polarity and acquisition of the motility and invasiveness associated with a mesenchymal phenotype (Kalluri and Weinberg, 2009). In one study by Liu et al., ZEB1 was overexpressed in a breast cancer cell line, media from these cells was then incubated with cultured HUVECs and the ability to induce tube formation was examined (Liu et al., 2016). The results from this study showed that HUVECs grown in ZEB1 overexpression cells media were able to form longer tubes than the control. This was found to be a result of ZEB1 inducing VEGF A and C secretion into the media, therefore stimulating angiogenesis in this environment (Liu et al., 2016).

The role of endothelial ZEB1 has not yet been established due to conflicting results. In mice, complete loss of ZEB1 is embryonic lethal, exhibiting skeletal defects such as limb defects, craniofacial abnormalities, fusion of ribs, hypoplasia of intervertebral discs and sternum defects (Takagi et al., 1998). Studies investigating loss of ZEB1 in mice should instead utilise a heterozygous model, cell specific and/or inducible model, or investigated at an embryonic stage. Isolating embryo fibroblasts at early stages in development has allowed for the investigation of the effects of complete loss of ZEB1 in the vasculature (Takagi et al., 1998; Jin et al., 2020). In a study investigating the effect of corneal neovascularisation, E19.5 homozygous, heterozygous and ZEB1 knockout embryos lungs were sectioned and stained for quantification of vasculogenesis. Jin et al., found that the ZEB1 heterozygous and

knockout mice has significantly underdeveloped lungs and reduced blood vessel formation (Jin et al., 2020). In adult mice, only heterozygous mice were studied compared to the control, and subjected to alkali-burn to stimulate corneal neovascularisation, where there was a reduction in angiogenesis following loss of one copy of ZEB1 (Jin et al., 2020). This was further investigated and thought to be a consequence of an inhibitory interaction with CtBP and through lack of repression of cyclin-dependent kinase inhibitors, which when repressed allow ZEB1 to drive tumour cell proliferation. It was therefore concluded that ZEB1 promotes angiogenesis in this model by regulating vascular EC proliferation (Jin et al., 2020). There are two papers which have used a mouse model of inducible ZEB1 knockout, specifically in ECs. This is favourable, as ZEB1 is an important transcription factor in most cell types. In a tumour model of ZEB1 inducible EC knockout, Fu et al., found that in the blood vasculature, ZEB1 levels are increased in tumour vessels, supporting tumour intravasation and metastasis, abnormal vessel formation and tumour growth. Following tumour cell implantation, reduced tumour growth was seen in comparison to the control, as well as increased E-cadherin and reduced vimentin, suggesting hindered EMT process (Fu, Li, et al., 2020). Vessel density of these mice was also measured, which was decreased in the ZEB1 knockout mice suggesting reduced tumour angiogenesis, these vessels had increased pericyte and basement membrane coverage, suggestive of vessel normalisation in comparison to badly formed leaky, tumour vessels. Overall survival of ZEB1 EC knockout mice was increased (Fu, Li, et al., 2020). This paper presents the idea that ZEB1 is a target for anti-tumour therapy, with involvement in tumour angiogenesis, vascular integrity, and anti-tumour immune response. No effects in (blood) vascular morphology, density or alterations in major organs were seen in ZEB1 inducible endothelial knockout mouse was seen in non-tumour bearing mice (Fu, Li, et al., 2020). The lymphatic vasculature was not investigated. The effect of ZEB1 expression seems to be tissue dependent as another paper by Fu et al., using the same mouse model of inducible EC knockout mouse, found in ZEB1 promotes angiogenesis-dependent bone formation, in a specific vessel subtype (Fu, Lv, et al., 2020). In this study, ZEB1 was seen predominantly expressed in the endothelium in human and juvenile (3-

week old) mouse bone, with a decrease seen in osteoporotic mice and human patients. Again, no change in vasculature growth was seen in non-skeletal organs. In cultured bone ECs, deletion of ZEB1 resulted in suppressed transcriptional activity of DLL4 and Notch1, downregulating the endothelial Notch signalling pathway. In bone, notch signalling is positive regulator of vascular growth, distinct from notch-mediated suppression of vessel sprouting in non-skeletal organs and malignant tumours (Fu, Lv, et al., 2020). In the lymphatic system, inhibition of notch signalling leads to lymphatic sprouting (Frye et al., 2018). Investigation of ZEB1 in the lymphatic endothelial system has not been researched.

1.5 Preliminary data

1.5.1 ZEB1 is present in the quiescent blood endothelium.

During angiogenesis, endothelial cells switch from a quiescent to an activated state. In unpublished work from the wider group, ZEB1 was identified as enriched in the quiescent endothelium, *in vivo* in the blood vessels of mouse retina (Figure 1.5.1.1, Panels A-D) and *in vitro* using HUVECs (Panel E-I). This finding contrasts the expression of other EMT markers such as SLUG and SNAIL which have previously been shown to drive angiogenic sprouting through induction of partial EndMT (Welch-Reardon et al., 2014, 2015). Expression of ZEB1 in blood vasculature was suggested to be induced by angiogenic tip anastomosis (Panel C) as expression of ZEB1 nuclei in the P5 plexus is equivalent to the expression in the adult quiescent vessels. In tip cells of P5 mice, ZEB1 expression is the lowest, suggesting ZEB1 is only expressed in areas of quiescence (Panels A and C). Investigating further in cultured HUVECs, ZEB1 expression was found highest in confluent (thought to be quiescent) conditions, in comparison to subconfluent (thought to represent angiogenic) conditions (Panels E-I). This was investigated at protein and RNA level by western blot and ddPCR respectively. This preliminary data suggests that unlike other markers of EMT, ZEB1 is expressed in the quiescent blood endothelium, and expression is lost during the angiogenic switch.

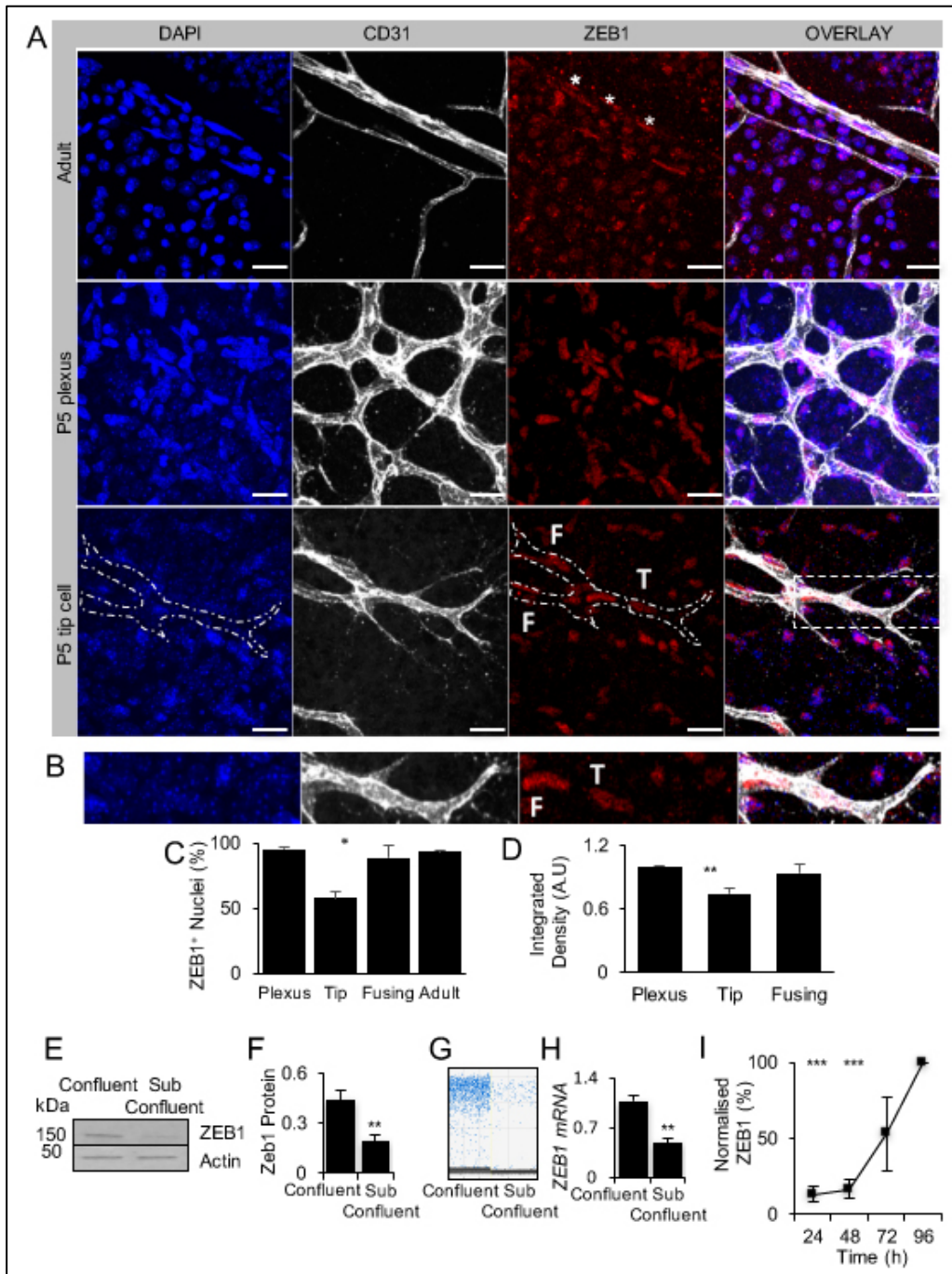


Figure 1.5.1.1 Preliminary data demonstrates that ZEB1 is expressed in quiescent HUVECs.

A. Representative images of CD31⁺ angiogenic blood vessels in murine P5 retina show heterogeneous ZEB1 expression *in vivo* compared with vessels in the quiescent vascular plexus. B. ZEB1 expression in fusing (F) versus tip (T) cell – where ZEB1 is in tip cells, it is expressed at a lower level than in the fusing cell behind it. There are fewer ZEB1⁺ tip cells (C), and less ZEB1 expression within those nuclei (D, P<0.001). Anastomosed tips (fusing) appear to regain their ZEB1 expression (A, B, C). Cultured HUVECs grown under confluent (quiescent) or sub-confluent (angiogenic) express less ZEB1 at the protein (E, F, P<0.001) or RNA level (measured by ddPCR, t-test, P<0.001, G, H) and increases with time as HUVECs plated as subconfluent monolayer grows to confluency (I). Data presented as mean ± SEM. N=3. Data from Amy Lynch and Andrew Benest, unpublished.

1.5.2 ZEB1 is present in the quiescent lymphatic endothelium.

Further to the findings of preliminary data in the blood endothelium, ZEB1 expression in the lymphatic endothelium was also investigated. Similar to the results in Figure 1.5.1.1, *in vitro* ZEB1 expression was highest in LECs grown to confluent (representing quiescent) conditions, as measured by ddPCR (Figure 1.5.2.1, Panel A). *In vivo*, adult mouse diaphragm was stained for ZEB1 and lymphatic specific marker PROX1, this revealed expression of ZEB1 in the lymphatic vessels. A condition of growth *in vivo* was not conducted. This data is preliminary and unpublished but allows for the creation of the hypothesis that ZEB1 is involved in maintaining lymphatic endothelial quiescence and gives supplies sufficient evidence to begin to investigate the effects of lack of ZEB1 both *in vitro* and *in vivo*.

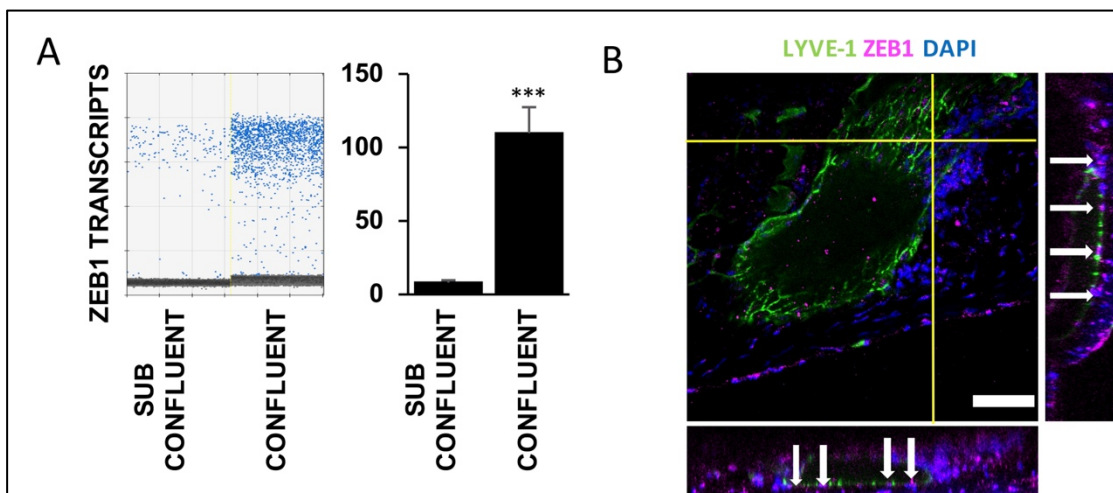


Figure 1.5.2.1 Preliminary data shows ZEB1 is expressed in LECs. A. LEC express increased ZEB1 when grown as a confluent monolayer compared with *in vitro* lymphangiogenic sub-confluent conditions *in vitro* (A, $P < 0.001$, $N = 3$). B. Murine diaphragm staining identifies LYVE1+ lymphatic vessels are ZEB1+, as shown by arrowheads, scale bar = 50 μm . Data from Amy Lynch and Andrew Benest, unpublished.

1.6 Aims and Hypothesis

Overall Hypothesis: Loss of endothelial ZEB1 will result in a lymphangiogenic phenotype by inducing partial EndMT.

Aims:

1. Investigate the RNA and Protein expression changes following ZEB1 knockdown (Chapters 3 & 4).
2. Investigate the change in metabolism following ZEB1 knockdown (Chapter 4).
3. In an inducible endothelial mouse model, investigate lymphatic-rich tissue for changes in morphology in developmental and adult stages (Chapter 5).
4. Investigate the lymphangiogenic response to injury in a mouse model of hindlimb ischaemia (Chapter 6).

Chapter 2. Methodology

2.1 Cell Culture

All cell culture took place in a category 2 microbiology cabinet. Primary Human Dermal Lymphatic Endothelial Cells (HDLECs) were isolated from adult skin, characterised and were thawed according to the manufacturer's instructions (PromoCell). The recommended culture medium, Endothelial Growth Medium MV2 (PromoCell) was supplemented with 10% FBS (Gibco) to make up complete media. Cells were cultured in T75 Cell Culture Flasks at 37°C and 5% CO₂. One vial (500,000 cells) was defrosted by removing from liquid nitrogen and placed into a waterbath set to 37°C until thawed, the cells were then transferred to a pre-warmed flask of complete media immediately. Cells were left to adhere overnight, and the media changed the following day. HDLECs required fresh media every 2-3 days and split when reaching 80-90% confluency, this involved aspirating off the current media, followed by two sterile Phosphate Buffered Saline (PBS, Gibco) washes. To detach the cells, 2 mL of Trypsin/EDTA (0.04%/0.03%) (PromoCell) was added to the flask, which was then returned to the incubator for 2 minutes. Use of a Leica DM750 microscope allowed visualisation of rounded, detached cells. To neutralise the trypsin, 4 mL of media was added, the total suspension was divided into three new T75 flasks containing pre-warmed media. Due to the nature of primary cells, HDLECs were passaged until morphology started to be lost, around P10-12. All experiments were conducted with HDLECs ranging from P3-10 with pooled adult male HDLECs.

2.1.1 Model of lymphangiogenic growth

To investigate the markers of a lymphangiogenic phenotype, two conditions were created to represent a growing and a quiescent environment. HDLECs were plated at a density of 25,000 cells per cm², creating an environment in which the cells have the space and nutrients to maintain and encourage growth. To represent a quiescent, state, HDLECs were plated at a density of 150,000 cells per cm² to reach confluency. Both conditions used media without FBS to maintain experimental conditions and not encourage excessive growth. For every confluent dish of 150,000 cells per cm², six sub-confluent, 25,000 cells per cm² dishes were made. This ensured the same

number of cells were being compared at the latter stages. The cells were incubated overnight at 37°C and 5% CO₂.

2.1.2 siRNA Knockdown

The protocol used for siRNA knockdown of HDLECs was optimised and published by the Endothelial Quiescence Group (Tabrizi et al., 2022). This protocol was upscaled up to increase the protein concentration and described in this section in full. Cells were plated into a sterile at a density of 133,333 cells per cm² with 5 mL complete media, for each condition there were three replicates. Confluency was checked the next day to be 80% before proceeding with the knockdown. The two conditions either involved the siRNA for ZEB1 (Dharmacon, L-006564-01-0050) or SLUG (Dharmacon, L-017386-00-0020), or ON-TARGETplus Non-targeting Control (Dharmacon, D-001810-10-20). These siRNAs are SMARTpools, therefore the target sequences of the pooled siRNAs are shown in Table 2.1.2.1.

Table 2.1.2.1 siRNA target sequences of the individual siRNAs which are pooled to reduce target gene expression. Information from Horizon Discovery.

Gene Target	siRNA Target Sequences
ZEB1	CUGUAAGAGAGAAGCGGAA CUGAAAUCCUCUCGAAUGA GCGCAAUAACGUUACAAAU GCAACAGGGAGAAUUAUUA
SLUG	UCUCUCCUCUUUCCGGAUA GCGAUGCCCAGUCUAGAAA ACAGCGAACUGGACACACA GAAUGUCUCUCCUGCACAA
Non-silencing control	UGGUUUACAUGUCGACUAA UGGUUUACAUGUUGUGUGA UGGUUUACAUGUUUUCUGA UGGUUUACAUGUUUUCUA

For each condition two solutions were made:

Table 2.1.2.2. Constituents of Solutions used in the siRNA knockdown of ZEB1. Quantities are given for 3 replicates of each condition for a LECs grown to 80% confluency on a 60 mm dish.

	Non-Silencing Control (NSC)	siRNA knockdown
Solution A	75 µL Non-silencing oligonucleotides (20 µM) 750 µL Opti-MEM	75 µL ZEB1 silencing siRNA (20 µM) 750 µL Opti-MEM
Solution B	37.5 µL Lipofectamine RNAiMax 750 µL Opti-MEM	37.5 µL Lipofectamine RNAiMax 750 µL Opti-MEM

Lipofectamine RNAiMax (Thermo Fisher) was kept on ice where possible. OptiMEM reduced serum medium (Gibco) was pre-warmed. Solutions A and B were incubated at room temperature separately for 10 minutes, then were combined, and incubated together at room temperature for 30 minutes. Media was aspirated from the cells, and the cells gently washed twice with PBS. To a final volume of 2.5 mL, to each dish 2 mL of Opti-MEM was added followed by 500 µL dropwise of the appropriate condition. Cells were incubated for 4 hours at 37°C and 5% CO₂. Transfection reagents were replaced with 5 mL complete media and left for 72 hours for protein quantification.

2.2 RNA Extraction

For RNASeq analysis, three ZEB1 knockdown and three Control samples were prepared as above, however only left for 48 hours. Prior to RNA extraction, the media was aspirated, and cells washed twice with PBS, each dish received 1 mL Trypsin/EDTA and incubated for 2 minutes at 37°C and 5% CO₂ until detached. The substrate was removed and placed into a corresponding sterile Eppendorf and spun at 1000 x g in a centrifuge (Sigma). The resulting cell pellets were placed on ice. Using the RNeasy Mini Kit (Cat No. 74104, QIAGEN), 600 µL Buffer RLT was added to each sample and vortexed to disrupt the pellet. One volume (600 µL) of 70% ethanol was added and the lysate pipetted up and down. 700 µL of each sample was then transferred to an individual spin column and centrifuged for 15 seconds at maximum

speed (8000 x g). The flow was discarded, and this step was repeated with the remainder of the sample. Buffer RW1 (700 µL) was added to the spin column and centrifuged at maximum speed for 15 seconds, with the flow through discarded. Buffer RPE (500 µL) was added to the spin column and centrifuged again at maximum speed and the flow through discarded. This step was repeated, however centrifugation at maximum speed for 2 minutes. At this point the spin columns were transferred to a new 2 mL collection tube, the tubes were spun at maximum speed for 1 minute to dry the membrane. The columns were transferred to a new 1.5 mL collection tube, 30 µL RNase-free water was added directly to spin column membrane. To elute the RNA, the samples were centrifuged at maximum speed for 1 minute. To maximise RNA yield, the elute from this step was pipetted onto the column membrane again, and centrifuges at maximum speed for 1 minute. The samples were kept at -80°C until sent off for sequencing by Novogene.

2.2.1 RNA Sequencing

Novogene conducted quality control on the ZEB1 KD samples via Qubit to ensure sample purity, minimal degradation and sufficient concentration, the results of which are indicated in Table 2.2.1.

Table 2.2.1 Quality control for LEC samples sent to Novogene for RNA Sequencing. Data from Novogene.

Sample	Concentration (ng/ul)	Vol (µl)	Total Amount (ng)	Pre-QC Method (qubit or nano)	RIN	OD 260/280	OD 260/230
LEC NSC	30.9	12	370.8	Qubit	9.3	2.17	2.82
LEC NSC	50.8	12	609.6	Qubit	9.7	2.15	2.13
LEC NSC	81.8	12	981.6	Qubit	9.6	2.13	2.44
LEC ZEB1 KD	30.3	12	363.6	Qubit	9.3	2.28	4.54
LEC ZEB1 KD	52.3	12	633.6	Qubit	9.6	2.16	2.08
LEC ZEB1 KD	59.9	12	718.8	Qubit	9.6	2.17	3.23

All samples met the minimum requirements, therefore the samples were run on Illumina platform for paired end 150 read depth sequencing. The raw counts to gene list analysis was completed by Joseph Horder. FASTQC was used for quality control and to identify adapters in the dataset. Cutadapt was used to trim adapters and

remove bases with a quality score of less than 20. The reference human genome GRCh38 was used to align the reads to the genome, using STAR. To align to a gene level, a featureCounts package from Subread was used. DESeq2 was used to normalise the read counts and perform differential expression analysis. Differentially expressed genes were inputted into Ingenuity Pathway Analysis (IPA, QIAGEN) for over representation analysis. IPA (version 94302991) was used to explore transcriptome changes that occur in HDLECs following ZEB1 knockdown. The differentially expressed gene list was uploaded to IPA, whereby canonical pathways, disease pathways and predicted upstream molecules were identified. A Z-score was calculated to provide directional information of two or more molecules in the dataset, to allow prediction of activation or inhibition of a particular pathway/protein. A negative Z-score suggests inhibition, and a positive Z-score indicates activation (Krämer et al., 2014).

2.3 ChIP Sequencing

To investigate potential ZEB1-DNA interactions, six samples (three using IgG antibody, and three using ZEB1 antibody) were prepared for chromatin immunoprecipitation (ChIP) sequencing. Using the active motif high sensitivity ChIP kit, the protocol was optimised to enhance the output, this involved increasing the recommended amount of input to 6 confluent 150 mm dishes, each initially seeded at a density of 333,333 cells per cm². Once 80-90% confluent, complete cell fixative solution was freshly prepared according to the kit instructions (180 µL fixation buffer, 1.57 mL sterile water, 750 µL 37% formaldehyde), for each dish containing 20 mL of growth media, 1/10 media volume of complete cell fixative was added. The dishes were gently rocked for 15 minutes. The final concentration of 11% formaldehyde (Sigma) is to cross link and preserve endogenous DNA-ZEB1 interactions. To stop the fixation (prevent over-fixing, artefacts and protein-protein cross linking resulting in false positive pulldowns) 1/20 media volume of Stop Solution was added to each dish. The dishes were placed on a rotator and incubated at room temperature for 5 minutes. The plates were scraped with a cell scraper to collect the lysates and placed on ice in a 50 mL falcon. Cells were pelleted by

centrifugation at 1,250 x g at 4°C. The supernatant was removed, and the pellet resuspended in 10 mL ice cold PBS wash buffer (21.25 mL sterile water, 2.5 mL 10X PBS and 1.25 mL detergent). The centrifugation was repeated, and the supernatant discarded. At this point, the three tubes were combined, first resuspending the first pellet in PBS wash buffer, then adding this to the next tube to resuspend the pellet, until all three pellets were resuspended in one tube. This is because HDLECs do not pack well therefore this method ensures adequate output. The single tube was centrifuged once more at 1,250 x g at 4°C and the supernatant discarded. Pellets were stored at -80°C until ready to do the next steps.

The pellet was thawed on ice and resuspended in 5 mL Chromatin Prep Buffer (prior supplemented with 5 µL Protein Inhibitor Cocktail and 5 µL 100 mM PMSF). The tube was incubated on ice for 10 minutes, followed by transfer to a chilled dounce homogeniser with a tight-fitting pestle (Active Motif). To ensure the cells were fully lysed the sample was homogenised by 40 strokes – this was checked using a phase contrast microscope to visualise the released nuclei. The sample was transferred to a 15 mL falcon tube and centrifuged for 3 minutes at 1,250 x g at 4°C. The supernatant was discarded, and the pellet resuspended in 500 µL Chromatin Prep Buffer (prior supplemented with 5 µL Protein Inhibitor Cocktail and 5 µL 100 mM PMSF). For optimal sonication, the sample was transferred to a 2 mL sonicator tube and incubated for 10 minutes on ice. The Sonicator used was the Bioruptor Pico sonicator set to 4°C. Sonication was optimised to 30 rounds of 30 seconds on, 30 seconds off. This was determined by visualising the fragment size and chromatin shearing efficiency on an agarose gel. The sample was spun in a microcentrifuge at maximum speed at 4°C to pellet debris, the supernatant contained the input DNA. For shearing analysis, 25 µL of input was transferred to a PCR tube. The remaining was kept at -80°C until adequate shearing has been confirmed.

To the PCR tube, 175 µL TE pH 8.0 and 1 µL RNase A was added, the tube was briefly vortexed and incubated in a thermocycler at 37°C for 30 minutes. To reverse the protein cross-links, 2 µL Proteinase K was added to the tube, briefly vortexed and further incubated in a thermocycler at 55°C for 30 minutes, then increased to 80°C

for 2 hours. The input was transferred to a larger 1.5 mL Eppendorf tube, with the addition 83 μ L Precipitation Buffer, 2 μ L Carrier and 750 μ L absolute ethanol (100% ethanol, Sigma). The tube was vortexed to mix and chilled at -80°C overnight.

The following day, the sample was spun at maximum speed for 15 minutes in a microcentrifuge (Sigma). The supernatant was discarded, washed with 500 μ L 70% ethanol and spun again at maximum speed for 5 minutes at 4°C . The supernatant was discarded, and the tube allowed to air dry for 15 minutes. Once dry, 25 μ L DNA Purification Elution Buffer was added to each tube and incubated at room temperature for 10 minutes. The tube was vortexed to resuspend the pellet in the solution. The absorption of the sample was read on a NanoDrop at 260 nm to determine DNA concentration. 500 ng of DNA was required for the analysis of shearing via agarose gel. The remaining was stored at -20°C .

The input DNA (500 ng) was transferred to a 250 μ L PCR tube, followed by 1 μ L 500 mM NaCl and adjusted to a final volume of 10 μ L with sterile water. Samples were heated in a thermocycler to 100°C for 20 minutes followed by a decrease down to 50°C for 5 minutes. The samples were removed from the thermocycler and incubated for 5 minutes at room temperature. A 1.5% agarose gel was created by dissolving 1.5g agarose powder (Sigma) into 100 mL TAE buffer in a microwave in short bursts. Once dissolved and cooled slightly on ice, and 8 μ L of Ethidium Bromide was added. Using 5X sample buffer (Biorad), 6.25 μ L buffer was added to 25 μ L sample, and 6 μ L of 100 bp ladder (New England Biolabs) and 1 Kb ladder (New England Biolabs) to help quantify the shearing efficiency. The gel was run for 13 minutes at 70 volts and scanned using a Gel Doc Imaging System (Biorad). Successful shearing was determined by a visible smear at around 500 bp.

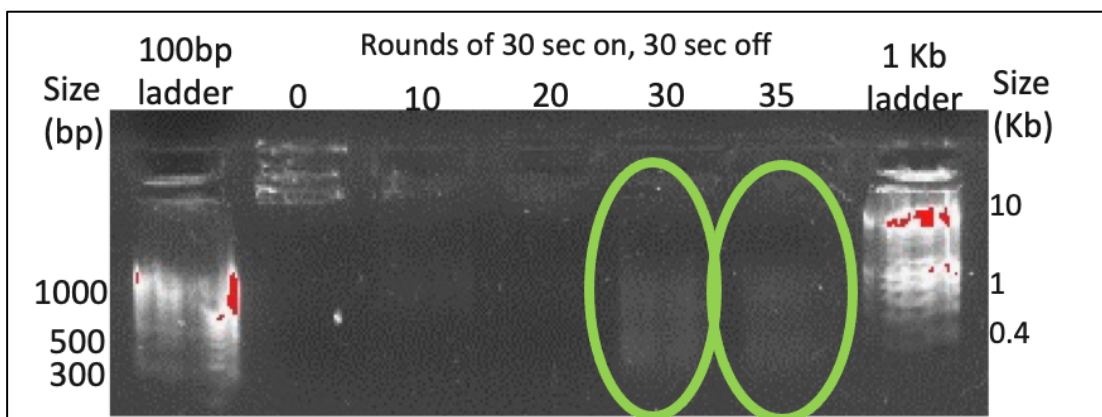


Figure 2.3.1. Optimisation of sonication of chromatin shearing of HDLECs. Chromatin was loaded onto a 1.5% agarose gel at 70 volts for 13 minutes. Successful shearing is visible by the smears visible (encircled in green). Negative control of the unsonicated sample is seen in the wells of 0 rounds of sonication.

The leftover sample from sonication was thawed on ice, followed by centrifugation at maximum speed for 2 minutes.

ChIP reactions were set up as shown in the table below:

Table 2.3.1. Reagents required for the precipitation of ZEB1 for Chromatin

Immunoprecipitation Sequencing. Quantities are given for three replicates of each condition.

Reagent	ZEB1	IgG
Sheared chromatin (10 µg-30 µg)	100 µL (depends on nanodrop concentration)	100 µL
ChIP Buffer	Adjust up to 200 µL (89 µL)	Adjust up to 200 µL (89 µL)
Protease Inhibitor Cocktail (PIC)	5 µL	5 µL
Antibody/Blocker mix	6 µL (ZEB1 ab 1:200 (final concentration) – final volume of 200 – 1 µL used with 5 µL blocker)	Not to exceed 35 µL (IgG concentration 10.2 mg/mg – 0.4 µL with 5 µL blocker)
Maximum Volume Allowed	240 µL	240 µL

The antibody/blocker mix was made with 5 μ L blocker and 4 μ g CHIP antibody, ZEB1 (Proteintech, 21544-1-AP) or IgG (Invitrogen, AB_2532938), this was incubated at 1 minute at room temperature before addition to the CHIP reactions. Three of each reaction was created. The tubes were then securely fastened and incubated on an end-to-end rotator overnight at 4°C.

The protein G agarose beads were resuspended in the tube, using a cut pipette tip, 30 μ L for each reaction (30 μ L x 6 – 180 μ L) were washed with an equal volume of TE pH 8.0, and inverted to mix. This was spun at 1250 x g for 1 minute. The exact volume of TE (180 μ L) was then removed. This was repeated, and the volume of TE removed. The CHIP reactions were spun for 1 minute at 1250 x g to collect all the liquid. Addition of 30 μ L of Protein G agarose beads was added to each CHIP reaction using a cut pipette tip and incubated on an end-to-end rotator for 3 hours at 4°C. For each reaction, a CHIP Filtration Column was placed in an empty 1 mL pipette tip box, this was to help contain the waste flow through. The CHIP reactions were spun to collect all the liquid at 1250 x g for 1 minute. To each reaction 600 μ L CHIP buffer was added before transferring the entire reaction to the column. Time was allowed for flow-through to occur by gravity. In this time, 100 μ L per reaction of Elution Buffer AM4 was added to a microcentrifuge tube to prewarm to 37°C. Each column was washed with 900 μ L Wash Buffer AM1 and left for 3 minutes, this step was repeated four times for a total of five washes. Columns were transferred to a new 1.5 mL microcentrifuge tube and spun at 1250 x g for 3 minutes at room temperature. This was to remove any residual wash buffer. The columns were transferred to a new 1.5 mL microcentrifuge tube, 50 μ L Elution Buffer AM4 warmed to 37°C was added and incubated at room temperature for 5 minutes. The sample was then spun at 1250 x g for 3 minutes in a microcentrifuge at room temperature. The flow through into the tube contained the CHIP DNA sample.

The eluted sample was transferred to a 250 μ L PCR tube and 2 μ L Proteinase K was added. The tube was vortexed to mix and placed in a thermocycler at 55°C for 30 minutes, then the temperature increased to 80°C for 2 hours. The sample was transferred to a new 1.5 mL tube with the addition of 500 μ L of DNA Purification

Binding Buffer and vortexed to mix. The pH of the sample was adjusted with 5 μ L 3M Sodium Acetate, correct pH was indicated by a bright yellow colour of the sample. A DNA Purification column (AM #103928) was placed in the collection tube and the sample added. The lid was shut and placed in a microcentrifuge and spun for 1 minute at 18,407 x g. The flow through was discarded and the column placed back into the collection tube. DNA Purification Wash Buffer was prepared and added to each column which was spun for 1 minute at 18,407 x g with the lid shut. The flow through was discarded, the column returned to the collection tube and spun with the lid open at 18,407 x g for 2 minutes. This was to remove any residual Wash Buffer from the column. The column was transferred to a clean microcentrifuge tube. For ChIPSeq, 36 μ L of pre-warmed 37°C DNA Purification Elution Buffer (AM #103498) was added to the centre of the column matrix and incubated at room temperature for 1 minute. The column was spun at 18,407 x g for 1 minute to elute the purified DNA. The three replicates of each condition were kept at -20°C until sequencing. Sequencing was completed by Novogene for ChIPSeq library preparation. The raw counts to gene list analysis were completed by Joseph Horder. Illumina sequencing was completed at paired end 150 read depth. FASTQ was used for quality control and identify adapters, these were trimmed using Cutadapt, and bases with <20 quality score were removed, and minimum read length was kept to 1. Bowtie2-build was used to align the reads to the referenced human genome GRCh38. MultiQC was used to check the alignment statistics. Unmapped reads were removed using Samtools, and Bedtools intersect to remove reads aligning to blacklist regions of the genome. Peak calling was completed using MACS2 on individual ZEB1 replicates against the combined the control. ChIPSeq quality was assessed using ChIPQC in R. The R package ChIPseeker was used to label the peaks to genes/transcripts. Promoter regions were defined as +/- 1000bp from the transcriptional start site. The annotated genes were cross-referenced with the differentially expressed genes (DEGs) produced by RNASeq to identify direct and indirect regulation of genes by ZEB1. To identify potential enhancer sites, publicly available data was utilised from ChIPSeq conducted with common histone modifications, along with DNase-Seq data. This data was aligned to the data using

IGV software. Accession numbers for the data used are: ENCFF091FMS (H3K27ac), ENCFF663PVP (H3K4me1), ENCFF065UIB (H3K4me3), ENCFF305BCB (DNase-Seq).

2.4 Measuring Oxygen Consumption Rate with Agilent Seahorse

HDLECs were transfected with NSC or ZEB1 siRNA as detailed in Section 2.1.2. After 48 hours, the cells were counted and replated into Agilent Seahorse 96-well XF Cell Culture Microplate at a seeding density of 43,859 cells per cm². Cells were incubated overnight at 37°C and 5% CO₂ to allow a confluent monolayer to form. XF Calibrant was used to hydrate the sensor cartridge (100 µL) per well, this was placed in a humidified 0% CO₂ incubator overnight. The XF96 was warmed to 37°C. XF Assay DMEM Medium (97 mL) pH 7.4 was supplemented with D-Glucose (10 mM, Sigma G7528), Sodium Pyruvate (0.1 mM, Sigma, P5280) and L-Glutamine (0.2 mM, Life Technologies, 25030-081) and the pH adjusted to 7.4. Cells were washed carefully twice with assay medium (200 µL), then 175 µL of assay medium was added before being placed in the 0% CO₂ incubator for 1 hour prior to the assay. The chosen drug concentrations were based on the concentrations used previously (García-Caballero et al., 2019). Oligomycin (10mM) was diluted to a port concentration of 9.6 µM by adding 2.88 µL of drug to 3 mL of supplemented XF assay medium, this gave a final well volume of 1.2 µM. FCCP (10 mM) was diluted to 45 µM by adding 13.5 µL into 3 mL media, giving a final well concentration of 5 µM. Rotenone (5 mM) was diluted to 10 µM by adding 6 µL to 3 mL media, giving a final concentration of 1 µM. Antimycin A (5 mM) was injected alongside rotenone, this was diluted by adding 6.6 µL of drug to the Rotenone and media solution, this gave a final concentration of 5 mM when injected into the well. Retrieving the hydrated cartridge and using the template as a loading guide, 25 µL of Port A solution (Oligomycin) was pipetted into Port A of all the wells with cells seeded. This was repeated for all ports. The mitochondrial stress programme was loaded on the Wave Desktop, and the utility cartridge inserted into the Agilent XFe 96 Analyser. The pH and temperature of each well was calibrated then the utility plate replaced with the cell microplate. Measurement of Oxygen Consumption Rate (OCR) were taken every 6 minutes (2 minutes mixing, 2 minutes delay, 2 minutes measuring). After the assay was completed, the media was

removed from the wells and replaced with 50 μ L RIPA buffer (Sigma), this was to normalise the data to μ g protein per well. The samples were diluted 1:5 with RIPA buffer and a BCA performed. The results were normalised and analysed using the Agilent Wave desktop.

2.5 Protein Extraction

For cell lysis, all steps took place on ice. Media was aspirated and the cells washed with ice cold PBS twice. RIPA (Sigma) was supplemented with 50X Protease inhibitor (Promega) 20 μ L/mL and phosphatase inhibitor (1 tablet per 10 mL RIPA [phosSTOP, Roche]). 300 μ L was to each dish and left for 5 minutes at 4°C gently rocking. The dishes are scraped for 3 minutes, and the lysate collected into Eppendorfs, then left to lyse on ice for 20 minutes. The lysates were centrifuged at maximum speed at 4°C for 20 minutes. The supernatant was stored in a new Eppendorf for protein quantification at -80°C.

To estimate the amount of protein in each sample, a BCA was performed using the Novagene BCA protein assay kit. This kit uses known protein concentrations to plot a standard curve, our unknown protein sample concentrations are then extrapolated from the calculated equation of the line. Protein standards were prepared using the RIPA supplemented with inhibitors and differing concentrations of bovine serum albumin (BSA). These are serially diluted from the highest concentration of 2000 μ g/mL to 1000 μ g/mL, 500 μ g/mL, 250 μ g/mL, 125 μ g/mL, 25 μ g/mL, and 0 μ g/mL. The samples were defrosted on ice and diluted 1:5 with RIPA (with inhibitors). In a 96 well plate, 200 μ L of BCA working reagent (BCA solution 50:1 4% Cupric Sulphate) was added to each of the standards (25 μ L) and samples (25 μ L). The plate was incubated at 37 °C for 30 minutes, left to cool at room temperature, then absorbance measures at 562 nm on a plate reader (BMG). Protein concentrations were estimated from the results and used to inform latter experiments.

2.6 Western Blotting

Samples were diluted with distilled water to ensure equal amounts of protein loading. Samples were prepared using 4X sample buffer (Thermo Fisher Scientific) supplemented with beta-mercaptoethanol (Sigma) (900:100). Samples were subject to 5 minutes at 95°C to denature the proteins, followed by sonication (Grant bench top sonicator) on ice for 15 minutes. Protein (30 µg) samples were loaded into a 4-12% gradient pre-cast gel (Bio-Rad) with a pre-stained protein ladder (ProteinTech) or dual colour ladder (BioRad). Proteins were separated by SDS-PAGE, ran at 120V for 1.5 hours in running buffer (10X running buffer constitutes of: 5g Tris base, 72g Glycine, 50mL 10% SDS, made up to 1L with distilled water, pH 8.6). Using the BioRad turbo blot machine the gel was transferred to a nitrocellulose membrane (BioRad) using a transfer stack (BioRad) soaked in Turbo 1X Transfer buffer (BioRad). The membrane was blocked in 5% bovine serum albumin (BSA) diluted in 1X Tris buffered saline (TBS) with 0.1% Tween-20 (Sigma) (TBS-t), for 1.5 hours at room temperature. Membranes were first probed with primary antibody (1:1000) ZEB1 (rabbit, 21544-I-AP, ProteinTech) and β -actin (mouse, SC-47778, Santa Cruz) in 1% BSA in TBS-t and incubated at 4°C on a roller overnight. The membranes were washed with TBS-t three times before the addition of appropriate secondary antibodies (1:5000), anti-rabbit IRDye 800RD (926-32211, LICOR) and anti-mouse IRDye 680RD (926-68070, LICOR), made up in 1% BSA in TBS-t. The membranes were incubated at room temperature on a roller for 1 hour in the dark before visualisation using Odyssey XF Imaging System (LICOR) and quantified with Odyssey Image Studio. Further probing of these membranes involves stripping the membrane for 10 minutes with 0.4M NaOH, re-blocking for 1.5 hours with TBS-t and adding the desired antibody and appropriate secondary antibody.

Table 2.6.1 List of antibodies used for protein expression analysis using Western Blotting.

Antibody	Dilution	Company
ZEB1	1:1000	Proteintech 21544-1-AP
B actin	1:1000	SantaCruz SC-47778
SLUG	1:1000	Cell Signalling, C19G7
SNAIL	1:1000	Cell Signalling, C15D3
ZEB2	1:1000	Cell Signalling, E6U7Z
VE-CADHERIN	1:1000	Invitrogen, AB_467495
PROX1	1:1000	Proteintech 11067-2-AP
Vimentin	1:1000	Cell Signalling, 5741T
JNK	1:1000	Cell Signalling, 4668S
ZO1	1:1000	Cell Signalling, 8193T
VEGFR2	1:1000	Cell Signalling, 55B11
VEGFR3	1:1000	Cell Signalling, 33566S
FOXC2	1:1000	Cell Signalling, 12974S
SOX18	1:1000	Invitrogen, MA5-32140
CD45	1:500	Abcam, ab10558

2.7 Animal iECKO model

All animal experiments were performed in compliance with the Animal Scientific Procedures Act of 1986 (ASPA) at the University of Nottingham. All experiments were conducted under UK Home Office Licence (PPL P375A76FE) held by Professor David Bates. Mice were bred and maintained in the Gene Targeting and Transgenic Unit in the Biological Support Unit, with genotyping outsourced to Transnetx Inc. Floxed loxP ZEB1 (Brabletz et al., 2017) mice were crossed with cdh5Cre-ERT2 mice

(Wang et al., 2010) to generate a $ZEB1^{fl/fl}Cdh5Cre^+$ and $ZEB1^{fl/fl}Cdh5Cre^-$ mixed population. This was through initial crossing, then backcrossing to generate a pure homozygous $ZEB1^{fl/fl}$. Genotyping was performed by Transnetyx with Cre maintained as heterozygous transgene. To induce gene excision, tamoxifen was injected at predetermined intervals. Sunflower oil (Sigma, S5007) was autoclaved in advance. In a laminar flow hood, 45 mg Tamoxifen (Sigma, T5648) was dissolved in 450 μ L sterile ethanol (Sigma, E7023) and vortexed final concentration (1 mg/10 μ L). 150 μ L of solution was added to a sterile Eppendorf and diluted further with sunflower oil to a final concentration of 1 mg/100 μ L. This was stored at -20°C until required. Tamoxifen injections and mouse sacrifice was completed by Nicholas Beazley-Long and Kathryn Green.

2.7.1 P5 model

Mice neonates were dosed with 50 μ g of tamoxifen in 5 μ L sunflower oil on three consecutive days, beginning on postnatal day 1 (P1-3) to induce endothelial cell knockout (iECKO). The mice were monitored closely throughout, then terminated on P5 and the tissue harvested.

2.7.2 Adult model

A mixed population of adult mice were intraperitoneally injected on five consecutive days with 1 mg tamoxifen in 100 μ L sunflower oil per 25g body weight. The mice underwent laser choroidal neovascularisation protocol for 2 weeks, with termination by cervical dislocation on the 14th day and the tissue harvested.

2.8 Immunofluorescence staining of ear dermis

The ears of humanly sacrificed mice were removed and placed immediately into a solution on 4% Paraformaldehyde (PFA) for 1 hour. The dermal layer of the ear was dissected using Leica M80 dissection microscope and placed into PBS. The tissue was washed 8*15 minutes with PBS-X (PBS with 0.3% Triton X-100 (Sigma)) on a rocking platform at room temperature. This was followed by blocking for 2 hours with 1% BSA in PBS-X. Primary antibodies were prepared in 1% BSA in PBS-X, primarily LYVE1

(Rabbit, Abcam, AB14917) at concentration of 1:100 was used. If necessary, CD31 (Rat, R&D Systems, AF114) was also added at concentration of 1:50. Primary antibodies were incubated with the tissue for 48 hours at 4°C on a rocking platform. To wash off unbound antibody, tissue was washed 8*30 minutes with PBS-X at room temperature on a rocking platform. Secondary antibodies were prepared in 1% BSA PBS-X, goat anti-rabbit Alexa Fluor 555 (Invitrogen, A21428) and goat anti-rat Alexa Fluor 488 1:500 (Invitrogen, A48262). Secondary antibodies were added to the tissue, protected from light, and incubated for 48 hours at 4°C. Tissue was washed 8*30 minutes with PBS-X at room temperature on a rocking platform, then mounted flat on a Superfrost glass slide (ThermoFisher) with 500 µL Flouoroshield (ThermoFisher) and a glass coverslip placed on top. The slides were cured overnight, protected from light at room temperature before sealing with nail varnish and stored at 4°C for imaging.

2.8.1 Analysis of lymphatic morphology

Images of the ear dermis were obtained using Leica Confocal SPE microscope. Z-stack images were taken at 20X magnification with equal laser power between samples. Using FIJI software, quantification of the lymphatic morphology was optimised and documented. The Z-stack images were maximally projected into a single image. The brightness was enhanced to clearly see the vessels, then the lengths of the vessels mapped with the freehand line tool, to measure the number and length of each lymphatic segment. From this, the node, how many times one vessel meets another, can also be manually quantified. Tip cells were manually quantified. Finally, the overall lymphatic area was quantified using the freehand selection tool, to map around the vessels. Initially, filopodia were attempted to be quantified by eye from these 20X magnification images, however, this was felt unreliable due to the low magnification for such small structures. New images were therefore obtained at a higher magnification (63X). Images were taken of sprouting and non-sprouting vessels and the visible filopodia quantified with the star tool.

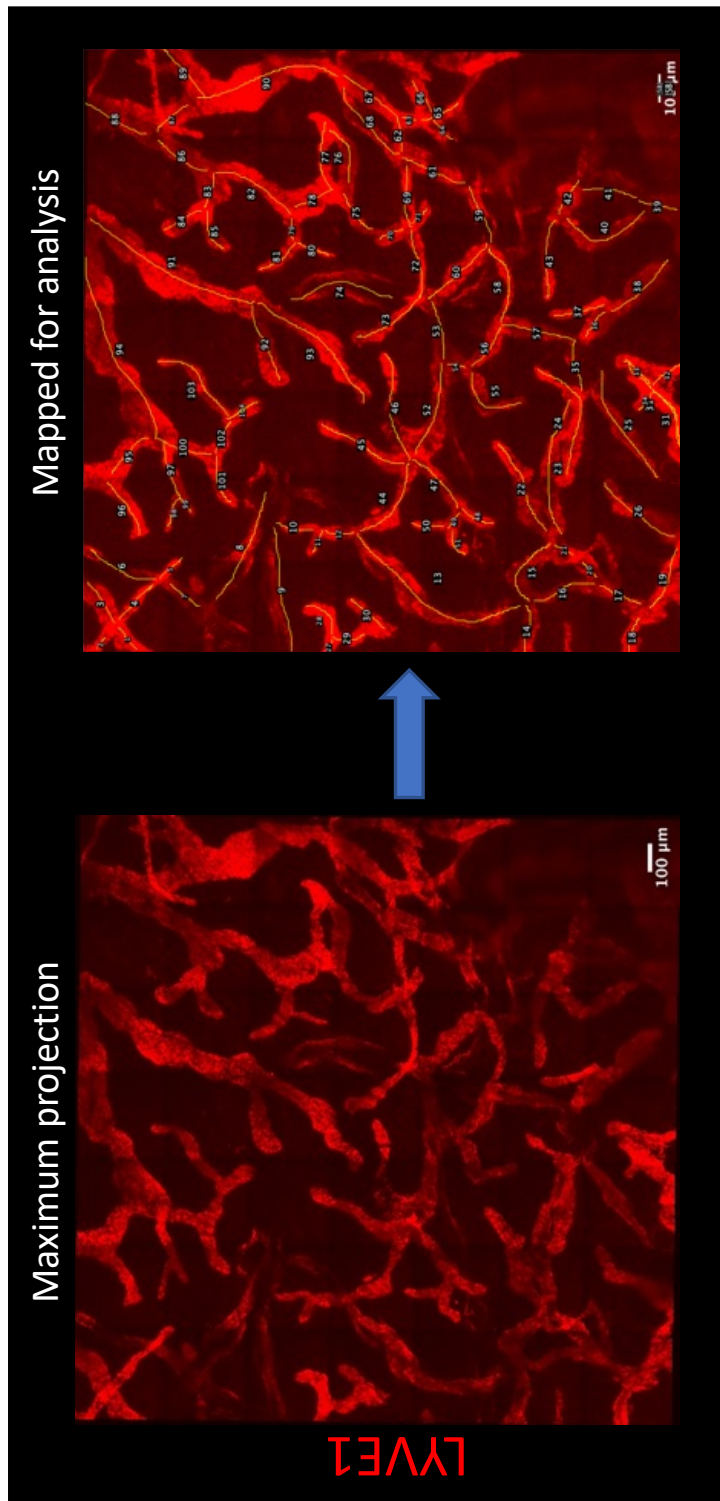


Figure 2.8.1 Analysis of lymphatic morphology in the mouse ear dermis using FIJI. A tilescan has been used for demonstration purposes. Ear dermis was isolated and stained for lymphatic specific marker LYVE1. This staining was visualised using a confocal microscope, maximum projections were used in FIJI for analysis.

2.9 Model of Hindlimb Ischaemia

To investigate the role of ZEB1 in a pathological model, we utilised the model of hindlimb ischaemia (HLI) (Bhalla et al., 2022) in the ZEB1^{iECKO} mice. This work was completed by Nicholas Beasley-Long, Mussarat Wahid, Sohni Ria Bhalla, Jason Amartey, and Kathryn Green. Adult mice underwent the tamoxifen dosing schedule as detailed in Chapter 2.8.2. After a week break, dosed mice were anaesthetised with 2% isoflurane (100% w/w IsoFlo (R)) in 100% oxygen at a flow rate of 2L/minute. Absence of withdrawal reflexes was confirmed with toe pinching to ensure lack of movement before the mouse was moved to the heat pad (Harvard Apparatus). Body temperature was monitored throughout surgery with the use of a rectal probe (Harvard Apparatus). Pre-surgery, confirmation of undisturbed blood flow to both hind paws using the laser speckle imaging system (FLPI-2, Moors Instruments). Analgesic (0.05 mg/kg buprenorphine) diluted in sterile saline (0.9% NaCl) was subcutaneously injected. Hair was removed from the left hindlimb using Nair and sterilised with hydrex derma spray (Scientific Laboratory Supplies). The mouse was transferred to the surgical platform where the paw was taped to secure and extend the leg, so the surgical area was easily accessible. With the use of a dissection microscope (Leica), a 1 cm cut from knee to abdomen was made. The layer of fat was separated from the connective tissue to expose the femoral artery. A suture (6-0 W812 Mersilk) was made to tie off above the superficial epigastric artery. A second suture was made close to the sapheno-popliteal bifurcation. The length of vessel between the two suture points was electro-coagulated using a cauteriser (Wuhan Spring Scenery Medical Instrument Co Ltd, Evergreen) at 18V. The incision was closed with surgical Adams clips (Scientific-Labs) and glued with a topical adhesive (GLUture, Zoetis). Post-surgery confirmation of successful ischaemia was visualised using the laser speckle imager. The mouse recovered post-operatively in a clean, warm cage with mash under close supervision. The animals were monitored twice daily for 7 days. Blood flow to the paws were imaged pre- and post-operatively via Moors Instruments laser perfusion imager. This allowed representation of blood flow via correlation with the velocity of the moving red blood cells, to confirm induction of ischaemia in the operated limb.

2.9.1 Immunofluorescence staining of muscle sections

For fixed perfusion of the mice, administration of 1mg/kg medetomidine (Sedastart, Animalcare group) and 75 mg/kg ketamine (Ketastart, Zoetis) was injected via intraperitoneal injection. After withdrawal reflexes were lost, cardiac perfusion was performed using 25 mL of sterile PBS followed by 25 mL of 4% PFA/PBS.

Gastrocnemius muscle from the hindlimbs of both operated and unoperated legs of the mice were dissected from the perfused mouse and immediately placed into 4% PFA. The following day, the muscle was placed into a 30% sucrose solution in PBS and incubated at 4°C until the muscle sunk (around 3 days). The tissue was embedded in OCT and immediately frozen at -80°C. To create thin sections for staining, muscle was sectioned to 16 µm and 40 µm thin using a Leica cryostat at -20°C, onto Superfrost Plus slides (ThermoFisher Scientific). Slides were kept at -20°C until stained. The sections were drawn around with a hydrophobic pen to keep the solutions on the slide, then gently washed with PBS 3*5 minutes. The sections were then blocked in 1% BSA in PBS-X (0.3%) for 1.5 hours. Appropriate antibody solutions were created, for visualisation of lymphatic vessels, a solution using LYVE1 at 1:100 (Rabbit, Abcam, AB14917) and IB₄ (Vector Laboratories, L-1104-1) 1:100 in 1% BSA in PBS-X (0.3%) was incubated with the sections overnight in a humid staining tray at 4°C. For visualisation of macrophages, a solution using CD45 1:100 (Goat, R&D Systems, AF114) and LYVE1 at 1:100 (Rabbit, Abcam, AB14917) was created and incubated with the sections overnight.

To wash away unbound antibody, sections were washed with PBS 3*5 minutes and appropriate secondary antibody solutions prepared. For the LYVE1 and IB₄ sections, goat anti-rabbit Alexa Fluor 555 (Invitrogen, A21428) and Streptavidin Alexa Fluor 488 (Invitrogen, S11223) was diluted 1:500 in 1% BSA in PBS-X (0.3%). For the CD45 and LYVE1 sections, Donkey anti-goat Alexa Fluor 555 (Invitrogen, A21432) 1:500 and Donkey anti-rabbit Alexa Fluor 488 (Invitrogen, A21206) was diluted in 1% BSA in PBS-X (0.3%) and left to incubate in a humid staining tray away from light at 4°C overnight. DAPI (1:1000) in 1% BSA with PBS-X (0.1%) was added the next day and left to incubate for one hour at room temperature. The sections were then washed 3*5 minutes and mounted by adding 200 µL Flourosshield (Thermofisher) and

covering with a coverslip. Slides were left to cure in the dark overnight, then sealed with nail varnish.

2.9.2 Analysis of HLI muscle sections

Muscle sections were imaged on a Leica confocal microscope. Z-stack tilescans were acquired at 20X magnification in a 3 x 3 field. Images were analysed using FIJI ImageJ software. The Z-stacks were projected into one image using the Z projection tool, showing the image as a maximum projection. Using the thresholding tool, the area of the fibres was selected and quantified (Figure 2.9.2.1). The threshold was then adjusted to identify positive LYVE1 or CD45 staining. These were automatically counted, and the area of positive staining quantified.



Figure 2.9.2.1 Analysis of lymphatic vessels in the hindlimb muscle using FIJI image analysis software. Muscle sections were stained for LYVE1, IB₄ and DAPI. These were visualised using a confocal microscope. Z stack tilescans were maximally projected. The area of the fibres was quantified, along with lymphatic density and area using FIJI image analysis.

2.10 Statistical Analysis

Statistical analysis was performed on the data sets based on recommended tests for the experiment design, number of variables and type of data output. An unpaired t-test was performed on data where the aim was to compare the means of two separate groups with equal variance. In this thesis, this was performed on the western blot data, where the mean of the ZEB1 knockdown cells was compared to the mean of the NSC cells. This was also performed on the Seahorse data which was provided as mean values between the groups through calculations performed by the Agilent software. For animal work where animals were split by sex and genotype, a two-way ANOVA was performed on the data. This was due to multiple variables being tested. Where data was unable to be split by sex, an unpaired t test was performed.

Chapter 3. The Effect of ZEB1 Knockdown on the Transcriptional Landscape of HDLECs

3.1 Introduction

Specific knockdown of gene expression in cultured cells is a widely used technique to investigate the importance of a specific gene within a specific cell subtype. From preliminary data in cultured endothelial cells conducted by the group (Chapter 1.5), we have suggestion that ZEB1 is expressed in confluent, and potentially quiescent conditions in blood and lymphatic ECs. In mouse blood vessels, this corresponded to ZEB1 expression in the stalk cells of established vessels, and lack of expression in the growing tip cells (Figure 1.5.1.1). ZEB1 expression in growing lymphatic vessels was not investigated. Examining the changes in the transcriptional landscape following loss of ZEB1 would allow indication of potential associated changes in cell phenotype. This can be used as rationale for further investigation at protein level, and knockdown in animal models.

Due to shared origins, mechanisms governing blood ECs often result in a similar effect on LECs (Srinivasan et al., 2007). From preliminary data, we have evidence that ZEB1 may have a role in governing a switch from a quiescent EC to an angiogenic EC. Translating this theory into LECs, this suggests that ZEB1 may play a role in mediating the same mechanism to a lymphangiogenic EC. To identify a lymphangiogenic EC *in vitro*, a broad analysis of gene expression can be conducted using RNA sequencing. Gene ontology analysis software can be utilised to group differential genes together to identify pathways significantly affected by loss of ZEB1. A specific lymphangiogenic signature has not yet been robustly defined, but theoretically would involve upregulation of key lymphangiogenic genes as well as changes in expression of metabolic genes, cell-cell junctional proteins and altered cell cycle mediators.

ZEB1 is a transcription factor, therefore following investigation of the RNA landscape following its depletion in the cell, we can unravel more detail about the site at which

ZEB1 is binding through methods such as Chromatin Immunoprecipitation Sequencing (ChIPSeq). TFs bind enhancers and promoters in different combinations, with enhancer regions, controlling the spatial and temporal control of gene expression (McCracken et al., 2023). A single gene can be regulated by multiple enhancers (Visel et al., 2009). Identification of enhancer regions provide a clear link between transcription factor binding and gene expression. Enhancer regions can be identified by increased levels of histone modifications, specifically H3K1Me1 and H3K27ac, and an absence of H3K4me3 (associated with promoters) (McCracken et al., 2023). By identifying which genes ZEB1 regulates, and where that regulation is taking place, we can use this to hypothesise what effect ZEB1 expression, or lack of, may have on the overall lymphatic cell phenotype and the underlying pathways responsible.

3.1.1. Gene silencing using siRNAs

The use of short interfering RNAs (siRNAs) can be used to study the effect of gene silencing in HDLECs. siRNAs are 21-23 base pair sequences which mediate post-transcriptional silencing (Elbashir et al., 2001). This process involves an RNase III family ribonuclease, Dicer, which recognises and processes the siRNA to dsRNA with 3'dinucleotide overhangs. The RNA-inducing silencing complex (RISC) assembles to incorporate the guide strand into the complex, degrades the target mRNA and silences endogenous gene expression (Sontheimer, 2005). siRNAs are now commercially available to target genes of interest and protocols are available for the specific transfection, including those optimised for transfection into HDLECs (Tabrizi et al., 2022). Methods optimised for HDLEC transfection utilise a lipid-based method of transfection, termed lipofection; this is a chemical gene transfer method, whereby a cationic lipid is mixed with a neutral lipid, forming liposome vesicles with a net positive charge by which nucleic acids (the target siRNA) is adsorbed. The net positive charge facilitates endocytosis into the cell (Gopalakrishnan and Wolff, 2009). The lipofection method optimised for siRNA delivery is high efficiency, allows transient and stable transfection and can transfect primary cells. Another method of siRNA transfection is electroporation, which involves high-voltage pulses of

electricity, however this has a poorer cell survival rate (Gopalakrishnan and Wolff, 2009).

The siRNA-mediated silencing should be as specific as possible to limit off-target effects. Off target transcript silencing can occur because of complementarity of transcripts to the seed region of the siRNA (Jackson et al., 2006). Designing a siRNA with a low seed complement frequency induced fewer off target effects (Anderson et al., 2008). Dharmacon uses this information to develop of mechanism of gene silencing, algorithms are used to eliminate common seed regions likely to cause off-target effects. Dharmacon also offer a SMARTpool of siRNAs, with 4 siRNAs provided in a mixture to maximise potency and specificity. Their ON-TARGETplus siRNA is guaranteed to silence target gene expression by 75% at mRNA level (Horizon Discovery, 2023).

3.1.2 RNA Sequencing

One unbiased, high throughput approach to investigate changes in gene expression is RNA Sequencing (RNASeq). Regulation of RNA transcription and translation has direct consequences on protein synthesis. RNASeq involves the isolation of mRNA from a given sample. This mRNA is fragmented to ensure equal chance of sequencing, then reverse transcribed to cDNA. The cDNA is fragmented into uniform sizes, ensuring equal chance of being sequenced. To each end of the fragmented cDNA, specialised adaptors are ligated, this allows the cDNA library to bind to the sequencer. To generate clusters of DNA for sequencing, target DNA must be amplified in the sample, this occurs by bridge PCR (Adessi, 2000). The DNA library is loaded onto a flow cell, where oligonucleotides complementary to the adaptors allow for capture of the cDNA fragments, and consequent amplification. These can be sequenced using several different platforms such as Illumina, pyrosequencing and Sequencing by Oligonucleotide Ligation and Detection (SOLiD) (Shendure and Ji, 2008). Illumina sequences the DNA using fluorescently labelled nucleotides with each base labelled with a different wavelength, these can be imaged as incorporated into the DNA, and the emission documented. The fluorescent tag is then cleaved,

and the process repeats. Once complete, the reads are aligned to a reference genome, and differences in reads counts can be determined (Shendure and Ji, 2008).

Qiagen's Ingenuity Pathway Analysis (IPA) is commercial online software which enables gene-set enrichment analysis of any gene or protein list. This tool was built help to understand the biological significance underlying a simple gene list, by using a purpose-built Ingenuity knowledge base. This is repository of over 26 million individually curated findings from sources, including published literature, which is maintained and updated daily (QIAGEN Digital Insights, 2023). This allows information on relationships between molecules, between molecules and diseases, and biological functions to be highlighted and investigated. Significant pathways are identified using over-representation analysis, and a further depth is achieved by predicting pathways that will be activated or inhibited based on the data. Additionally, upstream regulators are also identified, and their activity predicted allowing indication of the key mediators of the downstream affects present in the data (QIAGEN Digital Insights, 2023). Other gene ontology software is also available, such as Kyoto Encyclopedia of Genes and Genomes (KEGG).

3.1.3 Chromatin Immunoprecipitation

Chromatin is a mixture of DNA and any associated proteins. Chromatin packaging influences transcription by enabling or limiting access to DNA-binding proteins. Chromatin immunoprecipitation (ChIP) is an antibody-based experiment whereby the DNA-binding proteins along with their target DNA fragments, associated with the protein of interest are enriched in the sample. During ChIP, the native protein-chromatin interactions are initially preserved using a fixative, such as formaldehyde. This chromatin is then sheared either by enzymes or by sonication to smaller 200-600 base pair fragments, followed by the addition of the antibody against the protein of interest, and specific chromatin-protein complexes are immunoprecipitated. The cross links are then reversed, the released chromatin can either be sequenced genome-wide – by ChIP-chip utilising a DNA microarray, or by ChIPSeq or ChIP-PCR to identify single genes of interest (Park, 2009). For whole genome sequencing, ChIPSeq is a highly sensitive method of mapping DNA-binding

proteins to base pair resolution. This method utilises next generation sequencing such as Illumina, with paired end sequencing – where the 5' and 3' ends of the DNA are both sequenced – to map long range chromatin interactions (Park, 2009). The raw data produced from this process are images, this require a base caller, which converts the image data to sequence tags, which can be aligned to reference genome. This goes alongside with quality scores, indicative of the reliability of each base call. Peak calling requires a specific program, which will convert the aligned short reads to peaks in the dataset (Park, 2009). These peaks are cross-referenced with the reference genome. Statistical analysis of these enriched sites can then take place to identify true binding regions of the DNA (Park, 2009). The results of ChIPSeq can be utilised to inform other hypothesis and interpret results, such as gene expression data. For example, the differential expression of a gene correlating with the binding status of a transcriptional regulator.

In this chapter, bulk RNASeq was performed on siRNA ZEB1 knockdown HDLECs. Gene set enrichment, pathway analysis and prediction of upstream regulators was completed using IPA. ChIPSeq was also performed on HDLECs, using an antibody against ZEB1. The results of the RNASeq and the ChIPSeq were cross referenced, allowing identification of genes directly bound by ZEB1 resulting in a change in gene expression. Publicly available data of ChIPSeq binding tracks for histone modifications and DNase-Seq for DNase hypersensitivity sites were acquired from IGV for the identification of promoter and enhancer sites. The results and discussion sections of this chapter will be combined to allow for ease of reading and discussion depth in relation to the figures.

3.2 Hypothesis and Aims

Hypothesis: Loss of ZEB1 will produce a lymphangiogenic RNA signature

Aims:

1. Knockdown ZEB1 from HDLECs
2. Investigate the RNA changes as a result of loss of ZEB1
3. Investigate the direct binding partners of ZEB1 using ChIPSeq

3.3 ZEB1 Knockdown RNA Sequencing

ZEB1 was knocked down from HDLECs using siRNA protocol published (Tabrizi et al., 2022). This consistently achieved over 93% knockdown by protein quantification via western blot, shown in Figure 3.3.1. This is a representative western blot, the exact sample was sent off for sequencing and the knockdown not quantified, however this protocol has been thoroughly tested and consistently produced a successful knockdown of ZEB1 protein expression.

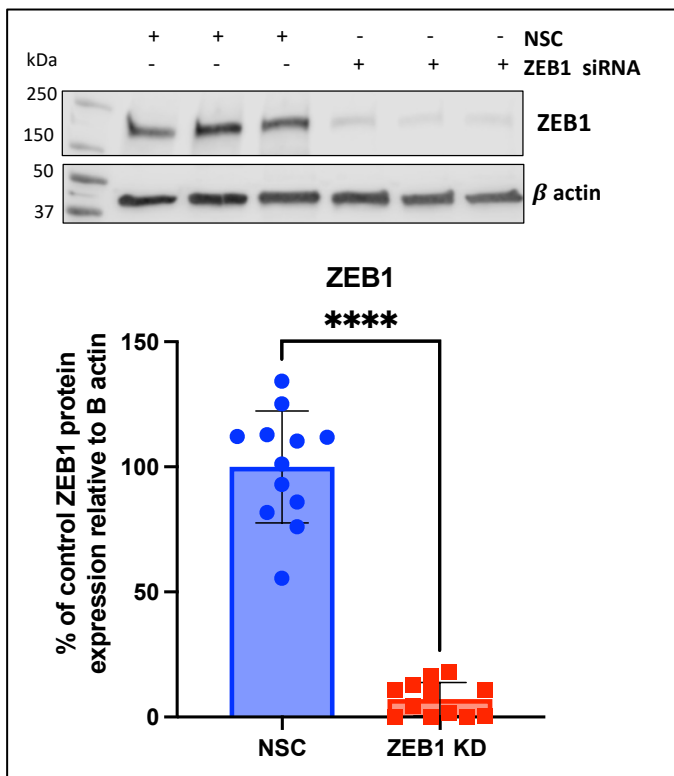


Figure 3.3.1 Consistent knockdown of ZEB1 protein in HDLECs was achieved via siRNA knockdown protocol. Western blot analysis of ZEB1 protein expression in HDLECs following siRNA knockdown of ZEB1. Representative image shown. N=12, statistical analysis by an unpaired t test, ****P<0.0001.

Three replicate samples for each condition were sequenced. The principal component analysis (PCA) plot (Figure 3.3.2) shows the variation between the samples within each condition. This plot shows distinct clusters containing the replicates for each condition, suggesting the transcription profiles of the replicates of

the experimental groups were similar, and the transcription patterns between the control and knockdown cells are distinct.

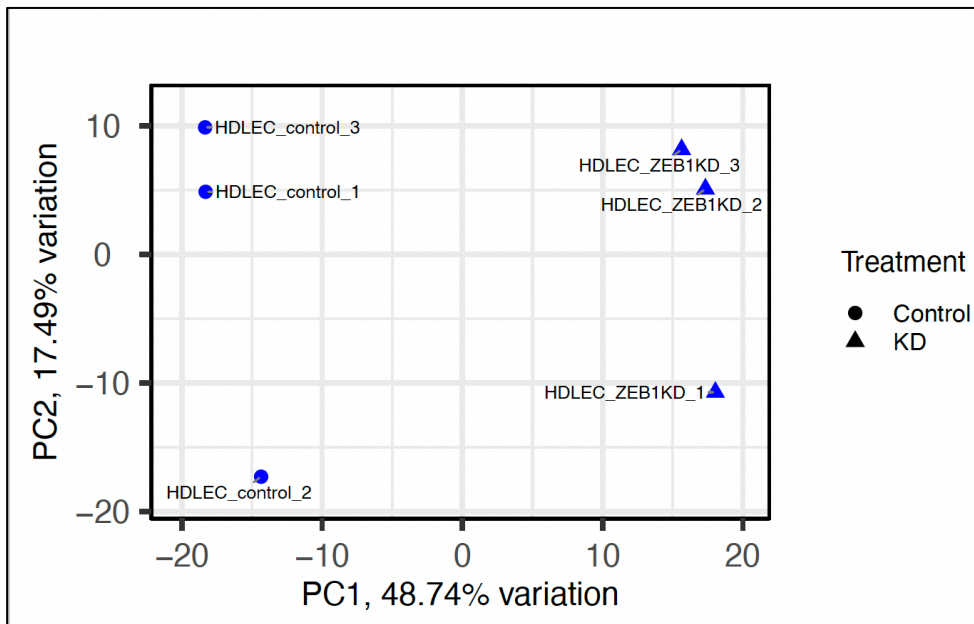


Figure 3.3.2. ZEB1 knockdown samples have a distinct transcriptional pattern in comparison to the control. The three replicates for each condition share similar transcriptional profiles. PCA plot generated by Joseph Horder.

The volcano plot (Figure 3.3.3) shows the statistical significance compared to the fold change of gene expression following ZEB1 knockdown. ZEB1 is visible as a significantly downregulated gene (Figure 3.3.3). A total of 2727 genes were differentially expressed following ZEB1 siRNA knockdown (1404 upregulated, 1323 downregulated).

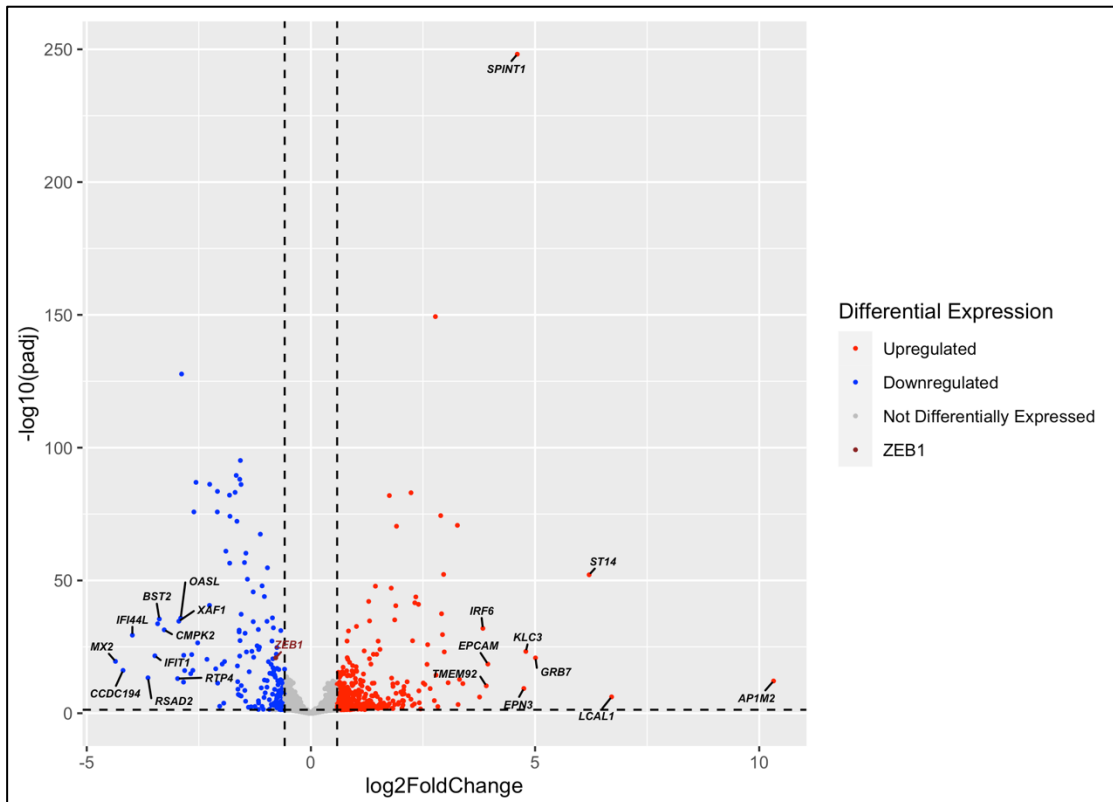


Figure 3.3.3. ZEB1 knockdown results in the differential expression of genes following RNA Sequencing. Volcano plot created by Joseph Horder. Genes are coloured if they pass the thresholds of false discovery rate (FDR) and log2FoldChange. Red dots are upregulated genes, blue dots are downregulated. The top 10 significantly upregulated and downregulated genes are labelled.

3.3.1 The Top 10 differentially expressed genes are representative of a lymphangiogenic phenotype

The top 10 differentially expressed upregulated and downregulated genes following ZEB1 knockdown in terms of Log2FoldChange are shown in Table 3.3.1. The top downregulated gene was MX2 (Log2FoldChange = -4.36, $P_{adj} = 2.85E-20$) this gene mediates interferon signalling (Juraleviciute et al., 2021), and is strongly expressed in lung LECs in the fetal lung (Norman et al., 2019). Interestingly MX2 was seen to regulate XAF1 in relation to the interferon pathways (Juraleviciute et al., 2021), which was also amongst the top 10 downregulated genes, suggesting this activity of this pathway (also seen in top canonical pathways, Figure 3.3.3.1) has been dysregulated following loss of ZEB1. The top upregulated gene was AP1M2 (Log2FoldChange 10.32, $P_{adj} = 7.23E-13$). This gene encodes the M2 subunit of the adhesive protein associated adapter protein complex 1 (AP-1), which functions in the

trans-golgi network to mediate protein sorting in the endothelium. This factor has been positively associated with poor prognosis in a variety of malignant tumours including breast, liver, and lung cancer (Yi et al., 2022). Specifically AP1M2 appeared to suppress immunocyte infiltration in these tumours, potentially enhancing tumour progression and malignancy (Yi et al., 2022). Another gene of interest which was upregulated in this dataset is epithelial cell adhesion molecule (EPCAM [Log2FoldChange 3.95, P_{adj} = 3.07E-19]), this protein is a pan epithelial marker, implicated in cell-cell adhesion and oncogenic signalling (Balzar et al., 1999; Osta et al., 2004). EPCAM is thought to exhibit oncogenic potential through the activation of Wnt/ β -catenin signalling in hepatocellular carcinoma (Yamashita et al., 2007). Interestingly the Wnt/ β -catenin signalling pathway has recently been implicated in lymphangiogenesis through induction of partial EndMT in LECs (Wang et al., 2017).

Table 3.3.1.1 Top 10 upregulated and downregulated genes in the Control versus ZEB1 knockdown treated HDLECs. Sorted by Log2FoldChange, P adjusted value is shown for each gene. Average basal expression of the normalised counts of three non-silencing control replicates.

Downregulated Genes				
ENSEMBLE ID	Gene Symbol	Log2FoldChange	P _{adj}	Basal Expression
ENSG00000183486	MX2	-4.3594712	2.85E-20	4385.40673
ENSG00000269720	CCDC194	-4.1905546	7.48E-17	91.7498908
ENSG00000137959	IFI44L	-3.9828376	4.05E-30	2908.926026
ENSG00000134321	RSAD2	-3.6341834	4.53E-14	2056.2868
ENSG00000185745	IFIT1	-3.4802755	2.42E-22	3239.387289
ENSG00000225886	Novel transcript	-3.4185795	2.02E-34	234.4803423
ENSG00000130303	BST2	-3.3813285	3.31E-36	2911.350391
ENSG00000134326	CMPK2	-3.2717992	4.02E-32	1401.266021
ENSG00000136514	RTP4	-2.9734449	9.13E-14	98.68966244
ENSG00000132530	XAF1	-2.9461024	2.27E-35	255.0696197

Upregulated Genes				
ENSEMBLE ID	Gene Symbol	Log2FoldChange	P _{adj}	Basal Expression
ENSG00000129354	AP1M2	10.3194733	7.23E-13	0
ENSG00000286042	LCAL1	6.70666165	6.89E-07	0.349686922
ENSG00000149418	ST14	6.20629985	7.29E-53	5.301891334
ENSG00000141738	GRB7	5.00909233	1.42E-21	3.129546995
ENSG00000104892	KLC3	4.79358929	5.34E-24	3.733881304
ENSG00000049283	EPN3	4.74935351	4.82E-10	1.418056664
ENSG00000166145	SPINT1	4.60337968	7.00E-25	67.357138
ENSG00000119888	EPCAM	3.94659242	3.07E-19	5.199876154
ENSG00000167105	TMEM92	3.91146172	4.71E-11	3.506021122
ENSG00000117595	IRF6	3.83616827	1.13E-32	7.071476922

3.3.2 ZEB1 knockdown in LECs affects the RNA expression of known upstream and downstream interactors

DEGs were uploaded into Ingenuity Pathway Analysis (IPA). ZEB1 was identified in the dataset as significantly downregulated (Log2FoldChange = -0.784 P_{adj} = 1.34E-21). The DEGs were explored using IPA to identify those genes with a known or putative interaction with ZEB1, with results shown in Figure 3.3.2.1. A large quantity of these genes had gene expression patterns which correlated differently to their known, published interaction with ZEB1 shown by a yellow connecting line. It is important to note that IPA does not distinguish cell type, thus the literature database it uses will include known interactions in a variety of cell types and environments. Each one of these relationships shown in Figure 3.3.2.1. can be investigated further by looking at the papers (Ingenuity knowledge base) used to establish this relationship. An example of this is ETS1, which had a decreased measurement in the dataset (Log2FoldChange= -0.195, P_{adj} = 0.034). IPA connects ETS1 and ZEB1 with inhibition; however, in the literature, there is a well-documented positive relationship between ETS1 and ZEB1 in epithelial cells, this was found via gene expression data, gene reporter assays and ChIP experiments (Loh et al., 2019; Sinh et al., 2017; Dave et al., 2011; Shirakihara et al., 2007). We have manually knocked down ZEB1 via siRNA,

thus we know the decreased measurement of ZEB1 was not through its relationship with ETS1, however, we could suggest that there is some kind of feedback loop in play, as ZEB1 appears to reciprocally regulate ETS1 expression. ITGB4, KRT18, MPZL2, BAX, ABCA3, CDKN2A, KRT19, BBC3, MAL2 and ESRP2 all have a significant increase in gene expression when ZEB1 was knocked down. These genes have also been identified by others using similar techniques to our work, for example, MPZL2 (EVA1) has been identified to be regulated by ZEB1 expression following siRNA knockdown in pancreatic cells, this data found increased MPZL2 expression following ZEB1 siRNA interference (Arumugam et al., 2009), as shown in our results (Log2FoldChange = 1.91, $P_{adj} = 3.86E-71$) (Figure 3.3.2.1). Interestingly, the MPZL2 gene encodes an epithelial junctional protein, involved in cell-cell interactions in developing tissues (Wesdorp et al., 2018).

There were also cases where alterations in gene expression are not predicted, for example the GATA2-ZEB1 relationship is derived from work carried out by Göös et al., in human embryonic kidney cells (HEK293). This paper states there is binding between GATA2 and ZEB1 in humans (Göös et al., 2022) but as for the effect on gene expression, this binding/interaction has not been investigated. In our data (Figure 3.3.2.1) we had a significant increase in GATA2 expression (Log2FoldChange = 0.22, $P_{adj} = 0.008$) following ZEB1 reduction. GATA2 is a zinc finger transcription factor which is essential for lymphatic valve development and maintenance (Kazenwadel et al., 2015). This transcription factor has also been involved in regulating other key members of lymphatic development, PROX1 and FOXC2 (Kazenwadel et al., 2015). PROX1 was downregulated in our dataset (Log2FoldChange = -0.633, $P_{adj} = 1.89E-10$), however FOXC2 was unchanged (Log2FoldChange = 0.168, $P_{adj} = 0.309$). FOXC2 is a mechanosensitive transcription factor, which executes its role in high areas of mechanical stress, such as valves (González-Loyola et al., 2021), as this dataset is from cultured HDLECs not experiencing a change in flow, no change in FOXC2 expression would be predicted. The changes in the RNA expression of GATA2 and PROX1 are enough to suggest a dysregulation of key markers of lymphatic development and maintenance with loss of ZEB1.

In our results, following ZEB1 downregulation, CDH2 expression was increased (Log2FoldChange = 0.48, P_{adj} = 0.0045), on Figure 3.3.2.1 this has been deemed inconsistent with the literature. CDH2 (N-Cadherin) expression has been associated with tumour aggressiveness, metastasis, and angiogenesis in cancers (Kaszak et al., 2020). This inconsistency could be due to a variety of reasons, for example the published literature used to establish a connection between CDH2 and ZEB1 is suggestive of an indirect (dashed line) relationship whereby decreased ZEB1 decreases CDH2 expression which is increased by ET1 protein (Sestito et al., 2022). However, this referenced literature is in a different cell type to our research, and in a disease (high grade ovarian cancer) environment. This interaction is also indirect, it could be the mediator of this interaction ET-1 (vasoconstrictor endothelin 1, EDN1) is not present, or upregulated in our sample (EDN1 is present in the RNA reads, but not differentially expressed in this dataset, P_{adj} value = 0.98). In tumour-derived ECs, CDH2 was found upregulated which promoted *in vitro* and *in vivo* angiogenesis (Zhuo et al., 2019). N-cadherin is generally considered a mesenchymal marker, with the gain of expression seen in EndMT (Gaikwad et al., 2023). Therefore, unlike in cancer settings, lack of ZEB1 appears to be promoting a mesenchymal, migratory phenotype, associated with vascular remodelling.

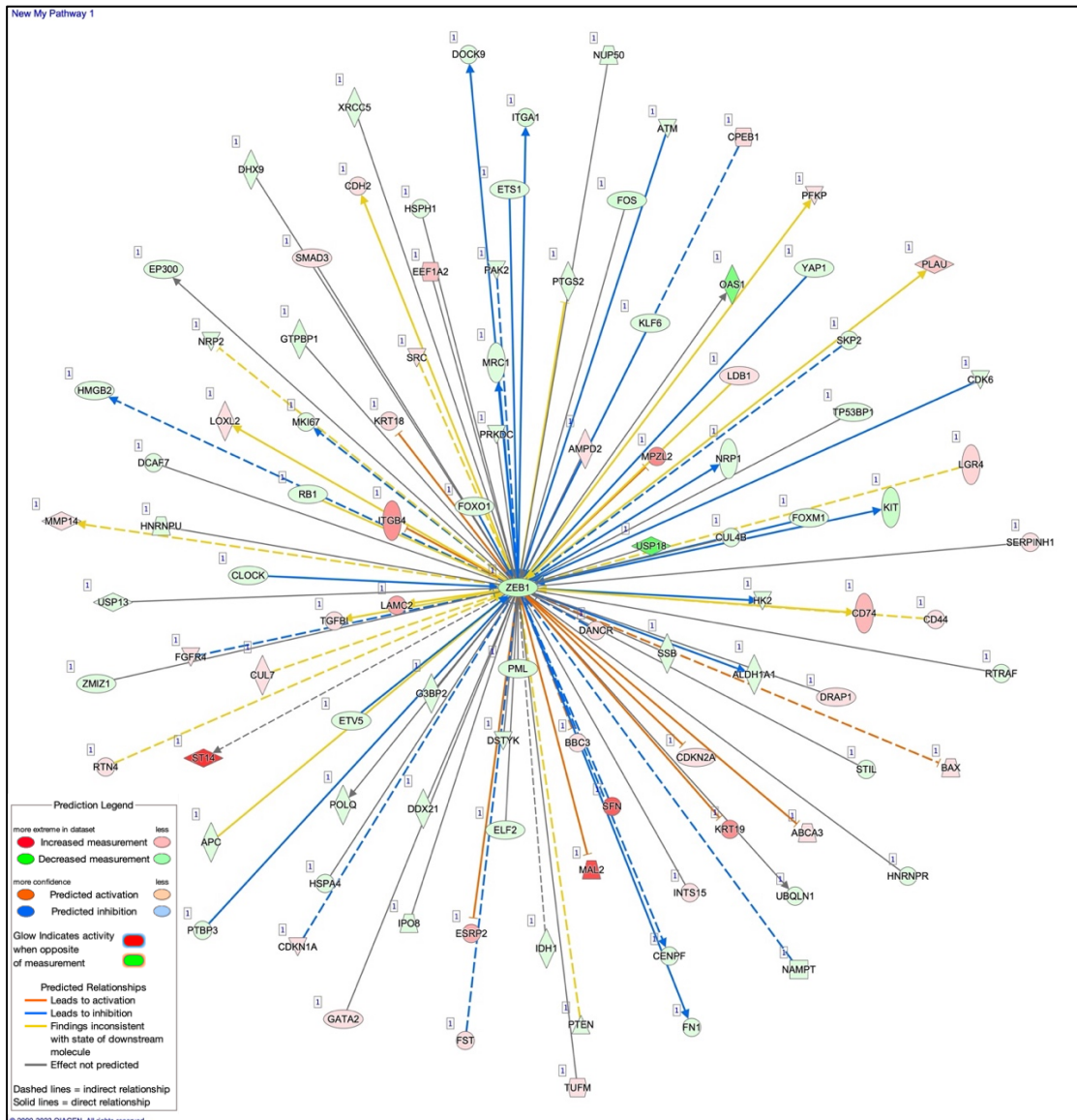


Figure 3.3.2.1 ZEB1 knockdown results in changes in expression of published interacting molecules. Based on the DEGs from the dataset, genes with a known relationship with ZEB1 are represented on the diagram using Ingenuity Pathway Analysis Software (QIAGEN).

3.3.3 Top canonical pathways

Alterations in APC involved in known canonical pathways can be grouped together to establish the effect of ZEB1 knockdown in known molecular mechanisms. The bar chart shown in Figure 3.3.3.1 shows the top five canonical pathways with the most alterations in gene expression in this dataset. As ZEB1 plays a known role in cancer progression (Joseph et al., 2014; Fu, Li, et al., 2020; Galván et al., 2015; Wels et al., 2011a) the top canonical pathway “Molecular Mechanisms of Cancer” is unsurprising. The overall activity pattern was unavailable for this pathway, this is

likely due to the sheer number of dysregulated genes in this large pathway (Figure 3.3.3.2).

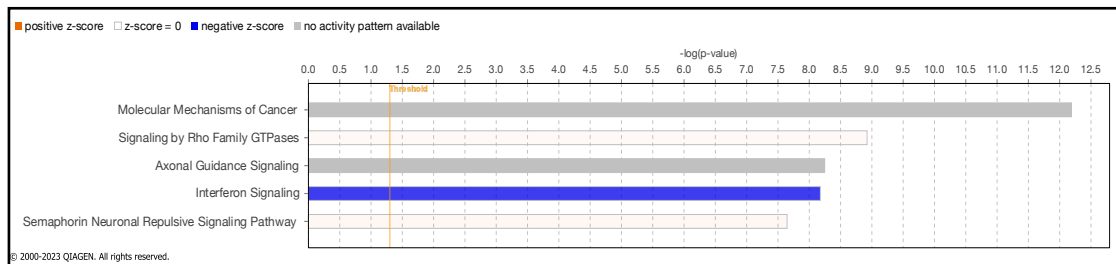


Figure 3.3.3.1 The top five canonical pathways with genes affected by ZEB1 knockdown.

Based on the differentially expressed genes from the dataset, genes canonically associated to established pathways represented on the bar chart. A positive Z-score suggests this pathway is activated in the sample; a negative Z-score is inhibition of this pathway. The grey bar is no activity pattern available. Generated using IPA.

In Molecular Mechanisms of Cancer, neither enhanced or downregulation of activity was predicted, genes included in the dataset and predicted changes of proteins not in the dataset, are displayed in Figure 3.3.3.2. In this figure, there is a mix of both activated and inhibited pathways, hence the overall activity pattern of this pathway was not predicted. Unexpected relationships where the predicted relationship between two proteins in the pathway do not fit the RNA expression pattern in our dataset, are also present. This canonical pathway is a disease mechanism which often results in dysregulation of many genes; thus, interactions will differ in comparison to our dataset, which is knockdown of one gene. However, there will be some mechanisms within this pathway, such as regulation of the cell cycle, apoptosis and metabolism that are common to all cell types. There was predicted of activation of the cell cycle, and inhibition of apoptosis through the decreased measurement of FOXO1 in the dataset ($\text{Log}_2\text{FoldChange} = -0.25$, $P_{\text{adj}} = 0.007$). FOXO1 is thought to be the master of quiescence, deletion of this gene in lymphatics enhanced valve formation in mice (Scallan et al., 2021). This suggests knockdown of ZEB1 may induce a growth-like phenotype, through decreased FOXO1. However, also seen in this figure are two incidences where cell survival is inhibited, through predicted inhibition of $\text{NF}\kappa\text{B}$ and of the BMP signalling pathway. These activity predictions are based on the differential expression of genes in the dataset which are up- or downstream of the predicted mediator.

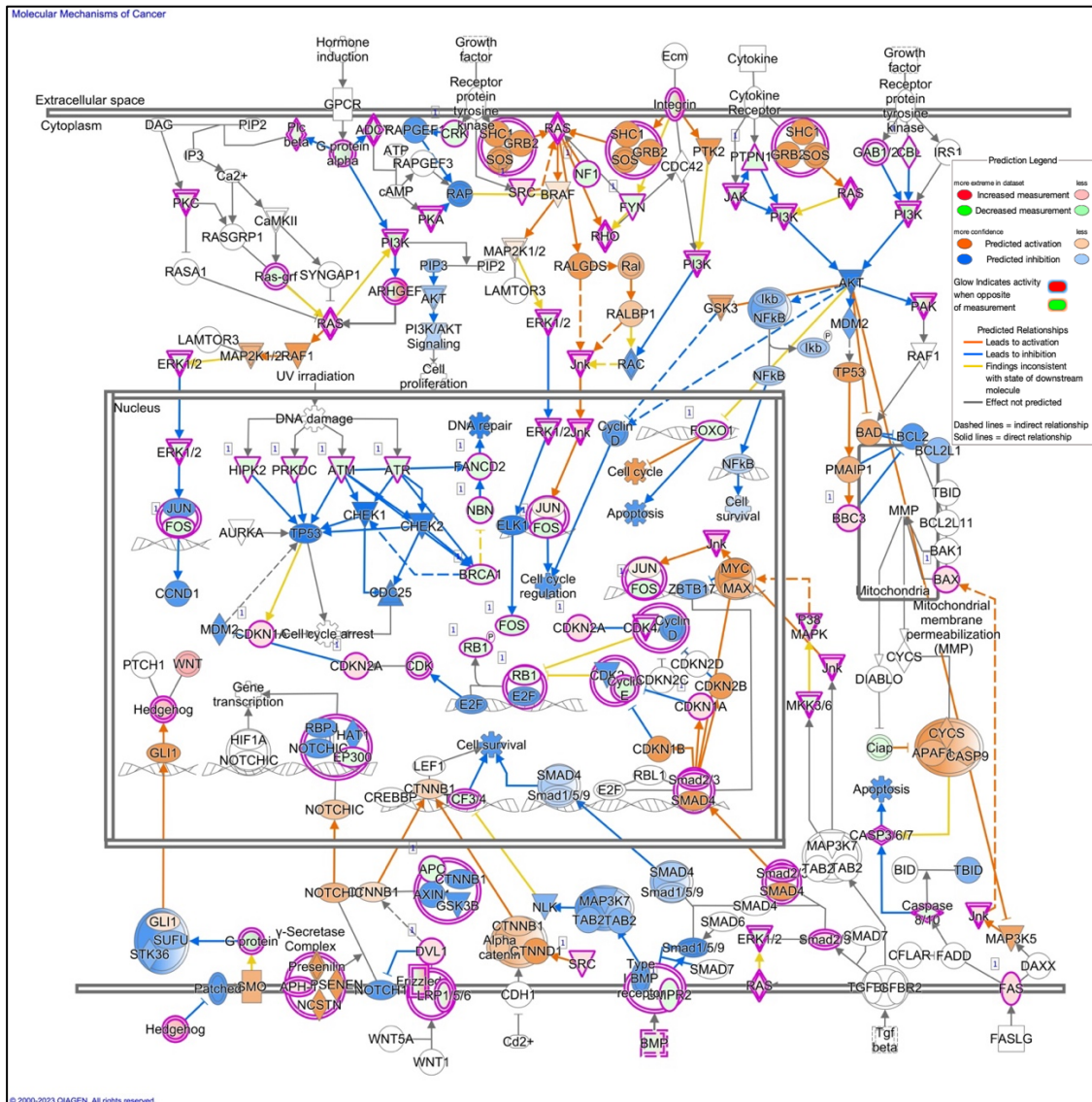


Figure 3.3.3.2 ZEB1 knockdown significantly impacts genes associated with the pathway Molecular Mechanisms of Cancer. Based on the differentially expressed genes from the dataset. Genes that form complexes as proteins are encircled in pink. Predicted effects are also shown (blue – inhibited, orange – activated) on downstream proteins in the pathway. Created using IPA (QIAGEN).

The Interferon Signalling Pathway was predicted to be inhibited following ZEB1 knockdown (Z-score = -2.828, $-\log(P\text{-value}) = 8.177$). This is due to the large quantity of downregulated genes within the pathway, present in the dataset (Figure 3.3.3.3). The interferon signalling pathway has anti-viral, anti-tumour and immunomodulatory effects (Takaoka and Yanai, 2006). Downregulation of this pathway is seen in tumours, decreasing the innate immune response, and aiding tumour progression. This is thought to be due to the increase in MYC expression (Zimmerli et al., 2022). In our dataset, MYC was not differentially expressed at the RNA level (Log2FoldChange

= -0.024, $P_{\text{adj}} = 0.46$) but predicted active at a protein level (Figure 3.3.3.2). ZEB1 has already been implicated in other cell types with controlling the gene expression of members of the interferon pathway. For example, IRF6 is directly negatively regulated by ZEB1 in gastric cancer (Li et al., 2019), in our dataset this idea is supported, as IRF6 was one of the most upregulated genes following ZEB1 knockdown ($\text{Log}_2\text{FoldChange} = 3.84$, $P_{\text{adj}} = 1.13\text{E-}32$). The overall effect on ZEB1 in this pathway is downregulation, as shown by the negative Z-score in Figure 3.3.3.1 ($Z\text{-score} = -2.828$). In tumours, this action of ZEB1 is thought to promote migration, invasion, and metastasis, leading to a poorer overall prognosis (Chen et al., 2014). The consequences of inhibition of interferon signalling in lung ECs has been shown to enhance proliferation, as when present, $\text{IFN}\gamma$ signals through JAK/STAT signalling resulting in an anti-proliferative effect (Laug et al., 2012). Therefore, we can suggest through inhibition of the interferon signalling pathway we may see an enhanced migratory phenotype in these LECs.

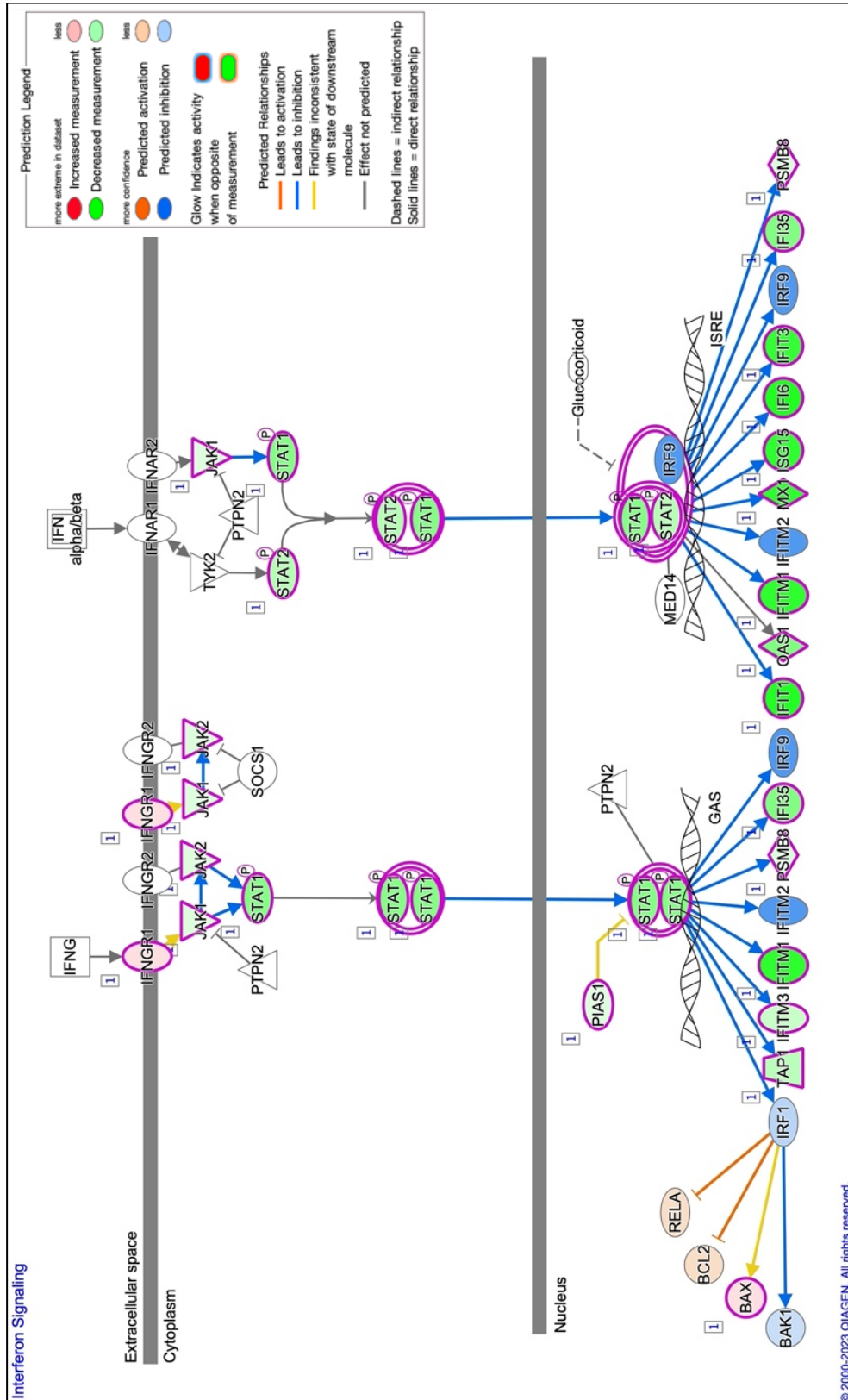


Figure 3.3.3.3 ZEB1 knockdown significantly impacts genes associated with Interferon Signaling. Based on the differentially expressed genes from the dataset. Genes that form complexes as proteins are encircled in pink. Predicted effects are also shown (blue – inhibited, orange – activated) on downstream proteins in the pathway. Created using IPA.

3.3.4 Loss of ZEB1 has an overall inhibitory effect on the EMT pathway

The epithelial to mesenchymal pathway is of significant interest to this work. ZEB1 is a key inducer of the EMT process. In Figure 3.3.4.1 we can see the predicted effect of knockdown of ZEB1 in the wider context of the EMT pathway. It is important to note the EMT process does not occur in ECs, we are using this canonical pathway to understand the effects of ZEB1 on an established pathway like EMT, which shares many similarities to EndMT. This pathway was predicted inhibited overall, with a Z-score = -0.781 and $-\log(\text{P-value}) = 5.787$. The EMT pathway is extensive, but only 44 of these molecules are present in the dataset, therefore the overall implications of the pathway are largely predictive based on the RNA expression of known interacting partners.

These predictions are contrasting at points. Both “EMT” and “mesenchymal cell activation” were predicted activated and inhibited in the sample due to multiple mechanisms of regulation. Following the TGF β side of the figure, based on the increased measurement of phosphorylated SMAD2/3, subsequent translocation into the nucleus where enhanced SMAD4 is predicted, this leads to increased CDH2 (N-cadherin), as seen in the dataset ($\text{Log2FoldChange} = 0.48$, $P_{\text{adj}} = 0.0045$), which leads to EMT (Loh et al., 2019).

Reaching other EMT markers of EMT, SNAI1 (SNAIL) and SNAI2 (SLUG) were predicted to be both activated and inhibited at different points in this pathway at a protein level. The RNA expression of these genes was unchanged between our control and ZEB1 knockdown samples ([SNAIL - $\text{Log2FoldChange} = 0.08$, $P_{\text{adj}} = 0.99$], [SLUG - $\text{Log2FoldChange} = -0.60$, $P_{\text{adj}} = 0.99$]). These transcription factors are known inducers of EMT and EndMT (Wels et al., 2011a; Cai et al., 2015; Kokudo et al., 2008). Downstream of these transcription factors, EMT was predicted inhibited when ZEB1 is involved, due to the downregulation of ZEB1 found in the dataset, and the predicted effects on the common node in this pathway CDH1. This gene encodes E-Cadherin, and was predicted activated, as inhibition of ZEB1 has been shown to

increase CDH1 expression previously (Loh et al., 2019; King et al., 2020; Sestito et al., 2022).

In pathways where ZEB1 is not directly involved, we saw predicted inhibition of both SLUG and SNAIL, largely due to decreased measurements of members of MEK/ERK signalling pathway. EGR1 (early growth response protein 1) is upstream of SNAI1 in this pathway and was downregulated in the dataset following ZEB1 knockdown ($\text{Log}_2\text{FoldChange} = -0.98$, $P_{\text{adj}} = 1.59\text{E-}10$). Through established interactions in epithelial cells, which state ERG1 enhances SNAI1 expression (Derynck et al., 2014; Grotegut et al., 2006), SNAIL was predicted at protein level to be inhibited.

We are faced with limitations of how much of this pathway can be interpreted, for example, E-cadherin is not expressed in ECs (Bobryshev, 1998). In our dataset, there were no reads of this gene in either sample, so several pathway predictions are not true for our dataset. Thus, although we can extrapolate some interpretation from this pathway, we are limited by cell specific proteins.

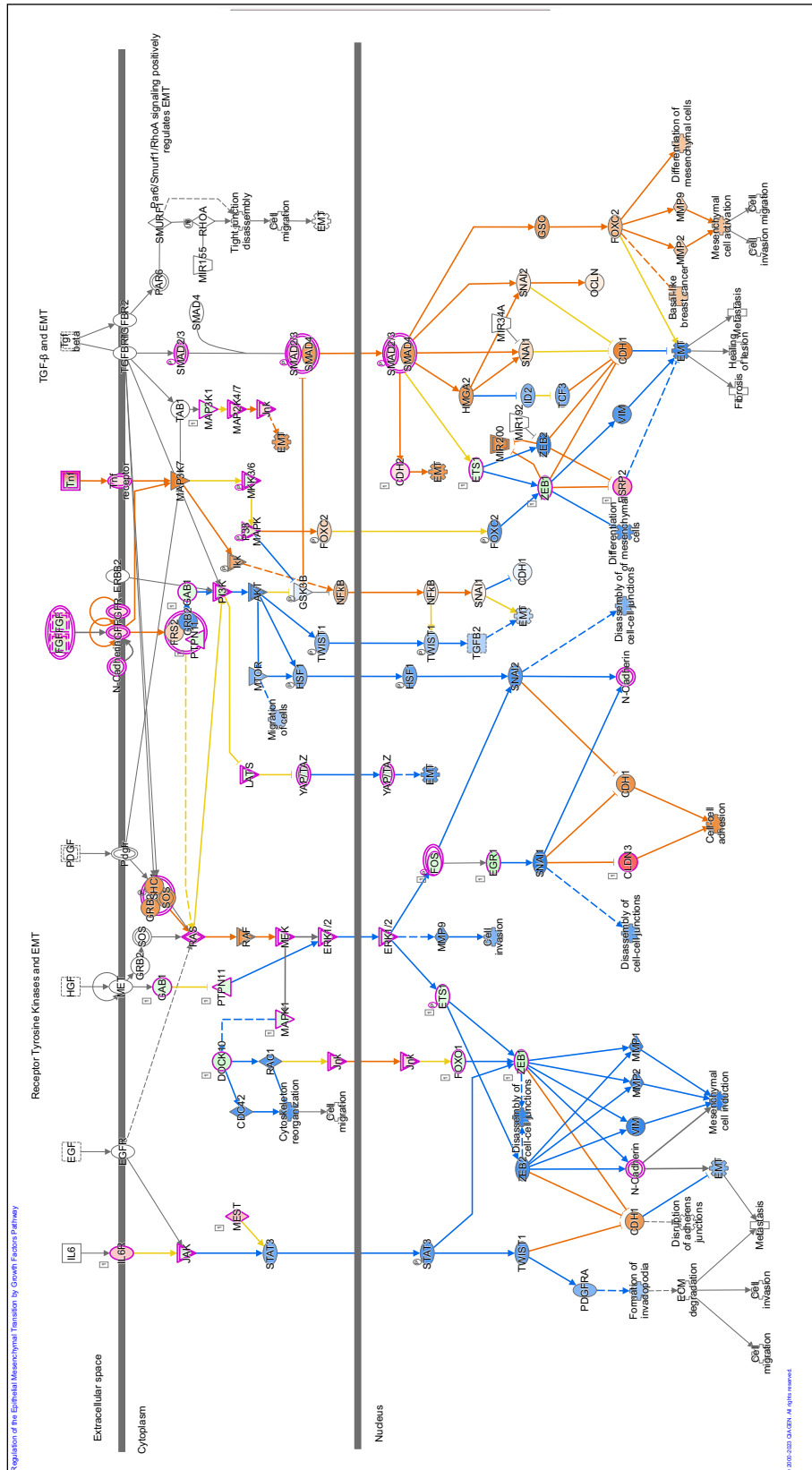


Figure 3.3.4.1 ZEB1 knockdown significantly impacts genes associated with Epithelial to Mesenchymal Transition by Growth Factors. Based on the differentially expressed genes from the dataset, genes from the dataset are highlighted in pink, alongside predicted effects (blue – inhibited, orange – activated) on downstream proteins in the pathway. Created using IPA.

3.3.5 Impact on Biological Functions and Disease

There were 2727 dysregulated genes in our dataset. These genes were analysed through IPA into categories based on their function in physiology and disease (Figure 3.3.5.1). From our gene list, 2602/2727 were involved in cancer pathophysiology, and 2626/2727 were involved in organismal injury and abnormalities. This suggests the loss of ZEB1 is highly relevant in disease, as many genes in this dataset have all previously been attributed in the literature to cancer and abnormalities in physiology. Biologically, this indicates the pathways which are under the control of ZEB1, or highly regulated by ZEB1 should be investigated for therapeutic intervention. Regarding molecular and cellular function, “cellular assembly and organisation” was the most significant with 932/2727 genes involved in this process. Similar terms “cellular function and maintenance” and “cellular development” highlight the impact of ZEB1 on these genes crucial for normal cell functioning. For our hypothesis, the term “Cellular movement” gives an indication of the endothelial to mesenchymal transition we believe may be partially occurring following ZEB1 knockdown, as we would see changes in cell-cell contacts, and ECM degradation facilitating cell movement from the endothelium. Regarding physiological systems, overall organism survival and development are top terms in this summary (Figure 3.3.5.1). This is perhaps not surprising as total ZEB1 knockout *in vivo* is embryonic and perinatal lethal (Takagi et al., 1998), combined with our results in LECs, we may suggest ZEB1 is essential for the normal functional development of LECs due to the molecular signature of genes regulated by its loss.

Top Diseases and Bio Functions		
Diseases and Disorders		
Name	p-value range	# Molecules
Cancer	2.05E-08 - 6.74E-199	2602
Organismal Injury and Abnormalities	2.09E-08 - 6.74E-199	2625
Endocrine System Disorders	1.25E-08 - 4.85E-178	2336
Gastrointestinal Disease	2.05E-08 - 3.30E-162	2409
Neurological Disease	1.81E-08 - 4.08E-129	2057
Molecular and Cellular Functions		
Name	p-value range	# Molecules
Cellular Assembly and Organization	1.27E-08 - 2.58E-54	932
Cellular Function and Maintenance	1.27E-08 - 2.58E-54	1074
Cellular Movement	2.03E-08 - 1.90E-51	881
Cell Death and Survival	1.59E-08 - 1.21E-50	1059
Cellular Development	1.97E-08 - 1.91E-49	1192
Physiological System Development and Function		
Name	p-value range	# Molecules
Organismal Survival	2.52E-10 - 5.00E-55	893
Cardiovascular System Development and Function	1.15E-08 - 4.00E-31	546
Organismal Development	1.84E-08 - 2.41E-29	1166
Tissue Development	1.65E-08 - 9.79E-29	937
Tissue Morphology	1.79E-08 - 1.59E-21	841

Figure 3.3.5.1 Summary of Biological Functions and Diseases which are enriched in a dataset of ZEB1 knockdown of HDLECs. Based on the differentially expressed genes from the dataset, which are categorised into known functions according to the literature. Created using IPA.

3.3.6 The effect of ZEB1 on transcriptional regulation

ZEB1 is zinc-finger E-box binding transcription factor, the impact of knockdown on this gene resulted in the differential expression of 2727 genes. It is highly likely the mechanism of action involves activation or inhibition of upstream transcription factors to enable this broad impact on gene expression in the sample. Using IPA, upstream analysis allowed for prediction of the activity of known transcriptional regulators, based on the expression of downstream molecules in the dataset. The top 10 most inhibited and activated transcriptional regulators are shown in Table 3.3.6.1. Five of the top 10 most inhibited transcriptional regulators are members of the Interferon family – IRF7, IRF1, IRF3, IRF9, IRF5. As shown in Figure 3.3.3.3, the Interferon Signalling Pathway was one of the most inhibited canonical pathways in this dataset. Therefore, based on this inhibition, there would be expected inhibition in transcriptional activators, and activation of transcriptional repressors upstream.

Two of the most activated transcriptional regulators are ETV6 (Z-score = 7.040) and ETV3 (Z-score = 7.000). These genes are known as transcriptional repressors, which have been shown to inhibit interferon stimulated genes (Villar et al., 2023). The

Interferon Signalling Pathway was also present in the top five dysregulated canonical pathways (Figure 3.3.3.1), further emphasising the impact of ZEB1 on regulation of this signalling. Another role of ETV3 and ETV6 is enabling monocyte differentiation to dendritic cells by repressing macrophage commitment (Villar et al., 2023). Therefore, we could speculate a role of these transcription factors in the control of cell state transitions, alike to EndMT.

Table 3.3.6.1 Top 10 Transcriptional Regulators predicted inhibited and activated as a result of ZEB1 knockdown. Based on the differentially expressed genes from the dataset, the activity of upstream transcriptional regulators is predicted. Created using IPA.

Upstream regulator	Molecule type	Predicted activation state	Activation Z-score
IRF7	transcription regulator	Inhibited	-7.634
COPS5	transcription regulator	Inhibited	-6.865
NONO	transcription regulator	Inhibited	-6.756
CEBPB	transcription regulator	Inhibited	-5.793
IRF1	transcription regulator	Inhibited	-5.517
IRF3	transcription regulator	Inhibited	-5.427
STAT1	transcription regulator	Inhibited	-5.297
IRF9	transcription regulator	Inhibited	-4.934
FOXC1	transcription regulator	Inhibited	-4.832
IRF5	transcription regulator	Inhibited	-4.304

Upstream regulator	Molecule type	Predicted activation state	Activation Z-score
ETV6	transcription regulator	Activated	7.040
ETV3	transcription regulator	Activated	7.000
NUPR1	transcription regulator	Activated	5.364
KMT2D	transcription regulator	Activated	5.155
TRIM24	transcription regulator	Activated	5.146

TCF4	transcription regulator	Activated	4.158
NKX2-3	transcription regulator	Activated	4.127
EHMT1	transcription regulator	Activated	3.771
CITED2	transcription regulator	Activated	3.628
NCOR1	transcription regulator	Activated	3.503

3.4 ZEB1 Chromatin Immunoprecipitation

To investigate direct interactions of ZEB1 in LECs, ChIPSeq was performed. The results of this experiment were cross-referenced and combined with the results from the RNASeq of ZEB1 knockdown of LECs, as shown in Figure 3.4.1. In the ChIPSeq data, 367 genes were identified as direct targets of ZEB1. The overlap between the RNASeq and ChIPSeq was 59 genes (Figure 3.4.1). These genes are displayed in Table 3.4.1. Half of the genes (55%) in this dataset (Table 3.4.1) appear to be regulated by ZEB1 binding outside of the promoter region. It is possible these transcriptional enhancer regions, as these can be found upstream and downstream of the gene, and even within introns (Pennacchio et al., 2013). Enhancer regions of genes are not well annotated, and cannot be identified from DNA sequence alone, additional histone markers such as H3K37ac can help annotate these regions (Pennacchio et al., 2013).

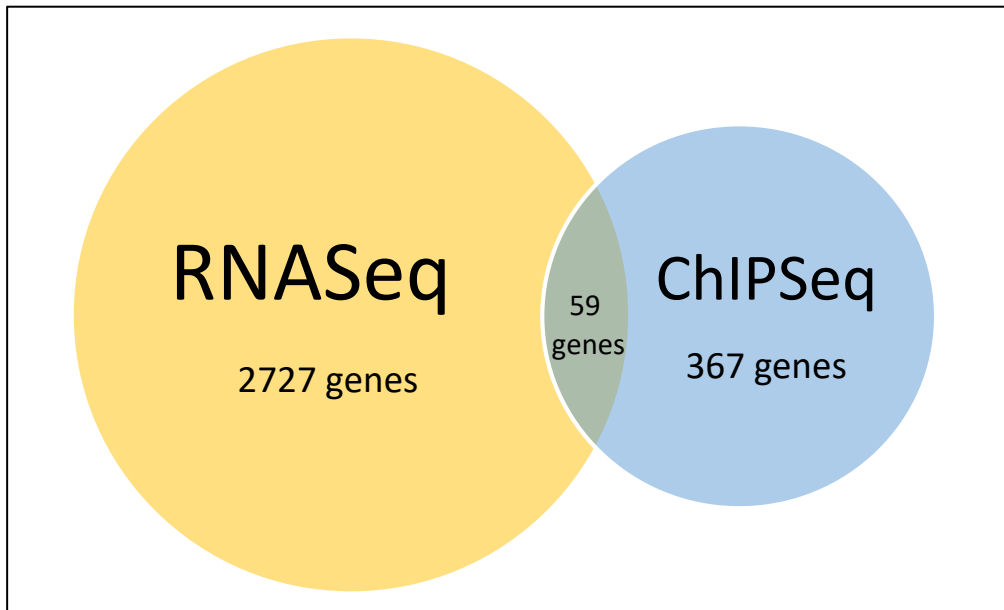


Figure 3.4.1. ZEB1 directly interacts with 367 target genes and alters the gene expression of 59 genes in HDLECs. RNA Sequencing of ZEB1 siRNA knockdown HDLECs and ChIP Sequencing of ZEB1 analysed using DESeq2. 59 genes appeared in both datasets when cross referenced.

Table 3.4.1 Genes which expression is differentially expressed through the direct binding of ZEB1. Results are from the sequencing of Chromatin Immunoprecipitation of LECs with a ZEB1 antibody, cross referenced with the RNA Sequencing results from siRNA knockdown of ZEB1 in LECs. Average basal expression from three non-silencing control replicates.

Symbol	Annotation	Distance ToTSS	ENSEMBL	Log2Fold Change	P _{adj}	Basal expression
HELZ2	Exon (ENST00000427522.6/85441, exon 3 of 14)	-1224	ENSG00000130589	-1.6501	5.28E-73	9056.5752
RNF213	Promoter	106	ENSG00000173821	-1.5869	8.06E-89	18444.0206
SMTNL1	Exon (ENST00000527972.6/219537, exon 3 of 8)	5997	ENSG00000214872	-1.4739	2.62E-09	163.3219
LRRC58	Promoter	181	ENSG00000163428	-0.5092	9.83E-05	652.0155
CPEB3	Exon (ENST00000412050.8/22849, exon 2 of 10)	3225	ENSG00000107864	-0.4620	0.0294	103.3614
ST3GAL5	Promoter	0	ENSG00000115525	-0.4168	0.0065	179.2397
TNS1	Distal Intergenic	22696	ENSG00000079308	-0.3888	0.0002	2111.1441

ZFYVE9	Promoter	0	ENSG00000157077	-0.2728	0.0111	726.2801
BMP2	5' UTR	2334	ENSG00000125845	-0.2704	0.0042	812.9018
TRIP13	Distal Intergenic	6346	ENSG00000071539	-0.2605	0.0060	704.8766
CHD9	Promoter	440	ENSG00000177200	-0.2118	0.0407	1430.1982
SESTD1	Promoter	0	ENSG00000187231	-0.2073	0.0344	1378.7132
IRF2BP2	Promoter	-488	ENSG00000168264	-0.1761	0.0361	2862.0203
UBP1	Distal Intergenic	-12063	ENSG00000153560	-0.1694	0.0173	2252.0436
NACC2	Intron (ENST00000371753.5/138151, intron 2 of 4)	4109	ENSG00000148411	0.1796	0.0455	1009.1097
APCDD1L	Promoter	556	ENSG00000198768	0.1990	0.0467	1.2004
COL18A1	Distal Intergenic	-14775	ENSG00000182871	0.2463	0.0018	16599.8690
CTSA	Promoter	732	ENSG00000064601	0.2488	0.0002	3575.8319
PITPNM2	Exon (ENST00000280562.9/57605, exon 9 of 25)	5139	ENSG00000090975	0.2603	0.0021	2077.6009
MROH1	Promoter	-79	ENSG00000179832	0.2764	0.0110	2014.4322
ARHGAP39	Intron (ENST00000377307.7/80728, intron 1 of 11)	-13925	ENSG00000147799	0.2798	0.050	287.6982
ZC3H12A	Promoter	0	ENSG00000163874	0.2814	0.0461	190.0609
LRP5	Exon (ENST00000294304.12/4041, exon 6 of 23)	-17310	ENSG00000162337	0.2822	0.0011	3767.8798
FASTK	Promoter	0	ENSG00000164896	0.2841	0.0046	1224.6926
LRFN3	Exon (ENST00000588831.5/79414, exon 3 of 4)	3755	ENSG00000126243	0.2953	0.0451	250.3098
SLC2A8	Promoter	285	ENSG00000136856	0.2975	0.0407	206.8612
MCOLN1	Exon (ENST00000597229.2/140467, exon 2 of 2)	-2436	ENSG00000090674	0.3193	0.0067	614.4669

VSIR	Promoter	0	ENSG00000107738	0.3221	0.0265	597.7092
MAP3K10	Promoter	0	ENSG00000130758	0.3315	0.0061	524.9668
ACAP3	Promoter	281	ENSG00000131584	0.3321	0.0195	1718.6732
GRN	Exon (ENST000002 93443.12/28 4069, exon 8 of 8)	2569	ENSG00000030582	0.3348	6.19E-05	11408.7523
SORBS3	Promoter	-20	ENSG00000120896	0.3592	2.84E-05	1761.4153
EXD3	Intron (ENST000003 40951.9/549 32, intron 1 of 21)	5380	ENSG00000187609	0.3723	0.0010	783.9838
EXD3	Promoter	114	ENSG00000187609	0.3723	0.0010	783.9838
MIB2	Promoter	-336	ENSG00000197530	0.3830	0.0045	1128.0948
MIB2	Promoter	0	ENSG00000197530	0.3830	0.0045	1128.0948
GPC1	Distal Intergenic	-44815	ENSG00000063660	0.3845	1.50E-05	755.3419
ABCA3	Exon (ENST000003 01732.10/21, exon 21 of 33)	-4083	ENSG00000167972	0.4062	1.01E-10	2177.59471
ZNF467	Exon (ENST000003 02017.4/168 544, exon 5 of 5)	7304	ENSG00000181444	0.4068	0.0030	385.6360
PIDD1	Promoter	0	ENSG00000177595	0.4162	0.0014	903.6097
LAMA5	Promoter	-626	ENSG00000130702	0.4239	1.75E-05	6115.5469
CKB	Promoter	0	ENSG00000166165	0.5319	0.0228	78.1230
PNPLA7	Exon (ENST000004 06427.6/375 775, exon 21 of 35)	-3895	ENSG00000130653	0.5449	0.0053	143.7567
SYNGR3	Promoter	214	ENSG00000127561	0.5693	0.0066	72.7742
GPR146	Intron (ENST000004 44847.2/115 330, intron 1 of 1)	-5057	ENSG00000164849	0.5760	0.0122	63.7256
MADCAM 1	Promoter	253	ENSG00000099866	0.7051	0.0319	36.9302
LOC10028 8175	Exon (ENST000004 12397.2/100	3227	ENSG00000217801	0.7218	1.68E-05	147.0441

	288175, exon 8 of 10)					
AMN	Promoter	0	ENSG00000166126	0.7781	0.0255	23.7617
LRP1	Promoter	0	ENSG00000123384	0.8377	0.0011	23.0182
CHPF	Exon (ENST000004 61395.5/555 15, exon 3 of 3)	10660	ENSG00000123989	0.8545	0.0300	10.4072
MST1R	Promoter	302	ENSG00000164078	0.9346	0.0050	25.1339
ABCA7	Promoter	749	ENSG00000064687	0.9396	2.51E-15	437.6137
ENTPD8	Exon (ENST000003 71506.7/377 841, exon 4 of 10)	1071	ENSG00000188833	1.2918	0.0005	20.6056
ENTPD8	Promoter	0	ENSG00000188833	1.2918	0.0005	20.6056
ESRP2	Promoter	0	ENSG00000103067	1.3058	3.04E-21	199.9452
SYTL1	Promoter	0	ENSG00000142765	2.2323	5.56E-06	6.8717
EPPK1	Exon (ENST000006 15648.2/834 81, exon 2 of 2)	9643	ENSG00000261150	2.6601	5.26E-10	8.4794
LMTK3	Exon (ENST000006 48216.1/114 783, exon 2 of 5)	4310	ENSG00000142235	2.7912	4.59E-15	14.5369
FAM83H	Promoter	0	ENSG00000180921	2.9138	3.52E-38	35.6370

The genes which were differentially regulated by ZEB1 binding in the promoter region is shown in Figure 3.4.2. RNF213 is one of the most changed genes in this figure, this gene encodes a ring finger protein, identified to have a role in vascular formation and vessel sprouting in zebrafish (Liu et al., 2011). In mice, RNF213 was found to regulate NFAT1 translocation, inhibiting its ability to transcribe target angiogenic genes (Scholz et al., 2016). RNF213 is also induced by interferon γ stimulation, which links to the Interferon Signalling Pathway highlighted in the RNA sequencing results (Figure 3.3.3.3). This pathway was predicted as inhibited, which corresponds to the decreased expression of RNF213 seen in Figure 3.4.2 as a direct consequence of ZEB1 binding.

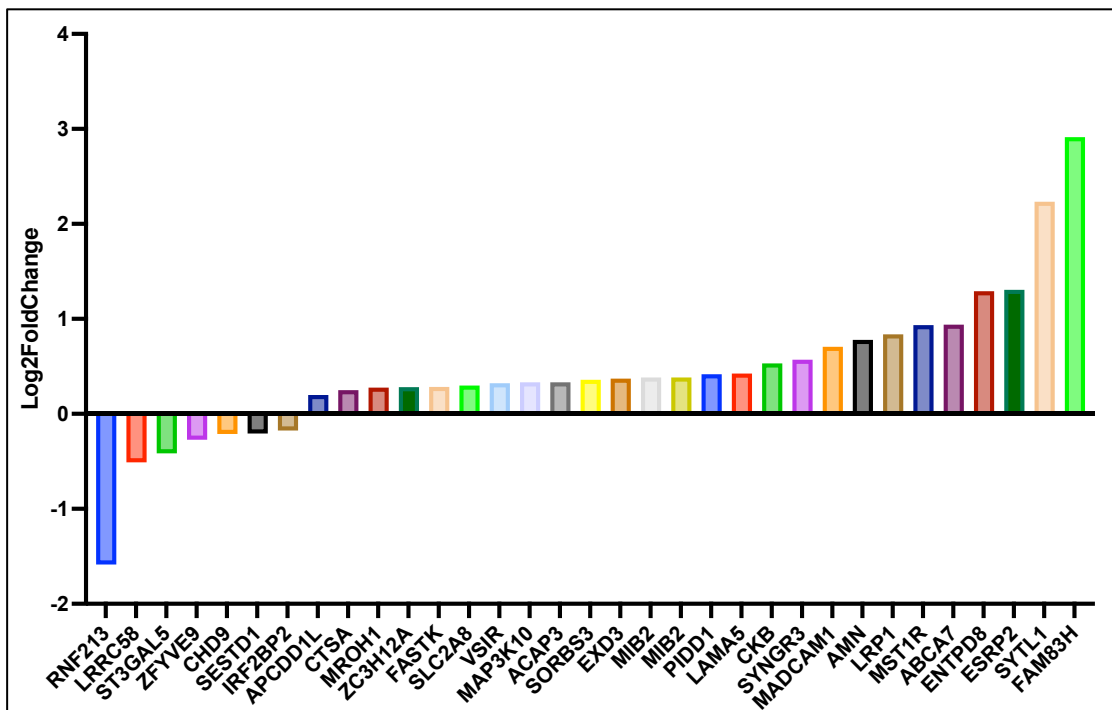


Figure 3.4.2 ZEB1 directly binds to the promoter region of genes identified via ChIPseq resulting in a significant change in gene expression. Identified by combining ChIPseq results identifying ZEB1 binding in the promoter regions of genes with the RNASeq of ZEB1 knockdown in HDLECs. Duplication of genes shown is due to multiple ZEB1 binding sites identified.

One gene, MIB2 appears twice in Figure 3.4.2, this is because ZEB1 was shown to bind to two different sites within the MIB2 promoter. MIB2 is mindbomb E3 ubiquitin ligase, which mediates the ubiquitination, and therefore consequent degradation of delta ligands within the Notch signalling pathway (Koo et al., 2005). This gene was upregulated with ZEB1 knockdown (Log2FoldChange = 0.38, P_{adj} = 0.0045). MIB2 has also been implicated in ubiquitination of RIPK1, inhibiting its pro-apoptotic and cytotoxic potential (Feltham et al., 2018). This pathway could be active in our dataset, as “cell death” was one of the molecular functions associated with DEGs in the dataset (Figure 3.3.5.1). Additionally, RIPK was downregulated following ZEB1 knockdown (Log2FoldChange = -0.24, P_{adj} = 0.0051), suggesting regulation of this pathway at a gene and protein level, aiding prevention of cell death. In ECs, MIB2 has reported to be regulated by FAT1, a member of the cadherin superfamily, which in turn regulates the YAP/TAZ signalling pathway (Li et al., 2023). In our results, MIB2 was upregulated (Figure 3.4.2), the YAP/TAZ complex was also

downregulated (shown in Figure 3.3.4.1). However, FAT1 was unchanged in the ZEB1 knockdown cells (Log2FoldChange = -0.29, P = 0.073, P_{adj} = 0.957), suggesting the control of YAP/TAZ signalling is not due to FAT1 enhancing MIB2 expression, but perhaps through the direct binding of ZEB1 to one or both sites in the promoter. In LECs, YAP/TAZ signalling has been shown to both positively (Cha et al., 2020) and negatively (Cho et al., 2019) regulate PROX1 during lymphangiogenesis. PROX1 is a key transcription factor necessary for the establishment and maintenance of lymphatic vessels, thus its regulation is tightly controlled (Ducoli and Detmar, 2021). In our dataset, PROX1 was downregulated in response to ZEB1 knockdown (Log2FoldChange = -0.633, P_{adj} = 1.89E-10), suggesting YAP/TAZ signalling would positively regulate PROX1 expression in this condition. The consequence of reduced PROX1 in the sample would negatively regulate lymphangiogenic potential, as continuous PROX1-VEGFR3 feedback is required for the maintenance of the lymphatic phenotype (Ma et al., 2021).

The gene with the largest positive Log2FoldChange in Figure 3.4.2 is FAM83H, this gene encodes a protein primarily involved calcification of the tooth enamel (Kim et al., 2008). However increased expression of this gene has been seen in various types of cancer, including colorectal cancer (Sasaroli et al., 2011). FAM83H was further investigated in cancer epithelial cells, where FAM83H was seen to regulate keratin cytoskeleton organisation, via recruitment of casein kinase 1 α (CK-1 α). Furthermore, FAM83H over-expressing cells had loss of epithelial cell polarity and E-cadherin expression, characteristic of a metastatic, invasive phenotype (Kuga et al., 2013). Applying these ideas to our dataset, we have a large increase (Log2FoldChange = 2.91, P_{adj} = 3.52E-28) in FAM83H expression with ZEB1 knockout (Table 3.4.1 and Figure 3.4.1), but there was no significant change in expression of CK-1 α (Log2FoldChange = -0.11, P_{adj} = 0.99). Our results are in a different cell type to the epithelial cells tested by Kuga et al.; however, “cellular assembly and organisation” was a significant term which was associated with many genes within the dataset (Figure 3.3.5.1). Therefore, we could hypothesise in LECs with ZEB1 knockdown,

FAM83H could play a role in altering the cell organisation to facilitate a potentially invasive phenotype.

3.4.1 Identification of enhancer regions

The ChIPSeq data was aligned with publicly available tracks of histone modifications to indicate the location of enhancer regions in the binding tracks. Select genes of interest highlighted from Chapter 3.4 have been aligned to tracks from several HUVEC ENCODE datasets acquired through IGV software. Histone modifications associated with promoter location (H3K4me3), enhancer location (H3K4me1) and enhancer activity (H3K27ac) tracks were selected to align to the ChIP dataset to help annotate regulatory elements of the genome. A DNase-seq track was also used to identify Transcriptional Start Sites (TSS), as DNaseI hypersensitive sites have been shown to lie distal to these sites in 125 cell types (Thurman et al., 2012). Included in Figure 3.4.1.1. are genes of interest RNF213, MIB2 and FAM83H, which have been highlighted to be alternatively expressed following ZEB1 knockdown, and directly bound by ZEB1 in the promoter region. By looking at the binding tracks, we can identify enhancer regions, which are associated with increased H3K4me1 and H3K27ac and the absence of H3K4me3. For RNF213, we can identify an enhancer region downstream from the TSS (identified by the DNaseI hypersensitive peak) and the promoter (H3K4me1 peak), highlighted by dual peaks in H3K4me1 and H3K27ac (Figure 3.4.1.1). This enhancer region has a peak in ZEB1 binding compared to the IgG sample, suggesting that ZEB1 binds the enhancer region of RNF213 to increase gene expression. In the binding tracks for MIB2, the promoter and enhancer regions are identified as adjacent to each other (Figure 3.4.1.1). The enhancer region has a clear peak in the ZEB1 sample, in the RNASeq, MIB2 was identified as upregulated in the absence of ZEB1, suggesting ZEB1 represses gene expression of MIB2, potentially by preventing activation by occupying the enhancer site. FAM83H has been identified as the most upregulated gene in absence of ZEB1 which has a binding site in the promoter, however when investigating the binding track of this gene, the histone tracks do not clearly identify a TSS, promoter or enhancer region (Figure 3.4.1.1). There is very low signal on the histone and DNase-seq tracks, therefore we

are unable to localise ZEB1 binding in through this alignment. Genes of interest which have appeared in the ChIPSeq data but are not highlighted as ZEB1 binding in the promoter can be further investigated, as enhancer regions can be responsible for temporal and spatial control of gene expression, and can be located next to, or at distance from the promoter sites. Further ZEB1 ChIPSeq binding track data is included in Chapter 4 alongside protein expression data of select markers of lymphatic identity and EndMT.

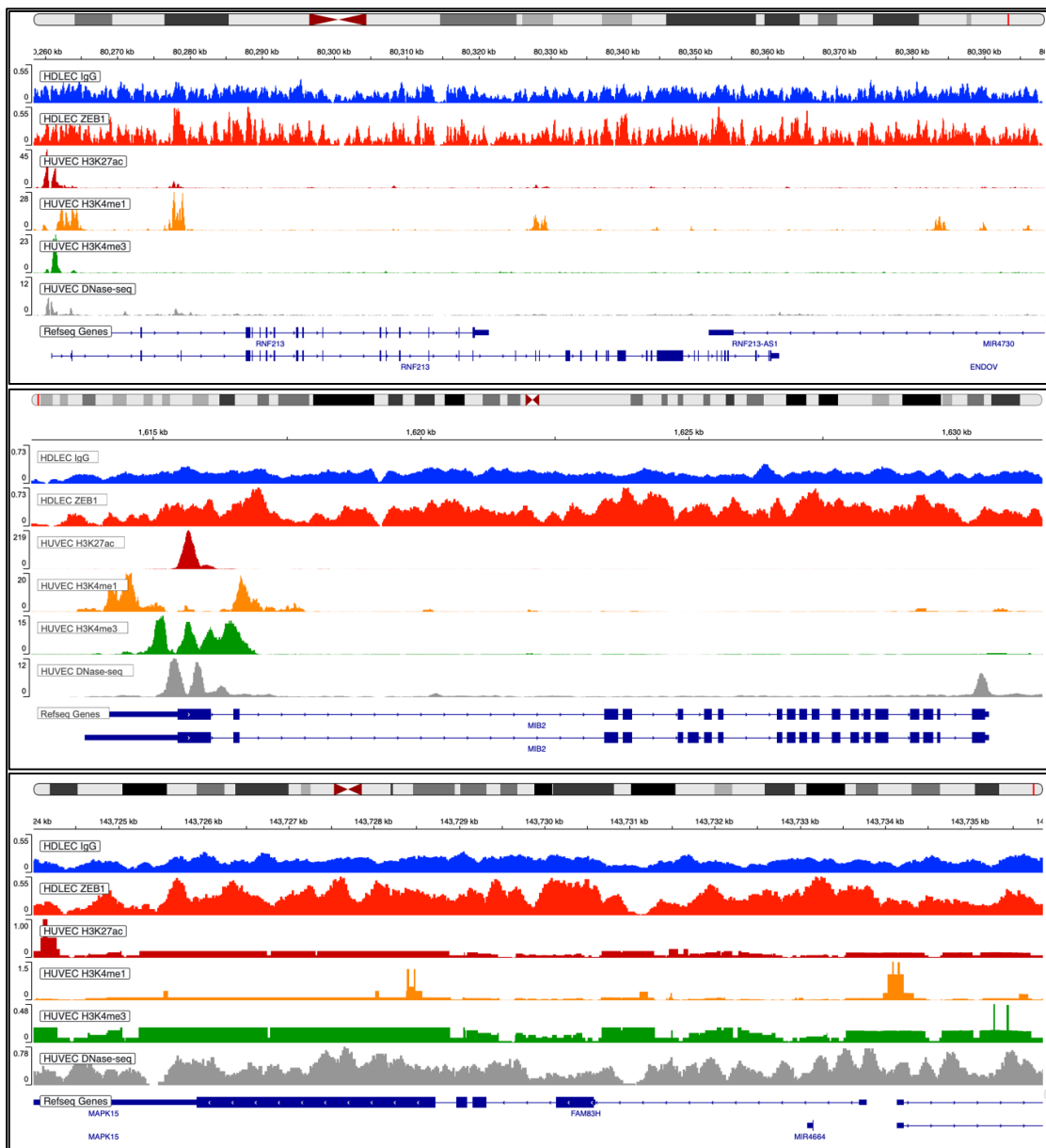


Figure 3.4.1.1. Histone modification binding tracks alongside ZEB1 ChIPSeq data allows for identification and visualisation of the TSS, promoter and enhancer regions. Histone ChIPSeq binding profiles was accessed through IGV software and aligned to ZEB1 ChIPSeq data. ChIPSeq binding profiles of ZEB1 in HDLECs, H3K27ac, H3K4me1, H3K4me3 in HUVECs. DNase-Seq shows DNase hypersensitivity sites in HUVECs. The x axis represents the genomic position; the y axis is the read depth normalised signal. Made using IGV.

3.5 Summary

The aim of this chapter was to investigate the impact of loss of ZEB1 on the wider LEC gene signature. Our hypothesis was that loss of ZEB1 will produce a lymphangiogenic RNA signature. Terms that could be associated with a

lymphangiogenic RNA signature included in our dataset are “cellular assembly” and “cellular movement”. Further to this, oncogenic drivers such as AP1M2, EPCAM and angiogenic transcription factor ETS1 point to a potentially invasive phenotype, concurrent with the characteristics required to drive lymphangiogenic growth. Expression of mesenchymal marker N-Cadherin suggests the mechanism of lymphangiogenic growth may be through an EndMT-like mechanism.

One signalling pathway, the Interferon Signalling Pathway, is repeatedly implicated by loss of ZEB1. Predicted inhibition of this pathway was suggested through downregulation of genes in the dataset such as MX2 and XAF1. ZEB1 was shown to directly bind to members of this pathway, such as RNF213, a stimulator of interferon γ , and decrease gene expression. Predicted upstream transcriptional mediators of this inhibition of the interferon pathway include inhibition of transcriptional activators – IRF1, 3, 5, 7, 9, and activation of transcriptional repressors ETV3 and ETV6. Biological consequences of inhibition of interferon signalling have been shown to influence cell proliferation (Laug et al., 2012), cell migration (Yang et al., 2017) and angiogenesis (Ciccarese et al., 2020). This combined with potentially oncogenic expression of EPCAM and FAM83H, and downregulation of master of quiescence FOXO1, leads us toward a more invasive gene signature with ZEB1 knockdown in LECs. EPCAM specifically exhibits this phenotype through activation of the Wnt/ β -catenin pathway (Yamashita et al., 2007). This pathway crucially has been implicated in a partial lymphatic EndMT mechanism, which resulted *in vitro* lymphangiogenesis (Wang et al., 2017).

The results of the RNASeq were not validated by other experiments. There is debate in the scientific community as to whether it is necessary to confirm data obtained by large scale transcriptomic studies. Prior to sequencing technologies such as Illumina, microarrays were used, which were subject to concerns over reproducibility and bias (Zhang et al., 2006; Balázs and Oltvai, 2007), therefore confirmation of changes in gene expression by methods such as quantitative and real time PCR were used. However, RNASeq has been shown to not encounter to the same issues as some

microarrays, extensive analysis of five RNASeq analysis platforms were compared to qPCR results, with only 1.8% of over 18,000 protein-coding genes showing opposing gene expression between the techniques, these genes were typically lower expressed and shorter in length (Everaert et al., 2017). The data from this study, and many others suggest current, advanced RNASeq technologies and data analysis are robust enough to not require confirmation. To investigate alterations at a protein level, select genes can be investigated by western blot, this adds value to the RNASeq dataset and allows for further interpretation of the effect the loss of ZEB1 on the overall cell phenotype.

Further work should be conducted to investigate if the pathways highlighted have phenotypic alterations within the HDLECs. Simple assays such as immunofluorescence staining with Ki-67, a proliferation marker, could detect cells in the growth phase, and compared with control cells. Additionally, a cell migration assay could also be completed, where cells are seeded into a dish with an insert, leaving a gap with no cells, the insert is then removed and the infiltration of cells into the available space is documented. Although no assay has been specifically marketed to measure lymphangiogenesis *in vitro*, angiogenesis assays, such as Ibidi's tube forming assay, and sprouting assays could be utilised to measure lymphangiogenic ability. These assays would first have to be optimised on control HDLECs to confirm suitability and may require usage of lymphatic specific growth factors such as VEGF C, before tested on siRNA knockdown cells.

Investigating the genomic landscape revealed by ChIPSeq, we have the ability to identify specific enhancer elements by which ZEB1 directly binds and alters gene transcription. Select genes were chosen in this chapter to give an example of the potential avenues of further investigation. This ChIPSeq data is used further in this thesis to support protein expression data in Chapter 4. Investigating how ZEB1 exerts mechanisms of gene expression and repression is critical to understand ZEB1 function, especially due to suspected opposing roles in endothelial and epithelial cells. The location and activation of enhancers within gene loci are thought to

mediate mechanisms of cell-specific transcriptional regulation (Heinz et al., 2015). Unfortunately, to date, there is no publicly available data for histone ChIPSeq or DNase-Seq in HDLECs, therefore HUVEC data was included in the analysis. There are obvious limitations with this, as minimal conclusions can be made relying on the location and activity of the enhancer as there is no guarantee this is the same in HUVECs and HDLECs. However, until histone ChIPSeq is completed in HDLECs and made publicly available, the data included in this chapter can be used as a guide, or as preliminary data for further hypotheses. Further follow up to the data shown could be centred around the functioning of enhancer regions in select gene loci, including investigating what controls expression of ZEB1 itself in LECs. Using our data, it is possible to identify select active enhancers, and combine this with *in vivo* validation, potentially through use of a zebrafish model as described by Neal et al. This method can be modified for the lymphatic vasculature and is quicker and cheaper than mouse models (Neal et al., 2022).

In conclusion, this chapter has sought to establish the *in vitro*, genomic consequences of loss of ZEB1 in LECs. Through RNASeq and ChIPSeq, novel interaction partners have been revealed with ZEB1 binding motifs, with some identifiable enhancer regions. The overall phenotype of the loss of the ZEB1 we hypothesise to be migratory, with enhanced proliferative ability and potentially lymphangiogenic. Further work should be conducted with HDLECs, and potentially whole animal models, to investigate the phenotypic functionality of ZEB1 in the lymphatic vasculature.

Chapter 4. ZEB1 Expression Influences the Protein Expression of EndMT Markers and Adjusts the Metabolic Profile of HDLECs

4.1 Introduction

4.1.1 EndMT

Endothelial to mesenchymal (EndMT) transition is a process by which ECs lose their endothelial characteristics and gain a more mesenchymal phenotype. This involves a loss of cell contacts, a loss of polarity and remodelling of the extracellular matrix. EndMT occurs in normal physiology, and is required for tissue morphogenesis, such as in the mitral valve (Armstrong and Bischoff, 2004) and pulmonary artery development (Arciniegas et al., 2005). The process can also be activated in pathological conditions such as wound healing (Singh et al., 2007), chronic inflammation (Lipton et al., 1992) and hypoxia (Zhu et al., 2006). Phenotypic drivers of this process are still debated but are often shared with EMT (Arciniegas et al., 2007). Markers lost in this transition (from work on vascular ECs) include VE-Cadherin, VEGFR1/2, Tie1/2 and CD31 (Arciniegas et al., 2007). Comparatively less research has been completed in LECs. In a recent study by Yoshimatsu et al., LECs were induced by TGF β to undergo EndMT. During this transition, markers of lymphatic identity, PROX1 and LYVE1 were decreased, and the mesenchymal phenotype of increased motility, decreased tube forming ability and increased vascular permeability was seen (Yoshimatsu et al., 2020). This process is thought to be driven by transcription factors common to EMT, SNAIL and SLUG have both been reported to be involved in the expressed in LECs (Yoshimatsu et al., 2020; Cai et al., 2015). Whereas, ZEB1 primarily has only been implicated in EMT (Wels et al., 2011b), emerging papers of the role of ZEB1 in ECs (Welch-Reardon et al., 2015; Fu et al., 2020; Yu et al., 2022) have yet to agree on the involvement of ZEB1 in EndMT. In blood vessel remodelling, the ECs are thought to go through a partial EndMT mechanism whereby not all the endothelial characteristics are lost. Specifically, the ECs do not lose their cell-cell contacts and migrate as a train of connected cells (Welch-Reardon et al., 2014). This mechanism supports angiogenesis, as the tip cells leading new sprouts lose polarity and disengage from the endothelium to lead the

sprout, while maintaining junctional connections with supporting trunk cells (Hultgren et al., 2020). The same mechanism is thought to be involved in lymphatic vessel remodelling, which has been shown *in vitro* (Wang et al., 2017).

4.1.2 Metabolic changes in EndMT

Changes in endothelial phenotype require a change in energy demand. Fatty acid β -oxidation (FAO) is the process by which fatty acids are broken down into molecules of acetyl CoA which enter the Krebs cycle to generate ATP. This involves a series of reactions which remove two-carbons from the fatty acid chain, generating acetyl CoA and reducing agents NADH and FADH₂. The reducing molecules can be used in oxidative phosphorylation as electron donors, to transfer electrons to the electron transport chain. This produces ATP in the most efficient way. Other methods of oxidative metabolism include the breakdown of other molecules, such as glucose in the process of aerobic glycolysis. Glycolysis can also take place anaerobically, this is comparatively low efficiency pathway of metabolism, however particularly useful in vessel sprouting where oxygen supply may be limited (De Bock, Georgiadou, Schoors, et al., 2013).

Aerobic glycolysis is a phenomenon only seen in ECs and cancer cells, despite inefficiency, in high glucose conditions, ATP can be produced faster and in greater quantities (Potente and Carmeliet, 2017). This is beneficial in vessel sprouting, where the tip cell leading the sprout requires energy for migration, often toward nutrient deprived and hypoxic tissue (Potente and Carmeliet, 2017). Phospho-fructokinase-2/fructose-2,6-bisphosphatase 3 (PFKFB3) is a key determinant of glycolysis activity. Proangiogenic molecules, such as VEGF, increase glycolysis and glucose uptake by increasing expression of glycolytic activators such as PFKFB3, to support sprouting behaviour (Potente and Carmeliet, 2017). The reliance of glycolysis for sprouting behaviour is shown by inhibition of PFKFB3 which compromised vessel outgrowth and tip cell formation (De Bock, Georgiadou, and Carmeliet, 2013). Another modulator of endothelial metabolism is the growth enhancing transcription factor MYC, which when phosphorylated by ERK, allows it to accumulate, and amplifies the

transcription of glycolysis-enhancing genes, as well as increasing mitochondrial function, and cell proliferation (Stine et al., 2015). In quiescent ECs, Forkhead Box O1 (FOXO1) is responsible for repressing MYC and decreasing the metabolic activity of the cell (Wilhelm et al., 2016). In a stable endothelium, ECs reduce glucose uptake and glycolysis, as the energy requirement is decreased. In sprouting vasculature, FOXO1 is suppressed through PI3K/AKT signalling through activation via VEGFR2 (Salih and Brunet, 2008). In LECs, there is also a reliance on glycolysis to generate ATP to facilitate sprouting, this was shown via fibroblast growth factor receptor (FGFR) control of MYC expression (Yu et al., 2017). One of the key enzymes of glycolysis is hexokinase 2 (HK2), which when downregulated, decreases glycolysis and therefore endothelial cell proliferation and migration (Yu et al., 2017). In comparison to BECs, LECs have higher rates FAO, shown to be essential in the differentiation of LECs from BECs during development (Wong et al., 2017). Inhibition of FAO was shown to induce dedifferentiation in ECs, suggesting FAO plays a role in maintaining endothelial cell identity (Xiong et al., 2018). This research has been reinforced in LECs in a study by Ma et al., which found that cells unable to respire through FAO in the mitochondria, were unable to maintain LEC identity. A decrease in VEGFR3 was seen in these deficient LECs, disrupting the VEGFR3-PROX1 feedback loop, key mediators of the lymphatic identity (Ma et al., 2021). PROX1 has been shown to upregulate CPT1a, a rate limiting enzyme in the outer mitochondrial membrane, promoting FAO thus increasing acetyl coA generation, shown to be a sensor for entrance to EndMT (Ma et al., 2021; Xiong et al., 2018). β oxidation in LECs also provides a source of fatty acid derived carbons for de novo nucleotide synthesis, supporting DNA replication and cell proliferation (Wong et al., 2017).

Regarding vessel remodelling as a partial EndMT mechanism, the associated metabolism changes are unclear. In a study by Xiong et al., acquisition of mesenchymal features, such as in EndMT, is accompanied by a lower energy status, where β -oxidation of fatty acids, the metabolic pathway producing the most amount of energy, is no longer needed or compensated by other pathways (Xiong et al., 2018). However, it is stated that although LECs use FAO more than BECs (Wong et al.,

2017), over 70% of their ATP supply is from glycolysis (Yu et al., 2018), therefore any change in FAO will not have a major impact on ATP generation, but may impact the cell identity (Xiong et al., 2018). During vessel sprouting, there is a requirement for enhanced energy production to fuel the growing sprout, which has shown to be compensated by increased glycolysis (De Bock, Georgiadou, and Carmeliet, 2013). Therefore, the lower energy status described by Xiong et al., could be a full endMT transition of the endothelial cell to a full mesenchymal state and not suggested in the partial EndMT associated with vessel remodelling. Thus, LECs require a change in metabolic activity during LEC growth and proliferation, suggesting that lymphangiogenic behaviour will be associated with alterations in cell metabolism.

4.1.3 Measuring Metabolism using Agilent Seahorse assay

The Seahorse assay (Agilent) is based on Mitchell's chemiosmotic theory of oxidative phosphorylation (Mitchell, 1961). This was adapted to the seahorse assay to measure the amount of oxygen consumption (OCR) and proton expulsion (extracellular acidification rate, ECAR) in the media surrounding cells in a cell culture plate-based assay. During oxidative phosphorylation, there is a coupling of oxygen consumption and ATP synthesis. Within the mitochondria, electrons transferred from the metabolism of glucose, amino acids and fatty acids are transported along the electron transport chain. This series of energetically downstream reactions reduce oxygen to water, are coupled with an upstream proton pumping across the matrix to the intermembrane space, generating a proton gradient across the inner mitochondrial membrane. ATP synthase utilises this force to drive catalysis of ADP+Pi to ATP, the end product of oxidative phosphorylation and ultimately the cellular source of energy. Thus, oxygen consumption can be used as a measurement of the number of electrons flowing through the electron transport chain, and an indirect measurement of protonmotive force (Divakaruni et al., 2014). The Seahorse Mitochondrial Stress Assay combines this theory with the addition of drugs which inhibit different components of the electron transport chain to enable calculations of the different metabolic pathways to the overall energy status of the cell. Oligomycin, an ATP synthase inhibitor, is the first drug administered after basal readings,

decreasing the electron flow through the electron transport chain, ATP production and mitochondrial respiration (Figure 4.1.1). The mitochondrial respiration unaffected by oligomycin administration is termed the proton leak-linked respiration, representing the proton leak across the inner membrane which can stimulate and consume the membrane potential, uncoupled from ATP synthesis. FCCP is an uncoupling agent which disrupts the mitochondrial membrane potential, which follows oligomycin administration. This disrupts the proton gradient, allowing electron flow to be uninhibited, allowing maximum respiratory capacity to be measured. Spare respiratory capacity can be calculated as the difference between basal and maximum respiration, allowing a measure of the cell's response to increased energy demand or stress. To completely stop mitochondrial electron transport chain, Rotenone (complex I inhibitor) and Antimycin A (complex III inhibitor) are dually added to the media, this enables the measurement of non-mitochondrial respiration from processes outside the mitochondria (Divakaruni et al., 2014). To quantify non-oxidative metabolism, extracellular acidification is measured throughout, this allows an indication of the level of glycolysis occurring in the cell. Anaerobic glycolysis is the metabolism of glucose to lactate, this produces protons which decrease the pH of the surrounding media, this is measured and allows indication of a switch and/or compensation of metabolic pathways (Plitzko and Loesgen, 2018).

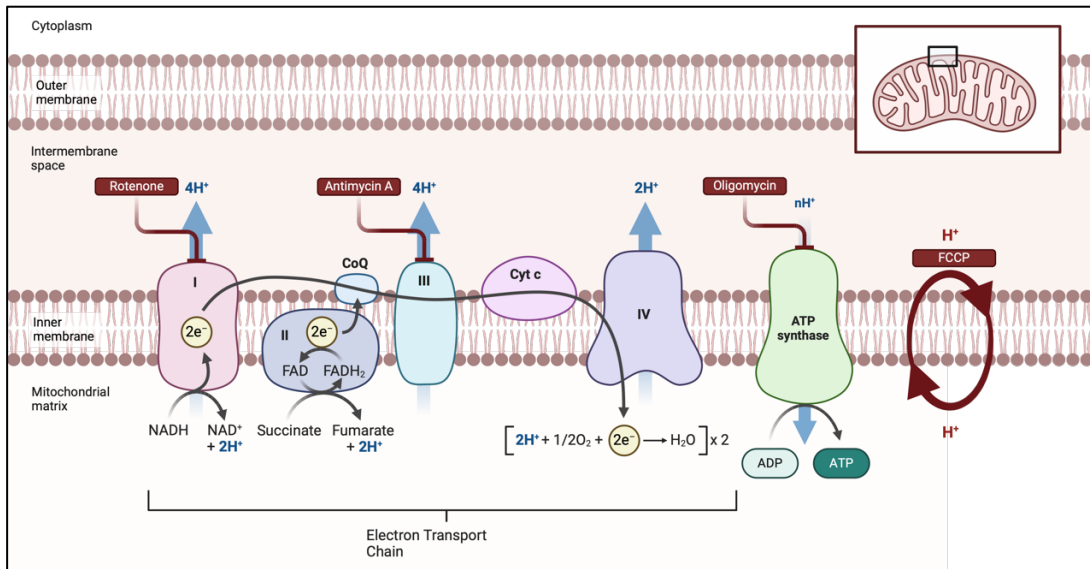


Figure 4.1.1 The principles of the Seahorse Mitochondrial Stress Assay. The electron transport chain is located on the inner mitochondrial membrane where electrons travel through redox reactions, resulting in a proton gradient which enables the catalysis of ADP to ATP through ATP synthase. The seahorse assay disturbs this process at key checkpoints to enable assessment of mitochondrial function. Created with Biorender.com.

HDLECs are widely used *in vitro* to understand LEC pathology. Commercially available primary cells undergo characterisation by flow cytometry using CD31 and Podoplanin to ensure a pure population allowing for reproducible results (PromoCell, 2023). Isolation from primary tissue is also possible, but is often time-consuming, limited by tissue availability and highly technical (Marelli-Berg et al., 2000; Kriehuber et al., 2001). Research effort has previously used animal models, such as mice and rats, this limits how translatable this research is to human physiology. Use of human LECs, not immortalised, preserves the native morphology and behaviour of these cells for a limited lifespan (Kriehuber et al., 2001). These cells do originate from different individuals, which may offer donor-variation, however immortalisation, or delayed senescence, involves the ectopic expression of human telomerase reverse transcriptase (Nisato et al., 2004), or originate from endotheliomas (Obeso et al., 1990). Before common use of primary cell lines, cell lines were used which were positive for only one or two desirable endothelial markers and often contained tumorigenic mutations which enhanced proliferative ability (Bouis et al., 2001). This removes the physiological accuracy of the cell line to the human physiological state.

To confirm successful gene silencing using siRNA knockdown, assessment of protein expression can be carried out following cell lysis. The gold standard for analysis of protein content is Western Blotting, a technique which involves separation of proteins by size using electrophoresis, and transfer to a membrane maintaining the pattern created. The membrane is probed using primary antibodies to a protein of interest, then this signal is amplified with the addition of secondary antibodies, which are labelled with a fluorophore. The signal is visualised using imaging systems equipped with lasers scanners or a digital charge coupled imager. This membrane can then be stripped to remove the bound antibodies and re-probed for further proteins of interest. Every re-probe will reduce the amount of protein on the membrane, thus will be finite. Protein can be quantified using image analysis software, with each sample normalised to the chosen loading control to normalise to protein content. Protein quantification prior to loading samples onto the gel is also beneficial to ensure even loading.

In this chapter, we utilised HDLECs in a model of growth, to understand the markers of EndMT. We investigated the consequences on protein expression of knocking down ZEB1 and how the metabolic profile of LECs responded to loss of ZEB1.

4.2 Hypothesis and Aims

Hypothesis: Actively growing LECs promote a partial EndMT-like phenotype which will be replicated by loss of ZEB1.

Aims:

1. Investigate differentially expressed EndMT markers in a model of growth
2. Investigate differentially expressed proteins following ZEB1 knockdown in HDLECs
3. Use the Seahorse Mitochondrial Stress Assay to investigate if loss of ZEB1 induces metabolic changes in HDLECs

4.3 Results

4.3.1 ZEB1 is differentially expressed in a model of lymphatic endothelial cell growth

To investigate ZEB1 protein expression in a model of growth, we cultured LECs in different conditions aiming to emulate a condition of growth (subconfluence), and a condition of quiescence (confluence). This was to test the hypothesis that ZEB1 protein expression is higher in quiescent (confluent) LECs. As shown in Figure 4.3.1.1 (Panel A) ZEB1 expression was decreased by 63% ($P = 0.0003$) in the subconfluent sample in comparison to the LECs grown in confluent conditions. Alongside ZEB1, other known markers of EndMT were investigated to understand how their protein expression changes in subconfluent and confluent conditions. SLUG was the only protein target identified (Figure 4.3.1.1, Panel B) to increase expression in subconfluent conditions (235% [$P = 0.0228$]). Whereas ZEB2, VE-Cadherin, SNAIL and PROX1 expression all decreased in subconfluent conditions (41% [$P = 0.0047$], 42% [$P = 0.0051$], 87% [$P = 0.0008$], and 84% [$P = 0.0009$] decrease respectively) suggesting these were upregulated in the confluent, and potentially quiescent conditions. SLUG expression was significantly increased in subconfluent conditions, SLUG is a known inducer of EndMT and acts via suppressing VE-Cadherin transcription (Lopez et al., 2009). This is consistent with results shown in Figure 4.3.1.1, as we saw SLUG expression highest in subconfluent conditions, where VE-Cadherin expression was reduced. SNAIL and SLUG have also reportedly had opposing (Ganesan et al., 2016) and enhancing (Kokudo et al., 2008; Lopez et al., 2009) roles in different conditions.

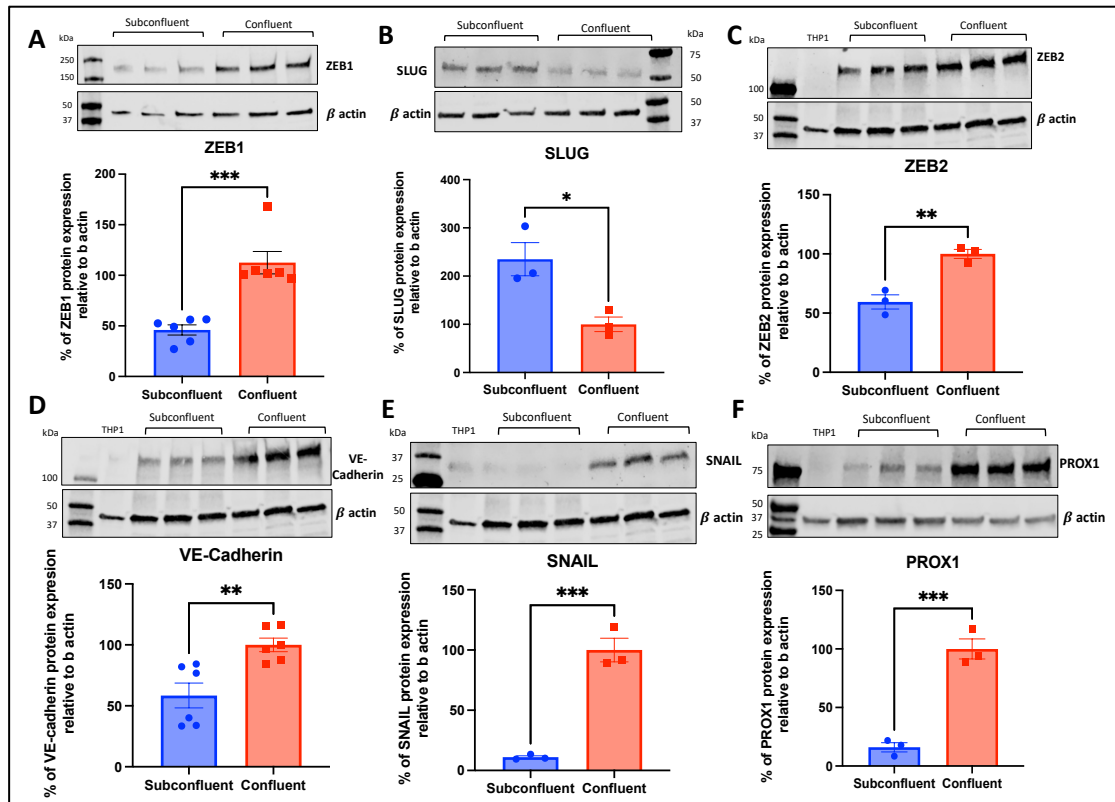


Figure 4.3.1.1 HDLECs exhibit a different protein expression profile when grown in subconfluent versus confluent conditions as measured by western blot analysis. LECs were plated at a density of 25,000 cells per cm^2 , and 150,000 cells per cm^2 . Western blots were stripped and reprobbed for markers of interest and analysed with Odyssey Image Studio with representative images shown. A. Western blot analysis of ZEB1 protein in subconfluent and confluent conditions, $N=6$, *** $P<0.001$. B. SLUG, $N=3$, * $P<0.05$. C. ZEB2, $N=3$, ** $P<0.005$. D. VE-Cadherin, $N=6$, ** $P<0.005$. E. SNAIL, $N=3$, ** $P<0.005$. F. PROX1 $N=3$, ** $P<0.005$. Data present as mean \pm SEM. Statistically analysed with an unpaired t test.

4.3.2 Optimisation of ZEB1 siRNA protocol

Following a lack of initial success with visualisation and consequently quantification of protein output (Figure 4.3.2.1), optimisation using 60 mm dishes was trialed to increase the amount protein input. The concentration of ZEB1 and non-silencing control siRNA was not adjusted from the manufacturers protocol, as the westerns were showing a lack of protein on the western gel, therefore this was determined as the first issue to fix, before looking at changing the knockdown protocol. The wells were loaded to maximum capacity in this trial, to observe the differences in protein concentration. Visible bands were detected in T75 and 60 mm dish lysates for ZEB1 and β actin (Figure 4.3.2.1). The knockdown experiment was therefore scaled from 6 well plates to 60 mm dishes, to allow more concentrated samples to be visible on

western blot, and therefore quantified. The lysate buffer was not scaled in future experiments to further increase protein concentration, allowing for multiple westerns to be ran with the same samples.

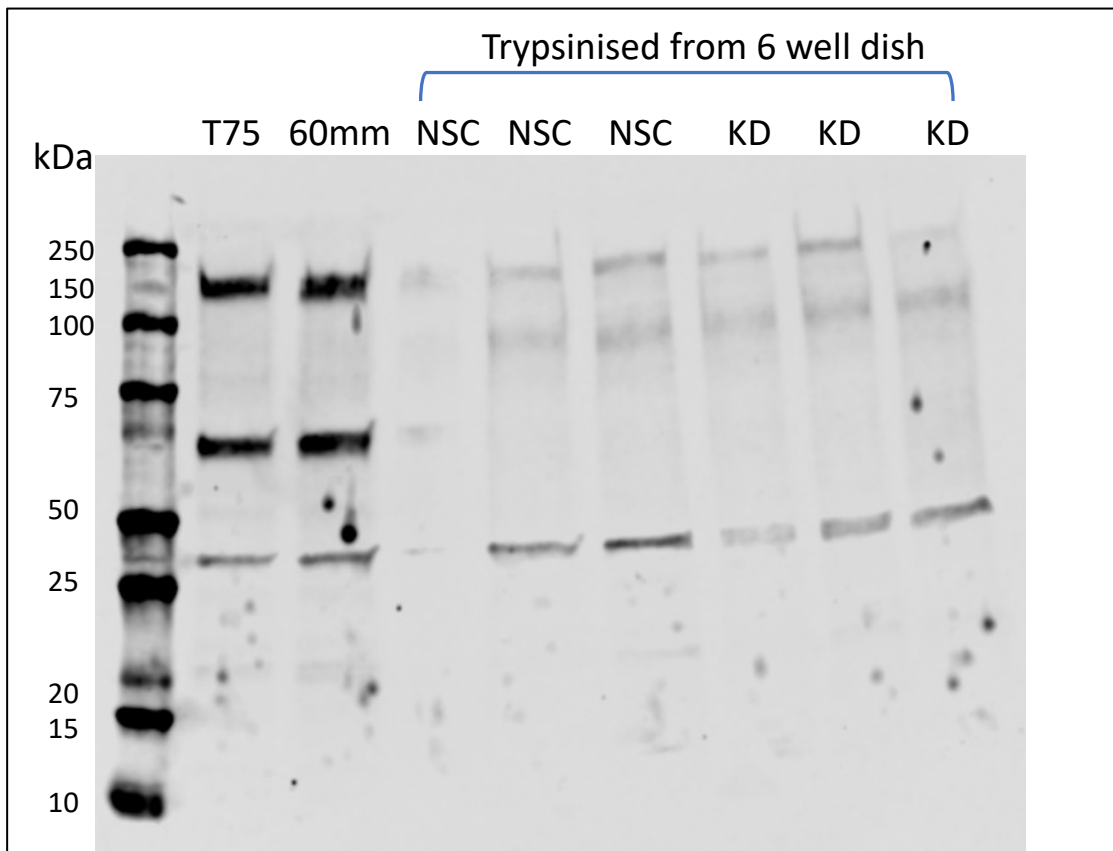


Figure 4.3.2.1 HDLECs grown to 80% confluency on 60 mm dishes were preferable for consistent protein visualisation on western blot during ZEB1 knockdown. Each lane was loaded to maximum capacity. ZEB1 band is visible around 150 kDa, and β actin between 25 and 50 kDa. Cells were collected from a T75 cell culture flask and 60 mm dish. ZEB1 knockdown was performed in a 6 well dish with 3 replicates.

4.3.3 ZEB1 siRNA knockdown influences expression of SLUG and SNAIL but no other markers of EMT/EndMT

To test the impact of ZEB1 protein expression in controlled growth conditions, LECs were grown to 80% confluency then subjected to ZEB1 siRNA knockdown. ZEB1 protein expression was successfully knocked down (Figure 4.3.3.1., Panel A) by 93% ($P < 0.0001$). Complementing Figure 4.3.1.1, SLUG expression significantly increased by 322% ($P = 0.0049$) with ZEB1 knockdown (Figure 4.3.3.1., Panel B), suggesting a relationship between these two transcription factors. In melanoma epithelial cells, SLUG was able to increase ZEB1 expression, with an increase following over expression of SLUG (Wels et al., 2011b). This has not been reflected in Figure 4.3.3.1

but requires further investigation to the cooperativity/inhibitory nature of SLUG and ZEB1 in ECs. We also investigated SNAIL expression following ZEB1 knockdown (Figure 4.3.3.1., Panel C), this was significantly increased in the knockdown cells (35% [P = 0.016]) potentially working with/following similar expression to SLUG in this condition. Reduction of ZEB1 did not affect the protein expression of the cell-cell junction marker VE-Cadherin (Figure 4.3.3.1., Panel E), or the mesenchymal marker vimentin (Figure 4.3.3.1., Panel E). Other markers of EMT/EndMT were also tested; JNK, ZO1, ZEB2, VEGFR2 (Figure 4.3.3.1., Panel F-I) and expression found unchanged (P = 0.115, 0.394, 0.679, 0.48 respectively). These results however were only a N=3 (N=5 for VEGFR2) it is possible a bigger sample size was required to be representative of the impact of ZEB1 knockdown. The results of the RNA Sequencing for the genes encoding the proteins shown in Figure 4.3.3.1 are displayed in Table 4.3.3.1. This table shows the basal levels of the RNA encoding the proteins, as well as the effect of loss of ZEB1 on this expression. From these results, we can see a significant reduction in ZO-1 and VEGFR2 RNA expression, which is not reflected in a change in protein expression as shown in Figure 4.3.3.1.

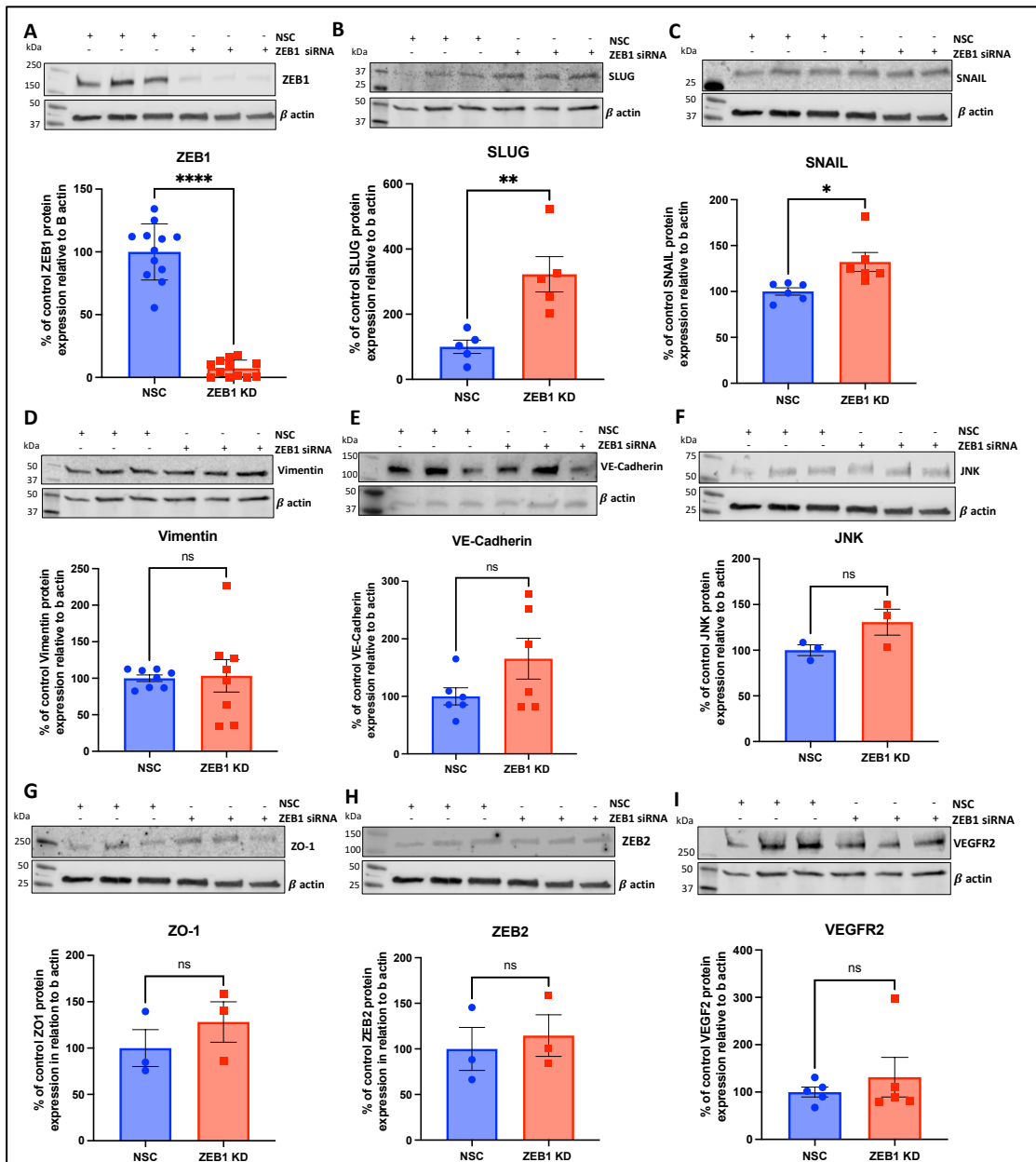


Figure 4.3.3.1. HDLECs treated with ZEB1 siRNA knockdown reduces ZEB1 protein expression.

A. Western blot image analysis following ZEB1 siRNA knockdown HDLECs for ZEB1 N=12, **** $P < 0.0001$. Western blots were stripped and reprobed for markers of interest and analysed with Odyssey Image Studio with representative images shown. B. SLUG, N=5, ** $P < 0.005$. C. SNAIL, N=6, * $P < 0.05$. D. Vimentin, N=9. E. VE-Cadherin N=6. F. JNK, N=3. G. ZO-1 N=3. H. ZEB2 N=3, I. VEGFR2 N=5. Data present as mean \pm SEM and analysed with an unpaired t test.

Table 4.3.3.1 ZEB1 siRNA knockdown affects ZO-1 and VEGFR2, but no other EMT/EndMT gene expression at an RNA level. RNA Sequencing of ZEB1 siRNA knockdown HDLECs. Average basal expression of the DESeq2 normalised counts of three non-silencing control replicates.

EMT/EndMT Genes				
ENSEMBLE ID	Gene Symbol	Log2FoldChange	P _{adj}	Basal Expression
ENSG00000148516	ZEB1	-0.784366384	1.39E-21	1864.771779
ENSG00000124216	SNAI2 (SLUG)	N/A	N/A	242.159109
ENSG00000124216	SNAI1 (SNAIL)	N/A	N/A	225.8461573
ENSG00000026025	VIM (Vimentin)	N/A	N/A	31033.9149
ENSG00000179776	CDH5 (VE-Cadherin)	N/A	N/A	23609.5968
ENSG00000107643	MAPK8 (JNK)	N/A	N/A	578.891946
ENSG00000104067	TJP1 (ZO-1)	-0.2860386	1.89E-06	4031.48441
ENSG00000169554	ZEB2	N/A	N/A	149.785969
ENSG00000128052	KDR (VEGFR2)	-0.3222236	3.20E-07	10583.9723

Utilising the ChIPSeq from Chapter 3, we investigated the ZEB1 binding tracks for select genes of interest highlighted in Figure 4.3.3.1 and Table 4.3.3.1. In Figure 4.3.3.2, the binding tracks for SNAIL, SLUG and VEGFR2 are displayed, along with publicly available data for histone modification tracks and DNaseI hypersensitivity sites. Out of these, only VEGFR2 was highlighted as significantly differentially expressed in the RNASeq data (Table 4.3.3.1). In the ChIPSeq, VEGFR2 was not identified as direct binding partner of ZEB1, the peaks shown in Figure 4.3.3.2 are similar between the IgG and ZEB1 samples. This suggests that ZEB1 alters VEGFR2 expression indirectly at an RNA level (Table 4.3.3.1) and not by binding to any regions of the KDR gene (Figure 4.3.3.2), however this does not translate to a change in VEGFR2 protein (Figure 4.3.3.1, Panel I) following loss of ZEB1. Neither SNAIL or SLUG were differentially expressed following loss of ZEB1 at RNA level (Table 4.3.3.1) or highlighted as direct binding partners of ZEB1 through ChIPSeq (Figure 4.3.3.2). Both these proteins are significantly increased following loss of ZEB1 (Figure 4.3.3.1, Panels B and C), however our ChIPSeq data suggests this effect on protein expression is not through direct ZEB1 binding.

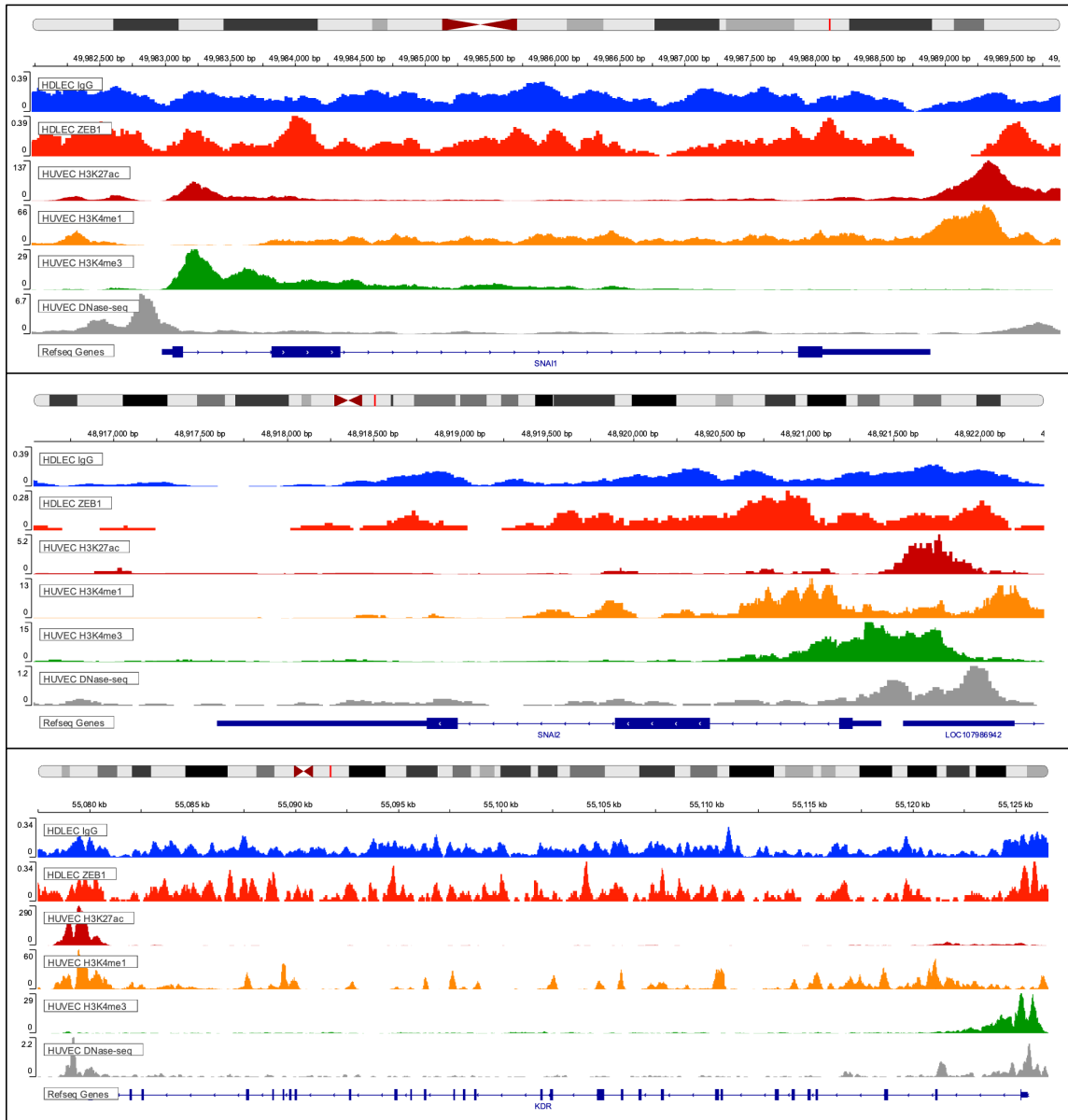


Figure 4.3.3.2. ChIPSeq binding tracks for SNAIL, SLUG and VEGFR2 found no significant peaks between ZEB1 and the IgG. Histone ChIPSeq binding profiles was accessed through IGV software and aligned to ZEB1 ChIPSeq data. ChIPSeq binding profiles of ZEB1 in HDLECs, H3K27ac, H3K4me1, H3K4me3 in HUVECs. DNase-Seq shows DNase hypersensitivity sites in HUVECs. The x axis represents the genomic position; the y axis is the read depth normalised signal. Made using IGV.

4.3.4 ZEB1 knockdown alters the expression of key mediators of lymphatic identity

To investigate the role of ZEB1 in lymphatic identity programming, ZEB1 knockdown samples were quantified by western blot for the expression of key markers of the lymphatic phenotype. PROX1 expression was significantly increased by 44% ($P = 0.0113$) following ZEB1 knockdown (Figure 4.3.4.1, Panel A). This result opposes the

result seen in Figure 4.3.1.1 whereby when ZEB1 expression was high in confluent conditions, as was PROX1. Cells were at 80% confluency when transfected with ZEB1 siRNA, whereas in the confluent conditions the aim was to grow the cells close to 100%, which may account for this difference, as lack of ZEB1 expression was not the only difference between experiments. VEGFR3 was found significantly downregulated by 50% ($P = 0.0018$) following ZEB1 knockdown (Figure 4.3.4.1, Panel B), this is interesting as expression of VEGFR3 is closely associated with the lymphatic phenotype, allowing cells to respond to VEGF-C stimulation and ultimately increase lymphangiogenesis. PROX1 and VEGFR3 have also been closely associated to regulate lymphatic identity, with VEGFR3 being identified to help maintain PROX1 expression in LECs (Srinivasan et al., 2014a). Our results (Figure 4.3.4.1, Panel B) show a decrease in VEGFR3 but an increase in PROX1 expression potentially suggesting due to ZEB1 decrease this feedback loop has been dysregulated. SOX18 causes differentiation of pre-LECs sprouting from the CV in the early embryo. SOX18 expression decreases over time as the vasculature matures. No difference in SOX18 expression was seen ($P = 0.1893$) with ZEB1 knockdown (Figure 4.3.4.1, Panel D). FOXC2 is a transcription factor involved in the differentiation of collecting lymphatics from capillaries, with specific roles in valve development. FOXC2 expression has also been linked to EMT in cancer, and in a study by Cai et al., was linked to PROX1 expression in LECs in terms of maintaining a more mesenchymal state (Cai et al., 2015). This was not reflected in the results in Figure 4.3.4.1 (Panel C) as FOXC2 expression was unchanged ($P = 0.0540$) despite an increase in PROX1. The results of the RNA Sequencing for the genes encoding the proteins shown in Figure 4.3.4.1 are displayed in Table 4.3.4.1. This table shows the basal levels of the RNA encoding the proteins, as well as the effect of loss of ZEB1 on this expression. Contrasting the results at protein level, PROX1 gene expression is reduced following loss of ZEB1 (Table 4.3.4.1). VEGFR3, FOXC2 and SOX18 RNA expression was unchanged (Table 4.3.4.1).

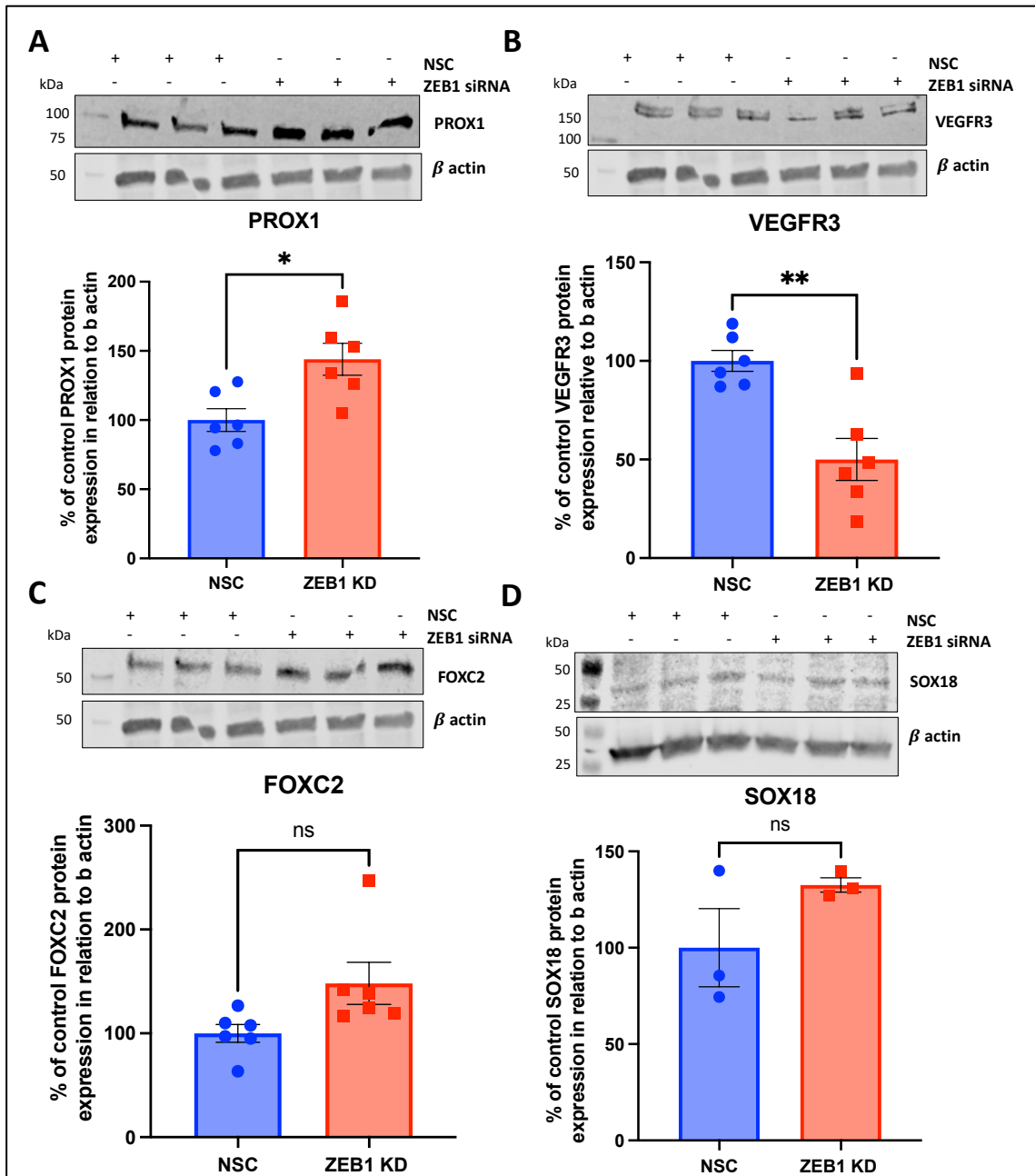


Figure 4.3.4.1. ZEB1 siRNA knockdown induces differential PROX1 and VEGFR3 protein expression as measured by western blot analysis. A. PROX1 protein was quantified following ZEB1 siRNA knockdown in HDLECs N=6, *P<0.05. Western blots were stripped and reprobed for markers of interest and analysed with Odyssey Image Studio with representative images shown. B. VEGFR3, N= 6, ** P<0.005. C. FOXC2, N=6. D. SOX18, N=6. Data present as mean \pm SEM and analysed with unpaired t test.

Table 4.3.4.1. ZEB1 knockdown downregulates PROX1 at RNA level. RNA Sequencing of ZEB1 siRNA knockdown HDLECs. Average basal expression of the DESeq2 normalised counts of three non-silencing control replicates.

Lymphatic Identity Genes				
ENSEMBL ID	Gene Symbol	Log2FoldChange	P _{adj}	Basal Expression
ENSG00000117707	PROX1	-0.6331544	1.89E-10	4740.20549
ENSG00000037280	FLT4 (VEGFR3)	N/A	N/A	20605.6448
ENSG00000176692	FOXC2	N/A	N/A	916.959132
ENSG00000203883	SOX18	N/A	N/A	4530.81837

PROX1 ChIPSeq binding tracks are shown in Figure 4.3.4.2. The ChIPSeq did not find PROX1 to have a significant peak suggesting ZEB1 binding, in comparison to the IgG. In a lymphatic specific gene such as PROX1, it may have been an issue to use histone modifications ChIPSeq and DNase-Seq which was conducted in HUVECs in order to locate regions of interest such as enhancer regions, as these are thought to be cell-type specific.

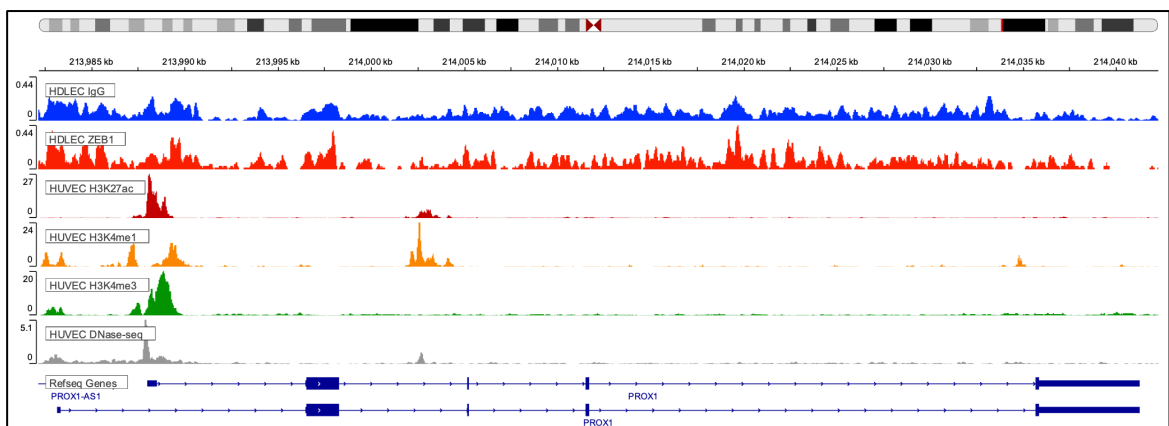


Figure 4.3.4.2. ChIPSeq binding tracks for PROX1 found no significant peaks between ZEB1 and the IgG. Histone ChIPSeq binding profiles was accessed through IGV software and aligned to ZEB1 ChIPSeq data. ChIPSeq binding profiles of ZEB1 in HDLECs, H3K27ac, H3K4me1, H3K4me3 in HUVECs. DNase-Seq shows DNase hypersensitivity sites in HUVECs. The x axis represents the genomic position; the y axis the read depth normalised signal. Made using IGV.

4.3.5 SLUG siRNA knockdown does not induce a change in ZEB1 protein expression

To investigate the connection of ZEB1/SLUG/SNAIL axis, SLUG knockdown was performed by siRNA following the same protocol as ZEB1. SLUG expression was significantly decreased by 64% ($P = 0.0001$) (Figure 4.3.5.1, Panel A). There no change in the expression of ZEB1 ($P = 0.1219$) or SNAIL ($P = 0.6474$) (Figure 4.3.5.1, Panel B and C). This could suggest the action of ZEB1 is upstream of SLUG, as decrease of SLUG did not reciprocally increase ZEB1 expression as seen in EMT (Wels et al., 2011a). A study by Cai et al., linked the supposed mesenchymal state of LECs to the action of SLUG, including affects in permeability, integrity of the endothelial monolayer and smooth muscle cell recruitment (Cai et al., 2015), more research is needed to investigate the role of ZEB1, shown to increase SLUG by 322% following knockdown (Figure 4.3.3.1, Panel B) to support this phenotype seen by Cai et al.

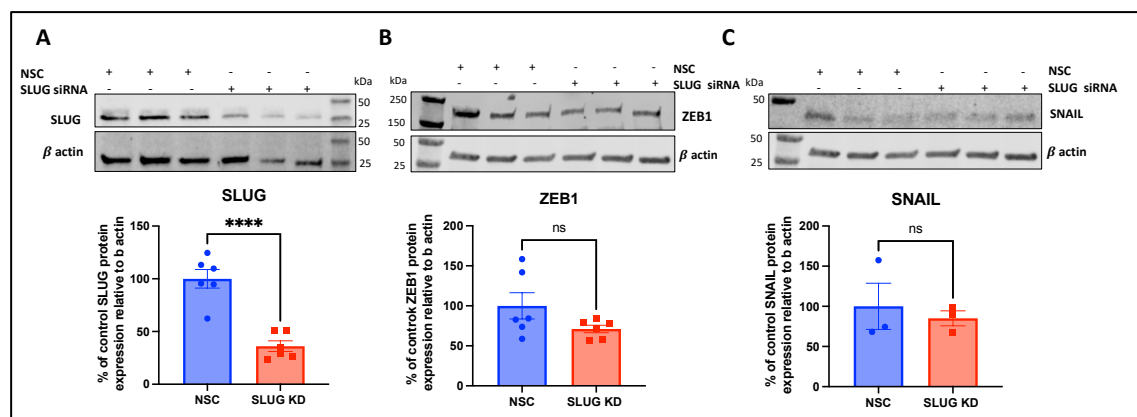


Figure 4.3.5.1 SLUG siRNA knockdown in HDLECs decreases SLUG protein expression. SLUG protein was quantified following SLUG siRNA knockdown in HDLECs $N=6$, **** $P < 0.0001$. Western blots were stripped and reprobed for markers of interest and analysed with Odyssey Image Studio with representative images shown. B. ZEB1, $N=6$. C. SNAIL, $N=3$. Data present as mean \pm SEM and analysed with an unpaired t test.

4.3.6 ZEB1 knockdown alters the metabolic profile of HDLECs

The metabolism of a cell is intrinsically linked to their behaviour. For changes in cellular identity to occur, such as in EndMT, the metabolic profile must be adjusted accordingly (Lovisa and Kalluri, 2018). Mitochondrial respiration has been shown to mediate LEC specification and maintenance via epigenetic regulation of VEGFR3 and PROX1 (Ma et al., 2021), which are dysregulated following ZEB1 knockdown (Figure 4.3.4.1, Panels A and B). RNA Sequencing of ZEB1 knockdown further suggests dysregulation of metabolism, as FOXO1 was significantly downregulated (Table

4.3.6.1.). FOXO1 is thought of as the master of quiescence, driving a change in metabolism, reducing both mitochondrial respiration and glycolysis (Wilhelm et al., 2016). C-MYC, a driver of cell division, is suppressed by FOXO1, in our RNA data C-MYC was not differentially expressed ($P_{adj} = 0.46$) but predicted activated (Chapter 3, Figure 3.3.2.2).

PFKFB3 opposes FOXO1, shown to be a glycolytic activator, promoting tip cell competition in the vasculature, and therefore vessel sprouting (De Bock, Georgiadou, Schoors, et al., 2013). Inhibition of PFKFB3 in proliferating ECs induces quiescence and reduces ATP consumption (De Bock, Georgiadou, Schoors, et al., 2013). PFKFB3 was not differentially expressed ($P_{adj} = 0.15$) at an RNA level (Table 4.3.6.1). Investigating these regulators of cell metabolism at a protein level (Figure 4.3.6.1), we found that these proteins were not significantly changed following ZEB1 knockdown. This was despite FOXO1 being significantly decreased at an RNA level, as shown in Table 4.3.6.1. Predictions of activation by IPA of C-MYC were not seen at protein level. There are of course multiple layers of regulation between RNA and protein, thus one cannot be completely predictive of the other.

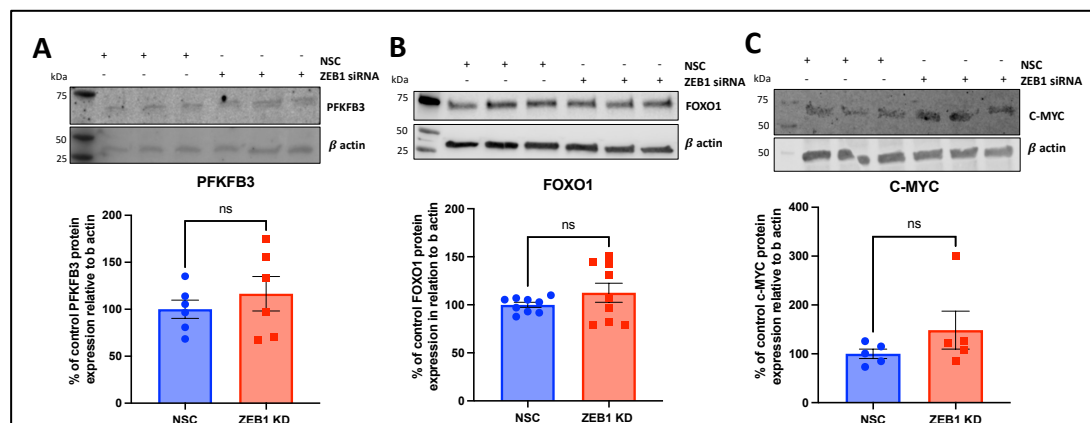


Figure 4.3.6.1. ZEB1 siRNA knockdown does not affect protein expression of metabolic markers as measured by western blot analysis. A. PFKFB3 protein was quantified following ZEB1 siRNA knockdown in HDLECs N=6. Western blots were stripped and reprobed for markers of interest and analysed with Odyssey Image Studio with representative images shown. B. FOXO1, N=9. C. C-MYC, N=6. Data present as mean \pm SEM and analysed using an unpaired t test.

Table 4.3.6.1 ZEB1 siRNA knockdown downregulates FOXO1 expression at RNA level. RNA Sequencing of ZEB1 siRNA knockdown HDLECs. Average basal expression of the DESeq2 normalised counts of three non-silencing control replicates.

Metabolic Genes				
ENSEMBLE ID	Gene Symbol	Log2FoldChange	P _{adj}	Basal Expression
ENSG00000170525	PFKFB3	N/A	N/A	1529.66819
ENSG00000150907	FOXO1	-0.2547273	0.00699297	1005.32767
ENSG00000136997	C-MYC	N/A	N/A	2142.13037

To understand how ZEB1 may impact the functional metabolism of LECs, the Mitochondrial Stress Seahorse Assay was performed on the ZEB1 knockdown LEC (Figure 4.3.6.2). The assay primarily measures oxygen consumption rate (OCR) in response to different drugs added to the media at pre-determined intervals. The expected trace for this assay is shown in Panel A, which also gives an indication of the metabolic parameters extrapolated (Agilent Technologies, 2019). Throughout the assay the ZEB1 knockdown cells maintained a significantly lower rate of respiration throughout, shown by Panels B and C (0.29 versus 0.2 pmol/min/ μ g [P = 0.0031]). This may suggest altered endogenous ATP demand of the knockdown cells. ATP-Production coupled regulation was also significantly decreased in the ZEB1 knockdown cells in comparison to the control (0.26 versus 0.15 pmol/min/ μ g [P = 0.0149]), suggesting this decrease in basal respiration is ATP-linked, and not driven by a decrease in other oxygen consumption activities. Maximum respiration was not significantly different between the control or knockdown cells (0.58 versus 0.52 pmol/min/ μ g [P = 0.317]), suggesting no alterations in the mitochondrial membrane proton gradients, metabolic enzyme activity or damage to the mitochondria. Spare respiratory capacity was also unchanged following knockdown (0.30 versus 0.34 pmol/min/ μ g [P = 0.482]). This is despite the decrease in basal respiration by the ZEB1 knockdown cells, suggesting although decreased respiration, these cells are still able to meet an increased energy demand and/or stress. Proton leak (Panel G) remained constant (0.03 versus 0.04 pmol/min/ μ g [P = 0.728]), suggesting the decrease in basal respiration is a result of decreased mitochondrial oxidative phosphorylation and not due to a decrease in oligomycin-insensitive respiration. The

negative results in the non-mitochondrial oxygen consumption suggests that all the respiration in the LECs is dependent on mitochondrial activity (-0.95 versus -0.93 pmol/min/ μ g [P = 0.774]), the negative values are a result of the last injection of drugs taking the respiration to below the initial basal rate, suggesting the contribution of non-mitochondrial oxidases to the oxygen consumption is minimal. The coupling efficiency shown in Panel I estimates the amount of percentage of basal respiration used to drive ATP synthesis ($100/[\text{ATP-Linked respiration}]/[\text{Basal Respiration}]$), this shows no difference between the two groups (68.83 versus 65.69% [P = 0.595]) suggesting the rate of basal respiration and ATP-production is not due to an uncoupling of the oxidative phosphorylation and ATP Synthesis. To investigate if the change seen is a result of an increase in anaerobic glycolysis, which produces protons (decreasing the extracellular pH), extracellular acidification rate is measured throughout (Panel J). This showed an overall increase in acidification throughout the assay, as aerobic respiration is halted through the inhibition of the electron transport chain. The ZEB1 knockdown cells therefore are predicted to maintain a lower rate of glycolysis throughout the assay in comparison to the control cells.

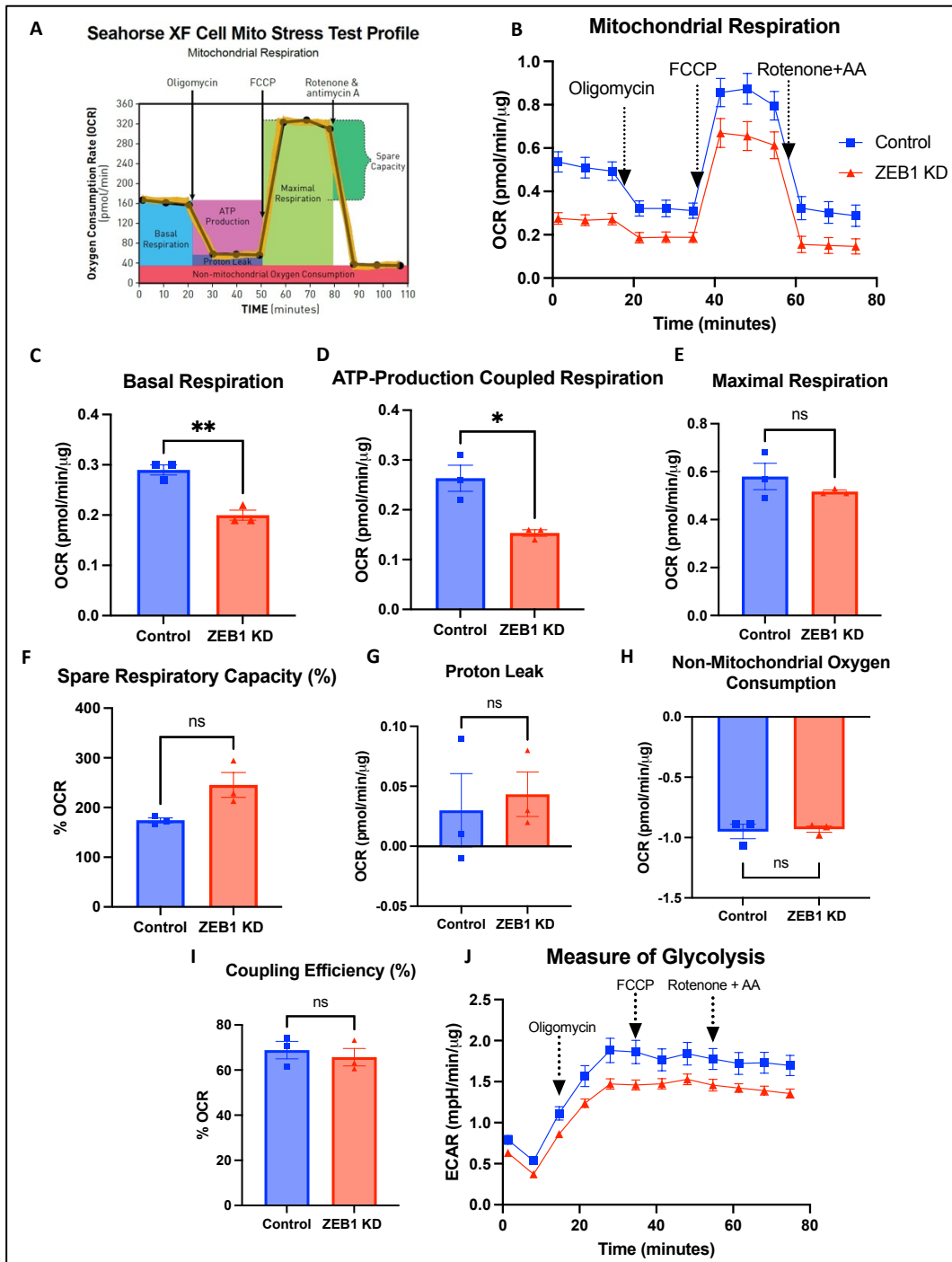


Figure 4.3.6.2 Metabolic analysis of HDLECs subjected to ZEB1 siRNA knockdown. HDLECs were re-plated following ZEB1 siRNA transfection and left to adhere overnight. Data represents three biological replicates and presented as mean \pm SEM of 10 wells. Data analysed primarily in Agilent Wave Desktop, then inputted into Prism and analysed with an unpaired t test. A. Seahorse Mitochondrial Stress Test trace from (Agilent Technologies, 2019) showing changes in oxygen consumption following addition of assay drugs at pre-determined timepoints. B. Oxygen consumption rate change following ZEB1 knockdown throughout the assay time course. C. Basal respiration of HDLECs following loss of ZEB1, $**P < 0.005$. D. ATP-production coupled respiration following loss of ZEB1, $*P < 0.05$. E. Comparison of maximal respiration of HDLECs as a consequence of loss of ZEB1. F. Spare

respiratory capacity as a percentage of the basal respiratory capacity. G. Measure of proton leak across the electron transport chain measured after the addition of Oligomycin, ATP synthase inhibitor. H. Non-mitochondrial oxygen consumption. I. Coupling efficiency of the electron transport chain to ATP production. J. Measure of glycolysis through extracellular acidification rate (ECAR) throughout the mitochondrial stress assay.

4.4 Discussion

The aim for this chapter was to investigate the role of ZEB1 in EndMT, with the hypothesis that actively growing LECs will promote a partial EndMT-like phenotype which will be replicated by loss of ZEB1. We utilised LECs to first understand the effect of different cell density on ZEB1 expression, as well as other markers of EndMT and lymphatic identity. In the subconfluent samples, whereby cells had the space to proliferate and were mostly without cell-cell contacts, ZEB1 expression was lower in comparison to the confluent cells, whereby cells had no room to grow, had established cell-cell contacts and ZEB1 expression was higher. The confluent samples we could imply were quiescent LECs in a static monolayer. Thus, the results show that in quiescent LECs we have increased ZEB1 expression (Figure 4.3.1.1). To investigate if ZEB1 plays a role in establishing this quiescence, ZEB1 was knocked down using siRNA. In these knockdown cells, drivers of EMT, and E-box binding transcription factors – SLUG and SNAIL were both significantly upregulated (Figure 4.3.3.1). Lymphatic identity markers PROX1 and VEGFR3 were also dysregulated in response to ZEB1 knockdown (Figure 4.3.4.1). There was no change in cell metabolism markers PFKFB3, FOXO1 or C-MYC (Figure 4.3.6.1) at a protein level. To understand the changes in the functional metabolism of these cells, the Seahorse Assay for Mitochondrial Stress was used to measure changes in oxygen consumption. The ZEB1 knockdown cells had a decreased basal metabolism and a significantly decreased change in ATP-linked respiration (Figure 4.3.6.2), suggesting a decreased energy requirement of these cells.

Investigating expression of EndMT markers in response to changes in cell density, ZEB1 was not the only dysregulated protein. SNAIL and ZEB2 expression were significantly higher in the confluent cells, which is unexpected, as both are drivers of EMT (Galván et al., 2015) and implicated in EndMT (Welch-Reardon et al., 2015). In a

model of breast cancer-cell conditioned ECs and embryonic stem cell-derived ECs, SLUG and SNAIL work together to induce endothelial to mesenchymal transition (Kokudo et al., 2008; Lopez et al., 2009). Also of note is the increased expression of ZEB2 in the confluent conditions. ZEB2 is also thought of as an inducer of EndMT, thus we expect the expression pattern to follow SLUG, but as ZEB1 and SNAIL, alternate roles for these transcription factors in altered conditions should be considered. PROX1 is a key marker of lymphatic identity, loss of PROX1 results in loss of key characteristics of LECs and even reversal of the lymphatic phenotype (Johnson et al., 2008). It is proposed that SLUG can regulated the fate of LECs by regulating PROX1 expression, a study by Cai et al, found that with SLUG depletion, PROX1 expression was also decreased (Cai et al., 2015). This is not reflected in the conditions tested in Figure 4.3.1.1. VE-Cadherin was also higher in the confluent cells, this is a protein implicated in formation of cell-cell junctions, as the confluent cells make more of these junctions as they were plated at a high density to establish quiescence. Thus, this increase in VE-Cadherin was expected and fits with published literature (Breviario et al., 1995; Dejana et al., 1999). PROX1 expression was also increased in the confluent samples (Figure 4.3.1.1). In development, PROX1 is a key marker of differentiating LECs (Wigle, 2002; Wigle and Oliver, 1999). LECs initially bud from the CV in an initially PROX1 independent manner, but maintenance of the activities required to establish the lymphatic vasculature such as migration and polarised budding depend on PROX1 expression (Wigle, 2002). On this basis, we might have expected PROX1 expression to be higher in the subconfluent samples, as we could imply the subconfluent conditions loosely replicating that on the initial conditions found in early development, however in early development, the cells maintain at least some cell-cell junctions, whereas in our subconfluent condition cells were mostly without contact to any cell neighbours, which could have affected their protein expression. SLUG expression was markedly decreased in the confluent cells, which fits with literature suggesting SLUG is a driver of EndMT and its expression in LECs is connected to a mesenchymal phenotype (Cai et al., 2015). The changes seen in this experiment of actively growing LECs versus quiescent LECs suggest that a better model is required to replicate a partial EndMT signature, for

partial EndMT like that seen in the vasculature, we would require the cells to remain in contact. In subconfluent conditions, although otherwise replicating a growth state alike to EndMT, the cells remain distant, this was shown by the increase in VE-Cadherin in confluent conditions (Figure 4.3.1.1). Following ZEB1 knockdown, SLUG expression was markedly increased (Figure 4.3.3.1), suggesting an interaction between SLUG and ZEB1 expression. This has been seen in other cell types, such as in melanoma, where SLUG is seen to directly bind to the ZEB1 promoter and induce an EMT-like phenotype (Wels et al., 2011a). The ChIPSeq results (Figure 4.3.3.2) revealed ZEB1 does not directly bind to SLUG, but SLUG ChIPSeq in HDLECs could be of interest. To investigate this relationship further, we subjected LECs to a SLUG siRNA knockdown, following the same protocol, these results are shown in Figure 4.3.5.1. These results suggest that in LECs, ZEB1 is upstream of SLUG in this pathway, as with SLUG expression decreased, ZEB1 expression was unaffected. SNAIL was also upregulated in response to ZEB1 knockdown, again a relationship of ZEB1-SLUG-SNAIL has been documented previously in other cell types in the context of EMT (Wels et al., 2011a). SNAIL was not affected by the loss of SLUG (Figure 4.3.5.1), and neither was ZEB1, suggesting SNAIL and ZEB1 may have upstream action before SLUG, or act independently of SLUG. Other markers of EMT/EndMT tested were unaffected by ZEB1 knockdown, this is indicative of the partial EndMT hypothesis, as it was documented that VE-Cadherin expression remains unchanged (Figure 4.3.3.1) as the cell-cell junctions remain, despite increase in other drivers of EndMT (Welch-Reardon et al., 2014).

Looking at markers of lymphatic identity, with ZEB1 knockdown we found altered expression of PROX1 and VEGFR3 (Figure 4.3.4.1). PROX1 expression was increased, opposing the result seen in Figure 4.3.1.1, where PROX1 expression was increased in the confluent condition, and ZEB1 protein expression was highest. However, there are multiple variables between the two experiments, in the siRNA knockdown, the cells were plated at 80% confluency, whereas the subconfluent versus confluent experiment (Figure 4.3.1.1) used extreme cell densities of around 25% and 100%, thus the protein expression of ZEB1 was not the only variable to differ, shown by the

significant differences in other protein expression, thus the level of PROX1 could be mediated by another factor in the experiment of lymphatic growth. In the literature there is well documented relationship between PROX1-VEGFR3 (Srinivasan et al., 2014b; Ma et al., 2021). In the early embryo, VEGFR3 is suggested to create a positive feedback loop to maintain identity of LECs through the expression of PROX1. VEGFR3 is downstream of PROX1, so in regulating PROX1 expression, regulates its own expression, this loop is thought to maintain lymphatic identity (Srinivasan et al., 2014b). Our results (Figure 4.3.4.1) show this feedback loop has been dysregulated by ZEB1 knockdown, we see an increase in PROX1, but a decrease in VEGFR3 expression, suggesting that PROX1 is not functioning downstream to increase VEGFR3 expression, or that at some point in the translation process, VEGFR3 is not being made. The VEGFR3 protein could also be ubiquitinated at a higher rate resulting in enhanced degradation, or the level of its ligand, VEGF-C is decreased in the knockdown cells. This should be investigated further in a chemiluminescence enzyme-linked immunosorbent assay (CL-ELISA) for detection of VEGF-C at high sensitivity (Ghavamipour et al., 2020).

Mitochondrial respiration has been shown to control the lymphatic endothelial phenotype (Ma et al., 2021; Wong et al., 2017). In lymphatic development, VEGFR3 expression has been shown to be influenced by mitochondrial complex III inhibition, specifically for histones H3K4me3 and H3K27ac function at the VEGFR3 loci which enables gene transcription (Ma et al., 2021). This mechanism activates and maintains the VEGFR3-PROX1 feedback loop and ultimately controls the amount and budding of LEC progenitor cells. Upon disruption of this feedback loop by respiratory changes, differentiation slows, eventually preventing further generation and budding (Ma et al., 2021). The HDLECs used in these experiments were from an adult, so we could imply that this feedback loop is not active in these cells or lowered in comparison to during development to maintain an LEC phenotype. PROX1 is reported to induce a metabolic switch toward increased fatty acid oxidation. This produces acetyl coA, which is consequently utilised in acetylation of key lymphangiogenic genes (Wong et al., 2017). In our results, we see ZEB1 knockdown

increases PROX1 expression (Figure 4.3.4.1), but we see no consequential increase in oxidative metabolism (Figure 4.3.6.2). This could be due to a decrease in VEGFR3 expression, seen in Figure 4.3.4.1, as inhibition of VEGFR3 has been shown to decrease FAO flux (Wong et al., 2017). Alternatively, this change in metabolism could be explained by the increase in SLUG expression (Figure 4.3.3.1). SLUG has been implicated in contributing to a mesenchymal status of LECs (Cai et al., 2015). SLUG is also known to induce EndMT by decreasing VE-Cadherin expression (Lopez et al., 2009). Although we do not see this reflected in our results (Figure 4.3.3.1), we do see a decreased metabolic activity associated with the mesenchymal phenotype (Figure 4.3.6.2). With knockdown studies *in vitro*, Cai et al., showed that SLUG may positively regulate PROX1 expression, thus SLUG may also play a role in maintaining the fate of LECs. Crucially, we can see that the decrease in basal respiration is not due to an increase in non-oxidative metabolism (Figure 4.3.6.2), which would otherwise suggest a switch in ATP generation from oxidative to anaerobic, instead we can conclude ZEB1 knockdown lymphatic cells are at a lower energy status.

Combining these ideas, we can suggest the metabolic changes seen with ZEB1 knockdown are a result of increased SLUG expression, resulting in a more mesenchymal phenotype with a lower energy requirement. FOXC2, a transcription factor primarily involved in valve development, has also been implicated in contributing to a mesenchymal status, with knockout cells highly plastic with poor differentiation (Cai et al., 2015), we saw no change in FOXC2 expression with ZEB1 knockdown. More research should be conducted to establish the role of SLUG and PROX1 in this scenario, as from the literature they theoretically have opposing roles on metabolism, as SLUG decreases the overall energy requirement of the cell but enhances PROX1 expression which increases fatty acid oxidation (Wong et al., 2017; Cai et al., 2015). Interestingly, there was no change in FOXO1/PFKFB3/MYC at protein level (Figure 4.3.6.1) signalling despite a change in basal metabolism following loss of ZEB1 (Figure 4.3.6.2). In a partial EndMT mechanism, alike to blood vessel sprouting, we would expect to see an increase in glycolysis to meet the energy demands of the tip cell leading the sprout, this would be shown by increased PFKFB3

and MYC and downregulation of FOXO1. It could be that loss of ZEB1 from the LECs has altered the reciprocal regulation of the EndMT signalling with SLUG and SNAIL, which has caused general dysregulation of the signalling pathways, and consequently the cell's metabolism, rather than producing a clear phenotype. It would be interesting to know the amount of acetyl CoA production in these cells to unpick the mechanisms at play and the exact role of ZEB1 in these pathways. Acetyl CoA can be detected by high performance liquid chromatography with high sensitivity (Shurubor et al., 2017). Other Seahorse assays could also be used, such as the Glycolytic Rate Assay, to further understand the changes in cell metabolism following loss of ZEB1.

In LECs, there is a heavy reliance on anaerobic glycolysis for ATP-production (Yu et al., 2017). The importance of the mechanisms controlling endothelial cell metabolism is reflected in the many disease mechanisms in which we see metabolic dysfunction. In cancer cells there is a high glycolytic metabolism even in abundant oxygen (Yang et al., 2012), this is also seen in fast-proliferating cells, despite being less efficient than oxidative phosphorylation (Lunt and Vander Heiden, 2011). Lymphatic malformations (LMs) are a congenital disease categorised by disordered lymphatic vessels in the embryo. The LECs in these vessels proliferate abnormally, causing excessive lymphangiogenesis (Boscolo et al., 2015). These abnormal vessels create cysts which are prone to infection and can affect the functionality of nearby organs (Gallagher et al., 2022). A study by Cai et al., suggested that LECs in LMs may lose their mesenchymal phenotype and contribute to pathogenesis of the disease, this change in phenotype will be reflected by a change in metabolism (Cai et al., 2015). A study by Jiang et al., found the lymphatics of LMs expressed the rate-limiting enzyme of glycolysis, pyruvate kinase M2, higher than healthy lymphatics of the skin (Jiang et al., 2021). This suggests that these LM lymphatics are utilising glycolysis to mediate pathogenic lymphangiogenesis. Our results show that ZEB1 knockdown may influence the cell to a mesenchymal energy profile, thus the pathway by which ZEB1 is acting through should be the topic of further research, as this could uncover a potential therapeutic target for the treatment of LMs

whereby, we could switch highly glycolytic, proliferating LECs to a lower energy, more mesenchymal phenotype.

Investigating the level of ZEB1 in a robust model of EndMT, and the effect of knockdown, would help uncover the role of ZEB1 in this transition. In our model of growth, we attempted to replicate a proliferating versus static monolayer condition, this has been investigated in HUVECs and documented to not replicate EndMT (Beloglazova et al., 2022). The addition of TGF β would improve this experiment to robustly induce EndMT in LECs (Yoshimatsu et al., 2020). An alternative model of EndMT would be to investigate tube formation using Matrigel, which supplies growth factors and extracellular matrix proteins required to form a tubular formation (Beloglazova et al., 2022). More mesenchymal cells have a reduced ability to form tubes and show increased motility (Yoshimatsu et al., 2020), we were unable to test the effect of ZEB1 on these characteristics using current chosen methods. Testing the exact measurement of glycolysis can also be more accurately measured by the Glycolytic Rate Seahorse Assay. Research effort should be placed into this avenue, as glycolytic dysfunction is a key marker of many diseases, including cancer and LMs.

In conclusion, this chapter has investigated the role of ZEB1 in lymphatic growth whereby expression was highest in a quiescent monolayer. When ZEB1 was knocked down, SLUG and SNAIL expression was increased, VE-cadherin expression was unchanged, which is potentially suggestive of a partial EndMT-like phenotype. Basal respiration was also decreased, therefore using published literature, we can infer these cells are in a mesenchymal, lower energy state. This ultimately suggests ZEB1 may play a role in lymphatic identity, as seen by an increase in PROX1 expression, and the metabolic status of the LEC.

Chapter 5. ZEB1 Plays No Major Role in the Early, Post-Natal Extension of the Lymphatic Vasculature of the Ear Dermis, or Adult Maintenance.

5.1 Introduction

5.1.1 Models of developmental lymphangiogenesis

Multiple models of lymphatic vascular are currently utilised in lymphatic research, including birds, tadpoles, zebrafish, and mice (Bruyère and Noël, 2010; Wilting et al., 2000). Each with their merits and drawbacks and there is not one optimal model for robust, translatable research. Zebrafish for example, have a very simple vascular system, which is easy to genetically modify, easy to visualise and allows for a high throughput (Suarez et al., 2023). However, zebrafish have no lymph nodes, do not experience the same environment as humans, or contain all the same organs (Suarez et al., 2023). Quail share similar developmental mechanisms as humans, with LECs sprouting from the CV at day 4 of incubation (Wilting et al., 2006). Cell lineage studies by Wilting et al., revealed PROX1 expression in prospective LECs in the jugular lymph sacs as well as those in established lymphatic vessels (Wilting et al., 2006). Similar to studies in mice, the dermal and more superficial lymphatics were derived from local lymphangioblasts, which are lymphatic progenitor cells which do not originate from the embryonic veins (Ribatti and Crivellato, 2010; Buttler et al., 2006; Wilting et al., 2001). Research by Ny et al., has proposed the frog as a lymphangiogenic model due to similarities in development of lymphatic development (Ny et al., 2005). Vessels have been detected to originate from lymphangioblasts and transdifferentiate from vascular ECs (Ny et al., 2005). However, frogs have a lymph heart, an organ whereby the lymph vessels circulate the lymph to, and which pumps it back into venous circulation (Baldwin et al., 1993). Like humans, knockdown studies of PROX1 in frogs caused lymphedema by impairing commitment to the lymphatic phenotype (Ny et al., 2005). Similarly, VEGF-C knockdown affected migration of LECs, but also affected blood vessel formation, suggesting VEGF-C plays a role in the establishment of both vascular systems in frogs (Ny et al., 2005). The divergence between human and frog lymphatic systems means the use of the xenopus model is an unpopular choice for investigating lymphatic development.

Mice have been routinely used for the research of lymphatic development, due to their small size, similarity to the human genome, and ease to genetically modify (Suarez et al., 2023). Many assays have been developed to specifically measure development, maintenance and response to disease or injury in mice. In development, back skin of the embryo has been utilised to measure outgrowth and expansion of the lymphatic network at different points in development (Cha et al., 2016; Geng et al., 2020; Majima et al., 2013; Dieterich et al., 2020). Dermal lymphatics are easy to access as they are close to the surface; this means they can be easily visualised by intradermal injections of FITC or prepared for immunohistochemistry (Suarez et al., 2023). The plexus of lymphatics can be measured for functionality based on drainage, or for levels of lymphatic coverage, vessel size and branching via image analysis after confocal microscopy (Suarez et al., 2023).

For immunofluorescence or immunohistochemistry studies, a robust marker of lymphatic vessels is essential, allowing one to distinguish blood vessels from lymphatics and lymphatics from macrophages (Gordon et al., 2010; Stacker et al., 2002). PROX1 is a transcription factor, enriched in LECs, therefore serves as a nuclear marker, however, is also expressed in cardiomyocytes, hepatocytes and pancreatic epithelial cells, thus double staining with a pan-endothelial cell marker is highly advised (Wilting et al., 2002). VEGFR3 is also commonly used as a marker of lymphatic vessels, however in early development, is expressed on all ECs, and only later expressed primarily on LECs, additionally, VEGFR3 has been found on tumour blood vessels, highly fenestrated blood vessels and macrophages (Stacker et al., 2002). Podoplanin is a podocyte membrane protein which shares similar expression pattern with VEGFR3, however is not present in larger lymphatic vessels that have smooth muscle coverage (Stacker et al., 2002). Lymphatic vessel endothelial hyaluronan receptor-1 (LYVE1) is a surface receptor for hyaluronan expressed in LECs prior to PROX1 in early embryonic development. LYVE1 is also expressed in some macrophages, which in development have been seen to incorporate into developing lymphatic vessels in the skin (Gordon et al., 2010). LYVE1 is currently regarded as

one of the most specific markers of the lymphatic endothelium, allowing to distinguish lymphatic vessels from blood vessels, this is especially beneficial in tumour models, where VEGFR3 can be expressed on blood vessels (Jackson, 2004; Johnson et al., 2017). The interpretation of LYVE1 staining can be impacted by expression in macrophages, co-stains should be utilised to mitigate this. However, LYVE1 positive macrophages are not reported in all tissues (Chakarov et al., 2019) and therefore use of LYVE1 remains a robust choice. LYVE1 is reported to be involved in the trafficking of leukocytes, thus is present at high density in the overlapping junctions of smaller lymphatics, however, has comparatively lower expression in the tight junctions of larger collecting lymphatics (Johnson et al., 2017).

5.1.2 Visualisation and quantification of lymphangiogenesis *in vivo*

One method of three-dimensional visualisation of the lymphatic vasculature is through flat-mount imaging. Using immunostaining, dermal lymphatics can be observed from E12.5 onwards (Betterman and Harvey, 2018). This is a crucial time for outgrowth, patterning and refining of the lymphatic network, this continues until approximately 10 weeks old when a mature vasculature is established (Martínez-Corral et al., 2012). Beyond this, lymphangiogenesis is present in the formation of the corpus luteum, during wound healing and in response to pathological stimuli (Karpanen and Alitalo, 2008). Adult lymphangiogenesis can be stimulated with enhanced expression growth factors such a VEGF-C, when subcutaneously injected via adenovirus (Enholm et al., 2001). Induced global knockout of VEGF-C in adult mice resulted in atrophy of the lacteals of the intestine (Nurmi et al., 2015), this suggests genes with a role in LEC maintenance will impact the lymphatic vasculature in adult mice when conditionally deleted.

Measurements of lymphangiogenesis often focus on the density of vessels in a certain area of interest (Clasper and Jackson, 2009), however, multiple parameters should be considered to determine the lymphangiogenic response. For example, enlargement of vessels via dilatation, or an increase in vessel width from proliferation resulting in radial growth, would not be accounted for in a simple

lymphatic count measurement, for this, the area positive for the lymphatic marker or lymphatic width should be considered (Wirzenius et al., 2007; Zhang et al., 2018; Cho et al., 2019; Thowsen et al., 2022). Other useful parameters include vessel segment length (Dieterich et al., 2020), filopodia per vessel segment (Wirzenius et al., 2007) branch point (also known as node) (Wälchli et al., 2021; Zhang et al., 2018), number of tip cells (Fatima et al., 2014) and number of “blunt ends” (Azimi et al., 2020). These parameters together encompass various features of hypoplasia, hyperplasia, sprouting lymphangiogenesis and disordered lymphatic development. A combination of these parameters is advisable when quantifying the lymphatic vasculature at any point *in vivo*.

5.1.3 Regulation of the lymphatic network in the dermis

The lymphatic network in the skin is organised into two plexuses. The superficial plexus is closest to the surface, made up of thin vessels without valves. This network has branches which drain into larger vessels in the lower dermis. The deeper lymphatic plexus is below the arterial network, these vessels are much bigger, with valves to help control the direction of interstitial fluid (Skobe and Detmar, 2000). The lymphatics in the skin require regulation to establish and maintain this structure. Loss of both VEGF-C alleles is incompatible with life, with loss of one allele resulting in lymphoedema of the skin (Karkkainen et al., 2004) emphasising the importance of the VEGF-C/VEGFR3 axis. Similarly with targeted Cre-mediated loss of VEGFR3 in the ear, non-targeted VEGFR3⁺ LECs arise in the tip cells in the ear, resulting in excess proliferation and hypersprouting (Zhang et al., 2018). The involvement of TGF β has been elucidated by James et al., who utilised embryonic dorsal skin to investigate the role of TGF β signalling in initial sprouting of the lymphatic vessel network. TGF β signals in LECs through two distinct receptors, TGF β R1 (also known as ALK5) which activates SMAD2 and SMAD3 or ALK1 which activates SMAD1 and SMAD5. Through induced Cre mediated deletions of TGF β R1 and R2, James et al., was able to discern that signalling through these receptors is essential in the development of the lymphatic network (James et al., 2013). A decrease in sprouting and branching was present in the double mutants, with an increase in proliferation resulting in

hyperplasia. TGF β R2 specifically, has the most significant impact in development, when activated TGF β R2 inhibits proliferation, and upregulates VEGFR3 in cultured human LECs (James et al., 2013). Initial LEC specification and primary sac formation were normal, but inducible deletion at the later stages of network extension was severely disrupted (James et al., 2013). It is important to note, the input of macrophages here in the dermal lymphatic network, which may or may not be incorporated into the developing vessel, are a major source of TGF β in the skin, thus enhancing this pathway of signalling (James et al., 2013). ZEB1 has reported be affected by TGF β signalling in many tissues and disease states such as glioblastoma (Joseph et al., 2014), lung adenocarcinoma (Guo et al., 2022), and corneal inflammation (Liang et al., 2022). In murine retina vascular ECs, ZEB1 is not present in angiogenic tip cells (Chapter 1, Figure 1.5.1.1), but expressed in the quiescent endothelium. Expression of ZEB1 in cultured LECs was also seen in quiescent conditions, and in quiescent lymphatic vessels of the murine diaphragm (Chapter 1, Figure 1.5.2.1). However, investigation of ZEB1 in lymphangiogenic conditions *in vivo* has not been conducted.

In this chapter, we used a transgenic animal mouse model of inducible endothelial cell knockout to investigate the effect of ZEB1 knockout in LECs. Mice were investigated at development (P5) and in adulthood. The level of lymphangiogenic remodelling was investigated through lymphatic morphology of the ear, visualised by immunofluorescence staining.

5.2 Hypothesis and Aims

Hypothesis: Loss of endothelial ZEB1 will result in a lymphangiogenic phenotype

Aims:

1. Characterise a mouse model of inducible endothelial cell ZEB1 knockout
2. Investigate the lymphatic beds in development for changes in lymphatic morphology following loss of ZEB1
3. Investigate the lymphatic beds in adult mice for changes in lymphatic morphology following loss of ZEB1

5.3 Results

5.3.1 Characterisation of ZEB1^{IECKO} transgenic mice

The Cre-ERT loxP system allows for inducible, conditional knockout of target floxed genes upon the administration of tamoxifen. Cre-recombinase is a protein from the bacteriophage P1, which recognises a 34-base pair loxP site, this site can be flanked either side of target DNA, with the recombinase removing the coding region between the sites (Figure 5.3.1.1). Restricting the expression of Cre recombinase is ensured by placing the Cre under the control of a promoter/enhancer sequence. This allows spatial control of the excision. Temporal control is enabled by fusing the Cre-recombinase with a mutated estrogen receptor ligand binding domain (ERT2), this sequesters the Cre into a complex with hsp90 in the cytoplasm unable to ligate the target DNA in the nucleus. Upon administration of tamoxifen, the active metabolite OHT is produced, this prevents interaction with hsp90 allowing the Cre into the nucleus where it can recombine the loxP sites and excise the target DNA (Payne et al., 2018). Tamoxifen can be injected at any point to induce gene deletion, with minimal side effects of toxicity (Feil et al., 2009). This model is particularly beneficial as global knockout of ZEB1 causes lethality, embryonically and perinatally (Takagi et al., 1998). For an endothelial specific knockout, the Cre-recombinase was placed under the promoter for endothelial junctional marker VE-Cadherin. This has been validated to knockout genes in vascular ECs and LECs (Wang et al., 2010).

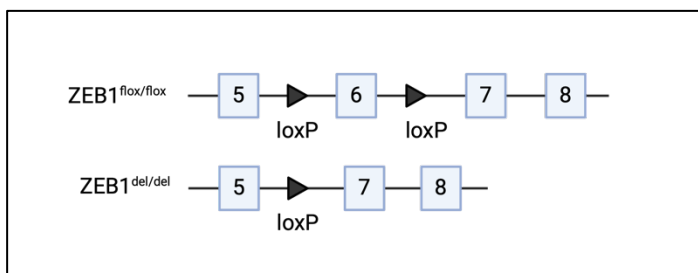


Figure 5.3.1.1. Schematic illustration of the loxP sites which flank exon 6 of ZEB1. Cre recombinase activity leads to excision of the flanked exon. Exon 6 was chosen due to the large central protein coding sequence contained within. Deletion of exon 6 results in a premature translational stop in exon 7, this leads to a reduction of ZEB1 full length transcripts (Brabletz et al., 2017). Blue boxes represent exons, triangles indicate the location of loxP sites.

To determine the genotype of the mice, ear (adult) or tail (P5) clippings were sent off to Transnetyx, an automated genotyping service which conducts real-time PCR to a high (99.97%) accuracy. The raw values of one of the reports is shown in Table 5.3.1.1. Any signal represents presence of the excision product of recombination of the ZEB1 gene locus as shown in Table 5.3.1.1. The result of a positive signal represents a Cre positive genotype, and therefore ZEB1^{iECKO} mouse. No signal is a negative result, representing Cre negative genotype, and therefore represents a Control mouse. The results from the genotyping have not been directly validated as a reliable method of confirmation of loss of gene and protein expression. It is advised this be confirmed by further investigation to confirm the level of mRNA and protein knockdown.

Table 5.3.1.1. Example of a Transnetyx raw data report. The signal correlates to the relative copy number of the excision product. Detection of the excision product resulted in a positive result.

ZEB1 ^{iECKO}			
Well	Sample Name	Signal	Result
A1	221853	0.00785	+
B1	221854	0	-
C1	221855	0	-
D1	221856	0.0092	+
E1	221857	0	-
F1	221860	0.008	+
G1	221861	0.01005	+
H1	221862	0	-
A2	221863	0.00945	+
B2	221865	0.0112	+
C2	221866	0.0114	+
D2	221852	0	-
E2	221858	0	-
F2	221859	0.0054	+
G2	221864	0.00605	+

Initial attempts of visualising the amount ZEB1 knockdown by immunofluorescent techniques were unsuccessful (Figure 5.3.1.2). The trachea of Control and ZEB1^{iECKO} mice was dissected and stained for endothelial marker IB₄ and ZEB1, although vessels were clearly visible in some samples (Figure 5.3.1.2), the expression of ZEB1 was either seen across the tissue (Figure 5.3.1.2) or devoid of any positive staining in

one or both chosen markers. The mouse model was chosen for specificity in gene knockdown from ECs, any tissues from the mouse will contain a multitude of different cell types, presenting difficulty to quantify ZEB1 expression specifically in the ECs. Therefore, isolation of the ECs from a whole tissue may offer a better solution to quantifying ZEB1 expression.

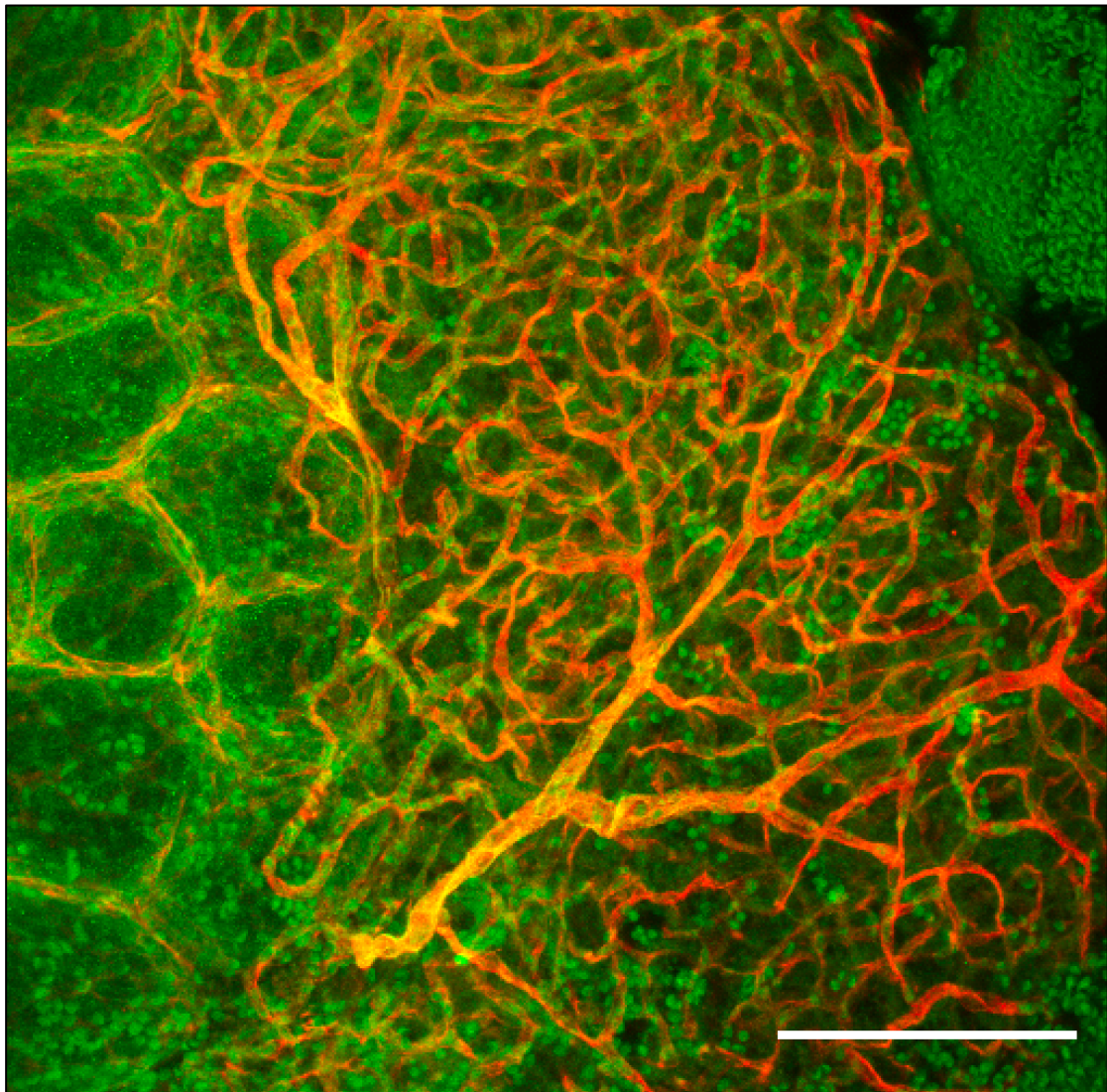


Figure 5.3.1.2. Mouse trachea was unable to be optimised for quantification of ZEB1 knockdown. Adult mouse trachea was stained with IB₄ (red) and ZEB1 (green). Vessel structures were visible but due to the promiscuity of ZEB1 expression, quantification was unable to take place. Scale bar = 100 μ m.

ECs were isolated from adult mice following five daily doses of tamoxifen via IP injection to induce Cre recombination. Three weeks later, mice were sacrificed, and the lungs dissected and dissociated into a cell suspension. The suspension was

followed by magnetic cell sorting to isolate a CD31⁺ population. The cell fractions were run on western blot as shown in Figure 5.3.1.3. Mouse A was Cre negative, and Mouse B was Cre positive. It was expected to see a difference in ZEB1 expression in comparison to the control in the CD31⁺ fraction, representing the endothelial cells. However, when analysed using Image Studio, expression of ZEB1 when normalised to the β actin control, the signal values were 21.22 and 24.55 for mouse A and B, respectively. This could suggest the mouse model was not translating to a decrease in protein expression, or that the ZEB1 protein has a long half-life, so is still present in the endothelial cells despite theoretical degradation of its mRNA.

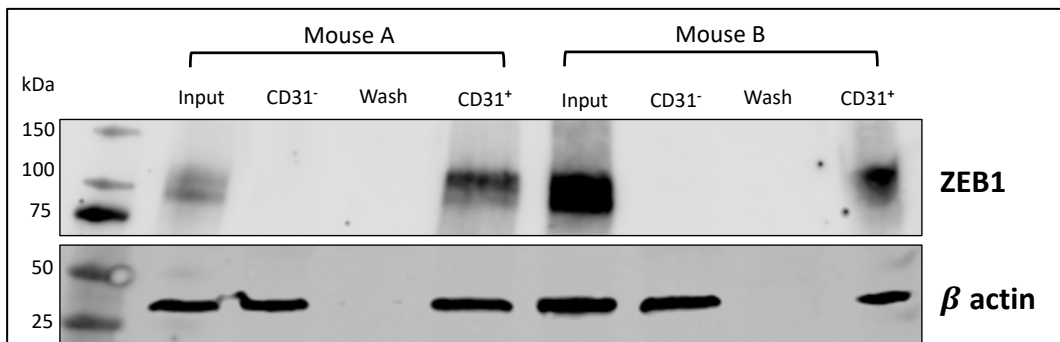


Figure 5.3.1.3. No change in the ZEB1 expression between the CD31⁺ fractions of Mouse A and B. Mouse A was Cre negative, and Mouse B Cre positive. The signal values were analysed using Image Studio software and normalised to β actin expression.

Successful confirmation of the level of knockout was completed using mRNA isolated from the CD31⁺ population. mRNA was extracted from this fraction, reverse transcribed into cDNA, and quantified for ZEB1 RNA expression using digital droplet polymerase chain reaction (ddPCR). This was normalised to housekeeping gene GAPDH. The data shown in Figure 5.3.1.4, shows a significant decrease of 57% ($P = 0.0006$) in the levels of ZEB1 mRNA expression in the CD31⁺ cell fraction compared to the Control.

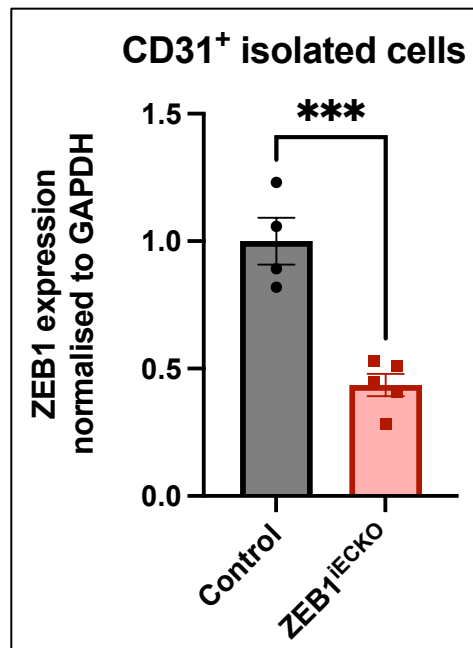


Figure 5.3.1.4. ZEB1 mRNA expression in adult mouse lung tissue in the CD31⁺ fraction of Control and ZEB1^{IECKO} mice. ZEB1 expression was normalised to GAPDH. Data relative to the control. Data present as \pm SEM and statistically analysed using a t test. N=4 Control, N=5 ZEB1^{IECKO} ***P <0.005. Data from Kathryn Green.

5.3.2 Ear dermis as a model of lymphangiogenesis

Lymphatic rich tissues were compared for use as a representative model to investigate a possible lymphatic phenotype between ZEB1^{IECKO} and Control mice (Figure 5.3.2.1). All the animal used in these experiments were primarily used in other studies, for example studying corneal neovascularisation. No tissue was used in the final analysis that may have been affected by the eye surgery or by the intraperitoneal injection of tamoxifen to induce the gene knockout. The ear dermis was concluded as the best tissue bed to utilise, it was easy to access, unaffected by procedures and was consistently well visualised. Other tissues stained included the trachea, diaphragm and tail dermis as shown in Figure 5.3.2.1. The trachea was hard to dissect and image due to its muscularity. The diaphragm was thin so easy to stain and image, but extremely hard to dissect from the mouse, and potentially affected by intraperitoneal injection of the tamoxifen. The tail dermis was investigated and posed as the next best choice after the ear, it was easy to access and dissect but failed to give consistent visualisation. The dermis of the mouse allows us to extrapolate and combine our *in vitro* work to a point, although human, our primary

cells originate from the dermis. This allows us to at least concentrate our field of lymphatic work to the dermal lymphatic network. The ear has been utilised previously (Zhang et al., 2018; Enholm et al., 2001) with established protocols (Johnson, 2022) and using LYVE1 (Tripp et al., 2008) providing a rationale to use this as our primary tissue in which to investigate a possible phenotype.

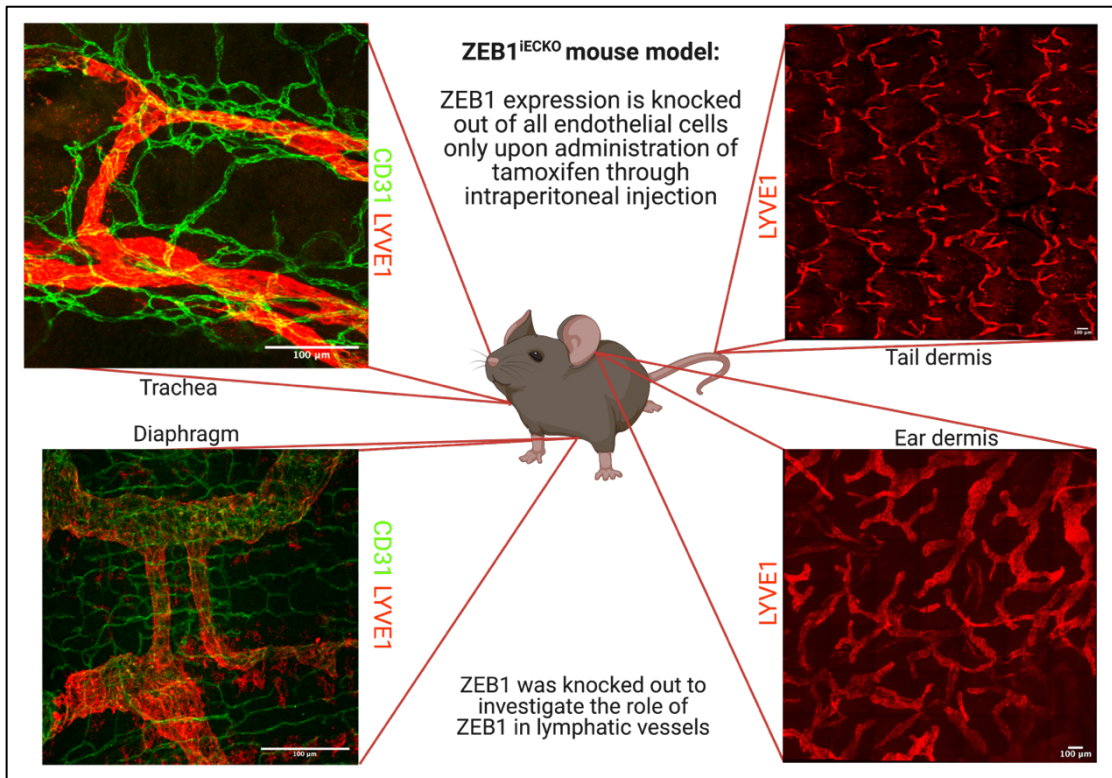


Figure 5.3.2.1. Different lymphatic-rich tissues could be utilised for the investigation of a lymphatic vessel phenotype. Representative images from the trachea and diaphragm stained with LYVE1 and CD31. The ear and tail dermis were stained with LYVE1. Image on a confocal microscope at 20X magnification, the ear and dermis images shown are 3 x 3 and 5 x 5 tilescans.

5.3.3 ZEB1 is dispensable in postnatal extension of dermal lymphatic vessels

To determine whether ZEB1 inducible endothelial cell knockout affects the early extension and morphology of lymphatic vessels, mice pups were subject to 3 consecutive doses of tamoxifen to induce knockout. At P5, the mice were killed by cervical dislocation and the ears removed for histological analysis, the results of which are shown in Figure 5.3.3.1.

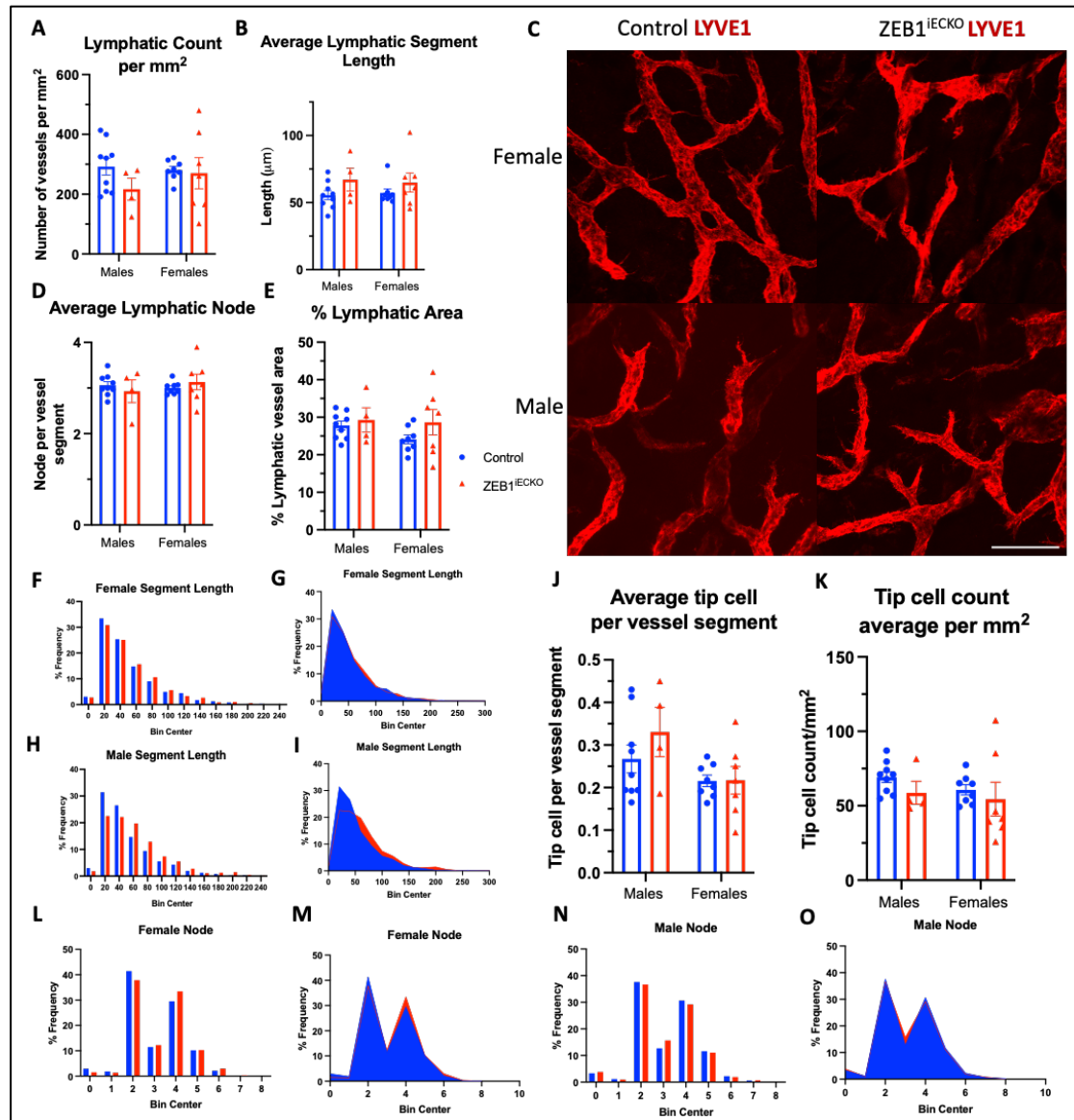


Figure 5.3.3.1. No significant morphological changes in the lymphatic vessels of P5 ear dermis of ZEB1^{iECKO} mice were found when knockdown was induced in comparison to the Control. The ear dermis was dissected post sacrifice and immediately fixed. Tissue was stained with the lymphatic specific marker LYVE1 and imaged with confocal microscopy at 20X magnification. Measurements were taken of vessels in the field of view using ImageJ software. Representative image is shown in Panel C. Scale bar = 100 μm. Male Control N=8 and Male ZEB1^{iECKO} N=4, Female Control N=8 and Female ZEB1^{iECKO} N=8. . Panels A, B, D and E are average measurements from multiple images of the field of view. Segment length (Panels F, G, H, I) and Node (Panel L, M, N, O) is representative of every measurement from each mouse, then shown as a percentage of the total readings. Statistically analysed by a two-way ANOVA.

Parameters of lymphatic morphology were chosen from a combination of protocols which quantified lymphatic vessels previously as described in Chapter 5.1.2. These parameters were established to be able to quantify any changes in length, number,

area, and overall patterning of the lymphatic vessels. No change was seen in the density, segment length, % LYVE1 area or average node between Control and ZEB1^{iECKO} mice at P5. There was also no sex difference in lymphatic morphology between the male and female mice in either Control or ZEB1^{iECKO} mice. There was no change in branching or segment length, as denoted by node (Figure 5.3.3.1, Panel D) when displayed as averages however changes in branching may attest to a change in hierarchy within the network, which may be lost when looking at averages of a large number of measurements, across multiple images, to then form an average for the individual mouse. To determine if just denoting the average may have masked a shift in the values, to an increase or decrease in distribution across the possible node numbers or “bins”, each measurement taken from every image from every animal was plotted, then grouped together creating a histogram and bar chart (Figure 5.3.3.1, Panels L-O). The same analysis was repeated for segment length (Figure 5.3.3.1, Panels F-I). This allowed visualisation of the distribution of values across each grouping to indicated if there has been a shift in values, rather than looking at the total means. There was no difference seen between ZEB1^{iECKO} and Control or between the sexes, suggesting loss of ZEB1 did not induce vessel remodelling in the P5 ear.

The number of filopodia was determined by imaging at a higher power magnification (63X) (Figure 5.3.3.2), as 20X magnification did not allow consistent visualisation. Vessels were divided as “sprouting” when connected to a vessel segment with a tip cell and “non-sprouting” when a segment is connected on both sides to other vessels. This was quantified and revealed no difference in filopodia number. There was a reduced range of results seen on the non-sprouting segments in ZEB1^{iECKO} mice versus Control. These results contain a mixture of sexes as slides were re-imaged, with only a limited number from the original results in Figure 5.3.3.1 retaining the ability to visualise these structures at high power.

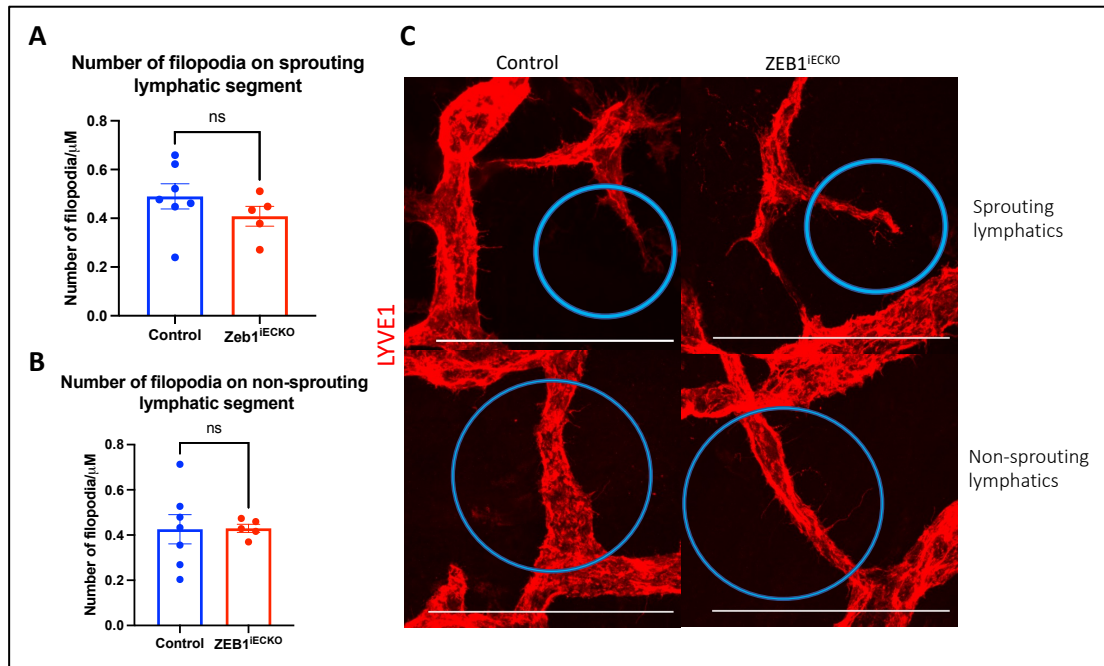


Figure 5.3.3.2. The number of filopodia on sprouting versus non-sprouting lymphatic vessels did not differ between Control and ZEB1^{IECKO} mice. Tissue from Figure 5.4.3.1 was imaged at higher power (63X) to visualise filopodia. Measurements were taken of vessels in the field of view using ImageJ software. A. Number of filopodia per micrometre of a sprouting lymphatic segment. B. Number of filopodia per micrometre on a non-sprouting lymphatic segment. Representative images of sprouting and non-sprouting lymphatic segments are shown in Panel C. Scale bar = 100 μm . Control N=7 and ZEB1^{IECKO} N=5. Statistically analysed using an unpaired t test.

5.3.4 ZEB1 may have a subtle effect on adult dermal lymphatic morphology

During development ECs are guided by innate genetic programs, local signals, and haemodynamic forces to determine cell fate. It is possible that in development the innate plasticity of LECs, which can differentiate to and from BECs (Oliver and Srinivasan, 2010), are able to overcome a loss in a signalling pathway and still establish functional vasculature. In established vasculature, LECs mostly retain a quiescent, terminally differentiated phenotype, due to continued expression of PROX1 (Johnson et al., 2008). This focussed our investigation to adult lymphatic loss of ZEB1, where tissue may not be able to compensate a change in transcription factor expression.

Adult lymphangiogenesis only traditionally occurs in pathological conditions, thus often requires a stimulus. However, alterations in lymphatic morphology were seen by the conditional adult knockout of VEGF-C (Nurmi et al., 2015), suggesting there

are essential required genes involved in the adult maintenance of lymphatic vasculature. Additionally, gut lymphatics are constantly remodelling even in adulthood (Cifarelli and Eichmann, 2019), suggesting adult tissues hold the ability to remodel from previously quiescent vasculature.

To investigate if ZEB1 plays a role in maintenance of lymphatic vessel physiology, adult mice (10-12 weeks old) were subject to five consecutive doses of tamoxifen to induce endothelial cell knockout. No difference was found between the Control and ZEB1^{iECKO} mice in any of the measured parameters in Figure 5.3.4.1. Furthermore, no difference was seen in the parameters measuring lymphatic morphology between male and female mice.

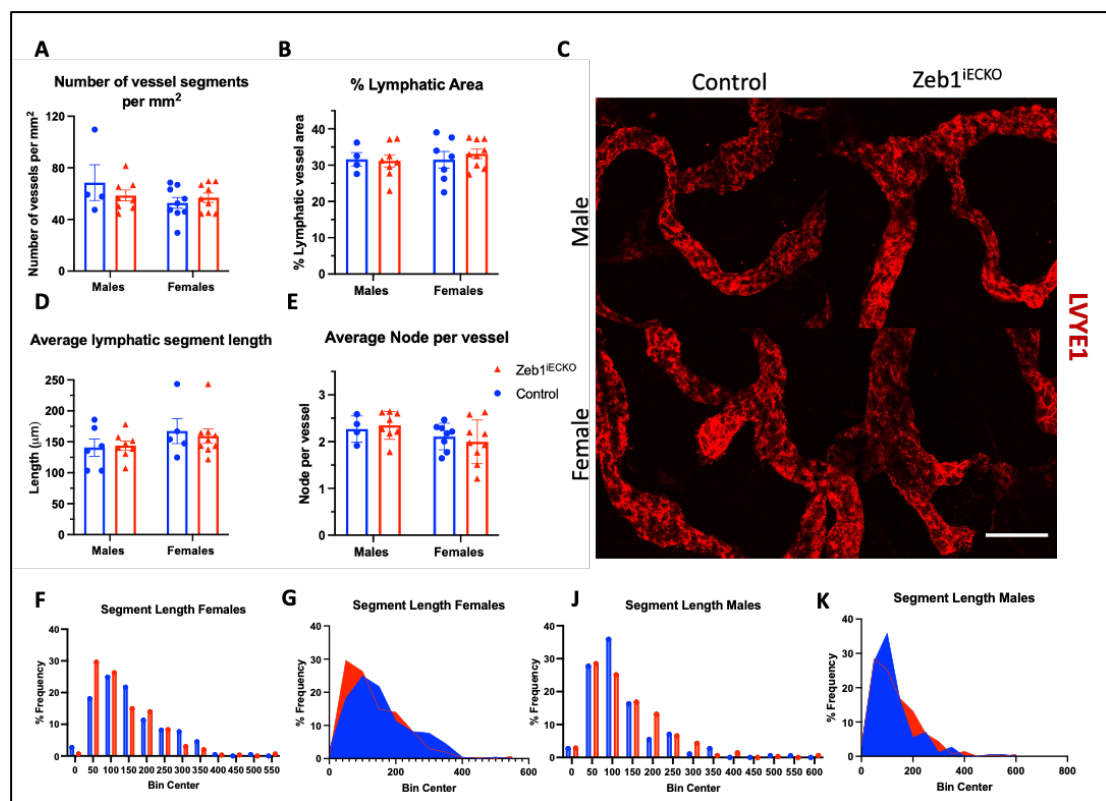


Figure 5.3.4.1 No change in the lymphatic morphology of the dermal ear lymphatics of male and female Control and ZEB1^{iECKO} adult mice. Tissue was dissected and stained for the lymphatic specific marker LYVE1. Images were acquired on a confocal microscope at 20x magnification and analysed using ImageJ. Measurements were taken of vessels in the field of view using ImageJ software. Representative images are shown in Panel C. Scale bar represents 100 μm. N=4 for Control male N=8 for ZEB1^{iECKO} males. N= 7 female Control mice, and N=9 for ZEB1^{iECKO} females. Panels A, B, D and E are average measurements from multiple images of the field of view. Segment length (Panels F-K) is representative of every

measurement from each mouse, then shown as a percentage of the total readings. Statistically analysed using a two-way ANOVA.

The node was investigated further, as described with the developmental work. This was to ensure any effect of remodelling was not masked by taking the overall mean of each animal from a large quantity of measurements. As the spread of node was easier to visualise (Figure 5.3.4.2) a slight difference was seen in the male mice at a node number of 4. ZEB1^{IECKO} mice had an increase of 68% at node 4 (24.7% ZEB1^{IECKO} versus 14.7% Control of total readings). This is seen in Panels A and B of Figure 5.3.4.2 and reflected in the representative images in Panel C. This is not seen in the measurements of the female mice. This suggests the male mice have an increase in branching and connections following loss of ZEB1.

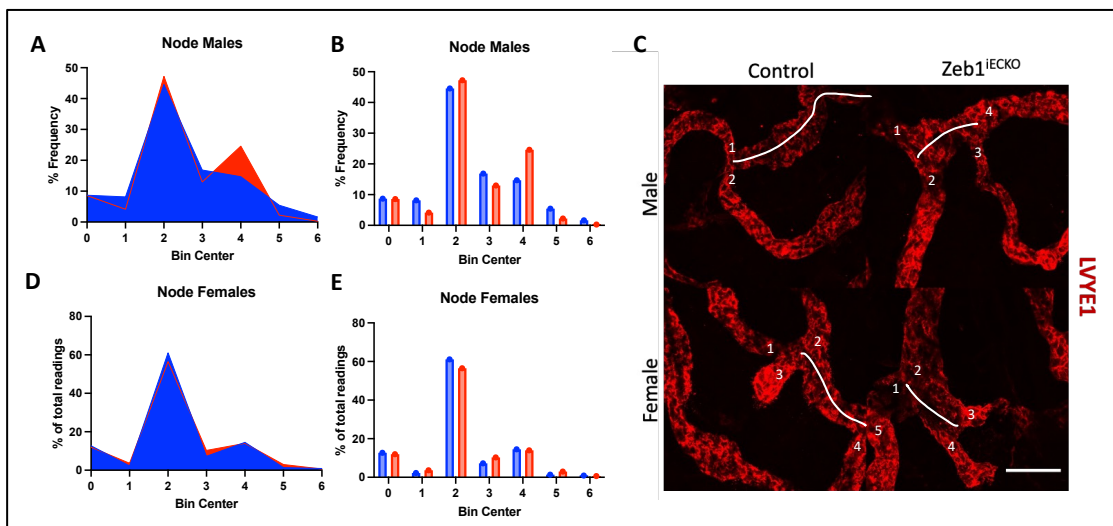


Figure 5.3.4.2. ZEB1^{IECKO} display altered lymphatic networking in comparison to the Control. Node was calculated for all vessels in the field of view, measurements are shown as a percentage of the total readings. Panel C is an example of this analysis using representative images.

5.4 Discussion

This chapter aimed to investigate the lymphatic beds in both a developmental and adult mouse model of ZEB1^{IECKO}. Based on preliminary data in blood endothelial cells (Chapter 1.5.1), we hypothesised loss of ZEB1 would result in a lymphangiogenic phenotype. However, from the results presented in this chapter, it is not clear as to the role of ZEB1 in lymphatic remodelling in the mouse ear. During developmental

lymphangiogenesis (P5 model), we saw no changes in lymphatic morphology in the parameters measured when ZEB1 is knocked out. We only measured this at P5, with tamoxifen dosing P1-3. It is possible that this is not enough of a time window to see an effect. Although the lymphatic vessels are growing rapidly in this time, if ZEB1 has a long protein half-life, it would be present in the cells for a longer duration post-knockout. To mitigate this, the mice pups could be left for a longer period to be sure ZEB1 protein levels have decreased in ECs. Ideally, quantification of ZEB1 protein knockout would also be quantified. A P21 timepoint has been used in similar studies (Scallan et al., 2021), by this time after dosing P1-3, the ECs should have been depleted from ZEB1 and allows time for this to potentially impact the proliferation of the LECs and extension of the lymphatic network. It is also possible that even at P5 we are too late in development to see the involvement of ZEB1. It could be ZEB1 plays a role in the initial migration of the primitive ECs from the CV, or any embryonic stage of lymphatic development. To investigate this, the knockout would have to happen in utero, and pups either sacrificed upon birth, or culled during a particular embryonic stage of interest (Wigle and Oliver, 1999). This would entail a dedicated study to investigate this, currently there is not enough evidence of the impact of ZEB1 to warrant this.

To determine the level of ZEB1 knockout in the ECs, mRNA extracted from CD31⁺ cells from the lung suspensions of ZEB1^{iECKO} and Control mice, this determined the mRNA level of ZEB1 has decreased by 57% following injection with tamoxifen (Figure 5.3.1.4). Specific decrease of ZEB1 levels in LECs was not completed. This could explain the lack of predicted lymphatic remodelling in these mice. As this mouse model chosen knocks ZEB1 out of all ECs, experiments should have been conducted whereby a LEC fraction was isolated from the lung suspension, therefore specific loss of ZEB1 from the LECs could be determined. The level of knockdown of the ZEB1 protein should also be completed, for example by optimisation of western blot. This would establish if our mouse model was sufficiently and successfully depleting the LECs of ZEB1 and therefore responsible for any differences seen between the Control and ZEB1^{iECKO} mice. The use of a Prox1 Cre-ERT2 mouse could also be suggested.

Prox1-CreERT2 would specifically target the LECs to ensure any change is a result of loss of ZEB1 in the LECs and not a downstream consequence of loss of ZEB1 from other ECs subtypes, however the lack of lymphatic phenotype seen using the Cdh5-CreERT2 seen in this chapter does not provide rationale for this.

It is also possible that different parameters for quantification could have been utilised, there seems to be a variety of methods by which lymphatic morphology can be analysed, with no clear standard methodology. Visual comparison of the images may influence which quantification may be suitable for analysis in a study. For this study general parameters were chosen which had also been used to quantify blood vessels previously. These parameters were suited to the study as this work was preliminary and utilised a mouse model which had primarily been used in other studies. If qualitatively a difference in morphology was seen that was missed out of the existing parameters, these parameters would have been adjusted. As shown in Figure 5.3.2.1, the arrangement of the lymphatics in the different tissue varies greatly, even from the dermis in both tail and ear. This is because the tail skin is thicker, so lymphatics are more uniform whereas in the ear, there is more variability as the tissue is thin and flexible. A more uniform patterning such as the hexagonal patterning may have been easier to quantify as potential disruption to this structure would be easier to visually define. The use of the ear as a model during development was decided as a suitable lymphatic bed to use as it was easy to access, visualise and unaffected by other procedures the mice were subjected to. The dermis was also favourable as it is common to use primary cells from the human dermis, allowing research to translate *in vitro* to *in vivo*. However, the origin of the lymphatics in the dermis is still questioned and should not be used as a representative of the whole lymphatic system in the animal. Deeper lymphatics such as those seen in the trachea may have been affected differently by the loss of ZEB1 as internal lymphatics may involve different mechanisms of development and maintenance, depending on the surrounding environment. Even in the skin, there is a superficial plexus, and deeper lymphatics which drain into larger vessels in the subcutaneous adipose, each type experiencing a different microenvironment by

which they grow, reach quiescence, and respond to local stimuli. The use of a second tissue in this study, such as the trachea, would have been beneficial to allow a more thorough investigation of the role of ZEB1 in development.

In adults, lymphatic vessels in the skin are quiescent until activated by a stimulus, such as injury or inflammation. In normal circumstances, anchoring filaments are attached to the LECs and work with collagen and elastin fibres to allow the vessels to adapt to increases in interstitial flow. However prolonged high interstitial flow can damage the integrity of the vessel, thus the lymphatic network must be able to maintain the ability to become activated to mitigate this. In our animal model, we had no inflammatory or injury stimulus, but did give ample time (14 days) once tamoxifen is injected until sacrifice. This tested the role of ZEB1 in normal physiological conditions within the lymphatic vessels. For most of the parameters measured, there was no difference between the Control and ZEB1^{iECKO} mice. However, in the node parameter, defined as how many times one vessel segment means another, there was a 68% increase in node 4 in the ZEB1^{iECKO} males in comparison to the Control males. This is notable for several reasons, the first being this is not replicated in the females. It has been debated before in experiments regarding the blood vasculature, that any effect seen by knocking out ZEB1 was more pronounced in the male mice versus females. This could be a sex-dependent effect, or due to a lesser knockdown of ZEB1 in the female mice, mice were not split by sex in Figure 5.3.1.4 due to time and tissue availability, but ideally should be quantified to investigate further.

The node of 4 being more pronounced in the ZEB1^{iECKO} mice is interesting, in general we see two peaks in nodes, at 2 and 4, which is also reflective of the nodes seen at P5 (Figure 5.3.3.1, Panels L-O). This could mean that our ZEB1^{iECKO} mice are reverting to this state of development, where there is still active lymphatic remodelling and outgrowth. Interestingly, where we see odd numbered nodes (Figure 5.3.4.2, Panel C) we also see a growing vessel with a tip cell/open ended vessel. This could mean we were deeper in the plexus in the ZEB1^{iECKO} mice, where vessels were connected as

they drained fluid from the surface down, and closer to the surface in Control mice, where open-ended vessels were stimulated to grow by the fluid accumulation. Or it could be that in our ZEB1^{IECKO} mice, the vessels were without this stimulation, or unable to respond to it, leaving more connected vessels with less open ends. As tip cell number was not quantified in the adult model (because they were rarely seen), a conclusion is also left open ended. Future work should attempt to more clearly decipher the level of plexus the images were taken at to analyse to mitigate this. Use of a stimulus could also help determine adjustments to the functionality of these vessels, such as induced oedema to see how the vessels react, or an inflammatory stimulus such as TNF α to see the contractile response (Chen et al., 2017).

This study has concentrated on looking at the morphology of the lymphatic vessels, with the aim of investigating the role of ZEB1 in lymphatic vessels. Functionality of the vessels cannot be determined by this; lymphatics can be dysfunctional whether open or collapsed. Furthermore, immunofluorescence cannot decipher between new lymphatics and already established vessels. Functionality of the lymphatics is highly dependent on the extracellular matrix supporting them, allowing response to changes in interstitial pressure. Functional assays can assess the functionality of vessels, such as injection of fluorescent tracers to measure lymphatic flow kinetics. In patients, isotope tracers are used in lymphography to diagnose lymphatic dysfunction. To distinguish new lymphatic vessels, the use of a tissue such as the cornea, which is physiologically devoid of lymphatics could be used. Any lymphatic invasion into this tissue would be newly developed vessels, perhaps undergoing partial EndMT to do so, in response to a carefully placed suture as the stimulus. In an adult model, the use of gut lymphatics would be an alternate lymphatic bed to investigate, these are vessels which help absorb lipids from the circulation and undergo active regeneration unlike most tissue beds (Cifarelli and Eichmann, 2019). To investigate the intestinal lacteals in the future, another route other than intraperitoneal injection of tamoxifen should be considered, in case of accidental injection into the intestine which may affect these vessels. It is also possible that a model of injury or other stimulus is needed to observe lymphatic remodelling, this

will allow changes in branching, or tip cell number to be accentuated in comparison to a physiological mouse model where the lymphatic vessels are mostly in a state of quiescence.

In conclusion, in this chapter we suggest ZEB1 is dispensable in the lymphatic outgrowth (P5) and maintenance (adult) of lymphatic morphology in the mouse ear. Further investigation of the functionality of these vessels should be conducted to investigate if loss of ZEB1 impacts the ability of lymphatic vessels to remodel in response to stimuli.

Chapter 6. Loss of ZEB1 Induces Remodelling in Mouse Hindlimb Lymphatic Vessels

6.1 Introduction

6.1.1 Lymphatic response to inflammation

Lymphangiogenesis has been closely linked with tissue inflammation in response to infection, or tissue injury. Termed inflammation associated lymphangiogenesis (IAL), this type of lymphangiogenesis is actively involved in the pathophysiology of many inflammatory diseases (Kim et al., 2014). During an inflammatory event, such as an infection, blood vessels expand and activate, this results in the five characteristics of inflammation - redness, heat, swelling, pain, and impaired function (Nathan, 2002). At the cellular level, these physiological adaptations are mediated by a shift in endothelial phenotype resulting in activation (Pober and Conran, 1990). The phenotypic changes enable the needs of immune cell recruitment to be met, such as upregulation of cell adhesion molecules, increased endothelial permeability and cytokine release from the endothelium (Moreira et al., 2018). Mast cells first respond to activation, pre-stationed in the tissue, they release histamine, TNF, cytokines, proteases, tryptases, eicosanoids and chemokines, which further recruit circulating neutrophils and leukocytes (Riley and West, 1953; Kunder et al., 2011). Histamine, eicosanoids and tryptases result in vasodilatation and extravasation of fluid, which contributes to oedema (Nathan, 2002). Neutrophils release active metalloproteinases promoting tissue breakdown, which continues as tissue resident and recruiting macrophages become active (Epstein and Weiss, 1989).

The lymphatic vessels facilitate the alleviation of the inflammation, by dilating to allow entry of fluid and immune cells and increasing pumping of collecting lymphatics to promote drainage of lymphatic capillaries (Skobe and Detmar, 2000). Should the inflammatory conditions persist, and lymphatic function is insufficient to clear the inflammation, further lymphatic remodelling takes place; this occurs via lymphatic expansion from pre-existing vessels in the inflamed tissue (Liao and von der Weid, 2014). The macrophages infiltrating the area of tissue damage release pro-lymphangiogenic stimuli, VEGF A, C and D, which activate VEGFR2 and VEGFR3

signalling pathways, resulting in an increase in growth of the lymphatic network toward the site of injury (Kim et al., 2012). The activated lymphatic vessels promote macrophages and dendritic cells to the site of tissue damage via expression of chemokines. Work by Johnson et al., using a mouse model of induced inflammation showed CCL21 was highly secreted in the lymphatic endothelium, and promoted the transmigration of mature dendritic cells (Johnson and Jackson, 2010). Secreted chemokines such as CCL21 and CXCL8 travel distally through the inflamed tissue, which attract CCR7⁺ dendritic cells and neutrophils from the inflammatory scene toward the lymphatic vessels (Bromley et al., 2005). The initial lymphatics in the tissue have button-like junctions, which allow as entry points for the immune cells (Pflücke and Sixt, 2009; Baluk et al., 2007). The immune cells are trafficked through the vasculature to draining lymph nodes through expression of leukocyte adhesion receptors – VCAM1, ICAM1 and E-Selectin by the LECs, which facilitate intravasation and migration, allowing tissue repair at the site of inflammation (Johnson et al., 2006; Martín-Fontecha et al., 2009; Johnson & Jackson, 2010). Failure of this mechanism, demonstrated by CCR7⁺ deficiency, resulted in accumulation of immune cells at the inflammatory site (Menning et al., 2007). Macrophages are also documented as a circulating progenitor which can be incorporated into a growing vessel and transdifferentiate into LECs, this theory is still being investigated, but inflammation results in an increase in the presence of these progenitors (Maruyama et al., 2005; Kataru et al., 2009; Hall et al., 2012).

6.1.2 Lymphatic response to ischaemia

The model of hindlimb ischaemia (HLI) is primarily used as a model of peripheral arterial disease (PAD), a progressive disorder which involves occlusion of arteries other than those supplying the brain or heart. PAD affects over 200 million people worldwide (Shu and Santulli, 2018). In the HLI model, ischaemia is induced via dual ligation of the femoral and iliac arteries, affecting the blood flow to the gastrocnemius muscle. The induced hypoxia to this muscle activates hypoxia-inducing factor (HIF) proteins, which in turn activate myeloid-cell infiltration and inflammation (Silvestre et al., 2008). HIF1 mediates the transcriptional response of

multiple cell types in the hypoxic tissue, including the hypoxic ECs. Cells within the tissue are stimulated to release pro-angiogenic growth factors in response to HIF, while the ECs upregulate cell-surface receptors for these growth factors, this results in angiogenesis to supply oxygen to the hypoxic tissue (Rey and Semenza, 2010). The effects of the HLI surgery on the lymphatic system have not been well documented. There is only one study that has investigated this model for its effect on lymphangiogenesis (Pu et al., 2021), primarily for investigation into a role in reparative angiogenesis. This study found that lymphangiogenesis did take place in response to ischaemia, and when enhanced, cleared the local artificially enhanced oedema and excessive inflammation (Pu et al., 2021). This study suggests the HLI model induces lymphatic remodelling, which has functional benefits in clearing inflammation and oedema in an artificially enhanced, prolonged oedema model (Pu et al., 2021). More research has been conducted regarding myocardial infarction (MI), also known as a temporary blockage of blood flow to a portion of the heart muscle, resulting in ischaemia. After the ischaemic event, cardiomyocytes in the affected area necrose, this is followed by an extensive inflammatory response (Sutton and Sharpe, 2000). The resulting oedema suggests that the lymphatic vasculature has also been impacted, this could be due to the inflammatory mediators and oxygen radicals generated during the chronic inflammation, which have a negative effect on lymphatic function (Aldrich and Sevick-Muraca, 2013; Zawieja et al., 1991). Therapeutic enhancement of lymphangiogenesis has been demonstrated by the targeted delivery of VEGF-C to the ischaemic site, which in mice, reduced the cardiac hypertrophy and improved lymphatic drainage (Henri et al., 2016). Cardiac macrophages are crucial in this process, accumulating in the tissue and producing VEGF-C, invoking cardiac lymphatic remodelling after MI (Glinton et al., 2022). The lymphatics resolve the inflammation and increase dendritic cell clearance, which dampens the immune response (Vieira et al., 2018). Prevention of escalation to a chronic inflammatory response is essential to protect the viability of the tissue and local lymphatic vessel function (Kraft et al., 2021).

6.1.3 Quantification of lymphatic remodelling

Lymphatic density is the simplest method of quantification of lymphangiogenesis but should be not taken alone to understand the lymphatic response. To account for changes in dilatation or enlargement of the existing vessels, % area of lymphatic coverage has also been included as a quantified parameter (Thowsen et al., 2022). The surface protein LYVE1 has been established as a reliable marker of LECs and has been used in the hindlimb previously using immunofluorescence (Pu et al., 2021). The influx of immune cells to the site of injury allows investigation of the extent of inflammatory activation in the chosen model. Pan-leukocyte marker CD45 is a protein tyrosine phosphatase, expressed at high levels in several types of nucleated hematopoietic cells, covering up to 10% of the cell surface (Altin and Sloan, 1997). CD45 has been used previously in many mouse tissues to quantify immune cell infiltration, including the kidney (Zheng and Epstein, 2021), brain (Nordstrand et al., 2001) and specifically in the HLI model (Hsieh et al., 2018). The number of CD45⁺ cells per field of view was quantified in these studies allows suggestion of the severity of activation of the immune response.

In this chapter we investigated the effect of inducing HLI on the lymphatic vasculature. We also sought to investigate any differences in lymphatic response to ischaemic insult between Control and ZEB1^{iECKO} mice. This was investigated using immunofluorescence staining of muscle sections of both the operated (ipsilateral) and non-operated leg (contralateral).

6.2 Hypothesis and Aims

Hypothesis: Loss of ZEB1 will induce lymphatic remodelling following ischaemic insult in the gastrocnemius.

Aims:

1. Establish if inducing hypoxia to the gastrocnemius induces a lymphangiogenic response
2. Investigate if loss of ZEB1 induces lymphatic remodelling following ischaemic insult
3. Investigate a connection if loss of ZEB1 alters the inflammation-induced lymphangiogenesis following ischaemic insult

6.3 Results

The hindlimb surgery successfully induced ischaemia into the ipsilateral leg following the protocol published by (Bhalla et al., 2022), as shown in Figure 6.3.1. To determine the baseline, blood flow measurements were taken prior to surgery of both Control and ZEB1^{IECKO} mice, this allowed comparison regardless of surgery of any effect the knockout might have on blood flow to the limb (Figure 6.3.1, Panel B). There was no difference found in baseline speckle flux intensity between Control and ZEB1^{IECKO} mice. Post-operatively, speckle flux was measured to confirm successful reduction in blood flow (Figure 6.3.1, Panel C). This was also compared to between ZEB1^{IECKO} and Control mice, revealing ZEB1^{IECKO} mice had an increased blood flow in the surgery limb, as a % of the contralateral limb ($17.33 \pm 0.84\%$), when compared to the Control mice ($14.06 \pm 1.00\%$). These could indicate a lesser response to the surgery in the ZEB1^{IECKO} mice. The return of blood flow was documented by speckle flux and plotted in Panel D. Mixed effect analysis of the measurements at selected time points revealed no significant difference in ischaemia recovery between ZEB1^{IECKO} and control mice. The purpose of this data is to establish the surgery was successful in inducing ischaemia before investigation of the lymphatic vasculature in the ischaemic tissue. HLI was successfully instigated in both groups, however there is a small, but significant, difference in the amount of reduction in blood flow immediately following surgery in the ZEB1^{IECKO} mice.

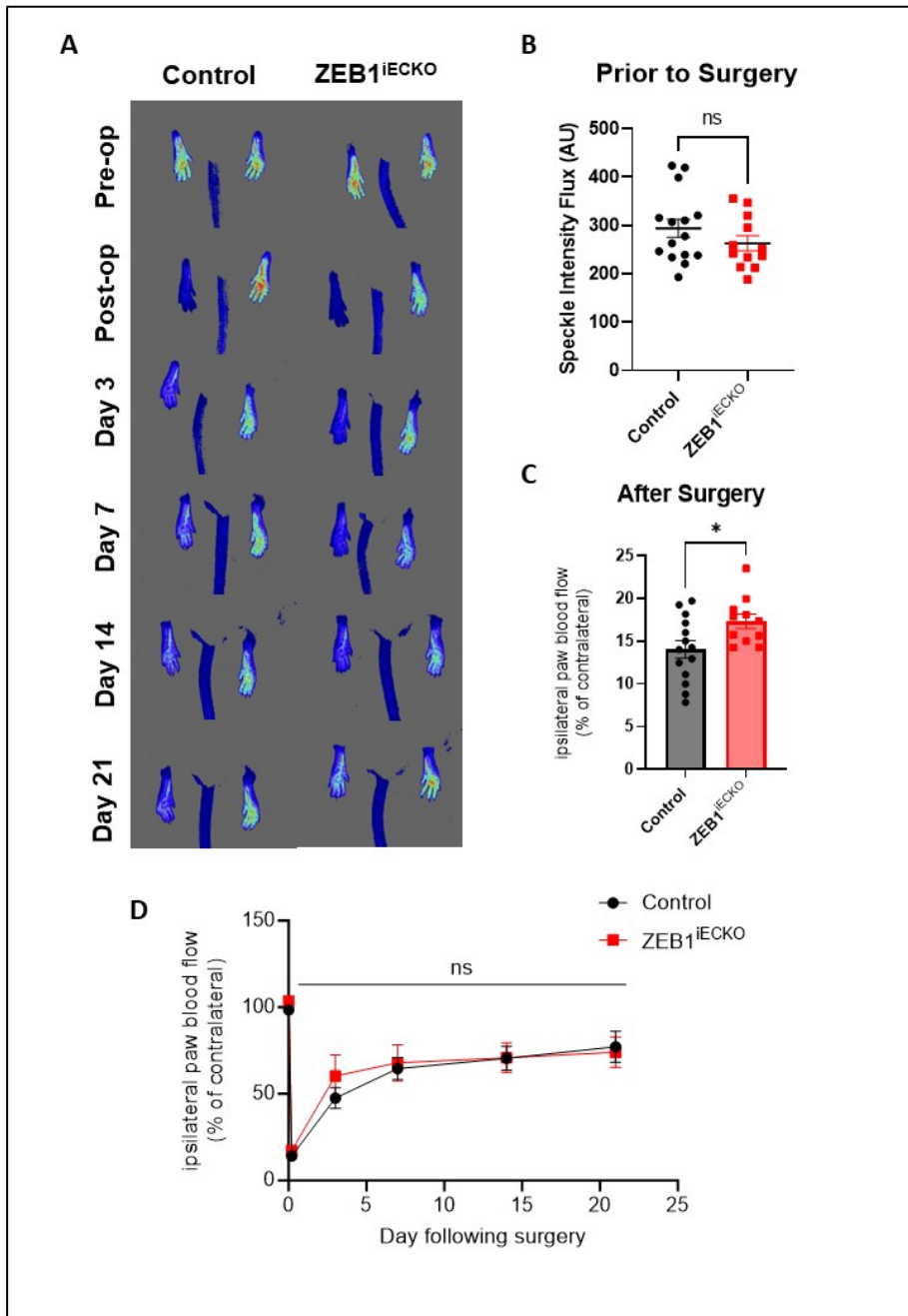


Figure 6.3.1 Loss of endothelial ZEB1 had no effect on blood flow recovery after successful induction of ischaemia in the hindlimb. A. Representative images of hind paw blood flow for all time points showing successful ligation of the left femoral artery. B. Raw values of speckle intensity flux showed no significant difference between ZEB1^{IECKO} and control mice using an unpaired t test. C. After surgery, % of blood flow normalised to the contralateral paw was significantly increased, analysed using an unpaired t test, *P<0.05. D. Mixed effects analysis of % of blood flow over time showed no significance in response to ischaemia between ZEB1^{IECKO} and the control in the time points analysed. Control N=5, ZEB1^{IECKO} N=12. Data from Nicholas Beazley-Long and Kathryn Green.

6.3.1 Lymphatic vessels in the skeletal muscle ZEB1^{IECKO} mice were remodelled in the unoperated limb

To investigate if knockout of ZEB1 effects pathological lymphangiogenesis, we utilised the model of hindlimb ischaemia. This restricts blood flow to the affected lower limb, inducing hypoxia and an inflammatory response. Mice underwent this surgery a week after tamoxifen dosing, left to recover for 28 days then cardiac perfused. The gastrocnemius was sectioned into 16 µm sections and stained for the lymphatic marker LYVE1. Both surgery (ipsilateral) and non-surgery (contralateral) were stained for investigation of lymphatic morphology. This allowed the effect of the surgery on the lymphatic vessels between the contralateral and ipsilateral legs to be quantified, as well as comparison between the Control and ZEB1^{IECKO} mice. The results in Figure 6.3.1.1 show that the HLI surgery did not illicit a lymphangiogenic response in the Control mice. As shown in Panel C, F and G, there was not a significant change in the number of lymphatic vessels or the percentage area between the contralateral and ipsilateral legs (116.5 versus 113.4 structures per mm²). In the ZEB1^{IECKO} mice, it is unclear if the surgery had elicited a lymphangiogenic response. What is clear, is that in the ZEB1^{IECKO} mice there was a significant increased number of LYVE1 positive structures per mm² in the contralateral leg compared to the Control mice, shown by Panel A (116.5 versus 158.5 structures per mm², P = 0.02) and visually represented in Panel C. There was also a slight increase in % LYVE1 positive area (0.471% versus 0.716%), although this was not statistically significant (P = 0.08). These differences suggest that regardless of the surgery, ZEB1^{IECKO} mice have altered lymphatic morphology in the gastrocnemius in comparison to the Control. No change in lymphatic morphology was seen between the Control and ZEB1^{IECKO} mice was seen in the ipsilateral leg, as shown by Panel B and E. In terms of altered response to ischaemia, Panels F and G show contralateral versus ipsilateral leg measurements of lymphatic parameters. In these panels, there was very little response from the Control mice, however in the ZEB1^{IECKO} mice, we did see more variation in the parameters between the legs. This could be influenced by the results in Panel A, as we saw in these mice, there was an increased number of vessels in the contralateral leg per mm², thus upon ischaemic

insult these mice may have sufficient ability to respond to without need for a lymphangiogenic response.

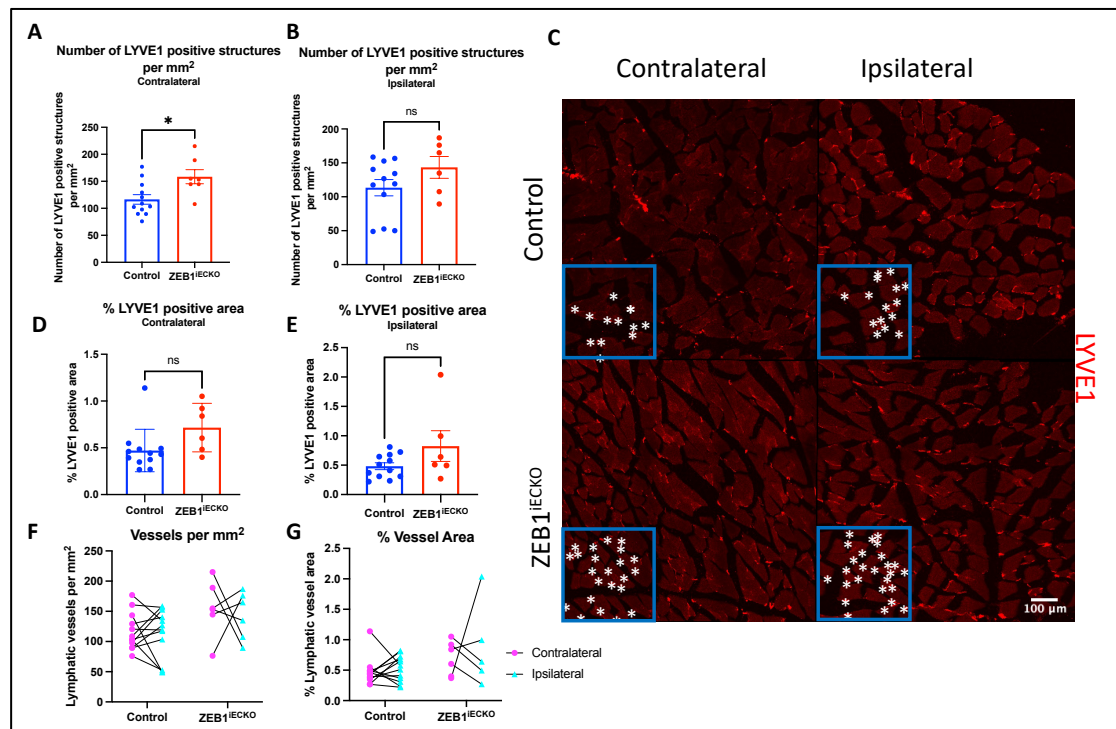


Figure 6.3.1.1. ZEB1^{IECKO} mice display increased lymphatic remodelling in contralateral and ipsilateral leg muscles following hindlimb ischaemia surgery. The muscle was sectioned to 0.16 μm thick and stained with LYVE1. Images obtained on a confocal microscope at 20X magnification and analysed using ImageJ. Panels A, B and D-G are average values from multiple fields of view of the section. % LYVE1 positive area (Panels D, E and G) is the area of muscle fibre which contains positive staining, to exclude the space between muscle fibres. Representative images are shown in Panel C, asterisks represent LYVE1 positive structures. Scale bar represents 100 μm . N=8 for Control, N=5 for ZEB1^{IECKO}. Statistically analysed using an unpaired t test *P<0.05.

6.3.2 ZEB1^{IECKO} mice have altered lymphatic morphology in the hindlimb regardless of surgery

To investigate if ZEB1^{IECKO} have altered morphology in the gastrocnemius in physiological conditions, we induced ZEB1 knockout in mice, then sacrificed a week later via cardiac perfusion. The gastrocnemius was sectioned as previous and quantified. Preliminary results from this small data set, show a change in % LYVE1 positive area (0.571% versus 1.037%) and LYVE1 positive structure density (105.297 versus 160.523 per mm^2) between the Control and ZEB1^{IECKO} mice (Figure 6.3.2.1).

This suggests a change in physiological lymphatic morphology; however, a larger dataset is required to robustly conclude this.

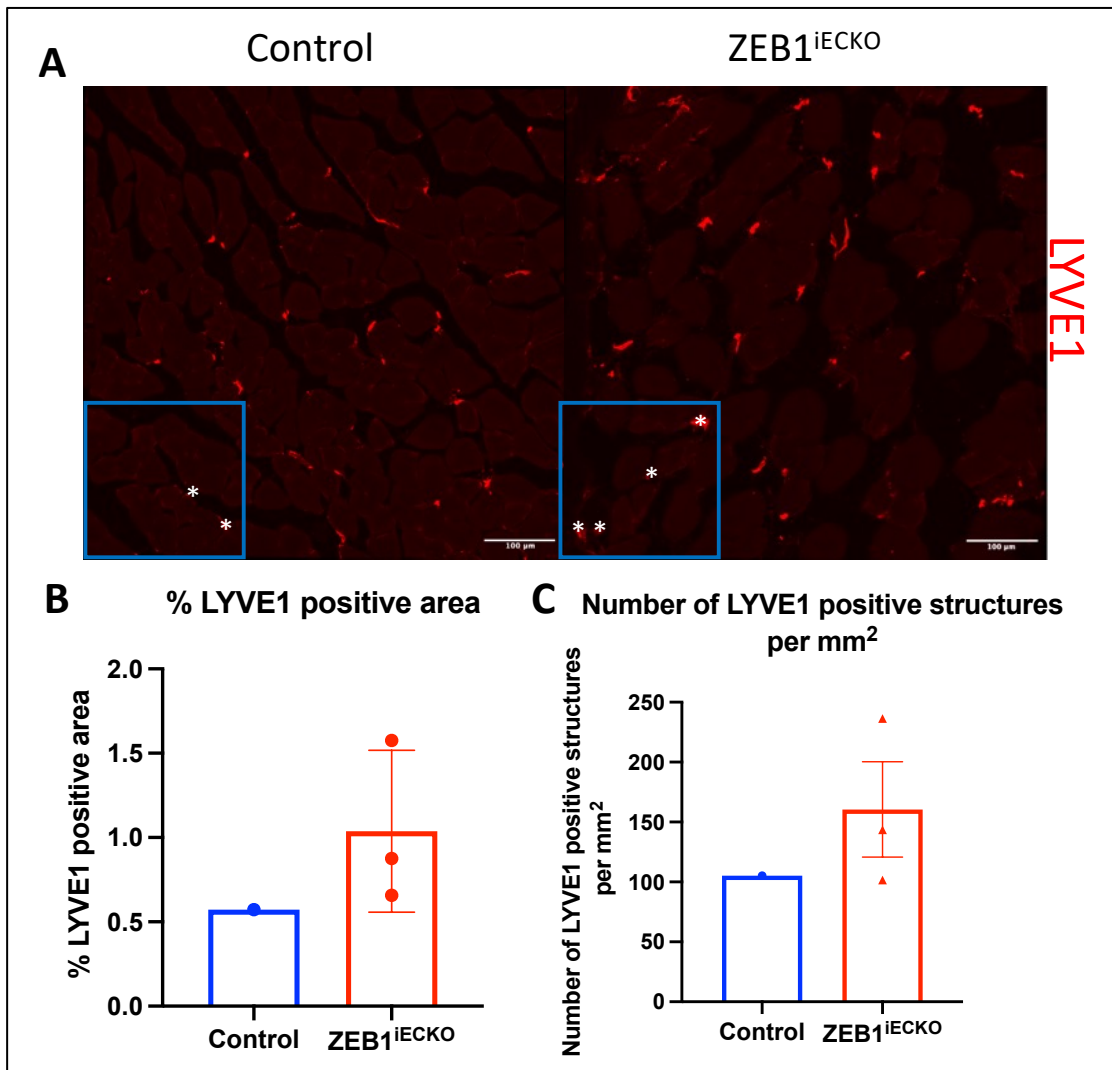


Figure 6.3.2.1. ZEB1^{iECKO} mice have altered lymphatic morphology in skeletal muscle of the gastrocnemius. The muscle was sectioned to 0.16 μm thick and stained with LYVE1. Images obtained on a confocal microscope at 20X magnification and analysed using ImageJ. Representative images are shown in Panel A, asterisks represent LYVE1 positive structures. Panel B and C are average values from multiple fields of view of the section. Scale bar represents 100 μm. Control N=1, ZEB1^{iECKO} N=3.

6.3.3 Lymphatic vessels of the mouse hindlimb are CD45 positive

Whilst attempting to investigate immune infiltration, we observed that the LYVE1 positive lymphatic vessels appear CD45 positive (Figure 6.3.3.1). To ensure these were in fact lymphatic vessels, rather than artefacts of resident macrophages, we increased the section width of the muscle sections, this allowed us to identify vessel-like morphology, as opposed to an immune cell such as a macrophage. These

sections were initially from the mice which underwent the surgery, however when section width was increased tissue availability was limited, thus the results shown in Figure 6.3.3.1 were from the mice which did not undergo ischaemia. As seen in Panel A and B, lymphatic vessel morphology was identifiable and positive for LYVE1, dual staining was seen with CD45 throughout the visible vessel. To the best of our knowledge, this is a novel finding. This dual staining was present in the Control and ZEB1^{IECKO} mice hindlimbs, suggesting this staining is not a consequence of loss of ZEB1.

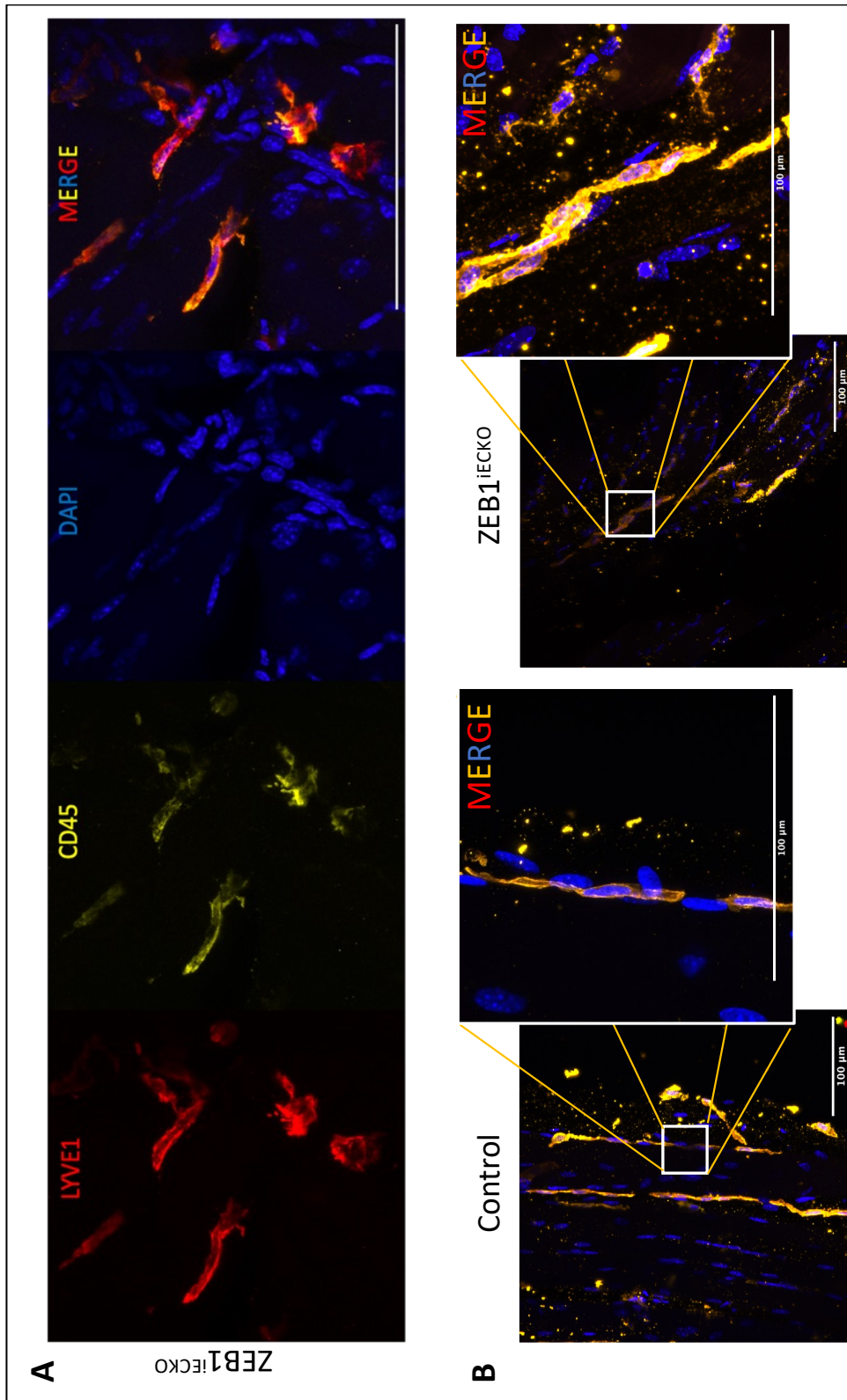


Figure 6.3.3.1 Lymphatic vessels of the gastrocnemius are LYVE1 and CD45 positive. Sectioned muscle (40 μm) from ZEB1^{IECKO} mice were stained for the immune marker CD45 revealing dual staining in the lymphatic vessels in both ZEB1^{IECKO} and Control mice. Panel A shows the separate channels plus overlay at 63X magnification. Panel B shows a 20X magnification image, with the inset showing a section of the image at 63X magnification. Images taken on confocal microscope. Scale bar = 100 μm.

6.3.4 Human *in vitro* data suggests a relationship between ZEB1 and CD45

The CD45 expression was not quantified in the ZEB1^{iECKO} mouse hindlimb, although qualitatively CD45 expression was similar seen in both Control and ZEB1^{iECKO} mice. We decided to investigate the level of CD45 expression using human dermal LECs. Utilising samples created for previous experiments, NSC and ZEB1 siRNA knockdown lysates were ran on western blot and quantified for CD45 protein expression. A positive control cell lysate THP1 derived from an acute monocytic leukaemia patient, which is known to constitutively express CD45 (Pfau et al., 2000) was ran alongside. These results show that HDLECs do not express CD45 in routine culture, however with ZEB1 knockdown, there was a 457% increase in CD45 expression, suggesting a relationship between ZEB1 expression and ectopic CD45 protein expression (Figure 6.3.4.1, Panel A). This was investigated further in the model of growth, whereby two conditions of cell density were compared as seen in Chapter 4. In this model, we see highest ZEB1 expression in the confluent LECs, and comparatively lower expression in subconfluent conditions. When we investigate these lysates for CD45 expression, we found the CD45 expression was highest in subconfluent conditions, where ZEB1 expression was lowest (Figure 6.3.4.1, Panel B). In confluent conditions, where ZEB1 expression was the highest, we see a fainter band, which is at a different molecular weight in each of the confluent samples, suggesting a potential change in isoform expression/post translational modification of CD45 in these conditions.

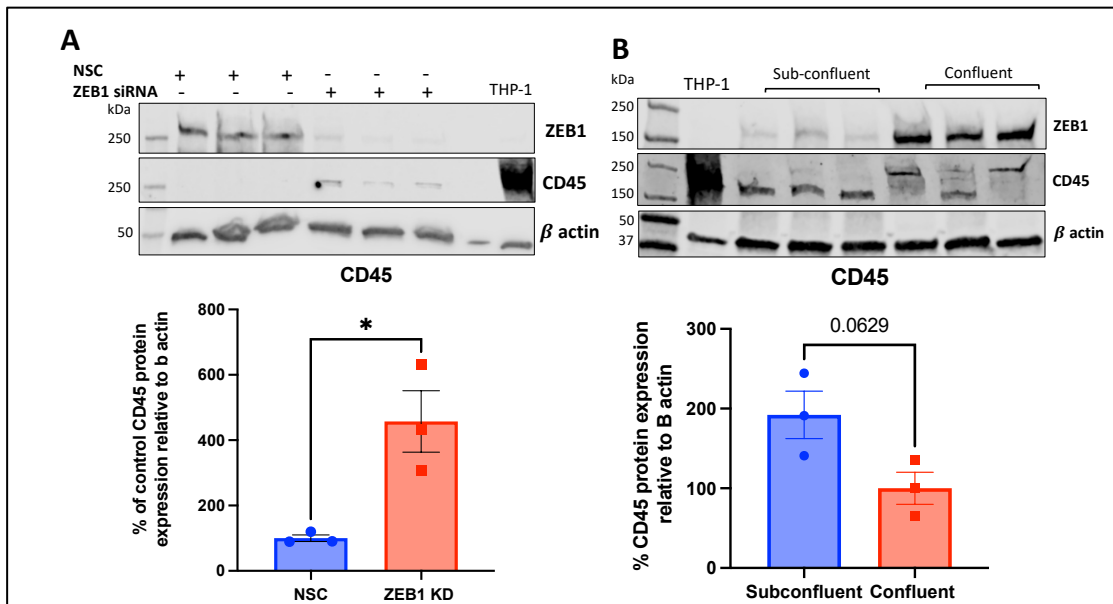


Figure 6.3.4.1 A potential relationship between ZEB1 and CD45 in HDLECs. A. ZEB1 siRNA knockdown enhanced CD45 expression in HDLECs. Data present as mean \pm SEM, statistically analysed using an unpaired t test, N=3, *P<0.05. B. Dysregulation of CD45 expression following culture of HDLECs grown in sub-confluent and confluent conditions. HDLECs were plated at a density of 25,000 cells per cm², and 150,000 cells per cm². Data present as mean \pm SEM, statistically analysed using an unpaired t test. N=3.

Investigating this phenomenon further at an RNA level, bulk RNA sequencing of ZEB1 knockdown HDLECs was compared to the NSC. CD45 (PTPRC) was not a differentially expressed gene in this data set. However, using IPA, based on differentially expressed genes of proteins known to interact upstream and downstream of CD45, a prediction is made of activation or inhibition of the protein. Shown in Figure 6.3.4.2, CD45 is at the centre of the diagram in orange, suggesting that based on the changes in genes encoding proteins of known interactions, at a protein level CD45 is in the ZEB1 knockdown sample is more active, in comparison to the Control. It is important to note these relationships are from the literature and do not discriminate for cell type, thus these relationships may include molecules/pathways/interactions that are not present, or not currently known to occur in LECs. The yellow connecting lines suggest a known relationship between CD45 and the molecule, but the differential gene expression of the molecule does not fit with the overall predicted activation of CD45 in this sample. For example, TIE1 has an increased measurement of gene expression in the dataset, however IPA has found literature detailing CD45 having an inhibitory effect on TIE1 thus if this pathway/relationship was present in our sample,

we would expect a decreased measurement of TIE1 in the sample. Looking into this paper used to understand this relationship, structural analysis revealed human CD45 dephosphorylates the TIE1 protein, thus rendering inactive (Barr et al., 2009).

However, this phosphatase assay does not replicate in-cell interactions, is predictive and there may be enhanced phosphorylation by kinases in our sample, which outweighs the activity of this phosphatase.

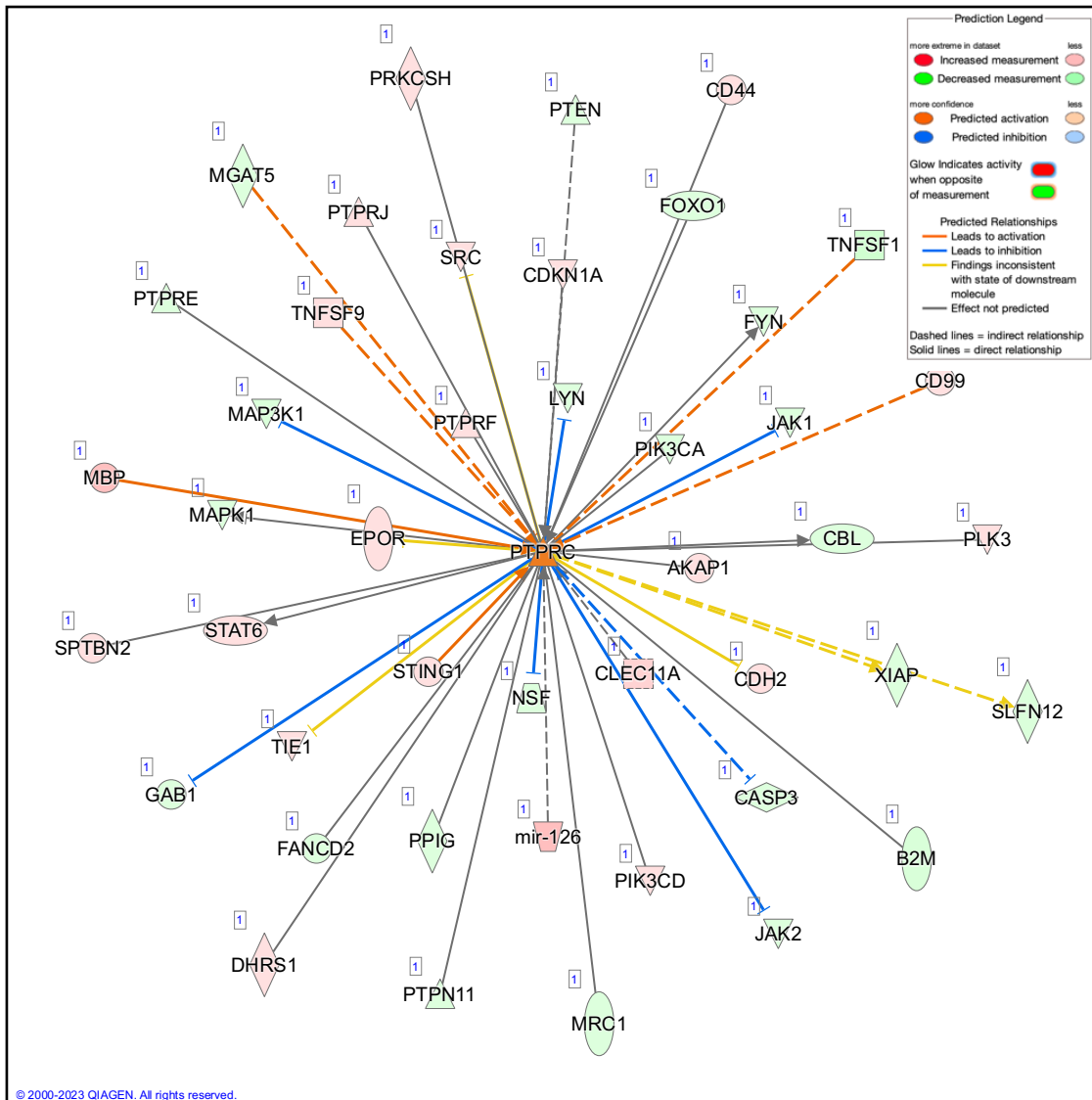


Figure 6.3.4.2 Interaction plot predicting effect of ZEB1 knockdown on PTPRC (CD45) protein expression in LECs. Using the dataset from ZEB1 knockdown of HDLECs, known interaction partners were identified within the data set, based on their differential expression, and their known interaction with CD45, CD45 protein expression was predicted using Ingenuity Pathway Analysis (QIAGEN).

To investigate at a single-cell level if CD45 is present in other organ-specific LECs, open-access data was sourced from Habermann et al., 2020. This study was primarily to investigate the mediators driving fibrotic lung remodelling, this study was purposely chosen as it was not endothelial cell specific, as often these datasets exclude CD45 positive cells, on the basis that ECs do not (canonically) express CD45. This study used the lungs of 20 patients with pulmonary fibrosis, and 10 control lungs. Potentially due to the increased samples, or due to increased cell population, LECs were only identifiable in our sorting method in the diseased samples, as shown in Figure 6.3.4.3. To identify the lymphatic population, cells were identified by PECAM, VE-Cadherin and PROX1 expression. From this population, we investigated CD45 (PTPRC) and ZEB1 expression amongst these cells. The results in Figure 6.3.4.3 show a distinct population which was PECAM1⁺, PROX1⁺, PTPRC⁺ and ZEB1⁻. This is a population that using common cell sorting techniques to isolate ECs would otherwise be lost.

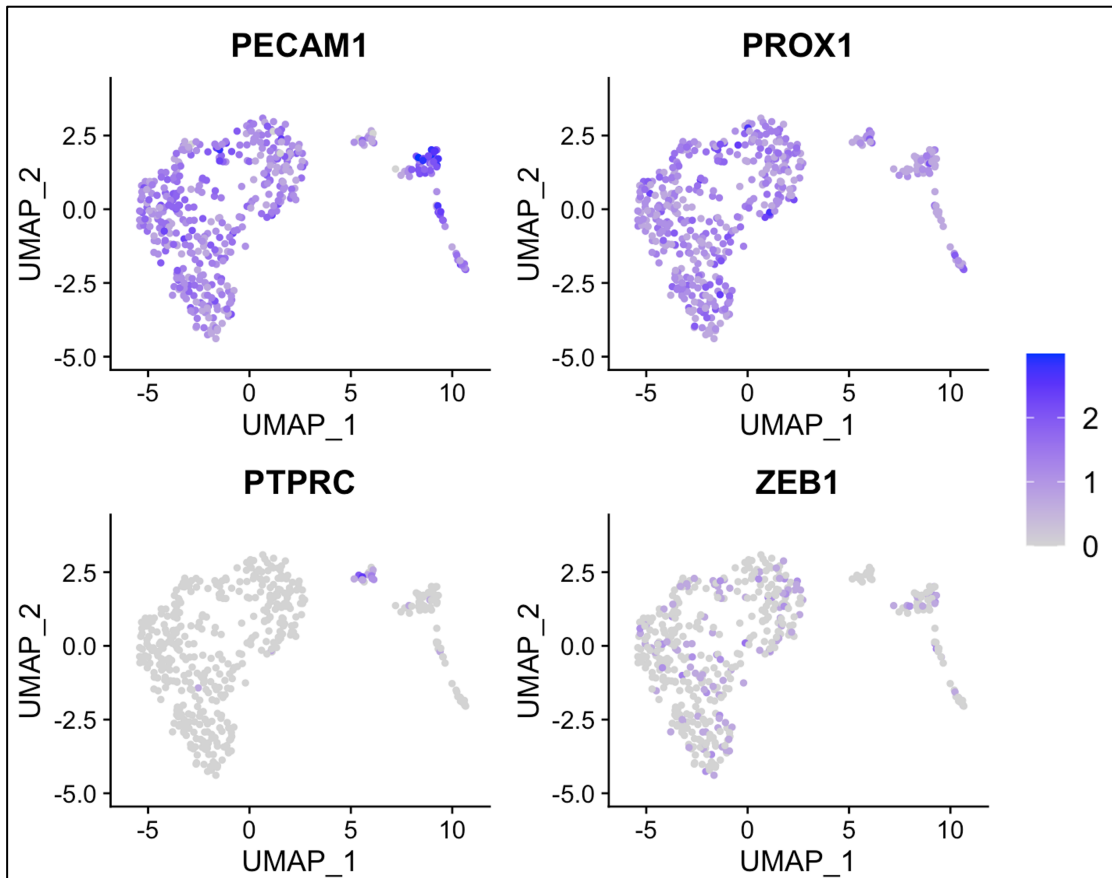


Figure 6.3.4.3 Feature plots representing expression profiles of lymphatic endothelial cells in lung fibrotic tissue. Each dot is representative of a cell and its expression profile. The colour of the dot corresponds to expression level of the gene of interest. A grey dot means no expression. The darker the colour, the higher the expression. Original data sourced from Habermann et al, 2020. GEO accession number GSE135893. Samples were from 20 pulmonary fibrotic lungs and processed by 10X Genomic scRNA-Sequencing. UMAP plot generated by Jade Manning.

6.4 Discussion

The aim of this chapter was to induce hypoxia to the gastrocnemius to induce a lymphangiogenic response, with the hypothesis that loss of ZEB1 will result in increased lymphatic remodelling. To investigate the effect of ZEB1 in pathological/inflammation-induced lymphangiogenesis, we utilised a model of HLI. While this model is documented to induce angiogenesis and inflammation (Silvestre et al., 2008), and was successful in reducing blood flow (Figure 6.3.1), we found this surgery did not induce a lymphangiogenic response in the Control mice (Figure 6.3.1.1, Panels C, F and G). However, upon investigation of the skeletal muscle sections, there was a significant difference between the lymphatic density of the non-surgery legs of ZEB1^{ieCKO} and Control mice (Figure 6.3.1.1, Panel A and C),

suggesting ZEB1 plays a role in the lymphatic morphology of the gastrocnemius muscle. To ensure this was not related to the surgery, a preliminary study on non-surgery mice was completed, the results of which are shown in Figure 6.3.2.1. Despite the low sample size, a difference in lymphatic density and area was potentially suggested between ZEB1^{IECKO} and Control mice, indicating ZEB1 may be involved in maintaining lymphatic maturation in this tissue bed, however more data is required to investigate this further. A novel discovery amongst this work was the expression of CD45 expression in lymphatic vessels of the skeletal muscle (Figure 6.3.3.1). This was present in both Control and ZEB1^{IECKO} mice. Upon further investigation in human dermal LECs and lung LECs, a relationship between ZEB1 and ectopic expression of CD45 has been suggested.

Regarding the HLI model, it is possible that sufficient ischaemia/inflammation was not induced through the surgery to induce lymphangiogenesis. There is only one study that has investigated this model for its effect on lymphangiogenesis (Pu et al., 2021). This study suggested the lymphangiogenic response aided the restorative angiogenic remodelling. Pu et al., took several time points for analysis, resulting in documentation of the increase in LYVE1⁺ cells per field over post-operative days 0, 3, 5, 7, 14 and 28, with the most significant increase seen by day 28 (Pu et al., 2021). In our experiment, we sacrificed the animals at day 28, suggesting we were correct in our choice of endpoint for analysis. Otherwise, the concern would be that this time point was too late, as it is documented that once the inflammation resolves, the newly formed lymphatic vessels can regress (Kataru et al., 2011; Tan et al., 2012; H. Kim et al., 2014). These studies however mainly concentrate on lymphatics nearby or within lymph nodes, so may not be true for insult to skeletal muscle. This regression is thought to be down to the presence of T-cells in the node, which secrete anti-lymphangiogenic factor INF- γ . Whereas, in peripheral tissues, the extra-nodal neo-lymphatic network is thought to remain (Yao et al., 2010; Tan et al., 2012), these studies were not quite representative of the ischaemia-induced inflammation, as both these studies concentrated on repeated inflammatory stimuli over a longer period to model chronic disease in the airways.

The model of cardiac ischaemia is a similar surgery-induced single induction of ischaemia, studies here have found the lymphatic response was documented from day 3 (Shimizu et al., 2018). This continued in various studies up to 42 days (Vuorio et al., 2018; Klotz et al., 2015). Combining this research, we assume that following a successful surgery of HLI, we should have been able to induce a lymphatic response, visible through immunofluorescence staining at our chosen 28-day end point. It is therefore possible, that the surgery potentially did not induce sufficient blood flow restriction to induce ischaemia to the tissue for a sufficient length of time, or the later induced inflammation induced lymphangiogenesis. Further to this, in this dataset, the consequences of the surgery on the remodelling of local blood vessels was not studied in this thesis. The mouse model used results in the loss of ZEB1 from all ECs, including blood vasculature. It is possible that altered blood vessel remodelling influenced the lymphatic response, such as lack of a blood vessel infiltration resulting in a failure of immune response, therefore decreasing the need for a lymphatic response. Alternatively, enhanced blood vessel infiltration could adequately re-oxygenate the hypoxic tissue, also resulting in a decreased immune response. To exclude these possibilities, a lymphatic specific mouse model, such as Prox1-Cre mouse could be utilised, along with monitoring the immune response with histological staining of neutrophils, leukocytes, and macrophages.

An unexpected result from this study was the lymphatic density difference between the non-surgery legs of ZEB1^{iECKO} and Control mice. This research discovered that inducing ZEB1^{iECKO} induces an increase in density of LYVE1 positive structures (Figure 6.3.1.1 and Figure 6.3.2.1). As this was seen initially seen in tissue from mice that had undergone surgery, we wanted to ensure the effects seen were not a side-effect of the surgery, such as increased weight-bearing on the contralateral leg. A preliminary study was conducted whereby mice were dosed with tamoxifen to induce ZEB1^{iECKO} a week prior to cardiac perfusion. The same process of sectioning, immunofluorescence staining and LYVE1 quantification took place, with these results (Figure 6.3.2.1) displaying a similar trend to that seen in the contralateral leg of the surgery leg. This suggests that loss of ZEB1 in the lymphatic vessels of the skeletal

muscle does induce a lymphatic response resulting in an increase in lymphatic density. These results support the initial hypothesis that presence of ZEB1 retains quiescence in LECs, therefore loss of this transcription factor may induce a more mesenchymal phenotype, whereby full mesenchymal transition has not taken place, supportive of vessel remodelling (Fang et al., 2021).

CD45 is a commonly used histological marker for immune cells, thus often used to quantify immune infiltration within a tissue bed. Due to its suggested specificity, it is also used in techniques such as endothelial cell sorting, whereby any CD45⁺ positive cells are removed from the sample as to remove any contaminating immune cells. Therefore, it was decided that ECs are CD45⁻, and this assumption is engrained in these established techniques and downstream applications. Similar to other researchers (Hsieh et al., 2018), we began to use CD45 as a marker of immune cell infiltration, however we discovered dual staining of CD45 alongside LYVE1. At first, we thought this may be suggestion our initial LYVE1 staining could be macrophage, as LYVE1 is present on macrophage subtypes (Lim et al., 2018). However, when we took thicker sections of the hindlimb muscle (increased from 0.16 μm to 0.40 μm) we discovered this dual-like staining on vessel-like structures (Figure 6.3.3.1), this allowed visual morphological assessment of the positive structures, which we were unable to do in Figures 6.3.1.1 and Figure 6.3.2.1. We assessed that the structures seen were lymphatic vessels, as they were elongated, vessel like structures positive for LYVE1. The literature suggests very little with why this might be, the most convincing is these vessels may have been formed using the progenitor pool of leukocytes, this has been documented once in adult mice by Buttler et al., (2016). In this study a significant number of leukocytes co-localised, and actively integrated, into newly formed lymphatics in Matrigel plug experiments, this represented inflammation-induced lymphangiogenesis. The integration of these leukocytes into the new vessels was assumed due to the endothelial-like morphology of these cells, not unlike what we have seen (Figure 6.3.3.1). These cells also co-expressed podoplanin, a marker of the lymphatic endothelium (Buttler et al., 2016). What is established by Buttler et al., and not in our results, is these vessels are newly formed,

as they are actively invading the Matrigel plug. In our model of HLI, and of the hindlimb muscle following ZEB1^{iECKO}, we are unable to distinguish newly formed vessels from the existing vasculature. Therefore, we are unable to conclude if the expression of CD45⁺ LYVE1⁺ structures are neo-vessels, or pre-established. Buttler et al., suggests their results are a result of adult lymphangiogenesis in response to inflammation, utilising leukocyte progenitors to aid this, then once incorporated into the vessels and CD45 expression is a relic of leukocyte origin. It could be that we are seeing the same, or that these vessels were not newly formed, but were expanded in normal developmental lymphangiogenesis using the progenitor pool of leukocytes, potentially retaining their CD45 expression. To investigate this further, in a developmental model of lymphangiogenesis, such as that seen in Chapter 4, co-staining for CD45 and a lymphatic marker should take place. We have previously justified our choice of lymphatic marker LYVE1, however, to fully establish that our results are showing LECs expressing CD45, an alternate or additional marker should be included. Markers such as podoplanin used by Buttler et al., VEGFR3 or PROX1 would also delineate LECs. This will help distinguish between LECs originating from leukocyte origin from the LYVE1 positive macrophages capable of adhering to the lymphatic walls, which do not express PROX1 (Gordon et al., 2010).

Another theory of CD45 expression in these ECs originate from a similar phenomenon seen in mitral valve ECs after MI in sheep. In this study, by Bishchoff et al., mitral valve ECs were seen to express CD45 in response to MI. This expression was detected in the tissue by immunohistochemistry and flow cytometry 6 months after the initial infarct. These cells were identified by their expression of VE-Cadherin, α -smooth muscle actin and CD45. Increased number of CD45⁺ cells correlated with enhanced fibrosis, severity, and infarct size. Furthermore, CD45 expression was induced *in vitro* in these ECs specifically, in response to TGF β , a known inducer of EndMT (Bischoff et al., 2016). Inhibition of CD45 PTPase activity reduced migration of these ECs, a hallmark of the EndMT process (von Gise and Pu, 2012), suggesting a role of CD45 in initiation of EndMT. Increased EndMT is necessary for recovery of the tissue from an initial infarct, however uncontrolled

EndMT has been shown to increase negative outcomes, as potentially shown in this study (Bischoff et al., 2016). However, Bischoff and colleagues concludes that due to the plasticity of mitral valve ECs, the expression of CD45 may be indicative of an adaptive phenotype, as this phenomenon was isolated to mitral valve ECs and not the other carotid arterial cardiac ECs also included in the experiments (Bischoff et al., 2016). This study gives suggestion to what was seen in our results in the *in vitro* results (Figure 6.3.4.1) as we have previously suggested ZEB1 has a role in EndMT (Chapter 4), where we found during siRNA knockdown the mesenchymal phenotype of LECs was enhanced, through upregulation of SLUG and SNAIL. In this chapter, we demonstrate *in vitro*, the ZEB1 knockdown enhanced CD45 expression at protein level, we could suggest that following Bischoff et al., we are also seeing an adaptive, more mesenchymal phenotype.

In a brief report by Nasim et al., which follows on from Bischoff et al., the idea has been reinforced. Nasim and colleagues induced expression of CD45 in human endothelial colony forming cells, a cell type that does not express CD45 physiologically or through induction with TGF β . Bulk RNASeq of these cells revealed an upregulation in EndMT markers in CD45-expressing cells, including TGF β 2, SLUG and α SMA (Nasim et al., 2023). Through functional assays, mesenchymal properties of these cells were revealed. Migration is a hallmark of EndMT, enabling movement from the endothelium to the subendothelial space allowing initial remodelling and/or repair (Bischoff et al., 2016). Using a transwell migration assay, enhanced migration of the CD45-expressing cells was seen, which was reduced upon addition of a CD45 PTPase inhibitor. Activated mesenchymal cells can modulate the extracellular matrix, this can be tested through the ability to contract collagen gels, again this was seen enhanced in the CD45-activated cells and reduced with the addition of the PTPase inhibitor. Finally, integrity of the endothelial barrier was tested, as a loosening of cell-cell junctions and increase in permeability is attributed to EndMT to facilitate detachment of ECs from their neighbours and migration. This assay found the CD45-activated cell had a decrease in transendothelial electrical resistance showing these cells formed a reduced electrically resistance endothelial

barrier (Nasim et al., 2023). By testing the functionality of these cells Nasim et al., have given an insight into the consequences physiologically of enhanced CD45 expression in this particular EC subtype. Combined with Bischoff et al., this idea of CD45 expression initiating EndMT has been seen in both sheep and human models in vascular ECs, suggesting this process is conserved through animal species. Our work is based in LECs of mice and humans, so requires some extrapolation through the ECs subtypes. In our results, we found significant amounts of CD45 expression in what we believe to be the LECs of the skeletal muscle (Figure 6.3.3.1) in mice. From the results shown in Nasim et al., we could infer these lymphatic vessels may function differently to non-CD45 expressing lymphatics vessels. Quantification of CD45 in the hindlimb between ZEB1^{iECKO} and Control mice did not take place, however qualitatively, there is no obvious difference in expression (Figure 6.3.3.1). We did however see an increase in expression *in vitro* in HDLECs upon ZEB1 knockdown (Figure 6.3.4.1). If we had tested *in vitro* for changes in the functionality of the ZEB1 knockdown cells in the way Nasim et al. had, along with PTPase inhibition to establish this was a direct consequence of CD45 expression, we might be able to extrapolate to our results shown Figure 6.3.1.1 and Figure 6.3.2.1. These results show enhanced LYVE1 density in the ZEB1^{iECKO} mice, regardless of hindlimb surgery. Although a difference in CD45 expression was not shown qualitatively through tissue visualisation, we have reason to believe there is enhanced CD45 activity following ZEB1 knockdown (Figure 6.3.4.1) in human LECs, although cross-species, enhanced density could be a result of enhanced EndMT which leads to enhanced remodelling. *In vitro* experiments, including functional assays as discussed using primary mouse LECs would help guide this research further, to understand if this developing idea is conserved. Future research effort should be made to measure any changes in CD45 expression *in vivo*, alongside ZEB1 expression in these CD45⁺ vessels. Previous research showed LECs express ZEB1 in a quiescent state (Chapter 4.3.1), therefore it is possible in the Control mice where we see CD45 expression, these hindlimb lymphatic vessels may be undergoing active remodelling, therefore may not be expressing ZEB1. Dual staining of Control and ZEB1^{iECKO} mice lymphatic beds with ZEB1 and CD45 antibodies would test this theory.

It is rare, but not unheard of, to enhance lymphatic density/activate lymphangiogenic in adult tissue without a stimulus such as injury or addition of lymphangiogenic factor (Enholm et al., 2001; Nurmi et al., 2015). However, what we have seen is the induction of knockout of ZEB1 has induced some form of remodelling in the skeletal muscle, even without stimulus of injury or inflammation (Figure 6.3.1.1 and Figure 6.3.2.1). To test the functional impact of this enhanced remodelling, an alternate model of injury, well documented to induce neo-lymphangiogenesis should be used. As discussed, our model of HLI did not induce a lymphangiogenic response in the Control mice (Figure 6.3.1.1). This suggests the level of inflammation, or perhaps insufficient prolonged ischaemia made this model not best suited for our research. Additionally, had we seen a lymphangiogenic response, we would have been unable to distinguish newly formed vessels from pre-existing ones. The cornea, however, is an avascular tissue bed which allows observation of neo-lymphangiogenesis with no physiological network interference (Cao et al., 2011). To induce inflammation-associated lymphangiogenesis, a suture is sown in the epithelial layer to induce a robust inflammatory, lymphangiogenic response (Maruyama et al., 2005). Alternatively, to study the formation of new vessels without inflammatory response, a pellet containing lymphangiogenic stimuli can be surgically inserted into a micropocket in the mouse cornea. The cornea can then be quantified by immunofluorescence staining to visualise the newly formed vessels (Cao et al., 2011). For our research, we would want to investigate the presence of CD45 in these neo-vessels.

The implications of this work discussed is significant, as mentioned many techniques of endothelial isolation and identification involve the idea that ECs are CD45⁻, from Bischoff et al., we see this is not the case in mitral valve ECs. In LECs, the presence of CD45⁺ has not previously been recorded, except for in the case of leukocyte integration (Buttler et al., 2016). This finding has not seemed to alter or optimise any protocol for the specific cell isolation of LECs from a mixed population. Presented here is further evidence that blanket ECs isolation techniques need adapting for

potential populations of CD45 expressing cells, these cells may only appear in diseased populations (Figure 6.3.4.3), upon gene knockout such as ZEB1 (Figure 6.3.4.1, Panel A) or certain growth conditions (Figure 6.3.4.1, Panel B). However, these adaptable cells could be crucial in our understanding of EndMT initiation, control, and therapeutic potential.

One obvious limitation of this work is the co-expression of some macrophages of LYVE1 and CD45 present in the skeletal muscle (Krasniewski et al., 2022). We hoped to overcome this with the morphological analysis of vessel-like structures, however ideally an alternate lymphatic marker should be considered to ensure a robust, well-rounded research finding. To test the functional consequences of ZEB1 knockdown, assays such as those describe by Nasim et al., would be interesting, especially with the addition of PTPase inhibitor. *In vivo*, investigating other tissue beds, at different stages of development would be desirable, to investigate if CD45 expression seen in the lymphatic vessels is just a phenomenon isolated to lymphatics of the skeletal muscle. Additionally, cell-lineage tracing may be a useful tool to investigate the origins of the LECs expressing CD45 as described specifically in mice LECs by Martinez-Corral & Makinen, 2018. This protocol involves a process with utilises the Cre/loxP system to fluorescently tag target LEC-specific progeny (Martinez-Corral and Makinen, 2018). This can be later visualised by immunofluorescence staining and stained for further markers such as CD45. This method would give insight into alternate contributors of lymphatic progenitors, and can be inducible at any stage, meaning we could investigate if CD45-expressing progenitors are only included in adult lymphatic remodelling, or in specific tissue beds such as the skeletal muscle as shown in this work.

In conclusion, this chapter aimed to focus on the inflammation-induced lymphangiogenesis in adult skeletal muscle. However, what was discovered was not a result of the HLI surgery. ZEB1 knockout was instead found to induce an increase in LYVE1 positive structures in the gastrocnemius in physiological conditions. Upon investigation of these structures using thicker sections, vessel-like structures were

visibly LYVE1 and CD45 positive in both the Control and ZEB1^{IECKO} mice. This is a novel finding which should be investigated further.

Chapter 7. Discussion

7.1 The role of ZEB1 in lymphatic endothelial cells

This research aimed to understand the involvement of ZEB1 in LECs. The overall hypothesis was that loss of endothelial ZEB1 will result in a lymphangiogenic phenotype by inducing partial EndMT. These ideas are based on the idea that LECs, like BECs, undergo partial EndMT during lymphatic vessel remodelling. Preliminary work by the group had highlighted the expression of ZEB1 in HUVECs and HDLECs in subconfluent, and potentially quiescent, conditions (Chapter 1.5). ZEB1 is a key driver of EMT, which shares many similarities with EndMT, however instead of driving EndMT and only expressed in activated state, ZEB1 is expressed in quiescent LECs (Chapter 4.3.1), suggesting an alternate role. ZEB1 knockdown in RNA (Chapter 3.3.1) and protein (Chapter 4.3.3) suggests that ZEB1 when present acts to maintain a quiescent, not active, state. A decrease in ZEB1 dysregulated some markers of EndMT, namely SLUG and SNAIL, while cell junctional protein VE-Cadherin expression was unaffected (Chapter 4.3.3), suggesting only partial EndMT is in progress, but not through direct ZEB1 binding (Chapter 4.3.3). ECs in vessels undergoing remodelling have been shown to go through partial EndMT, resulting in angiogenesis. In the hindlimb muscle (Chapter 6.3.2), we found increased presence of lymphatic vessels following ZEB1 knockdown, suggesting increased lymphangiogenesis in this tissue bed. This suggests ZEB1 may play a role in maintenance of lymphatic vessel quiescence. This is a crucial finding, to investigate how lymphatic vessels stop growing, is also to discover by which mechanisms they reinitiate growth.

Loss of ZEB1 has been shown throughout this thesis to suggest a change in cell phenotype away from quiescent, to a more activated state. In the bulk RNA sequencing of ZEB1 knockdown, 2727 genes were altered. Over-representation analysis pointed to changes in genes involved in cell movement, cell proliferation and function (Chapter 3.3.2), suggesting ZEB1 is crucial to the physiological functioning of LECs. The Interferon Signalling Pathway was a major signalling pathway predicted inhibited in this dataset, with key regulators of this pathway

appearing to be regulated by ZEB1. RNF213 was also present in the ChIPSeq/RNASeq cross over data set, showing ZEB1 directly binds to an enhancer region of RNF213 to control its expression. RNF213 is a stimulator of the interferon γ pathway. The effect of the interferon pathway on LECs specifically has not been elucidated and should be a focus of future research. In other cell types, the interferon pathway has been shown to influence cell proliferation, cell migration and angiogenesis (Laug et al., 2012; Yang et al., 2017; Ciccarese et al., 2020). Due to shared origins of blood and lymphatic vasculature, signalling pathways guiding angiogenesis often impact lymphangiogenesis. The lack of significant key regulators of lymphatic identity and lymphangiogenesis in both the RNASeq and ChIPSeq potentially suggests a lack of significance of ZEB1 in LECs and taken alone may prevent any further investigation. However, the lymphatic field is underdeveloped and what may be present in the data may be currently unknown key regulators of the lymphatic vasculature. Our hypothesis that a lymphangiogenic signature would be recognisable in our RNA data was potentially naïve, but we did see changes in key lymphangiogenic markers such as PROX1 and VEGFR3, which suggests although ZEB1 might not be the direct mediator, ZEB1 is indirectly affecting the expression of these genes. It would be interesting to investigate the effect of overexpression of ZEB1 in LECs, and conduct RNASeq on the samples, to investigate if it is a reciprocal relationship.

7.1.1 Does loss of ZEB1 initiate partial EndMT in LECs?

There is potential evidence within this thesis of activation of partial EndMT through loss of ZEB1. EndMT is characterised by loss of apical basal polarity, loss of cell-cell contacts, ability to remodel basement membrane and migration into the extracellular space (Bischoff, 2019). EMT and EndMT share overlap in signalling pathways and transcriptional mediators and epithelial and ECs share many characteristics, therefore much overlap is seen within the molecular mechanisms. FAM83H was identified as a significantly increased following ZEB1 knockdown (Chapter 3.4) and in the ChIPSeq (Chapter 3.5). In epithelial cells, there was a loss of epithelial polarity with FAM83H expression, and loss of cell junctional marker E-cadherin (Kuga et al., 2013). These are characteristic of a metastatic, invasive

phenotype, alike to EndMT. This idea is reinforced with a top downregulated gene, EPCAM, a pan epithelial marker implicated in cell adhesion and oncogenic signalling (Yamashita et al., 2007). Downregulation of this gene suggests alterations in cell-cell contact, which is required to attain a migratory phenotype. EPCAM has been linked to execute oncogenic potential through activation on the Wnt/ β -catenin pathway (Yamashita et al., 2007), which has been implicated in partial EndMT mechanism resulting in *in vitro* lymphangiogenesis (Wang et al., 2017). The results at a protein level of ZEB1 knockdown further point to a mechanism of partial EndMT (Chapter 4.3.2). SLUG and SNAIL were both upregulated following loss of ZEB1, but VE-Cadherin expression was unchanged (Chapter 4.3.2), SLUG and SNAIL are both documented drivers of EndMT. The lack of change in VE-Cadherin suggests partial EndMT, not full EndMT is in progress, as cell-cell junctions are still intact. Expression of CD45 (Chapter 6.3.4) following ZEB1 knockdown *in vitro* further supports this idea, as CD45 has been suggested as a novel marker of EndMT (Nasim et al., 2023). Metabolic analysis using the Seahorse Mitochondrial Stress Assay revealed a lower basal energy status of the ZEB1 knockdown cells (Chapter 4.3.5) this is suggestive of a mesenchymal phenotype, which has been associated with a lower energy requirement (Cai et al., 2015). This could be attributed to the increase in SLUG expression, as this has been implicated in contributing to the mesenchymal status of LECs (Cai et al., 2015). To investigate this further *in vitro*, function assays such as gel contraction, transwell migration and electrical resistance assays should be considered to elucidate a possible mesenchymal phenotype.

7.1.2 A relationship between ZEB1 and CD45 expression

A potential novel marker of EndMT, CD45 (Nasim et al., 2023) was found expressed in the lymphatics of the skeletal muscle (Chapter 6.3.3). This is a novel finding, with previous work by Nasim et al., conducted in mitral valve ECs. One paper has documented expression of CD45⁺ cells which have integrated into a growing vessel. Buttler et al., documented that leukocytes were incorporated into newly established lymphatic vessels, and able to co-express lymphatic markers such as podoplanin (Buttler et al., 2016). It is possible this is what has been seen in Chapter 6, CD45

expression was seen in both our ZEB1^{IECKO} and Control mice, although not quantified, qualitatively expression appeared unchanged. In the tissues investigated, the vessels could not be defined as newly formed, so it is unclear if leukocyte integration is an explanation for our results. Unfortunately, no other tissue beds were investigated for CD45 expression, however this should be investigated further as a matter of priority, along with co-expression of specific markers of LECs to establish the identity of the cells within the vessel. This includes suggestions of use of an avascular tissue bed, to determine a newly formed vessel, with consequent staining to investigate CD45 expression. Many techniques, involving cell sorting, isolate ECs from a mixed population by their expression patterns, relying on ECs being CD45⁻, here we present at least in the skeletal muscle, this is not the case for LECs in mice. In human primary dermal LECs this was first investigated at an RNA level, where CD45 was unchanged but predicted upregulated following loss of ZEB1. This was validated at a protein level whereby expression of CD45 was only seen following loss of ZEB1 (Chapter 6.3.4). These results fit with our overall hypothesis that loss of ZEB1 results in lymphangiogenic remodelling via induction of partial EndMT, however this is only seen in the mouse skeletal muscle. To investigate if it is the loss of ZEB1 induces lymphatic remodelling in humans, future work recommended would be to use functional assays such as tube formation using HDLECs, as well as, if possible, LECs originating from other tissue beds.

7.2 Limitations

Using the ChIPSeq in LECs, combined with HUVEC ChIPSeq for common histone modifications H3K4me1, H3K4me3 and H3K27ac, we can determine ZEB1 binding in regions associated with transcriptional regulation, such as promoter and enhancer regions. These tracks were selected due to the shared endothelial cell line, and the lack of available data in HDLECs. However, while this data can be used to inform hypothesis, it cannot be used alone to determine ZEB1 binding at active enhancer regions, as these are cell-specific in nature. This means we could be missing lymphatic specific active enhancer regions where ZEB1 is binding, as these are not highlighted as active in HUVECs. This is significant as no key lymphatic regulators

were present as in the ChIPSeq data, as shown in Chapter 4. This could mean that ZEB1 acts through other mechanisms to influence changes in regulators such as PROX1, such as binding to a co-factor, which directly binds to PROX1, or by influencing the expression of a protein upstream of PROX1, or by preventing degradation of the protein. Efforts should be made to acquire ChIPSeq data of histone modifications specifically in HDLECs so accurate interpretations of the data can be made, and further experiments to confirm these mechanisms. The lack of data available adds to the lymphatic field trailing behind the blood vasculature knowledge, despite the potential therapeutic benefits of treatment with lymphangiogenic agents.

Despite predictions *in vitro* of partial EndMT activation, and potentially lymphangiogenic response *in vitro*, in Chapter 5, there was no overall change in the lymphatic parameters measured in the *in vivo* mouse model. There are obvious differences between our *in vitro* and *in vivo* work, the most apparent is species. All the experiments *in vitro* utilised primary human dermal LECs. This allows translation into the human system, but a lesser extent to our mouse model. The cells did originate from the dermis, and we did choose the ear dermis as primary location for measurements of lymphatic morphology however, use of a mouse model to replicate the human system is not ideal. The protein coding regions of mouse and human genomes are approximately 85% similar (NIH, 2017). Additionally, *in vitro* with any cell line, we are also unable to reproduce the complex biological environment of an *in vivo* system. With LECs, the lymph flow providing shear stress is an important mediator of quiescence, our experiments used a 2D monolayer, therefore not replicating the tube formation of vessels, or experiencing any type of flow. This could be replicated using 3D cell culture models, some which account for flow, but these are technical and costly.

In a pathological model of injury, we found hindlimb ischaemic insult did not result in a substantial lymphangiogenic consequence. We could not therefore make any conclusions as to whether loss of ZEB1 impacted the pathogenic lymphangiogenic response. The HLI model was not the optimal model for the investigation of

lymphatic remodelling in response to injury. A more appropriate model would involve use of the cornea, an avascular tissue bed, which is a published model of neo-lymphangiogenesis in response to a suture or stimulus which induces inflammation. The HLI model is not validated for use in lymphatic research, however due to limitations in animal models was the only model of injury available for our research. This pathological model did reveal changes in a tissue-bed not investigated in Chapter 5. The lymphatics of the skeletal muscle were observed to increase in number and density following loss of ZEB1. This is suggestive that loss of ZEB1 induces lymphatic remodelling in a tissue-bed specific basis. Combined with the results from Chapter 3 and 4, we could suggest this lymphatic remodelling is due to activation of a partial EndMT mechanism. To determine this fully, alternate tissue beds should be investigated, as well as investigation of expression of EndMT markers such as SNAIL and SLUG, in these tissue beds.

The use of our mouse model which is not lymphatic specific is somewhat unusual for lymphatic research. Although there is some published literature (Wang et al., 2010) of use of the Cdh5-CreERT2 model for use in lymphatic research, it is primarily used to understand mechanisms regarding the blood vasculature. To exclude any effect seen in the blood vasculature influencing the lymphatic vasculature, the use of a Prox1-CreERT2 should be considered. The PROX1-CreERT2 model is widely used in lymphatic research, this places the Cre under the control of the promoter for PROX1, which is expressed in LECs, although not exclusively (Rudzinska et al., 2017; Lavado and Oliver, 2007). Alternative models include the LYVE1-CreERT2 mouse (Connor et al., 2016) however LYVE1 is also expressed in macrophages, which may further complicate the results seen in Chapter 6 regarding CD45 expression. Other models of the lymphatic vasculature could also be considered, such as the zebrafish model. This model is a convenient especially when investigating the early phases of development, as they are transparent allowing for individual LEC tracking via transgenic tagging and real time imaging (Kim and Jin, 2014). The role of ZEB1 in early development was not studied in this thesis, it could be ZEB1 plays a pivotal role in utero, which becomes redundant after birth. The use of a transgenic zebrafish model would help investigate this much quicker, easier, and cheaper than the

equivalent in a mouse. The use of zebrafish does not come without issues, the use of zebrafish moves away from the translatability of the findings to humans, for example in zebrafish, PROX1 is dispensable for lymphatic development (van Impel et al., 2014). Therefore, zebrafish could offer valuable insights to some aspects of the lymphatic vasculature but should complement rather than replace other models of lymphatic development and disease.

7.3 Implications

In disease, ZEB1 has been implicated primarily in cancer, driving EMT and a metastatic phenotype. In the eye, mutations which result in insufficient ZEB1 have been identified in ECs to be responsible for the several diseases associated with corneal dystrophies. In posterior polymorphous corneal dystrophy (PPCD), 30% of patients present with a mutation of the ZEB1 gene, resulting in decreased expression (Frausto et al., 2019). In an animal model of PPCD, lack of ZEB1 resulted in epithelial-like features in the endothelium, such as increased expression of E-cadherin and keratins, and decreased expression of N-cadherin (Frausto et al., 2019). These models had increased endothelial apoptosis, increased barrier function with Frausto et al., suggesting an endothelial to epithelial transition is occurring because of decreased ZEB1. Although not the same mechanism we are seeing Frausto et al., demonstrates a role of ZEB1 in maintaining endothelial phenotype and integrity, not unlike what was seen with loss of ZEB1 in the LECs (Chapter 4.3.3). Interestingly the cornea does not contain lymphatic vessels and has been suggested as an alternative tissue bed to investigate neo-lymphangiogenesis. This work by Frausto et al., presents a complication to this idea, as ZEB1 seems to have a key role in these ECs, therefore may interfere with the proposed experiment to measure lymphatics in an avascular tissue bed in the current mouse model. This issue could be mitigated with the use of a lymphatic specific mouse model such as the Prox1 Cre-ERT2.

Lack of remodelling of lymphatic vessels in response to injury/trauma, can lead to lymphoedema, which is currently incurable. Primary lymphoedema is a result of genetic defect and is rare. However secondary lymphoedema is common amongst breast cancer survivors, up to 1 in 5 patients who have undergone surgery to biopsy

the lymph nodes or remove a tumour (Ren et al., 2022). Lack of remodelling to repair the damaged tissue results in fluid accumulation in the upper arms, this is painful and has severe psychological impact on many patients (Ren et al., 2022). Currently, treatment focusses on management rather than cure. Similarly, excess lymphatic remodelling is associated with poorer prognosis in metastatic cancer, with lymphangiogenesis a hallmark of tumour dissemination (Hanahan and Weinberg, 2011). Thus, investigating the switch from quiescent vasculature to an active state of remodelling is essential to uncover potential therapeutic targets to ensure homeostasis of the vasculature. The results in this thesis present ZEB1 as a worthy avenue of research to find a targetable mechanism to initiate lymphatic growth in areas of damaged vasculature.

Specifically, the results in Chapter 6, whereby lack of expression of ZEB1 in humans, is linked to expression of CD45 in LECs has significant implications on the lymphatic field. The expression of CD45 alone in lymphatic vessels, shown in the hindlimb muscle in mice, and in human cultured cells, is a significant finding itself. Whether this be a relic of leukocyte origin as suggested by Buttler et al (2016), or potentially a novel marker of EndMT as suggested in other endothelial subtypes by Bischoff et al (2016) and Nasim et al (2023). This could unveil a mechanism by which ZEB1 when present in LECs, suppresses CD45 expression, therefore maintaining quiescence in these vessels. This mechanism, once fully characterised, could be utilised in cancer, where tumour lymphangiogenesis aids tumour progression and metastasis (Stacker et al., 2002). Preventing lymphatic growth in this disease by finding a druggable target in this pathway, could help restrict the cancer to the primary site, keeping the patient at an earlier, easier to treat, stage of disease. Opposingly, in cases such as lymphoedema where lymphatic growth is required, by reducing expression of ZEB1 such as in Chapter 6, and inducing CD45 expression, we could potentially induce partial EndMT in lymphatic vessels, inducing growth to revascularise the affected area. This could be a potential therapy for secondary lymphoedema as a consequence of lymph node dissection, breast cancer resection, or due to chronic illnesses where the lymphatic vessels have been damaged by excess inflammation,

such as Crohn's disease. Further research should research the proteins involved in the regulation of both ZEB1 and CD45 expression in LECs, as this could result in a landmark treatment in the control of lymphatic growth.

7.4 Conclusion

In conclusion, loss of ZEB1 does induce a partial EndMT signature in HDLECs. In the skeletal muscle of ZEB1^{iECKO} mice, this corresponded with enhance lymphatic remodelling, the suggested mechanism for this shown in Figure 7.1. Recommended further research would be to investigate alternate tissue beds to investigate this further, with the potential to use a lymphatic specific mouse model. Therapeutically, enhanced lymphatic remodelling would give rise to breakthrough treatments in cases of secondary lymphoedema, enhanced wound healing and chronic inflammatory diseases.

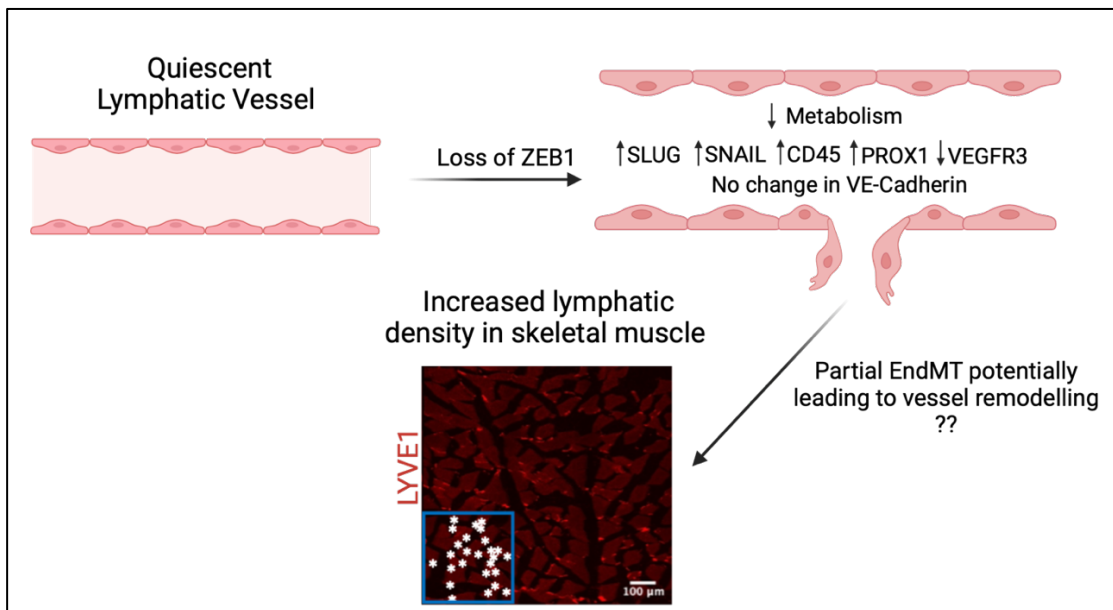


Figure 7.4. A proposed mechanism by which loss of ZEB1 leads to increased lymphatic density. Quiescent lymphatic vessels express ZEB1, following loss of ZEB1, markers of EndMT are upregulated, leading to a partial EndMT mechanism of vessel remodelling. In the skeletal muscle, this remodelling manifested as an increased lymphatic density, as observed by LYVE1 staining on 20 μm muscle sections. Made with Biorender.com

Chapter 8. Appendix

8.1 COVID Statement

This PhD was undertaken from September 2019 to September 2023. During this time there was undisputable difficulty and adaptation. During the lockdown, animal studies were mostly halted, and the building closed for five months. The limited animal work that was able to be completed, was isolated to the BSU, meaning the tissue was not processed until the building was reopened. This complicated the animal studies and limited the viable tissue available for analysis of lymphatic morphology. Regarding the hindlimb ischaemia surgery, preliminary data collected in this time suggested a lack of induction of ischaemia in the female mice, thus females were then excluded from further studies. Upon return from the pandemic, strict rules were placed on distancing, limiting access to equipment, and being taught by others. This limited the amount of guidance we received from senior lab members before their contracts ran out. Despite the difficulties faced during this time, I believe there is a sufficient amount of data collected to allow for completion of a doctoral thesis without need for an extension.

8.2 Professional Industry Placement

As part of the BBSRC DTP PhD programme, students are required to undertake a 3-month placement "away from the lab bench". These placements - PIPs (Professional Industry Placements) - can be anywhere, and encouraged to be different to your PhD project, this is so you can have time away from your project to learn other skills and gain new experiences to help further your personal development. Having taken on a Student Ambassador role with Promega earlier this year, I felt this would be an ideal company to undertake my PIP with. As the company had never had an intern of such before but having already established rapport with Head of Sales during my time as an ambassador, I was allowed to be their "guinea pig" for such placement. This was a great outcome for both sides, I was able to mould the project outline around my interests, and the company had confidence in my abilities already, so were willing to put their time into planning a project for me.

During my time, I spent time in the Promega UK HQ, a purpose-build, carbon neutral hub nestled in Southampton Science Park. Featuring a grass meadow roof, open green space, the most extra clock I've ever seen, and ground source heat pumps to regulate the temperature of the building.

My internship had time allocated in each department in the company, this enabled me to experience every team involved in a successful life science company, and the jobs available outside of academia after a PhD. I spent time in Marketing, where I focussed on recruitment of the next cohort of Student Ambassadors, completed data analysis, and was given the opportunity to present my findings to colleagues in the US. A major part of my project was in Sales support, where the work on setting up pre-prepared answers on an E-platform will help secure more successful bids faster, and with less resources. In Strategic Marketing, I was able experience jobs for technical PhD graduates, outside of sales, as a Product Manager. This was a role I never knew existed and shows the benefit of these placements. Product Managers are responsible for a portfolio of products, they mostly have PhD's so have the technical knowledge to strategically market these products, and converse with the Sales team on how best these products are applied in different research groups. In my time with the Product Managers, I designed and created an "emailer" for an assay, which was sent out to a specific emailing list of researchers from the Promega account.

Academia shields you from a lot of the "outside world", we know our project, our immediate surroundings, and often are inclined to be kept in that bubble.

Placements such as our PIPs allow us to see and experience roles outside of academia, without being tied to the role as a full-time job. I have really enjoyed my 3-months with Promega, I joked after the first month that "my personality has come back". A PhD is draining, and a lot of hard work, we often forget to incorporate into our projects what skills we had learnt previously, such as creativity and communication. Going from an academic to corporate setting, I was surprised how much freedom I was allowed to come up with new ideas to communicate to the

customer and how my opinion and contribution was appreciated and acknowledged throughout the company. I was apprehensive to say the least to go to take such a large chunk of time away from my PhD project, considering the lab time already taken away from us from the pandemic. However, the time spent away my project has helped me think about my future career and what I want from a future job, rather than what a future job wants from me.

Chapter 9. References

- Adams, R. H. & Alitalo, K. (2007) Molecular regulation of angiogenesis and lymphangiogenesis. *Nature Reviews Molecular Cell Biology*. [Online] 8 (6), 464–478. [online]. Available from: <https://www.nature.com/articles/nrm2183>.
- Adessi, C. (2000) Solid phase DNA amplification: characterisation of primer attachment and amplification mechanisms. *Nucleic Acids Research*. [Online] 28 (20), 87e–887. [online]. Available from: <https://academic.oup.com/nar/article-lookup/doi/10.1093/nar/28.20.e87>.
- Agilent Technologies (2019) *Agilent Seahorse XF Cell Mito Stress Test Kit*. [online]. Available from: https://www.agilent.com/cs/library/usermanuals/public/XF_Cell_Mito_Stress_Test_Kit_User_Guide.pdf (Accessed 26 September 2023).
- Aigner, K. et al. (2007) The transcription factor ZEB1 (δ EF1) promotes tumour cell dedifferentiation by repressing master regulators of epithelial polarity. *Oncogene*. [Online] 26 (49), 6979–6988. [online]. Available from: <https://www.nature.com/articles/1210508>.
- Aldrich, M. B. & Sevick-Muraca, E. M. (2013) Cytokines are systemic effectors of lymphatic function in acute inflammation. *Cytokine*. [Online] 64 (1), 362–369. [online]. Available from: <https://linkinghub.elsevier.com/retrieve/pii/S1043466613002597> (Accessed 18 July 2023).
- Alitalo, K. et al. (2005) Lymphangiogenesis in development and human disease. *Nature*. [Online] 438 (7070), 946–953. [online]. Available from: <https://www.nature.com/articles/nature04480>.
- Al-Niaimi, F. & Cox, N. (2009) Cellulitis and lymphoedema: a vicious cycle. *Journal of Lymphoedema*. 4 (2), 38–42.
- Altin, J. G. & Sloan, E. K. (1997) The role of CD45 and CD45-associated molecules in T cell activation. *Immunology & Cell Biology*. [Online] 75 (5), 430–445. [online]. Available from: <https://onlinelibrary.wiley.com/doi/10.1038/icb.1997.68>.
- Alva, J. A. et al. (2006) VE-Cadherin-Cre-recombinase transgenic mouse: A tool for lineage analysis and gene deletion in endothelial cells. *Developmental Dynamics*. [Online] 235 (3), 759–767. [online]. Available from: <https://anatomypubs.onlinelibrary.wiley.com/doi/10.1002/dvdy.20643>.
- Anderson, E. M. et al. (2008) Experimental validation of the importance of seed complement frequency to siRNA specificity. *RNA*. [Online] 14 (5), 853–861. [online]. Available from: <http://rnajournal.cshlp.org/lookup/doi/10.1261/rna.704708>.
- Arciniegas, E. et al. (2005) Endothelial-Mesenchymal Transition Occurs during Embryonic Pulmonary Artery Development. *Endothelium*. [Online] 12 (4), 193–200. [online]. Available from: <http://www.tandfonline.com/doi/full/10.1080/10623320500227283> (Accessed 10 July 2023).
- Arciniegas, E. et al. (2007) Perspectives on endothelial-to-mesenchymal transition: potential contribution to vascular remodeling in chronic pulmonary hypertension. *American Journal of Physiology-Lung Cellular and Molecular*

- Physiology*. [Online] 293 (1), L1–L8. [online]. Available from:
<https://www.physiology.org/doi/10.1152/ajplung.00378.2006>.
- Armstrong, E. J. & Bischoff, J. (2004) Heart Valve Development. *Circulation Research*. [Online] 95 (5), 459–470. [online]. Available from:
<https://www.ahajournals.org/doi/10.1161/01.RES.0000141146.95728.da>
(Accessed 10 July 2023).
- Arumugam, T. et al. (2009) Epithelial to Mesenchymal Transition Contributes to Drug Resistance in Pancreatic Cancer. *Cancer Research*. [Online] 69 (14), 5820–5828. [online]. Available from:
<https://aacrjournals.org/cancerres/article/69/14/5820/549748/Epithelial-to-Mesenchymal-Transition-Contributes>.
- Azimi, M. S. et al. (2020) Lymphatic-to-blood vessel transition in adult microvascular networks: A discovery made possible by a top-down approach to biomimetic model development. *Microcirculation*. [Online] 27 (2), . [online]. Available from:
<https://onlinelibrary.wiley.com/doi/10.1111/micc.12595>.
- Baeyens, N. et al. (2015) Vascular remodeling is governed by a VEGFR3-dependent fluid shear stress set point. *eLife*. [Online] 4 (4), . [online]. Available from:
<https://elifesciences.org/articles/04645>.
- Balázsi, G. & Oltvai, Z. N. (2007) ‘A Pitfall in Series of Microarrays: The Position of Probes Affects the Cross-Correlation of Gene Expression Profiles’, in *Microarray Data Analysis*. [Online]. New Jersey: Humana Press. pp. 153–162. [online]. Available from:
<http://www.springerlink.com/openurl.asp?genre=book&id=doi:10.1385/1-59745-390-0:153>.
- Baldwin, A. L. et al. (1993) Regulation of water balance between blood and lymph in the frog, *Rana pipiens*. *Lymphology*. 26 (1), .
- Baluk, P. et al. (2007) Functionally specialized junctions between endothelial cells of lymphatic vessels. *The Journal of Experimental Medicine*. [Online] 204 (10), 2349–2362. [online]. Available from:
<https://rupress.org/jem/article/204/10/2349/46664/Functionally-specialized-junctions-between>.
- Baluk, P. et al. (2009) TNF- α drives remodeling of blood vessels and lymphatics in sustained airway inflammation in mice. *Journal of Clinical Investigation*. [Online] 119 (10), 2954–2964. [online]. Available from:
<http://www.jci.org/articles/view/37626>.
- Balzar, M. et al. (1999) The biology of the 17–1A antigen (Ep-CAM). *Journal of Molecular Medicine*. [Online] 77 (10), 699–712. [online]. Available from:
<http://link.springer.com/10.1007/s001099900038>.
- Bannister, A. J. & Kouzarides, T. (2011) Regulation of chromatin by histone modifications. *Cell Research*. [Online] 21 (3), 381–395. [online]. Available from:
<https://www.nature.com/articles/cr201122>.
- Barr, A. J. et al. (2009) Large-Scale Structural Analysis of the Classical Human Protein Tyrosine Phosphatome. *Cell*. [Online] 136 (2), 352–363. [online]. Available from:
<https://linkinghub.elsevier.com/retrieve/pii/S0092867408015134>.
- Beloglazova, I. et al. (2022) New Insight on 2D In Vitro Angiogenesis Models: All That Stretches Is Not a Tube. *Cells*. [Online] 11 (20), 3278. [online]. Available from:
<https://www.mdpi.com/2073-4409/11/20/3278>.

- Benedito, R. et al. (2009) The Notch Ligands Dll4 and Jagged1 Have Opposing Effects on Angiogenesis. *Cell*. [Online] 137 (6), 1124–1135. [online]. Available from: <https://linkinghub.elsevier.com/retrieve/pii/S0092867409003249>.
- Benest, A. V et al. (2008) VEGF-C induced angiogenesis preferentially occurs at a distance from lymphangiogenesis. *Cardiovascular research*. [Online] 78 (2), 315–323. [online]. Available from: <http://www.ncbi.nlm.nih.gov/pubmed/18065770>.
- Bernier-Latmani, J. et al. (2015) DLL4 promotes continuous adult intestinal lacteal regeneration and dietary fat transport. *Journal of Clinical Investigation*. [Online] 125 (12), 4572–4586. [online]. Available from: <https://www.jci.org/articles/view/82045>.
- Betterman, K. L. & Harvey, N. L. (2018) 'Histological and Morphological Characterization of Developing Dermal Lymphatic Vessels', in *Methods in Molecular Biology*. [Online]. pp. 19–35. [online]. Available from: http://link.springer.com/10.1007/978-1-4939-8712-2_2.
- Bhalla, S. R. et al. (2022) 'Measurement of Revascularization in the Hind Limb After Experimental Ischemia in Mice', in *Methods in Molecular Biology*. [Online]. pp. 105–113. [online]. Available from: https://link.springer.com/10.1007/978-1-0716-2059-5_9.
- Bischoff, J. et al. (2016) CD45 Expression in Mitral Valve Endothelial Cells After Myocardial Infarction. *Circulation Research*. [Online] 119 (11), 1215–1225. [online]. Available from: <https://www.ahajournals.org/doi/10.1161/CIRCRESAHA.116.309598>.
- Bischoff, J. (2019) Endothelial-to-Mesenchymal Transition. *Circulation Research*. [Online] 124 (8), 1163–1165. [online]. Available from: <https://www.ahajournals.org/doi/10.1161/CIRCRESAHA.119.314813>.
- Boardman, K. C. & Swartz, M. A. (2003) Interstitial flow as a guide for lymphangiogenesis. *Circulation research*. [Online] 92 (7), 801–808. [online]. Available from: <http://www.ncbi.nlm.nih.gov/pubmed/12623882>.
- Bobryshev, Y. (1998) The cell adhesion molecule E-cadherin is widely expressed in human atherosclerotic lesions. *Cardiovascular Research*. [Online] 40 (1), 191–205. [online]. Available from: [https://academic.oup.com/cardiovasres/article-lookup/doi/10.1016/S0008-6363\(98\)00141-2](https://academic.oup.com/cardiovasres/article-lookup/doi/10.1016/S0008-6363(98)00141-2).
- Boehme, J. T. et al. (2021) HIF-1 α promotes cellular growth in lymphatic endothelial cells exposed to chronically elevated pulmonary lymph flow. *Scientific Reports*. [Online] 11 (1), 1468. [online]. Available from: <https://www.nature.com/articles/s41598-020-80882-1>.
- Boscolo, E. et al. (2015) AKT hyper-phosphorylation associated with PI3K mutations in lymphatic endothelial cells from a patient with lymphatic malformation. *Angiogenesis*. [Online] 18 (2), 151–162. [online]. Available from: <http://link.springer.com/10.1007/s10456-014-9453-2>.
- Bouïs, D. et al. (2001) Endothelium in vitro: A review of human vascular endothelial cell lines for blood vessel-related research. *Angiogenesis* 4 (2) p.91–102.
- Bouvrée, K. et al. (2012) Semaphorin3A, Neuropilin-1, and PlexinA1 Are Required for Lymphatic Valve Formation. *Circulation Research*. [Online] 111 (4), 437–445. [online]. Available from: <https://www.ahajournals.org/doi/10.1161/CIRCRESAHA.112.269316>.

- Brabletz, S. et al. (2017) Generation and characterization of mice for conditional inactivation of *Zeb1*. *genesis*. [Online] 55 (4), . [online]. Available from: <https://onlinelibrary.wiley.com/doi/10.1002/dvg.23024>.
- Brabletz, T. (2012) To differentiate or not — routes towards metastasis. *Nature Reviews Cancer*. [Online] 12 (6), 425–436. [online]. Available from: <https://www.nature.com/articles/nrc3265>.
- Braverman, I. M. & Yen, A. (1974) Microcirculation in Psoriatic Skin. *Journal of Investigative Dermatology*. [Online] 62 (5), 493–502. [online]. Available from: <https://linkinghub.elsevier.com/retrieve/pii/S0022202X15442800>.
- Breviario, F. et al. (1995) Functional Properties of Human Vascular Endothelial Cadherin (7B4/Cadherin-5), an Endothelium-Specific Cadherin. *Arteriosclerosis, Thrombosis, and Vascular Biology*. [Online] 15 (8), 1229–1239. [online]. Available from: <https://www.ahajournals.org/doi/10.1161/01.ATV.15.8.1229> (Accessed 17 July 2023).
- Bromley, S. K. et al. (2005) Chemokine receptor CCR7 guides T cell exit from peripheral tissues and entry into afferent lymphatics. *Nature Immunology*. [Online] 6 (9), 895–901. [online]. Available from: <https://www.nature.com/articles/ni1240>.
- Bruyère, F. & Noël, A. (2010) Lymphangiogenesis: *in vitro* and *in vivo* models. *The FASEB Journal*. [Online] 24 (1), 8–21. [online]. Available from: <https://onlinelibrary.wiley.com/doi/abs/10.1096/fj.09-132852>.
- Bujoreanu, I. & Gupta, V. (2023) *Anatomy, Lymph Nodes*. [online]. Available from: <http://www.ncbi.nlm.nih.gov/pubmed/26628065>.
- Buttler, K. et al. (2016) Integration of CD45-positive leukocytes into newly forming lymphatics of adult mice. *Histochemistry and Cell Biology*. [Online] 145 (6), 629–636. [online]. Available from: <http://link.springer.com/10.1007/s00418-015-1399-y>.
- Buttler, K. et al. (2006) Mesenchymal cells with leukocyte and lymphendothelial characteristics in murine embryos. *Developmental Dynamics*. [Online] 235 (6), 1554–1562. [online]. Available from: <https://onlinelibrary.wiley.com/doi/10.1002/dvdy.20737>.
- Cai, X. et al. (2015) Mesenchymal status of lymphatic endothelial cell: enlightening treatment of lymphatic malformation. *International journal of clinical and experimental medicine*. 8 (8), 12239–12251. [online]. Available from: <http://www.ncbi.nlm.nih.gov/pubmed/26550134>.
- Cao, R. et al. (2011) Mouse corneal lymphangiogenesis model. *Nature Protocols*. [Online] 6 (6), 817–826. [online]. Available from: <https://www.nature.com/articles/nprot.2011.359>.
- Caramel, J. et al. (2018) Pleiotropic Roles for ZEB1 in Cancer. *Cancer Research*. [Online] 78 (1), 30–35. [online]. Available from: <https://aacrjournals.org/cancerres/article/78/1/30/625031/Pleiotropic-Roles-for-ZEB1-in-CancerOncogenic>.
- Celià-Terrassa, T. et al. (2018) Hysteresis control of epithelial-mesenchymal transition dynamics conveys a distinct program with enhanced metastatic ability. *Nature Communications*. [Online] 9 (1), 5005. [online]. Available from: <https://www.nature.com/articles/s41467-018-07538-7>.

- Cha, B. et al. (2016) Mechanotransduction activates canonical Wnt/ β -catenin signaling to promote lymphatic vascular patterning and the development of lymphatic and lymphovenous valves. *Genes & Development*. [Online] 30 (12), 1454–1469. [online]. Available from: <http://genesdev.cshlp.org/lookup/doi/10.1101/gad.282400.116>.
- Cha, B. et al. (2020) YAP and TAZ maintain PROX1 expression in the developing lymphatic and lymphovenous valves in response to VEGF-C signaling. *Development*. [Online] [online]. Available from: <https://journals.biologists.com/dev/article/doi/10.1242/dev.195453/267080/YAP-and-TAZ-maintain-PROX1-expression-in-the>.
- Chakarov, S. et al. (2019) Two distinct interstitial macrophage populations coexist across tissues in specific subtissular niches. *Science*. [Online] 363 (6432), . [online]. Available from: <https://www.science.org/doi/10.1126/science.aau0964>.
- Chen, G. et al. (2019) Single-Cell RNA-Seq Technologies and Related Computational Data Analysis. *Frontiers in Genetics*. [Online] 10. [online]. Available from: <https://www.frontiersin.org/article/10.3389/fgene.2019.00317/full>.
- Chen, Limo et al. (2014) Metastasis is regulated via microRNA-200/ZEB1 axis control of tumour cell PD-L1 expression and intratumoral immunosuppression. *Nature Communications*. [Online] 5 (1), 5241. [online]. Available from: <https://www.nature.com/articles/ncomms6241>.
- Chen, Y. et al. (2017) The pro-inflammatory cytokine $\text{TNF-}\alpha$ inhibits lymphatic pumping via activation of the $\text{NF-}\kappa\text{B}$ - iNOS signaling pathway. *Microcirculation*. [Online] 24 (3), . [online]. Available from: <https://onlinelibrary.wiley.com/doi/10.1111/micc.12364>.
- Chiang, I. K. N. et al. (2023) The blood vasculature instructs lymphatic patterning in a SOX7-dependent manner. *The EMBO Journal*. [Online] 42 (5), . [online]. Available from: <https://www.embopress.org/doi/10.15252/emboj.2021109032>.
- Cho, H. et al. (2019) YAP and TAZ Negatively Regulate Prox1 During Developmental and Pathologic Lymphangiogenesis. *Circulation Research*. [Online] 124 (2), 225–242. [online]. Available from: <https://www.ahajournals.org/doi/10.1161/CIRCRESAHA.118.313707>.
- Choi, D. et al. (2017) ORAI1 Activates Proliferation of Lymphatic Endothelial Cells in Response to Laminar Flow Through Krüppel-Like Factors 2 and 4. *Circulation Research*. [Online] 120 (9), 1426–1439. [online]. Available from: <https://www.ahajournals.org/doi/10.1161/CIRCRESAHA.116.309548>.
- Cicarese, F. et al. (2020) Genetic perturbation of IFN- α transcriptional modulators in human endothelial cells uncovers pivotal regulators of angiogenesis. *Computational and Structural Biotechnology Journal*. [Online] 183977–3986. [online]. Available from: <https://linkinghub.elsevier.com/retrieve/pii/S2001037020305158>.
- Cifarelli, V. & Eichmann, A. (2019) The Intestinal Lymphatic System: Functions and Metabolic Implications. *Cellular and Molecular Gastroenterology and Hepatology*. [Online] 7 (3), 503–513. [online]. Available from: <https://linkinghub.elsevier.com/retrieve/pii/S2352345X18301772>.
- Clasper, S. & Jackson, D. G. (2009) 'Immunohistochemical Methods for Measuring Tissue Lymphangiogenesis', in *Methods in molecular biology (Clifton, N.J.)*.

- [Online]. pp. 79–91. [online]. Available from:
http://link.springer.com/10.1007/978-1-59745-241-0_4.
- Co, M. et al. (2020) FOXP transcription factors in vertebrate brain development, function, and disorders. *WIREs Developmental Biology*. [Online] 9 (5), . [online]. Available from: <https://wires.onlinelibrary.wiley.com/doi/10.1002/wdev.375>.
- Comijn, J. et al. (2001) The Two-Handed E Box Binding Zinc Finger Protein SIP1 Downregulates E-Cadherin and Induces Invasion. *Molecular Cell*. [Online] 7 (6), 1267–1278. [online]. Available from:
<https://linkinghub.elsevier.com/retrieve/pii/S109727650100260X>.
- Connor, A. L. et al. (2016) Lymphatic endothelial lineage assemblage during corneal lymphangiogenesis. *Laboratory Investigation*. [Online] 96 (3), 270–282. [online]. Available from:
<https://linkinghub.elsevier.com/retrieve/pii/S002368372201409X>.
- Cruys, B. et al. (2016) Glycolytic regulation of cell rearrangement in angiogenesis. *Nature Communications*. [Online] 7 (1), 12240. [online]. Available from:
<https://www.nature.com/articles/ncomms12240>.
- Cursiefen, C. et al. (2004) VEGF-A stimulates lymphangiogenesis and hemangiogenesis in inflammatory neovascularization via macrophage recruitment. *Journal of Clinical Investigation*. [Online] 113 (7), 1040–1050. [online]. Available from: <http://www.jci.org/articles/view/20465>.
- Dagenais, S. L. et al. (2004) Foxc2 is expressed in developing lymphatic vessels and other tissues associated with lymphedema–distichiasis syndrome. *Gene Expression Patterns*. [Online] 4 (6), 611–619. [online]. Available from:
<https://linkinghub.elsevier.com/retrieve/pii/S1567133X04001085>.
- D’Alessio, S. et al. (2014) VEGF-C–dependent stimulation of lymphatic function ameliorates experimental inflammatory bowel disease. *Journal of Clinical Investigation*. [Online] 124 (9), 3863–3878. [online]. Available from:
<http://www.jci.org/articles/view/72189>.
- Dave, N. et al. (2011) Functional Cooperation between Snail1 and Twist in the Regulation of ZEB1 Expression during Epithelial to Mesenchymal Transition. *Journal of Biological Chemistry*. [Online] 286 (14), 12024–12032. [online]. Available from:
<https://linkinghub.elsevier.com/retrieve/pii/S0021925820515810>.
- Davis, J. A. et al. (2018) ETS transcription factor Etsrp / Etv2 is required for lymphangiogenesis and directly regulates vegfr3 / flt4 expression. *Developmental Biology*. [Online] 440 (1), 40–52. [online]. Available from:
<https://linkinghub.elsevier.com/retrieve/pii/S0012160617308333>.
- De Bock, K., Georgiadou, M. & Carmeliet, P. (2013) Role of Endothelial Cell Metabolism in Vessel Sprouting. *Cell Metabolism*. [Online] 18 (5), 634–647. [online]. Available from:
<https://linkinghub.elsevier.com/retrieve/pii/S1550413113003252>.
- De Bock, K., Georgiadou, M., Schoors, S., et al. (2013) Role of PFKFB3-Driven Glycolysis in Vessel Sprouting. *Cell*. [Online] 154 (3), 651–663. [online]. Available from: <https://linkinghub.elsevier.com/retrieve/pii/S0092867413007769>.
- DEJANA, E. et al. (2007) Foxs and Ets in the transcriptional regulation of endothelial cell differentiation and angiogenesis. *Biochimica et Biophysica Acta (BBA)* -

- Reviews on Cancer*. [Online] 1775 (2), 298–312. [online]. Available from: <https://linkinghub.elsevier.com/retrieve/pii/S0304419X07000066>.
- Dejana, E. et al. (1999) Vascular Endothelial (VE)-Cadherin: Only an Intercellular Glue? *Experimental Cell Research*. [Online] 252 (1), 13–19. [online]. Available from: <https://linkinghub.elsevier.com/retrieve/pii/S0014482799946013> (Accessed 17 July 2023).
- Deng, Y. et al. (2013) Endothelial ERK signaling controls lymphatic fate specification. *Journal of Clinical Investigation*. [Online] 123 (3), 1202–1215. [online]. Available from: <http://www.jci.org/articles/view/63034>.
- Deng, Y. et al. (2015) Molecular Controls of Lymphatic VEGFR3 Signaling. *Arteriosclerosis, Thrombosis, and Vascular Biology*. [Online] 35 (2), 421–429. [online]. Available from: <https://www.ahajournals.org/doi/10.1161/ATVBAHA.114.304881>.
- Derynck, R. et al. (2014) Signaling pathway cooperation in TGF- β -induced epithelial–mesenchymal transition. *Current Opinion in Cell Biology*. [Online] 3156–66. [online]. Available from: <https://linkinghub.elsevier.com/retrieve/pii/S0955067414001033>.
- Detry, B. et al. (2012) Matrix metalloproteinase-2 governs lymphatic vessel formation as an interstitial collagenase. *Blood*. [Online] 119 (21), 5048–5056. [online]. Available from: <https://ashpublications.org/blood/article/119/21/5048/29950/Matrix-metalloproteinase2-governs-lymphatic-vessel>.
- Dieterich, L. C. et al. (2015) DeepCAGE Transcriptomics Reveal an Important Role of the Transcription Factor MAFB in the Lymphatic Endothelium. *Cell Reports*. [Online] 13 (7), 1493–1504. [online]. Available from: <https://linkinghub.elsevier.com/retrieve/pii/S2211124715011419>.
- Dieterich, L. C. et al. (2020) Lymphatic MAFB regulates vascular patterning during developmental and pathological lymphangiogenesis. *Angiogenesis*. [Online] 23 (3), 411–423. [online]. Available from: <https://link.springer.com/10.1007/s10456-020-09721-1>.
- Divakaruni, A. S. et al. (2014) ‘Analysis and Interpretation of Microplate-Based Oxygen Consumption and pH Data’, in *Methods in Enzymology*. [Online]. Academic Press. pp. 309–354. [online]. Available from: <https://linkinghub.elsevier.com/retrieve/pii/B9780128014158000163> (Accessed 10 July 2023).
- Drápela, S. et al. (2020) ZEB1: A Critical Regulator of Cell Plasticity, DNA Damage Response, and Therapy Resistance. *Frontiers in Molecular Biosciences*. [Online] 7. [online]. Available from: <https://www.frontiersin.org/article/10.3389/fmolb.2020.00036/full>.
- Ducoli, L. & Detmar, M. (2021) Beyond PROX1: transcriptional, epigenetic, and noncoding RNA regulation of lymphatic identity and function. *Developmental Cell*. [Online] 56 (4), 406–426. [online]. Available from: <https://linkinghub.elsevier.com/retrieve/pii/S1534580721000769>.
- Elbashir, S. M. et al. (2001) Duplexes of 21-nucleotide RNAs mediate RNA interference in cultured mammalian cells. *Nature*. [Online] 411 (6836), 494–498. [online]. Available from: <https://www.nature.com/articles/35078107>.

- Enholm, B. et al. (2001) Adenoviral Expression of Vascular Endothelial Growth Factor-C Induces Lymphangiogenesis in the Skin. *Circulation Research*. [Online] 88 (6), 623–629. [online]. Available from: <https://www.ahajournals.org/doi/10.1161/01.RES.88.6.623>.
- Epstein, F. H. & Weiss, S. J. (1989) Tissue Destruction by Neutrophils. *New England Journal of Medicine*. [Online] 320 (6), 365–376. [online]. Available from: <http://www.nejm.org/doi/abs/10.1056/NEJM198902093200606>.
- Escobedo, N. & Oliver, G. (2017) The Lymphatic Vasculature: Its Role in Adipose Metabolism and Obesity. *Cell Metabolism*. [Online] 26 (4), 598–609. [online]. Available from: <https://linkinghub.elsevier.com/retrieve/pii/S1550413117304850>.
- Everaert, C. et al. (2017) Benchmarking of RNA-sequencing analysis workflows using whole-transcriptome RT-qPCR expression data. *Scientific Reports*. [Online] 7 (1), 1559. [online]. Available from: <https://www.nature.com/articles/s41598-017-01617-3>.
- Fan, C. M. & Maniatis, T. (1990) A DNA-binding protein containing two widely separated zinc finger motifs that recognize the same DNA sequence. *Genes & Development*. [Online] 4 (1), 29–42. [online]. Available from: <http://genesdev.cshlp.org/lookup/doi/10.1101/gad.4.1.29>.
- Fang, J. S. et al. (2021) Regulation of Partial and Reversible Endothelial-to-Mesenchymal Transition in Angiogenesis. *Frontiers in Cell and Developmental Biology*. [Online] 9. [online]. Available from: <https://www.frontiersin.org/articles/10.3389/fcell.2021.702021/full>.
- Fatima, A. et al. (2014) Murine *Notch1* is required for lymphatic vascular morphogenesis during development. *Developmental Dynamics*. [Online] 243 (7), 957–964. [online]. Available from: <https://anatomypubs.onlinelibrary.wiley.com/doi/10.1002/dvdy.24129>.
- Feil, S. et al. (2009) ‘Inducible Cre Mice’, in *Methods in Molecular Biology*. [Online]. pp. 343–363. [online]. Available from: http://link.springer.com/10.1007/978-1-59745-471-1_18.
- Feltham, R. et al. (2018) Mind Bomb Regulates Cell Death during TNF Signaling by Suppressing RIPK1’s Cytotoxic Potential. *Cell Reports*. [Online] 23 (2), 470–484. [online]. Available from: <https://linkinghub.elsevier.com/retrieve/pii/S2211124718303991>.
- Flum, M. et al. (2022) Canonical TGFβ signaling induces collective invasion in colorectal carcinogenesis through a Snail1- and Zeb1-independent partial EMT. *Oncogene*. [Online] 41 (10), 1492–1506. [online]. Available from: <https://www.nature.com/articles/s41388-022-02190-4>.
- François, M. et al. (2008) Sox18 induces development of the lymphatic vasculature in mice. *Nature*. [Online] 456 (7222), 643–647. [online]. Available from: <https://www.nature.com/articles/nature07391>.
- Frausto, R. F. et al. (2019) ZEB1 insufficiency causes corneal endothelial cell state transition and altered cellular processing Jung Weon Lee (ed.). *PLOS ONE*. [Online] 14 (6), e0218279. [online]. Available from: <https://dx.plos.org/10.1371/journal.pone.0218279>.
- Frye, M. et al. (2018) Matrix stiffness controls lymphatic vessel formation through regulation of a GATA2-dependent transcriptional program. *Nature*

- Communications*. [Online] 9 (1), 1511. [online]. Available from: <https://www.nature.com/articles/s41467-018-03959-6>.
- Fu, R., Lv, W.-C., et al. (2020) Endothelial ZEB1 promotes angiogenesis-dependent bone formation and reverses osteoporosis. *Nature Communications*. [Online] 11 (1), 460. [online]. Available from: <https://www.nature.com/articles/s41467-019-14076-3>.
- Fu, R., Li, Y., et al. (2020) Inactivation of endothelial ZEB1 impedes tumor progression and sensitizes tumors to conventional therapies. *Journal of Clinical Investigation*. [Online] 130 (3), 1252–1270. [online]. Available from: <https://www.jci.org/articles/view/131507>.
- Gaikwad, A. V. et al. (2023) Endothelial-to-mesenchymal transition: a precursor to pulmonary arterial remodelling in patients with idiopathic pulmonary fibrosis. *ERJ Open Research*. [Online] 9 (2), 00487–02022. [online]. Available from: <http://openres.ersjournals.com/lookup/doi/10.1183/23120541.00487-2022>.
- Gallagher, J. R. et al. (2022) Annual prevalence estimation of lymphatic malformation with a cutaneous component: observational study of a national representative sample of physicians. *Orphanet Journal of Rare Diseases*. [Online] 17 (1), 192. [online]. Available from: <https://ojrd.biomedcentral.com/articles/10.1186/s13023-022-02336-3>.
- Galván, J. A. et al. (2015) Expression of E-cadherin repressors SNAIL, ZEB1 and ZEB2 by tumour and stromal cells influences tumour-budding phenotype and suggests heterogeneity of stromal cells in pancreatic cancer. *British Journal of Cancer*. [Online] 112 (12), 1944–1950. [online]. Available from: <https://www.nature.com/articles/bjc2015177> (Accessed 13 July 2023).
- Ganesan, R. et al. (2016) The transcription factors Slug (SNAI2) and Snail (SNAI1) regulate phospholipase D (PLD) promoter in opposite ways towards cancer cell invasion. *Molecular Oncology*. [Online] 10 (5), 663–676. [online]. Available from: <https://febs.onlinelibrary.wiley.com/doi/10.1016/j.molonc.2015.12.006>.
- García-Caballero, M. et al. (2019) Role and therapeutic potential of dietary ketone bodies in lymph vessel growth. *Nature Metabolism*. [Online] 1 (7), 666–675. [online]. Available from: <https://www.nature.com/articles/s42255-019-0087-y> (Accessed 5 July 2023).
- Gauvrit, S. et al. (2018) HHEX is a transcriptional regulator of the VEGFC/FLT4/PROX1 signaling axis during vascular development. *Nature Communications*. [Online] 9 (1), 2704. [online]. Available from: <https://www.nature.com/articles/s41467-018-05039-1>.
- Geng, X. et al. (2016) Multiple mouse models of primary lymphedema exhibit distinct defects in lymphovenous valve development. *Developmental Biology*. [Online] 409 (1), 218–233. [online]. Available from: <https://linkinghub.elsevier.com/retrieve/pii/S0012160615301032>.
- Geng, X. et al. (2020) S1PR1 regulates the quiescence of lymphatic vessels by inhibiting laminar shear stress–dependent VEGF-C signaling. *JCI Insight*. [Online] 5 (14), . [online]. Available from: <https://insight.jci.org/articles/view/137652>.
- Ghavamipour, F. et al. (2020) Enhanced sensitivity of VEGF detection using catalase-mediated chemiluminescence immunoassay based on CdTe QD/H₂O₂ system. *Journal of Nanobiotechnology*. [Online] 18 (1), 93. [online]. Available from:

- <https://jnanobiotechnology.biomedcentral.com/articles/10.1186/s12951-020-00648-9> (Accessed 17 July 2023).
- von Gise, A. & Pu, W. T. (2012) Endocardial and Epicardial Epithelial to Mesenchymal Transitions in Heart Development and Disease. *Circulation Research*. [Online] 110 (12), 1628–1645. [online]. Available from: <https://www.ahajournals.org/doi/10.1161/CIRCRESAHA.111.259960>.
- Glinton, K. E. et al. (2022) Macrophage-produced VEGFC is induced by efferocytosis to ameliorate cardiac injury and inflammation. *Journal of Clinical Investigation*. [Online] 132 (9), . [online]. Available from: <https://www.jci.org/articles/view/140685>.
- González-Loyola, A. et al. (2021) FOXC2 controls adult lymphatic endothelial specialization, function, and gut lymphatic barrier preventing multiorgan failure. *Science Advances*. [Online] 7 (29), . [online]. Available from: <https://www.science.org/doi/10.1126/sciadv.abf4335>.
- Göös, H. et al. (2022) Human transcription factor protein interaction networks. *Nature Communications*. [Online] 13 (1), 766. [online]. Available from: <https://www.nature.com/articles/s41467-022-28341-5>.
- Gopalakrishnan, B. & Wolff, J. (2009) ‘siRNA and DNA Transfer to Cultured Cells’, in *Methods in Molecular Biology*. [Online]. pp. 31–52. [online]. Available from: http://link.springer.com/10.1007/978-1-59745-429-2_3.
- Gordon, E. J. et al. (2010) Macrophages define dermal lymphatic vessel calibre during development by regulating lymphatic endothelial cell proliferation. *Development*. [Online] 137 (22), 3899–3910. [online]. Available from: <https://journals.biologists.com/dev/article/137/22/3899/44110/Macrophages-define-dermal-lymphatic-vessel-calibre>.
- Goveia, J. et al. (2020) An Integrated Gene Expression Landscape Profiling Approach to Identify Lung Tumor Endothelial Cell Heterogeneity and Angiogenic Candidates. *Cancer Cell*. [Online] 37 (3), 421. [online]. Available from: <https://linkinghub.elsevier.com/retrieve/pii/S1535610820301021>.
- Grotegut, S. et al. (2006) Hepatocyte growth factor induces cell scattering through MAPK/Egr-1-mediated upregulation of Snail. *The EMBO Journal*. [Online] 25 (15), 3534–3545. [online]. Available from: <http://emboj.embopress.org/cgi/doi/10.1038/sj.emboj.7601213>.
- Guo, Y. et al. (2022) Opposing roles of ZEB1 in the cytoplasm and nucleus control cytoskeletal assembly and YAP1 activity. *Cell Reports*. [Online] 41 (1), 111452. [online]. Available from: <https://linkinghub.elsevier.com/retrieve/pii/S2211124722012931>.
- Hall, K. L. et al. (2012) New Model of Macrophage Acquisition of the Lymphatic Endothelial Phenotype Raffaella Bonecchi (ed.). *PLoS ONE*. [Online] 7 (3), e31794. [online]. Available from: <https://dx.plos.org/10.1371/journal.pone.0031794>.
- Hanahan, D. & Weinberg, R. A. (2011) Hallmarks of Cancer: The Next Generation. *Cell*. [Online] 144 (5), 646–674. [online]. Available from: <https://linkinghub.elsevier.com/retrieve/pii/S0092867411001279>.
- Heinz, S. et al. (2015) The selection and function of cell type-specific enhancers. *Nature Reviews Molecular Cell Biology*. [Online] 16 (3), 144–154. [online]. Available from: <https://www.nature.com/articles/nrm3949>.

- Hellström, M. et al. (2007) Dll4 signalling through Notch1 regulates formation of tip cells during angiogenesis. *Nature*. [Online] 445 (7129), 776–780. [online]. Available from: <https://www.nature.com/articles/nature05571>.
- Henri, O. et al. (2016) Selective Stimulation of Cardiac Lymphangiogenesis Reduces Myocardial Edema and Fibrosis Leading to Improved Cardiac Function Following Myocardial Infarction. *Circulation*. [Online] 133 (15), 1484–1497. [online]. Available from: <https://www.ahajournals.org/doi/10.1161/CIRCULATIONAHA.115.020143>.
- Hernández Vásquez, M. N. et al. (2021) Transcription factor FOXP2 is a flow-induced regulator of collecting lymphatic vessels. *The EMBO Journal*. [Online] 40 (12), e107192. [online]. Available from: <https://www.embopress.org/doi/10.15252/embj.2020107192>.
- Ho, C.-Y. et al. (1999) A role for the extraembryonic yolk syncytial layer in patterning the zebrafish embryo suggested by properties of the hex gene. *Current Biology*. [Online] 9 (19), 1131–S4. [online]. Available from: <https://linkinghub.elsevier.com/retrieve/pii/S0960982299804850>.
- Hollenhorst, P. C. et al. (2007) Genome-wide analyses reveal properties of redundant and specific promoter occupancy within the *ETS* gene family. *Genes & Development*. [Online] 21 (15), 1882–1894. [online]. Available from: <http://genesdev.cshlp.org/lookup/doi/10.1101/gad.1561707>.
- Horizon Discovery (2023) *ON-TARGETplus siRNA* [online]. Available from: <https://horizondiscovery.com/en/gene-modulation/knockdown/sirna/products/on-targetplus-sirna-reagents#guarantee> (Accessed 26 September 2023).
- Hosking, B. M. et al. (2004) The VCAM-1 Gene That Encodes the Vascular Cell Adhesion Molecule Is a Target of the Sry-related High Mobility Group Box Gene, Sox18. *Journal of Biological Chemistry*. [Online] 279 (7), 5314–5322. [online]. Available from: <https://linkinghub.elsevier.com/retrieve/pii/S0021925820748593>.
- Hsieh, P.-L. et al. (2018) Recruitment and therapeutic application of macrophages in skeletal muscles after hind limb ischemia. *Journal of Vascular Surgery*. [Online] 67 (6), 1908–1920.e1. [online]. Available from: <https://linkinghub.elsevier.com/retrieve/pii/S0741521417315823>.
- Hultgren, N. W. et al. (2020) Slug regulates the Dll4-Notch-VEGFR2 axis to control endothelial cell activation and angiogenesis. *Nature Communications*. [Online] 11 (1), 5400. [online]. Available from: <https://www.nature.com/articles/s41467-020-18633-z>.
- Iftakhar-E-Khuda, I. et al. (2016) Gene-expression profiling of different arms of lymphatic vasculature identifies candidates for manipulation of cell traffic. *Proceedings of the National Academy of Sciences*. [Online] 113 (38), 10643–10648. [online]. Available from: <https://pnas.org/doi/full/10.1073/pnas.1602357113>.
- van Impel, A. et al. (2014) Divergence of zebrafish and mouse lymphatic cell fate specification pathways. *Development*. [Online] 141 (6), 1228–1238. [online]. Available from: <https://journals.biologists.com/dev/article/141/6/1228/46683/Divergence-of-zebrafish-and-mouse-lymphatic-cell>.

- Jackson, A. L. et al. (2006) Widespread siRNA “off-target” transcript silencing mediated by seed region sequence complementarity. *RNA*. [Online] 12 (7), 1179–1187. [online]. Available from: <http://rnajournal.cshlp.org/lookup/doi/10.1261/rna.25706>.
- Jackson, D. G. (2004) Biology of the lymphatic marker LYVE-1 and applications in research into lymphatic trafficking and lymphangiogenesis. *APMIS*. [Online] 112 (7–8), 526–538. [online]. Available from: <https://onlinelibrary.wiley.com/doi/10.1111/j.1600-0463.2004.apm11207-0811.x>.
- James, J. M. et al. (2013) TGF β signaling is required for sprouting lymphangiogenesis during lymphatic network development in the skin. *Development*. [Online] 140 (18), 3903–3914. [online]. Available from: <https://journals.biologists.com/dev/article/140/18/3903/45866/TGF-signaling-is-required-for-sprouting>.
- Jiang, H. et al. (2021) Pyruvate Kinase M2 Mediates Glycolysis in the Lymphatic Endothelial Cells and Promotes the Progression of Lymphatic Malformations. *The American Journal of Pathology*. [Online] 191 (1), 204–215. [online]. Available from: <https://linkinghub.elsevier.com/retrieve/pii/S000294402030482X>.
- Jin, L. et al. (2020) Zeb1 promotes corneal neovascularization by regulation of vascular endothelial cell proliferation. *Communications Biology*. [Online] 3 (1), 349. [online]. Available from: <https://www.nature.com/articles/s42003-020-1069-z>.
- Johnson, L. A. et al. (2006) An inflammation-induced mechanism for leukocyte transmigration across lymphatic vessel endothelium. *The Journal of Experimental Medicine*. [Online] 203 (12), 2763–2777. [online]. Available from: <https://rupress.org/jem/article/203/12/2763/46322/An-inflammation-induced-mechanism-for-leukocyte> (Accessed 18 July 2023).
- Johnson, L. A. (2022) ‘Analyzing Lymphatic Vessel Patterning in Adult Tissue’, in *Methods in Molecular Biology*. [Online]. pp. 85–94. [online]. Available from: https://link.springer.com/10.1007/978-1-0716-2059-5_7.
- Johnson, L. A. et al. (2017) Dendritic cells enter lymph vessels by hyaluronan-mediated docking to the endothelial receptor LYVE-1. *Nature Immunology*. [Online] 18 (7), 762–770. [online]. Available from: <https://www.nature.com/articles/ni.3750>.
- Johnson, L. A. & Jackson, D. G. (2010) Inflammation-induced secretion of CCL21 in lymphatic endothelium is a key regulator of integrin-mediated dendritic cell transmigration. *International Immunology*. [Online] 22 (10), 839–849. [online]. Available from: <https://academic.oup.com/intimm/article-lookup/doi/10.1093/intimm/dxq435> (Accessed 18 July 2023).
- Johnson, N. C. et al. (2008) Lymphatic endothelial cell identity is reversible and its maintenance requires Prox1 activity. *Genes & Development*. [Online] 22 (23), 3282–3291. [online]. Available from: <http://genesdev.cshlp.org/lookup/doi/10.1101/gad.1727208>.
- Joseph, J. V et al. (2014) TGF- β is an inducer of ZEB1-dependent mesenchymal transdifferentiation in glioblastoma that is associated with tumor invasion. *Cell*

- Death & Disease*. [Online] 5 (10), e1443–e1443. [online]. Available from: <https://www.nature.com/articles/cddis2014395>.
- Joukov, V. et al. (1997) Proteolytic processing regulates receptor specificity and activity of VEGF-C. *The EMBO journal*. [Online] 16 (13), 3898–3911. [online]. Available from: <http://www.ncbi.nlm.nih.gov/pubmed/9233800>.
- Juraleviciute, M. et al. (2021) MX2 mediates establishment of interferon response profile, regulates XAF1, and can sensitize melanoma cells to targeted therapy. *Cancer Medicine*. [Online] 10 (8), 2840–2854. [online]. Available from: <https://onlinelibrary.wiley.com/doi/10.1002/cam4.3846>.
- Kaipainen, A. et al. (1995) Expression of the fms-like tyrosine kinase 4 gene becomes restricted to lymphatic endothelium during development. *Proceedings of the National Academy of Sciences of the United States of America*. [Online] 92 (8), 3566–3570. [online]. Available from: <http://www.ncbi.nlm.nih.gov/pubmed/7724599>.
- Kalluri, R. & Weinberg, R. A. (2009) The basics of epithelial-mesenchymal transition. *Journal of Clinical Investigation*. [Online] 119 (6), 1420–1428. [online]. Available from: <http://www.jci.org/articles/view/39104>.
- Kalucka, J. et al. (2018) Quiescent Endothelial Cells Upregulate Fatty Acid β -Oxidation for Vasculoprotection via Redox Homeostasis. *Cell Metabolism*. [Online] 28 (6), 881–894.e13. [online]. Available from: <https://linkinghub.elsevier.com/retrieve/pii/S1550413118304595>.
- Kanapathy, M. et al. (2014) Tissue-engineered lymphatic graft for the treatment of lymphedema. *Journal of Surgical Research*. [Online] 192 (2), 544–554. [online]. Available from: <https://linkinghub.elsevier.com/retrieve/pii/S0022480414007239>.
- Karkkainen, M. J. et al. (2004) Vascular endothelial growth factor C is required for sprouting of the first lymphatic vessels from embryonic veins. *Nature Immunology*. [Online] 5 (1), 74–80. [online]. Available from: <https://www.nature.com/articles/ni1013>.
- Karpanen, T. & Alitalo, K. (2008) Molecular Biology and Pathology of Lymphangiogenesis. *Annual Review of Pathology: Mechanisms of Disease*. [Online] 3 (1), 367–397. [online]. Available from: <https://www.annualreviews.org/doi/10.1146/annurev.pathmechdis.3.121806.151515>.
- Kaszak, I. et al. (2020) Role of Cadherins in Cancer—A Review. *International Journal of Molecular Sciences*. [Online] 21 (20), 7624. [online]. Available from: <https://www.mdpi.com/1422-0067/21/20/7624>.
- Kataru, R. P. et al. (2009) Critical role of CD11b+ macrophages and VEGF in inflammatory lymphangiogenesis, antigen clearance, and inflammation resolution. *Blood*. [Online] 113 (22), 5650–5659. [online]. Available from: <https://ashpublications.org/blood/article/113/22/5650/107798/Critical-role-of-CD11b-macrophages-and-VEGF-in>.
- Kataru, R. P. et al. (2011) T Lymphocytes Negatively Regulate Lymph Node Lymphatic Vessel Formation. *Immunity*. [Online] 34 (1), 96–107. [online]. Available from: <https://linkinghub.elsevier.com/retrieve/pii/S1074761310004954>.

- Kazenwadel, J. et al. (2023) A Prox1 enhancer represses haematopoiesis in the lymphatic vasculature. *Nature*. [Online] 614 (7947), 343–348. [online]. Available from: <https://www.nature.com/articles/s41586-022-05650-9>.
- Kazenwadel, J. et al. (2015) GATA2 is required for lymphatic vessel valve development and maintenance. *Journal of Clinical Investigation*. [Online] 125 (8), 2979–2994. [online]. Available from: <http://www.jci.org/articles/view/78888>.
- Kim, H. et al. (2014) Inflammation-associated lymphangiogenesis: a double-edged sword? *Journal of Clinical Investigation*. [Online] 124 (3), 936–942. [online]. Available from: <http://www.jci.org/articles/view/71607> (Accessed 18 July 2023).
- Kim, H. et al. (2012) Regulation and implications of inflammatory lymphangiogenesis. *Trends in Immunology*. [Online] 33 (7), 350–356. [online]. Available from: <https://linkinghub.elsevier.com/retrieve/pii/S1471490612000567>.
- Kim, J.-D. & Jin, S.-W. (2014) A Tale of Two Models: Mouse and Zebrafish as Complementary Models for Lymphatic Studies. *Molecules and Cells*. [Online] 37 (7), 503–510. [online]. Available from: <https://linkinghub.elsevier.com/retrieve/pii/S1016847823053372>.
- Kim, J.-W. et al. (2008) FAM83H Mutations in Families with Autosomal-Dominant Hypocalcified Amelogenesis Imperfecta. *The American Journal of Human Genetics*. [Online] 82 (2), 489–494. [online]. Available from: <https://linkinghub.elsevier.com/retrieve/pii/S000292970800075X>.
- King, L. E. et al. (2020) Genes regulating membrane-associated E-cadherin and proliferation in adenomatous polyposis coli mutant colon cancer cells: High content siRNA screen Chunming Liu (ed.). *PLOS ONE*. [Online] 15 (10), e0240746. [online]. Available from: <https://dx.plos.org/10.1371/journal.pone.0240746>.
- Klotz, L. et al. (2015) Cardiac lymphatics are heterogeneous in origin and respond to injury. *Nature*. [Online] 522 (7554), 62–67. [online]. Available from: <https://www.nature.com/articles/nature14483>.
- Kokudo, T. et al. (2008) Snail is required for TGF β -induced endothelial-mesenchymal transition of embryonic stem cell-derived endothelial cells. *Journal of Cell Science*. [Online] 121 (20), 3317–3324. [online]. Available from: <https://journals.biologists.com/jcs/article/121/20/3317/35317/Snail-is-required-for-TGF-induced-endothelial>.
- Koo, B.-K. et al. (2005) Mind Bomb-2 Is an E3 Ligase for Notch Ligand. *Journal of Biological Chemistry*. [Online] 280 (23), 22335–22342. [online]. Available from: <https://linkinghub.elsevier.com/retrieve/pii/S0021925820691815>.
- Kraft, J. D. et al. (2021) Specialized Pro-Resolving Mediators and the Lymphatic System. *International Journal of Molecular Sciences*. [Online] 22 (5), 2750. [online]. Available from: <https://www.mdpi.com/1422-0067/22/5/2750>.
- Krämer, A. et al. (2014) Causal analysis approaches in Ingenuity Pathway Analysis. *Bioinformatics*. [Online] 30 (4), 523–530. [online]. Available from: <https://academic.oup.com/bioinformatics/article/30/4/523/202720>.
- Krasniewski, L. K. et al. (2022) Single-cell analysis of skeletal muscle macrophages reveals age-associated functional subpopulations. *eLife*. [Online] 11. [online]. Available from: <https://elifesciences.org/articles/77974>.

- Kriehuber, E. et al. (2001) Isolation and Characterization of Dermal Lymphatic and Blood Endothelial Cells Reveal Stable and Functionally Specialized Cell Lineages. *The Journal of Experimental Medicine*. [Online] 194 (6), 797–808. [online]. Available from: <https://rupress.org/jem/article/194/6/797/30009/Isolation-and-Characterization-of-Dermal-Lymphatic> (Accessed 17 July 2023).
- Kuga, T. et al. (2013) A novel mechanism of keratin cytoskeleton organization through casein kinase I α and FAM83H in colorectal cancer. *Journal of Cell Science*. [Online] 126 (20), . [online]. Available from: <https://journals.biologists.com/jcs/article/doi/10.1242/jcs.129684/263462/A-novel-mechanism-of-keratin-cytoskeleton>.
- Kukk, E. et al. (1996) VEGF-C receptor binding and pattern of expression with VEGFR-3 suggests a role in lymphatic vascular development. *Development (Cambridge, England)*. [Online] 122 (12), 3829–3837. [online]. Available from: <http://www.ncbi.nlm.nih.gov/pubmed/9012504>.
- Kume, T. (2008) Foxc2 Transcription Factor: A Newly Described Regulator of Angiogenesis. *Trends in Cardiovascular Medicine*. [Online] 18 (6), 224–228. [online]. Available from: <https://linkinghub.elsevier.com/retrieve/pii/S1050173808001266>.
- Kunder, C. A. et al. (2011) Mast cell modulation of the vascular and lymphatic endothelium. *Blood*. [Online] 118 (20), 5383–5393. [online]. Available from: <https://ashpublications.org/blood/article/118/20/5383/29763/Mast-cell-modulation-of-the-vascular-and-lymphatic>.
- Laug, R. et al. (2012) IFN- γ and TNF- α Synergize to Inhibit CTGF Expression in Human Lung Endothelial Cells Shree Ram Singh (ed.). *PLoS ONE*. [Online] 7 (9), e45430. [online]. Available from: <https://dx.plos.org/10.1371/journal.pone.0045430>.
- Lavado, A. & Oliver, G. (2007) *Prox1* expression patterns in the developing and adult murine brain. *Developmental Dynamics*. [Online] 236 (2), 518–524. [online]. Available from: <https://anatomypubs.onlinelibrary.wiley.com/doi/10.1002/dvdy.21024>.
- Lee, H.-W. et al. (2018) Recent advances in understanding lymphangiogenesis and metabolism. *F1000Research*. [Online] 71114. [online]. Available from: <https://f1000research.com/articles/7-1114/v1>.
- Lee, J. et al. (2007) The novel PIAS-like protein hZimp10 is a transcriptional co-activator of the p53 tumor suppressor. *Nucleic Acids Research*. [Online] 35 (13), 4523–4534. [online]. Available from: <https://academic.oup.com/nar/article-lookup/doi/10.1093/nar/gkm476>.
- Li, D. et al. (2019) IRF6 Is Directly Regulated by ZEB1 and ELF3, and Predicts a Favorable Prognosis in Gastric Cancer. *Frontiers in Oncology*. [Online] 9 (APR), . [online]. Available from: <https://www.frontiersin.org/article/10.3389/fonc.2019.00220/full>.
- Li, R. et al. (2023) Endothelial FAT1 inhibits angiogenesis by controlling YAP/TAZ protein degradation via E3 ligase MIB2. *Nature Communications*. [Online] 14 (1), 1980. [online]. Available from: <https://www.nature.com/articles/s41467-023-37671-x>.
- Li, X. et al. (2019) Hallmarks of Endothelial Cell Metabolism in Health and Disease. *Cell Metabolism*. [Online] 30 (3), 414–433. [online]. Available from: <https://linkinghub.elsevier.com/retrieve/pii/S1550413119304401>.

- Li, X. et al. (2006) The Novel PIAS-like Protein hZimp10 Enhances Smad Transcriptional Activity. *Journal of Biological Chemistry*. [Online] 281 (33), 23748–23756. [online]. Available from: <https://linkinghub.elsevier.com/retrieve/pii/S0021925819464132>.
- Liang, Q. et al. (2019) Avian Reticuloendotheliosis Viral Oncogene Related B Regulates Lymphatic Endothelial Cells during Vessel Maturation and Is Required for Lymphatic Vessel Function in Adult Mice. *The American Journal of Pathology*. [Online] 189 (12), 2516–2530. [online]. Available from: <https://linkinghub.elsevier.com/retrieve/pii/S0002944019307138>.
- Liang, W. et al. (2022) Zeb1 regulation of wound-healing-induced inflammation in alkali-damaged corneas. *iScience*. [Online] 25 (4), 104038. [online]. Available from: <https://linkinghub.elsevier.com/retrieve/pii/S258900422200308X>.
- Liao, S. & von der Weid, P.-Y. (2014) Inflammation-induced lymphangiogenesis and lymphatic dysfunction. *Angiogenesis*. [Online] 17 (2), 325–334. [online]. Available from: <http://link.springer.com/10.1007/s10456-014-9416-7>.
- Lim, H. Y. et al. (2018) Hyaluronan Receptor LYVE-1-Expressing Macrophages Maintain Arterial Tone through Hyaluronan-Mediated Regulation of Smooth Muscle Cell Collagen. *Immunity*. [Online] 49 (2), 326–341.e7. [online]. Available from: <https://linkinghub.elsevier.com/retrieve/pii/S1074761318302905>.
- Lin, F.-J. et al. (2010) Direct transcriptional regulation of neuropilin-2 by COUP-TFII modulates multiple steps in murine lymphatic vessel development. *Journal of Clinical Investigation*. [Online] 120 (5), 1694–1707. [online]. Available from: <http://www.jci.org/articles/view/40101>.
- Lipton, B. H. et al. (1992) Histamine-modulated transdifferentiation of dermal microvascular endothelial cells. *Experimental Cell Research*. [Online] 199 (2), 279–291. [online]. Available from: <https://linkinghub.elsevier.com/retrieve/pii/001448279290436C> (Accessed 10 July 2023).
- Liu, F. et al. (2015) Induction of hematopoietic and endothelial cell program orchestrated by <sc>ETS</sc> transcription factor <sc>ER</sc> 71/ <sc>ETV</sc> 2. *EMBO reports*. [Online] 16 (5), 654–669. [online]. Available from: <https://www.embopress.org/doi/10.15252/embr.201439939>.
- Liu, L. et al. (2016) ZEB1 Upregulates VEGF Expression and Stimulates Angiogenesis in Breast Cancer Ramani Ramchandran (ed.). *PLOS ONE*. [Online] 11 (2), e0148774. [online]. Available from: <https://dx.plos.org/10.1371/journal.pone.0148774>.
- Liu, W. et al. (2011) Identification of RNF213 as a Susceptibility Gene for Moyamoya Disease and Its Possible Role in Vascular Development Andreas Meisel (ed.). *PLoS ONE*. [Online] 6 (7), e22542. [online]. Available from: <https://dx.plos.org/10.1371/journal.pone.0022542>.
- Loh, C.-Y. et al. (2019) The E-Cadherin and N-Cadherin Switch in Epithelial-to-Mesenchymal Transition: Signaling, Therapeutic Implications, and Challenges. *Cells*. [Online] 8 (10), 1118. [online]. Available from: <https://www.mdpi.com/2073-4409/8/10/1118>.
- Lomelí, H. (2022) ZMIZ proteins: partners in transcriptional regulation and risk factors for human disease. *Journal of Molecular Medicine*. [Online] 100 (7), 973–983. [online]. Available from: <https://link.springer.com/10.1007/s00109-022-02216-0>.

- Long, J. et al. (2005) Pc2-mediated Sumoylation of Smad-interacting Protein 1 Attenuates Transcriptional Repression of E-cadherin. *Journal of Biological Chemistry*. [Online] 280 (42), 35477–35489. [online]. Available from: <https://linkinghub.elsevier.com/retrieve/pii/S0021925819482227>.
- Lopez, D. et al. (2009) Tumor-induced upregulation of Twist, Snail, and Slug represses the activity of the human VE-cadherin promoter. *Archives of Biochemistry and Biophysics*. [Online] 482 (1–2), 77–82. [online]. Available from: <https://linkinghub.elsevier.com/retrieve/pii/S0003986108005390>.
- Lovisa, S. & Kalluri, R. (2018) Fatty Acid Oxidation Regulates the Activation of Endothelial-to-Mesenchymal Transition. *Trends in Molecular Medicine*. [Online] 24 (5), 432–434. [online]. Available from: <https://linkinghub.elsevier.com/retrieve/pii/S1471491418300492> (Accessed 4 July 2023).
- Lunt, S. Y. & Vander Heiden, M. G. (2011) Aerobic Glycolysis: Meeting the Metabolic Requirements of Cell Proliferation. *Annual Review of Cell and Developmental Biology*. [Online] 27 (1), 441–464. [online]. Available from: <https://www.annualreviews.org/doi/10.1146/annurev-cellbio-092910-154237>.
- Ma, W. et al. (2021) Mitochondrial respiration controls the Prox1-Vegfr3 feedback loop during lymphatic endothelial cell fate specification and maintenance. *Science Advances*. [Online] 7 (18), 7359. [online]. Available from: <https://www.science.org/doi/10.1126/sciadv.abe7359>.
- Ma, W. & Oliver, G. (2017) Lymphatic Endothelial Cell Plasticity in Development and Disease. *Physiology*. [Online] 32 (6), 444–452. [online]. Available from: <https://www.physiology.org/doi/10.1152/physiol.00015.2017>.
- Mahamud, Md. R. et al. (2019) GATA2 controls lymphatic endothelial cell junctional integrity and lymphovenous valve morphogenesis through *miR-126*. *Development*. [Online] [online]. Available from: <https://journals.biologists.com/dev/article/doi/10.1242/dev.184218/266719/GATA2-controls-lymphatic-endothelial-cell>.
- Majima, T. et al. (2013) An Adaptor Molecule Afadin Regulates Lymphangiogenesis by Modulating RhoA Activity in the Developing Mouse Embryo Ryuichi Morishita (ed.). *PLoS ONE*. [Online] 8 (6), e68134. [online]. Available from: <https://dx.plos.org/10.1371/journal.pone.0068134>.
- Marelli-Berg, F. M. et al. (2000) Isolation of endothelial cells from murine tissue. *Journal of Immunological Methods*. [Online] 244 (1–2), 205–215. [online]. Available from: <https://linkinghub.elsevier.com/retrieve/pii/S0022175900002581>.
- Martínez-Corral, I. et al. (2012) In vivo imaging of lymphatic vessels in development, wound healing, inflammation, and tumor metastasis. *Proceedings of the National Academy of Sciences*. [Online] 109 (16), 6223–6228. [online]. Available from: <https://pnas.org/doi/full/10.1073/pnas.1115542109>.
- Martinez-Corral, I. & Makinen, T. (2018) ‘Genetic Lineage Tracing of Lymphatic Endothelial Cells in Mice’, in *Methods in Molecular Biology*. [Online]. pp. 37–53. [online]. Available from: http://link.springer.com/10.1007/978-1-4939-8712-2_3.
- Martín-Fontecha, A. et al. (2009) ‘Dendritic Cell Migration to Peripheral Lymph Nodes’, in *Dendritic Cells*. [Online]. Berlin, Heidelberg: Springer Berlin

- Heidelberg. pp. 31–49. [online]. Available from: http://link.springer.com/10.1007/978-3-540-71029-5_2 (Accessed 18 July 2023).
- Maruyama, K. et al. (2005) Inflammation-induced lymphangiogenesis in the cornea arises from CD11b-positive macrophages. *The Journal of clinical investigation*. [Online] 115 (9), 2363–2372. [online]. Available from: <http://www.ncbi.nlm.nih.gov/pubmed/16138190>.
- Maturi, V. et al. (2018) Genome-wide binding of transcription factor ZEB1 in triple-negative breast cancer cells. *Journal of Cellular Physiology*. [Online] 233 (10), 7113–7127. [online]. Available from: <https://onlinelibrary.wiley.com/doi/10.1002/jcp.26634>.
- Mazzone, M. & Bergers, G. (2019) Regulation of Blood and Lymphatic Vessels by Immune Cells in Tumors and Metastasis. *Annual Review of Physiology*. [Online] 81 (1), 535–560. [online]. Available from: <https://www.annualreviews.org/doi/10.1146/annurev-physiol-020518-114721>.
- McCracken, I. R. et al. (2023) Transcriptional regulators of arterial and venous identity in the developing mammalian embryo. *Current Opinion in Physiology*. [Online] 35100691. [online]. Available from: <https://linkinghub.elsevier.com/retrieve/pii/S2468867323000615>.
- McNamee, E. N. & Rivera-Nieves, J. (2017) Defective Lymphatics in Crohn’s Disease: Tertiary Lymphoid Follicles Plug the Gap. *Gastroenterology*. [Online] 152 (4), 908–910. [online]. Available from: <https://linkinghub.elsevier.com/retrieve/pii/S0016508517300823>.
- Menning, A. et al. (2007) Distinctive role of CCR7 in migration and functional activity of naive- and effector/memory-like Treg subsets. *European Journal of Immunology*. [Online] 37 (6), 1575–1583. [online]. Available from: <https://onlinelibrary.wiley.com/doi/10.1002/eji.200737201>.
- Da Mesquita, S. et al. (2018) Functional aspects of meningeal lymphatics in ageing and Alzheimer’s disease. *Nature*. [Online] 560 (7717), 185–191. [online]. Available from: <https://www.nature.com/articles/s41586-018-0368-8>.
- Mishima, K. et al. (2007) Prox1 Induces Lymphatic Endothelial Differentiation via Integrin $\alpha 9$ and Other Signaling Cascades Ben Margolis (ed.). *Molecular Biology of the Cell*. [Online] 18 (4), 1421–1429. [online]. Available from: <https://www.molbiolcell.org/doi/10.1091/mbc.e06-09-0780>.
- Mitchell, P. (1961) Coupling of Phosphorylation to Electron and Hydrogen Transfer by a Chemi-Osmotic type of Mechanism. *Nature*. [Online] 191 (4784), 144–148. [online]. Available from: <https://www.nature.com/articles/191144a0> (Accessed 10 July 2023).
- Moreira, M. B. et al. (2018) ‘Endothelium: A Coordinator of Acute and Chronic Inflammation’, in *Endothelium and Cardiovascular Diseases*. [Online]. Elsevier. pp. 485–491. [online]. Available from: <https://linkinghub.elsevier.com/retrieve/pii/B9780128123485000325>.
- Morris, C. J. et al. (2018) KLF2-mediated disruption of PPAR- γ signaling in lymphatic endothelial cells exposed to chronically increased pulmonary lymph flow. *American Journal of Physiology-Heart and Circulatory Physiology*. [Online] 315 (1), H173–H181. [online]. Available from: <https://www.physiology.org/doi/10.1152/ajpheart.00635.2017>.

- Moyon, D. et al. (2001) Selective expression of angiopoietin 1 and 2 in mesenchymal cells surrounding veins and arteries of the avian embryo. *Mechanisms of development*. [Online] 106 (1–2), 133–136. [online]. Available from: <http://www.ncbi.nlm.nih.gov/pubmed/11472842>.
- Nasim, S. et al. (2023) CD45 Is Sufficient to Initiate Endothelial-to-Mesenchymal Transition in Human Endothelial Cells—Brief Report. *Arteriosclerosis, Thrombosis, and Vascular Biology*. [Online] 43 (5), . [online]. Available from: <https://www.ahajournals.org/doi/10.1161/ATVBAHA.122.318172>.
- Nathan, C. (2002) Points of control in inflammation. *Nature*. [Online] 420 (6917), 846–852. [online]. Available from: <https://www.nature.com/articles/nature01320>.
- Neal, A. et al. (2022) ‘Finding and Verifying Enhancers for Endothelial-Expressed Genes’, in *Methods in Molecular Biology*. [Online]. pp. 351–368. [online]. Available from: https://link.springer.com/10.1007/978-1-0716-2059-5_28.
- NIH (2017) *Studying Genes*. [online]. Available from: https://www.nigms.nih.gov/education/Documents/Studying_genes_final.pdf (Accessed 26 September 2023).
- Nisato, R. E. et al. (2004) Generation and Characterization of Telomerase-Transfected Human Lymphatic Endothelial Cells with an Extended Life Span. *The American Journal of Pathology*. [Online] 165 (1), 11–24. [online]. Available from: <https://linkinghub.elsevier.com/retrieve/pii/S0002944010632713> (Accessed 17 July 2023).
- Nordstrand, A. et al. (2001) Delayed Invasion of the Kidney and Brain by *Borrelia crocidurae* in Plasminogen-Deficient Mice W. A. Petri (ed.). *Infection and Immunity*. [Online] 69 (9), 5832–5839. [online]. Available from: <https://journals.asm.org/doi/10.1128/IAI.69.9.5832-5839.2001>.
- Norman, T. A. et al. (2019) Transcriptional landscape of pulmonary lymphatic endothelial cells during fetal gestation Vladimir V. Kalinichenko (ed.). *PLOS ONE*. [Online] 14 (5), e0216795. [online]. Available from: <https://dx.plos.org/10.1371/journal.pone.0216795>.
- Norrmén, C. et al. (2009) FOXC2 controls formation and maturation of lymphatic collecting vessels through cooperation with NFATc1. *Journal of Cell Biology*. [Online] 185 (3), 439–457. [online]. Available from: <https://rupress.org/jcb/article/185/3/439/35548/FOXC2-controls-formation-and-maturation-of>.
- Nurmi, H. et al. (2015) VEGF-C is required for intestinal lymphatic vessel maintenance and lipid absorption. *EMBO Molecular Medicine*. [Online] 7 (11), 1418–1425. [online]. Available from: <https://www.embopress.org/doi/10.15252/emmm.201505731>.
- Ny, A. et al. (2005) A genetic *Xenopus laevis* tadpole model to study lymphangiogenesis. *Nature Medicine*. [Online] 11 (9), 998–1004. [online]. Available from: <https://www.nature.com/articles/nm1285>.
- Obeso, J. et al. (1990) A hemangioendothelioma-derived cell line: Its use as a model for the study of endothelial cell biology. *Laboratory Investigation*. 63 (2), 259–69.
- Oliver, G. et al. (2020) The Lymphatic Vasculature in the 21st Century: Novel Functional Roles in Homeostasis and Disease. *Cell*. [Online] 182 (2), 270–296.

- [online]. Available from:
<https://linkinghub.elsevier.com/retrieve/pii/S0092867420308163>.
- Oliver, G. & Srinivasan, R. S. (2010) Endothelial cell plasticity: how to become and remain a lymphatic endothelial cell. *Development*. [Online] 137 (3), 363–372. [online]. Available from:
<https://journals.biologists.com/dev/article/137/3/363/44149/Endothelial-cell-plasticity-how-to-become-and>.
- Oliver, G. & Srinivasan, R. S. (2008) Lymphatic Vasculature Development. *Annals of the New York Academy of Sciences*. [Online] 1131 (1), 75–81. [online]. Available from: <https://nyaspubs.onlinelibrary.wiley.com/doi/10.1196/annals.1413.006>.
- Osta, W. A. et al. (2004) EpCAM Is Overexpressed in Breast Cancer and Is a Potential Target for Breast Cancer Gene Therapy. *Cancer Research*. [Online] 64 (16), 5818–5824. [online]. Available from:
<https://aacrjournals.org/cancerres/article/64/16/5818/511554/EpCAM-Is-Overexpressed-in-Breast-Cancer-and-Is-a>.
- Park, P. J. (2009) ChIP–seq: advantages and challenges of a maturing technology. *Nature Reviews Genetics*. [Online] 10 (10), 669–680. [online]. Available from:
<https://www.nature.com/articles/nrg2641>.
- Park, S. M. et al. (2014) Mapping the Distinctive Populations of Lymphatic Endothelial Cells in Different Zones of Human Lymph Nodes Dimas Tadeu Covas (ed.). *PLoS ONE*. [Online] 9 (4), e94781. [online]. Available from:
<https://dx.plos.org/10.1371/journal.pone.0094781>.
- Payne, S. et al. (2018) Endothelial-Specific Cre Mouse Models. *Arteriosclerosis, Thrombosis, and Vascular Biology*. [Online] 38 (11), 2550–2561. [online]. Available from:
<https://www.ahajournals.org/doi/10.1161/ATVBAHA.118.309669>.
- Peng, D. H. et al. (2017) ZEB1 induces LOXL2-mediated collagen stabilization and deposition in the extracellular matrix to drive lung cancer invasion and metastasis. *Oncogene*. [Online] 36 (14), 1925–1938. [online]. Available from:
<https://www.nature.com/articles/onc2016358>.
- Pennacchio, L. A. et al. (2013) Enhancers: five essential questions. *Nature Reviews Genetics*. [Online] 14 (4), 288–295. [online]. Available from:
<https://www.nature.com/articles/nrg3458>.
- Perez-Oquendo, M. & Gibbons, D. L. (2022) Regulation of ZEB1 Function and Molecular Associations in Tumor Progression and Metastasis. *Cancers*. [Online] 14 (8), 1864. [online]. Available from: <https://www.mdpi.com/2072-6694/14/8/1864>.
- Petrova, T. V et al. (2004) Defective valves and abnormal mural cell recruitment underlie lymphatic vascular failure in lymphedema distichiasis. *Nature Medicine*. [Online] 10 (9), 974–981. [online]. Available from:
<https://www.nature.com/articles/nm1094>.
- Petrova, T. V. (2002) Lymphatic endothelial reprogramming of vascular endothelial cells by the Prox-1 homeobox transcription factor. *The EMBO Journal*. [Online] 21 (17), 4593–4599. [online]. Available from:
<http://emboj.embopress.org/cgi/doi/10.1093/emboj/cdf470>.
- Pfau, J. C. et al. (2000) Monoclonal antibodies to CD45 modify LPS-induced arachidonic acid metabolism in macrophages. *Biochimica et Biophysica Acta*

- (*BBA*) - *Molecular Cell Research*. [Online] 1495 (3), 212–222. [online]. Available from: <https://linkinghub.elsevier.com/retrieve/pii/S0167488999001718>.
- Pflicke, H. & Sixt, M. (2009) Preformed portals facilitate dendritic cell entry into afferent lymphatic vessels. *Journal of Experimental Medicine*. [Online] 206 (13), 2925–2935. [online]. Available from: <https://rupress.org/jem/article/206/13/2925/40788/Preformed-portals-facilitate-dendritic-cell-entry>.
- Pinnell, N. et al. (2015) The PIAS-like Coactivator Zmiz1 Is a Direct and Selective Cofactor of Notch1 in T Cell Development and Leukemia. *Immunity*. [Online] 43 (5), 870–883. [online]. Available from: <https://linkinghub.elsevier.com/retrieve/pii/S1074761315004070>.
- Planas-Paz, L. & Lammert, E. (2013) Mechanical forces in lymphatic vascular development and disease. *Cellular and Molecular Life Sciences*. [Online] 70 (22), 4341–4354. [online]. Available from: <http://link.springer.com/10.1007/s00018-013-1358-5>.
- Plitzko, B. & Loesgen, S. (2018) Measurement of Oxygen Consumption Rate (OCR) and Extracellular Acidification Rate (ECAR) in Culture Cells for Assessment of the Energy Metabolism. *BIO-PROTOCOL*. [Online] 8 (10), . [online]. Available from: <https://bio-protocol.org/e2850>.
- Pober, J. S. & Conran, R. S. (1990) The Role of Endothelial Cells in Inflammation. *Transplantation*. [Online] 50 (4), 537–544. [online]. Available from: <http://journals.lww.com/00007890-199010000-00001>.
- Postigo, A. A. (2003) Regulation of Smad signaling through a differential recruitment of coactivators and corepressors by ZEB proteins. *The EMBO Journal*. [Online] 22 (10), 2453–2462. [online]. Available from: <http://emboj.embopress.org/cgi/doi/10.1093/emboj/cdg226>.
- Potente, M. & Carmeliet, P. (2017) The Link Between Angiogenesis and Endothelial Metabolism. *Annual Review of Physiology*. [Online] 79 (1), 43–66. [online]. Available from: <https://www.annualreviews.org/doi/10.1146/annurev-physiol-021115-105134>.
- PromoCell (2023) *Human Dermal Lymphatic Endothelial Cells* [online]. Available from: https://promocell.com/product/human-dermal-lymphatic-endothelial-cells-hdlec/#tab-reference_literature (Accessed 26 September 2023).
- Pu, Z. et al. (2021) Important Role of Concomitant Lymphangiogenesis for Reparative Angiogenesis in Hindlimb Ischemia. *Arteriosclerosis, Thrombosis, and Vascular Biology*. [Online] 41 (6), 2006–2018. [online]. Available from: <https://www.ahajournals.org/doi/10.1161/ATVBAHA.121.316191>.
- QIAGEN Digital Insights (2023) *QIAGEN Digital Insights* [online]. Available from: <https://digitalinsights.qiagen.com> (Accessed 26 September 2023).
- Rajan, K. C. et al. (2023) Zmiz1 is a novel regulator of lymphatic endothelial cell gene expression and function. *bioRxiv [Preprint]*. [Online] [online]. Available from: <https://doi.org/10.1101/2023.07.22.550165>.
- Ren, Y. et al. (2022) Burden of lymphedema in long-term breast cancer survivors by race and age. *Cancer*. [Online] 128 (23), 4119–4128. [online]. Available from: <https://acsjournals.onlinelibrary.wiley.com/doi/10.1002/cncr.34489>.

- Renò, F. & Sabbatini, M. (2023) Breaking a Vicious Circle: Lymphangiogenesis as a New Therapeutic Target in Wound Healing. *Biomedicines*. [Online] 11 (3), 656. [online]. Available from: <https://www.mdpi.com/2227-9059/11/3/656>.
- Rey, S. & Semenza, G. L. (2010) Hypoxia-inducible factor-1-dependent mechanisms of vascularization and vascular remodelling. *Cardiovascular Research*. [Online] 86 (2), 236–242. [online]. Available from: <https://academic.oup.com/cvres/article-lookup/doi/10.1093/cvr/cvq045>.
- Ribatti, D. & Crivellato, E. (2010) The embryonic origins of lymphatic vessels: an historical review. *British Journal of Haematology*. [Online] 149 (5), 669–674. [online]. Available from: <https://onlinelibrary.wiley.com/doi/10.1111/j.1365-2141.2009.08053.x>.
- Riley, J. F. & West, G. B. (1953) The presence of histamine in tissue mast cells. *The Journal of Physiology*. [Online] 120 (4), 528–537. [online]. Available from: <https://physoc.onlinelibrary.wiley.com/doi/10.1113/jphysiol.1953.sp004915>.
- Rondon-Galeano, M. et al. (2020) <scp>MAFB</scp> modulates the maturation of lymphatic vascular networks in mice. *Developmental Dynamics*. [Online] 249 (10), 1201–1216. [online]. Available from: <https://anatomypubs.onlinelibrary.wiley.com/doi/10.1002/dvdy.209>.
- Rudzinska, M. et al. (2017) The role of prospero homeobox 1 (PROX1) expression in follicular thyroid carcinoma cells. *Oncotarget*. [Online] 8 (69), 114136–114155. [online]. Available from: <https://www.oncotarget.com/lookup/doi/10.18632/oncotarget.23167>.
- Sabine, A. et al. (2015) FOXC2 and fluid shear stress stabilize postnatal lymphatic vasculature. *Journal of Clinical Investigation*. [Online] 125 (10), 3861–3877. [online]. Available from: <https://www.jci.org/articles/view/80454>.
- Salih, D. A. & Brunet, A. (2008) FoxO transcription factors in the maintenance of cellular homeostasis during aging. *Current Opinion in Cell Biology*. [Online] 20 (2), 126–136. [online]. Available from: <https://linkinghub.elsevier.com/retrieve/pii/S0955067408000318>.
- Sánchez-Tilló, E. et al. (2012) EMT-activating transcription factors in cancer: beyond EMT and tumor invasiveness. *Cellular and Molecular Life Sciences*. [Online] 69 (20), 3429–3456. [online]. Available from: <http://link.springer.com/10.1007/s00018-012-1122-2>.
- Sasaroli, D. et al. (2011) Novel surface targets and serum biomarkers from the ovarian cancer vasculature. *Cancer Biology & Therapy*. [Online] 12 (3), 169–180. [online]. Available from: <http://www.tandfonline.com/doi/abs/10.4161/cbt.12.3.16260>.
- Scallan, J. P. et al. (2021) Foxo1 deletion promotes the growth of new lymphatic valves. *Journal of Clinical Investigation*. [Online] 131 (14), . [online]. Available from: <https://www.jci.org/articles/view/142341>.
- Scallan, J. P. et al. (2016) Lymphatic pumping: mechanics, mechanisms and malfunction. *The Journal of Physiology*. [Online] 594 (20), 5749–5768. [online]. Available from: <https://physoc.onlinelibrary.wiley.com/doi/10.1113/JP272088>.
- Scholz, B. et al. (2016) Endothelial RSPO3 Controls Vascular Stability and Pruning through Non-canonical WNT/Ca²⁺/NFAT Signaling. *Developmental Cell*.

- [Online] 36 (1), 79–93. [online]. Available from:
<https://linkinghub.elsevier.com/retrieve/pii/S153458071500800X>.
- Schoors, S. et al. (2015) Fatty acid carbon is essential for dNTP synthesis in endothelial cells. *Nature*. [Online] 520 (7546), 192–197. [online]. Available from:
<https://www.nature.com/articles/nature14362>.
- Schoppmann, S. F. et al. (2006a) Hypoxia inducible factor-1 α correlates with VEGF-C expression and lymphangiogenesis in breast cancer. *Breast Cancer Research and Treatment*. [Online] 99 (2), 135–141. [online]. Available from:
<http://link.springer.com/10.1007/s10549-006-9190-3>.
- Schoppmann, S. F. et al. (2006b) Hypoxia inducible factor-1 α correlates with VEGF-C expression and lymphangiogenesis in breast cancer. *Breast Cancer Research and Treatment*. [Online] 99 (2), 135–141. [online]. Available from:
<http://link.springer.com/10.1007/s10549-006-9190-3>.
- Semenza, G. L. (2013) HIF-1 mediates metabolic responses to intratumoral hypoxia and oncogenic mutations. *Journal of Clinical Investigation*. [Online] 123 (9), 3664–3671. [online]. Available from: <http://www.jci.org/articles/view/67230>.
- Sestito, R. et al. (2022) Functional interaction between endothelin-1 and ZEB1/YAP signaling regulates cellular plasticity and metastasis in high-grade serous ovarian cancer. *Journal of Experimental & Clinical Cancer Research*. [Online] 41 (1), 157. [online]. Available from:
<https://jeccr.biomedcentral.com/articles/10.1186/s13046-022-02317-1>.
- Shendure, J. & Ji, H. (2008) Next-generation DNA sequencing. *Nature Biotechnology*. [Online] 26 (10), 1135–1145. [online]. Available from:
<https://www.nature.com/articles/nbt1486>.
- Shi, Yujiang et al. (2003) Coordinated histone modifications mediated by a CtBP co-repressor complex. *Nature*. [Online] 422 (6933), 735–738. [online]. Available from: <https://www.nature.com/articles/nature01550>.
- Shimizu, Y. et al. (2018) Impact of Lymphangiogenesis on Cardiac Remodeling After Ischemia and Reperfusion Injury. *Journal of the American Heart Association*. [Online] 7 (19), . [online]. Available from:
<https://www.ahajournals.org/doi/10.1161/JAHA.118.009565>.
- Shirakihara, T. et al. (2007) Differential Regulation of Epithelial and Mesenchymal Markers by δ EF1 Proteins in Epithelial–Mesenchymal Transition Induced by TGF- β Carl-Henrik Heldin (ed.). *Molecular Biology of the Cell*. [Online] 18 (9), 3533–3544. [online]. Available from:
<https://www.molbiolcell.org/doi/10.1091/mbc.e07-03-0249>.
- Shu, J. & Santulli, G. (2018) Update on peripheral artery disease: Epidemiology and evidence-based facts. *Atherosclerosis*. [Online] 275379–381. [online]. Available from: <https://linkinghub.elsevier.com/retrieve/pii/S0021915018302764>.
- Shurubor, Y. et al. (2017) Determination of Coenzyme A and Acetyl-Coenzyme A in Biological Samples Using HPLC with UV Detection. *Molecules*. [Online] 22 (9), 1388. [online]. Available from: <http://www.mdpi.com/1420-3049/22/9/1388>.
- Silvestre, J.-S. et al. (2008) Post-ischaemic neovascularization and inflammation. *Cardiovascular Research*. [Online] 78 (2), 242–249. [online]. Available from:
<https://academic.oup.com/cvres/article-lookup/doi/10.1093/cvr/cvn027>.

- Singh, A. K. et al. (2007) Impaired integration of endothelial progenitor cells in capillaries of diabetic wounds is reversible with vascular endothelial growth factor infusion. *Translational Research*. [Online] 149 (5), 282–291. [online]. Available from: <https://linkinghub.elsevier.com/retrieve/pii/S1931524406004130> (Accessed 10 July 2023).
- Sinh, N. D. et al. (2017) Ets1 and ESE1 reciprocally regulate expression of ZEB1/ZEB2, dependent on ERK1/2 activity, in breast cancer cells. *Cancer Science*. [Online] 108 (5), 952–960. [online]. Available from: <https://onlinelibrary.wiley.com/doi/10.1111/cas.13214>.
- Skobe, M. & Detmar, M. (2000) Structure, Function, and Molecular Control of the Skin Lymphatic System. *Journal of Investigative Dermatology Symposium Proceedings*. [Online] 5 (1), 14–19. [online]. Available from: <https://linkinghub.elsevier.com/retrieve/pii/S0022202X15528534>.
- De Smet, F. et al. (2009) Mechanisms of Vessel Branching. *Arteriosclerosis, Thrombosis, and Vascular Biology*. [Online] 29 (5), 639–649. [online]. Available from: <https://www.ahajournals.org/doi/10.1161/ATVBAHA.109.185165>.
- Sontheimer, E. J. (2005) Assembly and function of RNA silencing complexes. *Nature Reviews Molecular Cell Biology*. [Online] 6 (2), 127–138. [online]. Available from: <https://www.nature.com/articles/nrm1568> (Accessed 11 July 2023).
- Srinivasan, R. S. et al. (2007) Lineage tracing demonstrates the venous origin of the mammalian lymphatic vasculature. *Genes & Development*. [Online] 21 (19), 2422–2432. [online]. Available from: <http://genesdev.cshlp.org/lookup/doi/10.1101/gad.1588407>.
- Srinivasan, R. S. et al. (2014a) The Prox1–Vegfr3 feedback loop maintains the identity and the number of lymphatic endothelial cell progenitors. *Genes & Development*. [Online] 28 (19), 2175–2187. [online]. Available from: <http://genesdev.cshlp.org/lookup/doi/10.1101/gad.216226.113>.
- Srinivasan, R. S. et al. (2014b) The Prox1–Vegfr3 feedback loop maintains the identity and the number of lymphatic endothelial cell progenitors. *Genes & Development*. [Online] 28 (19), 2175–2187. [online]. Available from: <http://genesdev.cshlp.org/lookup/doi/10.1101/gad.216226.113> (Accessed 12 July 2023).
- Srinivasan, R. S. & Oliver, G. (2011) Prox1 dosage controls the number of lymphatic endothelial cell progenitors and the formation of the lymphovenous valves. *Genes & Development*. [Online] 25 (20), 2187–2197. [online]. Available from: <http://genesdev.cshlp.org/lookup/doi/10.1101/gad.16974811>.
- Stacker, S. A. et al. (2002) Lymphangiogenesis and cancer metastasis. *Nature Reviews Cancer*. [Online] 2 (8), 573–583. [online]. Available from: <https://www.nature.com/articles/nrc863>.
- Stacker, S. A. et al. (2014) Lymphangiogenesis and lymphatic vessel remodelling in cancer. *Nature Reviews Cancer*. [Online] 14 (3), 159–172. [online]. Available from: <https://www.nature.com/articles/nrc3677>.
- Stine, Z. E. et al. (2015) MYC, Metabolism, and Cancer. *Cancer Discovery*. [Online] 5 (10), 1024–1039. [online]. Available from: <https://aacrjournals.org/cancerdiscovery/article/5/10/1024/4488/MYC-Metabolism-and-CancerMYC-Metabolism-and-Cancer>.

- Stone, O. A. et al. (2021) Endothelial ontogeny and the establishment of vascular heterogeneity. *BioEssays*. [Online] 43 (7), . [online]. Available from: <https://onlinelibrary.wiley.com/doi/10.1002/bies.202100036>.
- Stone, O. A. & Stainier, D. Y. R. (2019) Paraxial Mesoderm Is the Major Source of Lymphatic Endothelium. *Developmental Cell*. [Online] 50 (2), 247-255.e3. [online]. Available from: <https://linkinghub.elsevier.com/retrieve/pii/S1534580719303314>.
- Suarez, A. C. et al. (2023) Modeling lymphangiogenesis: Pairing in vitro and in vivo metrics. *Microcirculation*. [Online] 30 (2–3), . [online]. Available from: <https://onlinelibrary.wiley.com/doi/10.1111/micc.12802>.
- Suchting, S. et al. (2007) The Notch ligand Delta-like 4 negatively regulates endothelial tip cell formation and vessel branching. *Proceedings of the National Academy of Sciences*. [Online] 104 (9), 3225–3230. [online]. Available from: <https://pnas.org/doi/full/10.1073/pnas.0611177104>.
- Sutton, M. G. & Sharpe, N. (2000) Left ventricular remodeling after myocardial infarction: pathophysiology and therapy. *Circulation*. [Online] 101 (25), 2981–2988. [online]. Available from: <http://www.ncbi.nlm.nih.gov/pubmed/10869273> (Accessed 18 July 2023).
- Tabrizi, Z. B. et al. (2022) ‘Simple Gene Knockdown in Endothelial Cells Using Short Interfering RNA Oligonucleotides’, in *Methods in Molecular Biology*. [Online]. pp. 251–255. [online]. Available from: https://link.springer.com/10.1007/978-1-0716-2059-5_19.
- Takagi, T. et al. (1998) δ EF1, a zinc finger and homeodomain transcription factor, is required for skeleton patterning in multiple lineages. *Development*. [Online] 125 (1), 21–31. [online]. Available from: <https://journals.biologists.com/dev/article/125/1/21/39767/EF1-a-zinc-finger-and-homeodomain-transcription>.
- Takaoka, A. & Yanai, H. (2006) Interferon signalling network in innate defence. *Cellular Microbiology*. [Online] 8 (6), 907–922. [online]. Available from: <https://onlinelibrary.wiley.com/doi/10.1111/j.1462-5822.2006.00716.x>.
- Takeda, A. et al. (2019) Single-Cell Survey of Human Lymphatics Unveils Marked Endothelial Cell Heterogeneity and Mechanisms of Homing for Neutrophils. *Immunity*. [Online] 51 (3), 561-572.e5. [online]. Available from: <https://linkinghub.elsevier.com/retrieve/pii/S1074761319302973>.
- Tammela, T. & Alitalo, K. (2010) Lymphangiogenesis: Molecular Mechanisms and Future Promise. *Cell*. [Online] 140 (4), 460–476. [online]. Available from: <https://linkinghub.elsevier.com/retrieve/pii/S0092867410001157>.
- Tan, K. W. et al. (2012) Expansion of Cortical and Medullary Sinuses Restrains Lymph Node Hypertrophy during Prolonged Inflammation. *The Journal of Immunology*. [Online] 188 (8), 4065–4080. [online]. Available from: <https://journals.aai.org/jimmunol/article/188/8/4065/86114/Expansion-of-Cortical-and-Medullary-Sinuses>.
- Thowsen, I. M. et al. (2022) Genetic Engineering of Lymphangiogenesis in Skin Does Not Affect Blood Pressure in Mouse Models of Salt-Sensitive Hypertension. *Hypertension*. [Online] 79 (11), 2451–2462. [online]. Available from: <https://www.ahajournals.org/doi/10.1161/HYPERTENSIONAHA.122.19777>.

- Thurman, R. E. et al. (2012) The accessible chromatin landscape of the human genome. *Nature*. [Online] 489 (7414), 75–82. [online]. Available from: <https://www.nature.com/articles/nature11232>.
- Trincot, C. E. & Caron, K. M. (2019) Lymphatic Function and Dysfunction in the Context of Sex Differences. *ACS Pharmacology & Translational Science*. [Online] 2 (5), 311–324. [online]. Available from: <https://pubs.acs.org/doi/10.1021/acspsci.9b00051>.
- Tripp, C. H. et al. (2008) The lymph vessel network in mouse skin visualised with antibodies against the hyaluronan receptor LYVE-1. *Immunobiology*. [Online] 213 (9–10), 715–728. [online]. Available from: <https://linkinghub.elsevier.com/retrieve/pii/S0171298508001022>.
- Ulvmar, M. H. et al. (2014) The atypical chemokine receptor CCRL1 shapes functional CCL21 gradients in lymph nodes. *Nature Immunology*. [Online] 15 (7), 623–630. [online]. Available from: <https://www.nature.com/articles/ni.2889>.
- De Val, S. et al. (2008) Combinatorial Regulation of Endothelial Gene Expression by Ets and Forkhead Transcription Factors. *Cell*. [Online] 135 (6), 1053–1064. [online]. Available from: <https://linkinghub.elsevier.com/retrieve/pii/S0092867408013871>.
- De Val, S. & Black, B. L. (2009) Transcriptional Control of Endothelial Cell Development. *Developmental Cell*. [Online] 16 (2), 180–195. [online]. Available from: <https://linkinghub.elsevier.com/retrieve/pii/S1534580709000422>.
- Vieira, J. M. et al. (2018) The cardiac lymphatic system stimulates resolution of inflammation following myocardial infarction. *Journal of Clinical Investigation*. [Online] 128 (8), 3402–3412. [online]. Available from: <https://www.jci.org/articles/view/97192>.
- Villar, J. et al. (2023) ETV3 and ETV6 enable monocyte differentiation into dendritic cells by repressing macrophage fate commitment. *Nature Immunology*. [Online] 24 (1), 84–95. [online]. Available from: <https://www.nature.com/articles/s41590-022-01374-0>.
- Visel, A. et al. (2009) Genomic views of distant-acting enhancers. *Nature*. [Online] 461 (7261), 199–205. [online]. Available from: <https://www.nature.com/articles/nature08451>.
- Vuorio, T. et al. (2018) Downregulation of VEGFR3 signaling alters cardiac lymphatic vessel organization and leads to a higher mortality after acute myocardial infarction. *Scientific Reports*. [Online] 8 (1), 16709. [online]. Available from: <https://www.nature.com/articles/s41598-018-34770-4>.
- Wälchli, T. et al. (2021) Hierarchical imaging and computational analysis of three-dimensional vascular network architecture in the entire postnatal and adult mouse brain. *Nature Protocols*. [Online] 16 (10), 4564–4610. [online]. Available from: <https://www.nature.com/articles/s41596-021-00587-1>.
- Wang, S.-H. et al. (2017) Tumour cell-derived WNT5B modulates in vitro lymphangiogenesis via induction of partial endothelial-mesenchymal transition of lymphatic endothelial cells. *Oncogene*. [Online] 36 (11), 1503–1515. [online]. Available from: <https://www.nature.com/articles/onc2016317>.
- Wang, Y. et al. (2010) Ephrin-B2 controls VEGF-induced angiogenesis and lymphangiogenesis. *Nature*. [Online] 465 (7297), 483–486. [online]. Available from: <https://www.nature.com/articles/nature09002>.

- Wang, Z. et al. (2008) Combinatorial patterns of histone acetylations and methylations in the human genome. *Nature Genetics*. [Online] 40 (7), 897–903. [online]. Available from: <https://www.nature.com/articles/ng.154>.
- Welch-Reardon, K. M. et al. (2015) A Role for Partial Endothelial–Mesenchymal Transitions in Angiogenesis? *Arteriosclerosis, Thrombosis, and Vascular Biology*. [Online] 35 (2), 303–308. [online]. Available from: <https://www.ahajournals.org/doi/10.1161/ATVBAHA.114.303220>.
- Welch-Reardon, K. M. et al. (2014) Angiogenic sprouting is regulated by endothelial cell expression of Slug (Snai2). *Journal of Cell Science*. [Online] 127 (9), . [online]. Available from: <https://journals.biologists.com/jcs/article/doi/10.1242/jcs.143420/259914/Angiogenic-sprouting-is-regulated-by-endothelial>.
- Wels, C. et al. (2011a) Transcriptional Activation of ZEB1 by Slug Leads to Cooperative Regulation of the Epithelial–Mesenchymal Transition-Like Phenotype in Melanoma. *Journal of Investigative Dermatology*. [Online] 131 (9), 1877–1885. [online]. Available from: <https://linkinghub.elsevier.com/retrieve/pii/S0022202X15354075> (Accessed 12 July 2023).
- Wels, C. et al. (2011b) Transcriptional Activation of ZEB1 by Slug Leads to Cooperative Regulation of the Epithelial–Mesenchymal Transition-Like Phenotype in Melanoma. *Journal of Investigative Dermatology*. [Online] 131 (9), 1877–1885. [online]. Available from: <https://linkinghub.elsevier.com/retrieve/pii/S0022202X15354075>.
- Wesdorp, M. et al. (2018) MPZL2, Encoding the Epithelial Junctional Protein Myelin Protein Zero-like 2, Is Essential for Hearing in Man and Mouse. *The American Journal of Human Genetics*. [Online] 103 (1), 74–88. [online]. Available from: <https://linkinghub.elsevier.com/retrieve/pii/S0002929718301721>.
- Wigle, J. T. (2002) An essential role for Prox1 in the induction of the lymphatic endothelial cell phenotype. *The EMBO Journal*. [Online] 21 (7), 1505–1513. [online]. Available from: <http://emboj.embopress.org/cgi/doi/10.1093/emboj/21.7.1505>.
- Wigle, J. T. & Oliver, G. (1999) Prox1 Function Is Required for the Development of the Murine Lymphatic System. *Cell*. [Online] 98 (6), 769–778. [online]. Available from: <https://linkinghub.elsevier.com/retrieve/pii/S0092867400815111>.
- Wilhelm, K. et al. (2016) FOXO1 couples metabolic activity and growth state in the vascular endothelium. *Nature*. [Online] 529 (7585), 216–220. [online]. Available from: <https://www.nature.com/articles/nature16498>.
- Williams, T. M. et al. (1992) The TCF8 gene encoding a zinc finger protein (Nil-2-a) resides on human chromosome 10p11.2. *Genomics*. [Online] 14 (1), 194–196. [online]. Available from: <https://linkinghub.elsevier.com/retrieve/pii/S0888754305803076>.
- Wilting, J. et al. (2000) An avian model for studies of embryonic lymphangiogenesis. *Lymphology*. 33 (3), .
- Wilting, J. et al. (2001) Development of the avian lymphatic system. *Microscopy Research and Technique*. [Online] 55 (2), 81–91. [online]. Available from: <https://analyticalsciencejournals.onlinelibrary.wiley.com/doi/10.1002/jemt.1159>.

- Wilting, J. et al. (2006) Dual origin of avian lymphatics. *Developmental Biology*. [Online] 292 (1), 165–173. [online]. Available from: <https://linkinghub.elsevier.com/retrieve/pii/S0012160605009395>.
- Wilting, J. et al. (2002) The transcription factor Prox1 is a marker for lymphatic endothelial cells in normal and diseased human tissues. *The FASEB Journal*. [Online] 16 (10), 1271–1273. [online]. Available from: <https://onlinelibrary.wiley.com/doi/10.1096/fj.01-1010fje>.
- Wirzenius, M. et al. (2007) Distinct vascular endothelial growth factor signals for lymphatic vessel enlargement and sprouting. *The Journal of Experimental Medicine*. [Online] 204 (6), 1431–1440. [online]. Available from: <https://rupress.org/jem/article/204/6/1431/46931/Distinct-vascular-endothelial-growth-factor>.
- Wong, B. W. et al. (2018) Emerging Concepts in Organ-Specific Lymphatic Vessels and Metabolic Regulation of Lymphatic Development. *Developmental Cell*. [Online] 45 (3), 289–301. [online]. Available from: <https://linkinghub.elsevier.com/retrieve/pii/S1534580718302417>.
- Wong, B. W. et al. (2017) The role of fatty acid β -oxidation in lymphangiogenesis. *Nature*. [Online] 542 (7639), 49–54. [online]. Available from: <https://www.nature.com/articles/nature21028>.
- Xiang, M. et al. (2020) A Single-Cell Transcriptional Roadmap of the Mouse and Human Lymph Node Lymphatic Vasculature. *Frontiers in Cardiovascular Medicine*. [Online] 7. [online]. Available from: <https://www.frontiersin.org/article/10.3389/fcvm.2020.00052/full>.
- Xiong, J. et al. (2018) A Metabolic Basis for Endothelial-to-Mesenchymal Transition. *Molecular Cell*. [Online] 69 (4), 689-698.e7. [online]. Available from: <https://linkinghub.elsevier.com/retrieve/pii/S109727651830039X> (Accessed 4 July 2023).
- Xu, Y. et al. (2010) Neuropilin-2 mediates VEGF-C–induced lymphatic sprouting together with VEGFR3. *Journal of Cell Biology*. [Online] 188 (1), 115–130. [online]. Available from: <https://rupress.org/jcb/article/188/1/115/35665/Neuropilin-2-mediates-VEGF-C-induced-lymphatic>.
- Yamashita, T. et al. (2007) Activation of Hepatic Stem Cell Marker EpCAM by Wnt– β -Catenin Signaling in Hepatocellular Carcinoma. *Cancer Research*. [Online] 67 (22), 10831–10839. [online]. Available from: <https://aacrjournals.org/cancerres/article/67/22/10831/533669/Activation-of-Hepatic-Stem-Cell-Marker-EpCAM-by>.
- Yamazaki, T. et al. (2009) COUP-TFII regulates the functions of Prox1 in lymphatic endothelial cells through direct interaction. *Genes to Cells*. [Online] 14 (3), 425–434. [online]. Available from: <https://onlinelibrary.wiley.com/doi/10.1111/j.1365-2443.2008.01279.x>.
- Yang, M. et al. (2019) Biological characteristics of transcription factor RelB in different immune cell types: implications for the treatment of multiple sclerosis. *Molecular Brain*. [Online] 12 (1), 115. [online]. Available from: <https://molecularbrain.biomedcentral.com/articles/10.1186/s13041-019-0532-6>.

- Yang, Q. et al. (2017) Interferon- α inhibits cell migration and invasion and induces the expression of antiviral proteins in Huh-7 cells transfected with hepatitis B virus X gene-expressing lentivirus. *Experimental and Therapeutic Medicine*. [Online] 14 (6), . [online]. Available from: <http://www.spandidos-publications.com/10.3892/etm.2017.5288>.
- Yang, W. et al. (2012) PKM2 Phosphorylates Histone H3 and Promotes Gene Transcription and Tumorigenesis. *Cell*. [Online] 150 (4), 685–696. [online]. Available from: <https://linkinghub.elsevier.com/retrieve/pii/S0092867412008823> (Accessed 13 July 2023).
- Yao, L.-C. et al. (2012) Plasticity of Button-Like Junctions in the Endothelium of Airway Lymphatics in Development and Inflammation. *The American Journal of Pathology*. [Online] 180 (6), 2561–2575. [online]. Available from: <https://linkinghub.elsevier.com/retrieve/pii/S0002944012002428>.
- Yao, L.-C. et al. (2010) Steroid-Resistant Lymphatic Remodeling in Chronically Inflamed Mouse Airways. *The American Journal of Pathology*. [Online] 176 (3), 1525–1541. [online]. Available from: <https://linkinghub.elsevier.com/retrieve/pii/S0002944010604634>.
- Yi, Y. et al. (2022) System Analysis of Adaptor-Related Protein Complex 1 Subunit Mu 2 (AP1M2) on Malignant Tumors: A Pan-Cancer Analysis Fu Wang (ed.). *Journal of Oncology*. [Online] 20221–17. [online]. Available from: <https://www.hindawi.com/journals/jo/2022/7945077/>.
- Yoshimatsu, Y. et al. (2011) Ets family members induce lymphangiogenesis through physical and functional interaction with Prox1. *Journal of Cell Science*. [Online] 124 (16), 2753–2762. [online]. Available from: <https://journals.biologists.com/jcs/article/124/16/2753/31902/Ets-family-members-induce-lymphangiogenesis>.
- Yoshimatsu, Y. et al. (2020) TGF-beta and TNF-alpha cooperatively induce mesenchymal transition of lymphatic endothelial cells via activation of Activin signals Nobuyuki Takakura (ed.). *PLOS ONE*. [Online] 15 (5), e0232356. [online]. Available from: <https://dx.plos.org/10.1371/journal.pone.0232356> (Accessed 10 July 2023).
- Yoshimatsu, Y. & Watabe, T. (2011) Roles of TGF- β Signals in Endothelial-Mesenchymal Transition during Cardiac Fibrosis. *International Journal of Inflammation*. [Online] 20111–8. [online]. Available from: <http://www.hindawi.com/journals/iji/2011/724080/>.
- Yu, P. et al. (2017) FGF-dependent metabolic control of vascular development. *Nature*. [Online] 545 (7653), 224–228. [online]. Available from: <https://www.nature.com/articles/nature22322>.
- Yu, P. et al. (2018) ‘Metabolic Analysis of Lymphatic Endothelial Cells’, in Guillermo Oliver & Mark L Kahn (eds.) *Lymphangiogenesis: Methods and Protocols*. [Online]. New York, NY: Springer New York. pp. 325–334. [online]. Available from: http://link.springer.com/10.1007/978-1-4939-8712-2_22.
- Yu, Q. C. et al. (2022) Activation of Wnt/ β -catenin signaling by Zeb1 in endothelial progenitors induces vascular quiescence entry. *Cell Reports*. [Online] 41 (8), 111694. [online]. Available from: <https://linkinghub.elsevier.com/retrieve/pii/S2211124722015686>.

- Yuan, L. et al. (2002) Abnormal lymphatic vessel development in neuropilin 2 mutant mice. *Development (Cambridge, England)*. [Online] 129 (20), 4797–4806. [online]. Available from: <http://www.ncbi.nlm.nih.gov/pubmed/12361971>.
- Zawieja, D. C. et al. (1991) Reactive oxygen metabolites inhibit spontaneous lymphatic contractions. *American Journal of Physiology-Heart and Circulatory Physiology*. [Online] 260 (6), H1935–H1943. [online]. Available from: <https://www.physiology.org/doi/10.1152/ajpheart.1991.260.6.H1935>.
- Zegerman, P. et al. (2002) Histone H3 Lysine 4 Methylation Disrupts Binding of Nucleosome Remodeling and Deacetylase (NuRD) Repressor Complex. *Journal of Biological Chemistry*. [Online] 277 (14), 11621–11624. [online]. Available from: <https://linkinghub.elsevier.com/retrieve/pii/S0021925818519682>.
- Zhang, L. et al. (2006) Identical probes on different high-density oligonucleotide microarrays can produce different measurements of gene expression. *BMC Genomics*. [Online] 7 (1), 153. [online]. Available from: <https://bmcbgenomics.biomedcentral.com/articles/10.1186/1471-2164-7-153>.
- Zhang, Y. et al. (2018) Heterogeneity in VEGFR3 levels drives lymphatic vessel hyperplasia through cell-autonomous and non-cell-autonomous mechanisms. *Nature Communications*. [Online] 9 (1), 1296. [online]. Available from: <https://www.nature.com/articles/s41467-018-03692-0>.
- Zhang, Y. et al. (2019) The roles of ZEB1 in tumorigenic progression and epigenetic modifications. *Biomedicine & Pharmacotherapy*. [Online] 110400–408. [online]. Available from: <https://linkinghub.elsevier.com/retrieve/pii/S0753332218362048>.
- Zheng, S. & Epstein, P. (2021) CD45 Immunohistochemistry in Mouse Kidney. *BIO-PROTOCOL*. [Online] 11 (22), . [online]. Available from: <https://bio-protocol.org/e4230>.
- Zhu, P. et al. (2006) Transdifferentiation of pulmonary arteriolar endothelial cells into smooth muscle-like cells regulated by myocardin involved in hypoxia-induced pulmonary vascular remodelling. *International Journal of Experimental Pathology*. [Online] 87 (6), 463–474. [online]. Available from: <https://onlinelibrary.wiley.com/doi/10.1111/j.1365-2613.2006.00503.x> (Accessed 10 July 2023).
- Zhuo, H. et al. (2019) Tumor endothelial cell-derived cadherin-2 promotes angiogenesis and has prognostic significance for lung adenocarcinoma. *Molecular Cancer*. [Online] 18 (1), 34. [online]. Available from: <https://molecular-cancer.biomedcentral.com/articles/10.1186/s12943-019-0987-1>.
- Zimmerli, D. et al. (2022) MYC promotes immune-suppression in triple-negative breast cancer via inhibition of interferon signaling. *Nature Communications*. [Online] 13 (1), 6579. [online]. Available from: <https://www.nature.com/articles/s41467-022-34000-6>.